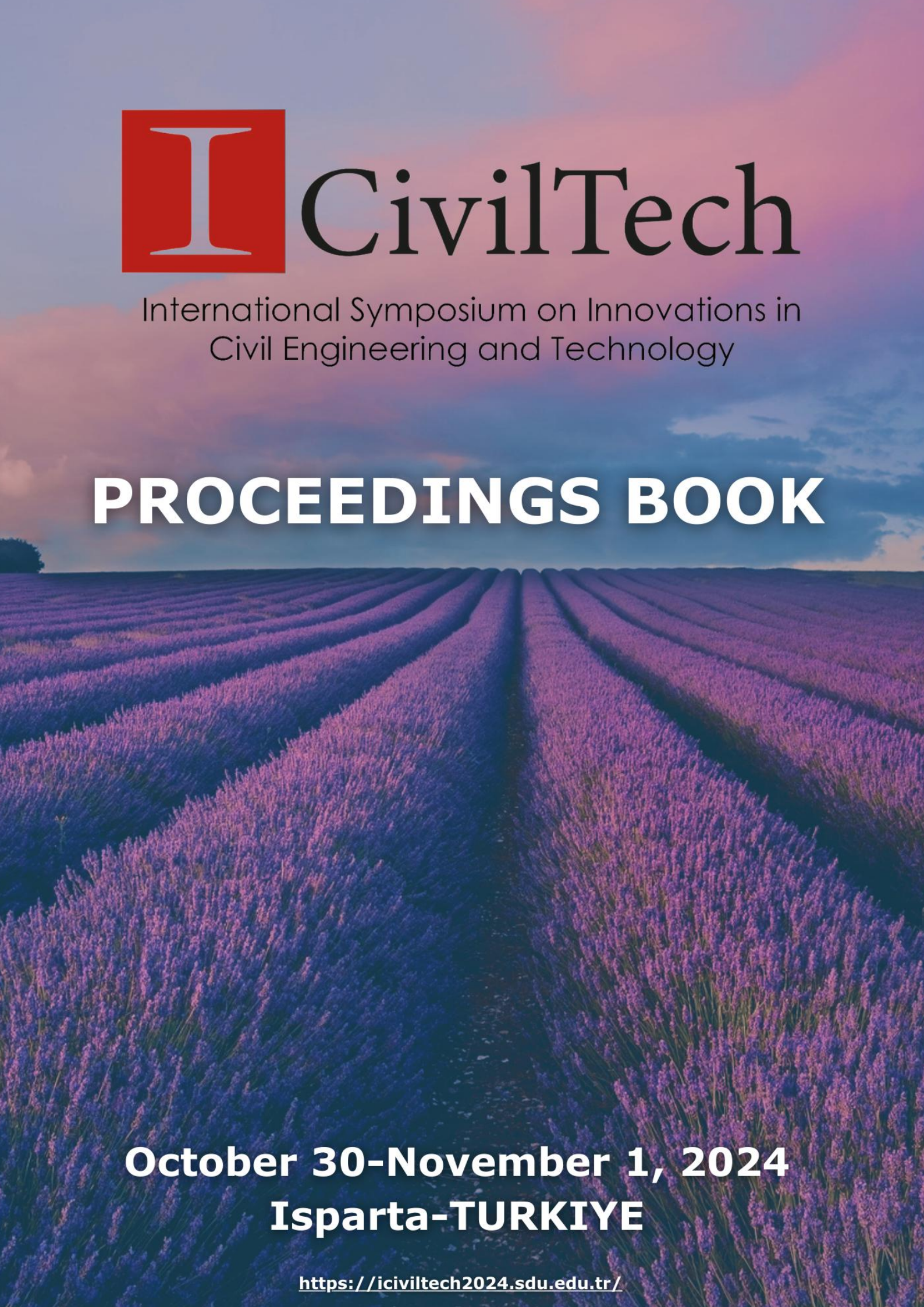

ICivilTech

International Symposium on Innovations in Civil Engineering and Technology

PROCEEDINGS BOOK

October 30-November 1, 2024
Isparta-TURKIYE

https://iciviltech2024.sdu.edu.tr/

2nd International Symposium on Innovations in Civil Engineering and Technology

(I CivilTech 2024)

PROCEEDINGS BOOK

Isparta-TURKIYE
October 30-November 1, 2024

SYMPOSIUM PROCEEDINGS BOOK

Second International Symposium on Innovations in Civil Engineering and Technology (2nd I CivilTech)

THEME: Innovations in Civil Engineering and Technology

PUBLISHER: Prof. Dr. Hüseyin AKBULUT

EDITORS: Hüseyin AKBULUT, Cahit GÜRER, Serdal TERZİ, Burak Enis KORKMAZ

COMPILATION BY: Burak Enis KORKMAZ, Ayfer ELMACI KORKMAZ and Şule YARCI

PLACE OF PUBLICATION: Isparta - TURKİYE

PRINT DATE: 23.12.2024

VOLUME: 1

ISBN: 978-605-69928-3-4

This book is available on the website: https://iciviltech2024.sdu.edu.tr/

Symposium Boards

Honor Committee

Rector of Suleyman Demirel University – Prof. Dr. Mehmet SALTAN

Rector of Afyon Kocatepe University – Prof. Dr. Mehmet KARAKAŞ

Rector of Isparta University of Applied Sciences – Prof. Dr. Yılmaz ÇATAL

Rector of Konya Teknik University – Prof. Dr. Osman Nuri ÇELİK

Rector of Istanbul Gelisim University – Prof. Dr. Bahri ŞAHİN

Rector of Fırat University – Prof. Dr. Fahrettin GÖKTAŞ

Organization Committee

Prof. Dr. Hüseyin AKBULUT (Chair), Afyon Kocatepe University, TURKIYE

Prof. Dr. Cahit GÜRER (Co Chair), Afyon Kocatepe University, TURKIYE

Prof. Dr. Mustafa KARAŞAHİN, Istanbul Gelisim University, TURKIYE

Prof. Dr. Serdal TERZİ, Süleyman Demirel University, TURKIYE

Prof. Dr. Özlem TERZİ, Isparta University of Applied Sciences, TURKIYE

Prof. Dr. Mehmet YILMAZ, Fırat University, TURKIYE

Assoc. Prof. Şebnem KARAHANÇER, Isparta University of Applied Sciences, TURKIYE

Assist. Prof. Ekinhan ERİŞKİN, Süleyman Demirel University, TURKIYE

Assist. Prof. Süleyman GÜCEK, Afyon Kocatepe University, TURKIYE

Assist. Prof. Tahsin BAYKAL, Kırıkkale University, TURKIYE

Lecturer Ayfer ELMACI KORKMAZ, Afyon Kocatepe University, TURKIYE

Lecturer M. Törehan TURAN, Alanya Alaaddin Keykubat University, TURKIYE

Res. Assist. Aydın KICI, Süleyman Demirel University, TURKIYE

Res. Assist. Burak Enis KORKMAZ, Afyon Kocatepe University, TURKIYE

Res. Assist. Burak İKİNCİ, Süleyman Demirel University, TURKIYE

Res. Assist. Fatih ERGEZER, Süleyman Demirel University, TURKIYE

Res. Assist. Şule YARCI, Afyon Kocatepe University, TURKIYE

Gökçe KURNAZ (MSc Student), Isparta University of Applied Sciences, TURKIYE

Scientific Committee

Prof. Dr. Agus Setyo Muntohar, Universitas Muhammadiyah Yogyakarta, INDONESIA
Prof. Dr. Ahmet Alper Öner, Kayseri Erciyes University, TURKIYE
Prof. Dr. Ahmet Tortum, Atatürk University, TURKIYE
Prof. Dr. Ahmet Yıldız, Afyon Kocatepe University, TURKIYE
Prof. Dr. Ali Hakan Ören, Dokuz Eylül University, TURKIYE
Prof. Dr. Ali Topal, Dokuz Eylül University, TURKIYE
Prof. Dr. Altan Çetin, Bartın University, TURKIYE
Prof. Dr. Amir Kavussı, Tarbiat Modares University, IRAN
Prof. Dr. Atmaja P. Rosyidi, Muhammadiyah University of Yogyakarta, INDONESIA
Prof. Dr. Baha Vural Kök, Fırat University, TURKIYE
Prof. Dr. Barış Sevim, Yıldız Teknik University, TURKIYE
Prof. Dr. Bekir Aktaş, Erciyes University, TURKIYE
Prof. Dr. Bojan Zlender, University of Maribor, Maribor, SLOVENIA
Prof. Dr. Burak Şengöz, Dokuz Eylül University, TURKIYE
Prof. Dr. Çağlar Özkaymak, Afyon Kocatepe University, TURKIYE
Prof. Dr. Cahit Gürer, Afyon Kocatepe University, TURKIYE
Prof. Dr. Cengiz Özel, Isparta Applied Sciences University, TURKIYE
Prof. Dr. Cenk Karakurt, Bilecik Şeyh Edebali University, TURKIYE
Prof. Dr. Cesare Sangiorgi, University of Bologna, İTALYA
Prof. Dr. Chong-Chen Wang, Beijing University of Civil Engineering and Architecture, CHINA
Prof. Dr. Constantin E. Chalioris, Democritus University of Thrace, GREECE
Prof. Dr. Dunja Perıc, Kansas State University, USA
Prof. Dr. Ender Demirel, Eskişehir Osmangazi University, TURKIYE
Prof. Dr. Erol Tutumluer, University of Illinois at Urbana-Champaign, USA
Prof. Dr. Evandro Tolentino, Federal Center for Technological Education of Minas Gerais, BRAZIL
Prof. Dr. Fatih Özcan, Mersin University, TURKIYE
Prof. Dr. Gülser Çelebi, Çankaya University, TURKIYE
Prof. Dr. Hakan Tongal, Suleyman Demirel University, TURKIYE
Prof. Dr. Halil Ceylan, Iowa State University, USA
Prof. Dr. Halim Ceylan, Pamukkale University, TURKIYE
Prof. Dr. Hasbi Yaprak, Kastamonu University, TURKIYE
Prof. Dr. Hashem R. Al-Masaeid, Jordan University of Science and Technology, JORDAN
Prof. Dr. Hong-Hu Zhu, Nanjing University, CHINA
Prof. Dr. Hung-Jiun Liao, National Taiwan University of Science and Technology, TAIWAN
Prof. Dr. Hüseyin Akbulut, Afyon Kocatepe University, TURKIYE
Prof. Dr. Hüseyin Temiz, Kahramanmaraş Sütçü İmam University, TURKIYE
Prof. Dr. İbrahim Özgür Deneme, Aksaray University, TURKIYE
Prof. Dr. İlhami Demir, Kırıkkale University, TURKIYE
Prof. Dr. İlker Bekir Topçu, Eskişehir Osmangazi University, TURKIYE
Prof. Dr. İlker Fatih KARA, Mersin University, TURKIYE
Prof. Dr. İlker KAZAZ, Erzurum Technical University, TURKIYE
Prof. Dr. Imad L. Al-Quadi, University of Illinois at Urbana-Champaign, USA
Prof. Dr. Iqbal Khan, King Saud University, SAUDI ARABIA
Prof. Dr. İsmail Demir, Afyon Kocatepe University, TURKIYE
Prof. Dr. İsmail Hakkı Özölçer, Zonguldak Bülent Ecevit University, TURKIYE
Prof. Dr. İsmail Zorluer, Afyon Kocatepe University, TURKIYE
Prof. Dr. Jalal Taqi Shaker Al-Obaedi, University of Al- Quadisiyah, IRAQ
Prof. Dr. João Pedro Silva, Polytechnic Institute of Leiria, PORTUGAL
Prof. Dr. Juan Carlos Vielma, Pontifical Catholic University of Valparaíso, CHILE

Prof. Dr. Julian Carrillo, Nueva Granada Military University, COLOMBIA
Prof. Dr. Ka-Veng Yuen, University of Macau, MACAO
Prof. Dr. Kemalettin Yılmaz - Sakarya University, TURKIYE
Prof. Dr. Khan Shahzada, University of Engineering and Technology Peshawar, PAKISTAN
Prof. Dr. K.M. Mini, Amrita School of Engineering, INDIA
Prof. Dr. Kubilay Akçaözoğlu, Niğde Ömer Halis Demir University, TURKIYE
Prof. Dr. Malaya Chetia, Assam Engineering College, INDIA
Prof. Dr. Masayasu Ohtsu, Kyoto University, JAPAN
Prof. Dr. Matjaz Sraml, University of Maribor, Maribor, SLOVENIA
Prof. Dr. Md Safıuddin, George Brown College, CANADA
Prof. Dr. Mehmet Avcar, Suleyman Demirel University, TURKIYE
Prof. Dr. Mehmet Orhan, Gazi University, TURKIYE
Prof. Dr. Mehmet Saltan, Suleyman Demirel University, TURKIYE
Prof. Dr. Mehmet Uğur Toprak, Dumlupınar University, TURKIYE
Prof. Dr. Mehmet Yılmaz, Fırat University, TURKIYE
Prof. Dr. Meor Othman Hamzah, University Sains Malaysia, MALAYSIA
Prof. Dr. Mesut Çimen, Suleyman Demirel University, TURKIYE
Prof. Dr. Mesut Tığdemir, Suleyman Demirel University, TURKIYE
Prof. Dr. Metin Hakan Severcan, Niğde Ömer Halis Demir University, TURKIYE
Prof. Dr. Murat Kankal, Uludağ University, TURKIYE
Prof. Dr. Murat Karacasu, Eskişehir Osmangazi University, TURKIYE
Prof. Dr. Murat Öztürk, Konya Teknik University, TURKIYE
Prof. Dr. Murat Türköz, Eskişehir Osmangazi University, TURKIYE
Prof. Dr. Musharraf Zaman, University of Oklahoma, USA
Prof. Dr. Mustafa Erol Keskin, Suleyman Demirel University, TURKIYE
Prof. Dr. Mustafa Karaşahin, İstanbul Gelişim University, TURKIYE
Prof. Dr. Mustafa Sarıdemir, Niğde Ömer Halis Demir University, TURKIYE
Prof. Dr. Mustafa Yıldız, Konya Technical University, TURKIYE
Prof. Dr. Mustafa Özer, Gazi University, TURKIYE
Prof. Dr. Mustaque Hossain, Kansas State University, Kansas, USA
Prof. Dr. Nabi Yüzer, Yıldız Technical University, TURKIYE
Prof. Dr. Nurdan Memişoğlu Apaydin, İstanbul University Cerrahpaşa, TURKIYE
Prof. Dr. Okan Karahan, Kayseri Erciyes University, TURKIYE
Prof. Dr. Osman Günaydin, Adıyaman University, TURKIYE
Prof. Dr. Osman Nuri Çelik, Konya Technical University, TURKIYE
Prof. Dr. Özge Andiç, Ege University, TURKIYE
Prof. Dr. Özgür Yaman, Middle East Technical University (METU), TURKIYE
Prof. Dr. Özlem Terzi, Isparta Aplied Sciences University, TURKIYE
Prof. Dr. Hasan Özkaynak, Beykent University, TURKIYE
Prof. Dr. Paula Folino, Universidad de Buenos Aires, ARGENTİNA
Prof. Dr. Rafat Siddique, Thapar University, INDIA
Prof. Dr. Recep Bakış, Eskişehir Technical University, TURKIYE
Prof. Dr. Regita Bendikienė, Kaunas University of Technology, LITHUANIAN
Prof. Dr. Rüstem Gül, Iğdır University, TURKIYE
Prof. Dr. Ş. Ebru Okuyucu, Afyon Kocatepe University, TURKIYE
Prof. Dr. Sabit Oymael, Arel University, TURKIYE
Prof. Dr. Salih Yazıcıoğlu, Gazi University, TURKIYE
Prof. Dr. Sarad Das, Indian Institute of Technology (ISM), INDIA
Prof. Dr. Şemsettin Kılınçarslan, Suleyman Demirel University, TURKIYE
Prof. Dr. Serdal Terzi, Suleyman Demirel University, TURKIYE
Prof. Dr. Şeref Sağıroğlu, Gazi University, TURKIYE
Prof. Dr. Serhan Tanyel, Dokuz Eylül University, TURKIYE

Prof. Dr. Servet Karasu, Zonguldak Bülent Ecevit University, TURKIYE
Prof. Dr. Servet Yıldız, Fırat University, TURKIYE
Prof. Dr. Seyhan Fırat, Gazi University, TURKIYE
Prof. Dr. Soner Haldenbilen, Pamukkale University, TURKIYE
Prof. Dr. Stanishlav Jovanovic, University of Novi Sad, SERBIA
Prof. Dr. Taha Taşkıran, Ankara Yıldırım Beyazıt University, TURKIYE
Prof. Dr. Tamer Baybura, Afyon Kocatepe University, TURKIYE
Prof. Dr. Tomaž Tollazzi, University of Maribor, SLOVENIA
Prof. Dr. Turan Özturan, Boğaziçi University, TURKIYE
Prof. Dr. Volkan Emre Uz, Izmir Institute of Technology, TURKIYE
Prof. Dr. Yeliz Yükselen Aksoy, Dokuz Eylul University, TURKIYE
Prof. Dr. Yılmaz Aruntaş, Gazi University, TURKIYE
Prof. Dr. Yılmaz İçağa, Afyon Kocatepe University, TURKIYE
Prof. Dr. Yüksel Taşdemir, Bozok University, TURKIYE
Prof. Dr. Yusuf Arayici, Northumbria University, UK
Assoc. Prof. Dr. Ahmet Atalay, Atatürk University, TURKIYE
Assoc. Prof. Dr. Ahmet Raif Boğa, Afyon Kocatepe University, TURKIYE
Assoc. Prof. Dr. Altan Yilmaz, Mehmet Akif Ersoy University, TURKIYE
Assoc. Prof. Dr. Diego Lopez-Garcia, Pontifical Catholic University of Chile, CHILE
Assoc. Prof. Dr. Emine Dilek Taylan, Süleyman Demirel University, TURKIYE
Assoc. Prof. Dr. Evren Seyrek, Kütahya Dumlupınar University, TURKIYE
Assoc. Prof. Dr. Gökhan Durmuş, Gazi University, TURKIYE
Assoc. Prof. Dr. Hakan Özbaşaran, Eskişehir Osmangazi University, TURKIYE
Assoc. Prof. Dr. Halil Ibrahim Burgan, Akdeniz University, TURKIYE
Assoc. Prof. Dr. Hamide Kabaş, Suleyman Demirel University, TURKIYE
Assoc. Prof. Dr. Hasan Savaş, Eskişehir Osmangazi University, TURKIYE
Assoc. Prof. Dr. Hümeyra Bolakar Tosun, Aksaray University, TURKIYE
Assoc. Prof. Dr. Jülide Öner, Uşak University, TURKIYE
Assoc. Prof. Dr. Kadir Güçlüer, Adiyaman University, TURKIYE
Assoc. Prof. Dr. Kamil Bekir Afacan, Eskişehir Osmangazi University, TURKIYE
Assoc. Prof. Dr. Kemal Saplioğlu, Suleyman Demirel University, TURKIYE
Assoc. Prof. Dr. Kıvanç Taşkin, Eskişehir Technical University, TURKIYE
Assoc. Prof. Dr. Lilian Rezende, Federal University of Goiás, BRAZIL
Assoc. Prof. Dr. Manuel Chiachio Ruano, University of Granada, SPAIN
Assoc. Prof. Dr. Mehmet Canbaz, Eskişehir Osmangazi University, TURKIYE
Assoc. Prof. Dr. Mehmet Rıfat Kahyaoğlu, Muğla Sıtkı Koçman University, TURKIYE
Assoc. Prof. Dr. Mehmet Sarikahya, Afyon Kocatepe University, TURKIYE
Assoc. Prof. Dr. Meltem Saplioğlu, Suleyman Demirel University, TURKIYE
Assoc. Prof. Dr. Metin Mutlu Aydin, Ondokuz Mayıs University, TURKIYE
Assoc. Prof. Dr. Murat Kilit, Afyon Kocatepe University, TURKIYE
Assoc. Prof. Dr. Mustafa Yalçın, Afyon Kocatepe University, TURKIYE
Assoc. Prof. Dr. Nihat Morova, Isparta University of Applied Sciences, TURKIYE
Assoc. Prof. Dr. Niyazi Özgür Bezgin, İstanbul University Cerrahpaşa, TURKIYE
Assoc. Prof. Dr. Osman Şimşek, Gazi University, TURKIYE
Assoc. Prof. Dr. Ricardo Duarte, Polytechnic of Leiria, PORTUGAL
Assoc. Prof. Dr. Roumiana Zaharieva, University of Architecture, BULGARIA
Assoc. Prof. Dr. Şebnem Karahançer, Isparta University of Applied Sciences, TURKIYE
Assoc. Prof. Dr. Tuba Kütük Sert, Recep Tayyip Erdoğan University, TURKIYE
Assoc. Prof. Dr. Ümit Yurt, Düzce University, TURKIYE
Assoc. Prof. Dr. Weal M. Hassan, University of Alaska, ABD
Assoc. Prof. Dr. Yue Xiao, Wuhan University, CHINESE
Assist. Prof. Dr. Abdullah Demir, Dumlupınar University, TURKIYE

FOREWORD

Civil engineering is a fundamental discipline that creates and maintains the infrastructure of societies. Civil engineers are responsible for designing safe, durable and sustainable structures, from buildings to bridges, highways, railways, airports, ports and dams.

Turkiye is a country that frequently experiences earthquakes. The earthquakes centered in Kahramanmaras that occurred on February 6, 2023 and affected 11 provinces, once again revealed how important the profession of civil engineering is. This tragic event brought to the agenda not only the loss of life and destruction, but also the importance of awareness about the earthquake resistance of structures.

Similar situations are experienced worldwide; natural disasters, climate change and environmental conditions require the development of civil engineers and their updating according to the requirements of the age. Sustainable designs, green building applications, smart city solutions, artificial intelligence applications are important trends in the field of civil engineering. At this point, civil engineers need to not only design structures but also take environmental impacts into consideration.

As a result, civil engineering is of great importance worldwide. The February 6 earthquake reminded us that this profession is not just a construction activity, but also a critical area that directly affects human life and safety. In this context, the responsibilities of civil engineers are increasing; they need to continuously develop the knowledge and skills required to ensure the safety of structures, protect human life and develop sustainable solutions.

For this purpose, the first International Symposium on Innovations in Civil Engineering and Technologies (ICivilTech) hosted by Afyon Kocatepe University in Afyonkarahisar, Turkiye in 2019 was a great scientific event where academicians, industry representatives and students came together to present and discuss the latest developments and innovations in the field of Civil Engineering. Due to the pandemic process, we are experiencing, it was decided that the second symposium after 5 years will be held in Isparta/Turkiye on October 30th-November 1st, 2024 hosted by Suleyman Demirel University.

The symposium aims to bring together academicians, industry representatives and students at Süleyman Demirel University to promote new ideas, innovative applications and knowledge sharing at the intersection of civil engineering and technology and to discuss the latest developments in the field. In the 2nd iCivilTech symposium, a total of 86 papers from 18 different countries (Algeria, Bangladesh, China, Croatia, Georgia, Greece, India, Iraq, Italy, Kazakhstan, Pakistan, Poland, Russian Federation, Slovenia, Sweden, Ukraine, United States, Vietnam) will be presented face-to-face and online. In addition, invited speakers from five different countries, Prof. Dr. Halil Ceylan, Assoc. Prof. Dr. Luigi Pariota, Assoc. Prof. Dr. Borut Macuh, Assoc. Prof. Dr. Aman Garg, Assist. Prof. Dr. Selçuk İz will make presentations on the latest developments in traffic, geotechnical, mechanical and steel structures. In the sessions to be held, expert academics, researchers and industry representatives will share with us and the relevant industry the research results and technologies that will shape the future of civil engineering. I believe that the interactions between the participants will allow our knowledge and experience to be

further enriched. I hope that the 2nd ICivilTech symposium will open the door to new academic collaborations, creative solution suggestions and inspiring exchanges of ideas in the field of civil engineering. I would like to thank all participants, the members of the executive board who contributed to the work of the symposium, our valuable researchers who supported us with their papers, our participants and all the universities that supported us. I hope that the symposium will be beneficial.

Prof. Dr. Mehmet SALTAN
Rector of Suleyman Demirel University

Programme

2ND INTERNATIONAL SYMPOSIUM ON INNOVATIONS IN CIVIL ENGINEERING AND TECHNOLOGIES

31 OCT 2024 | THURSDAY

DAY2 - LÜTFÜ ÇAKMAKÇI CONVENTION CENTER HALL A

09:15-10:00	**OPENING CEREMONY**
10:00-10:30	**KEYNOTE SESSION** **LUIGI PARIOTA (PH.D.) (INVITED SPEAKER)** EXPERIMENTS CONCERNING THE USE OF MACROSCOPIC FUNDAMENTAL DIAGRAM-BASED HIERARCHICAL CONTROL OF URBAN TRAFFIC
10:30-12:15	**SESSION 1** — **SESSION CHAIR: PROF. DR. SERDAL TERZİ**
10:30-10:45	INVESTIGATION OF THE NYLON BAG WASTE MODIFIED BITUMEN PROPERTIES CAHİT GÜRER, BOJAN ZLENDER, SÜLEYMAN GÜCEK, PRIMOZ JELUSIK, BURAK ENİS KORKMAZ, ŞULE YARCI, MURAT VERGİ TACİROĞLU, TAMARA BRAČKO, BORUT MAČUH, ROK VARGA
10:45-11:00	CATEGORIZING URBAN NETWORK SEGMENTS FOR CYCLISTS' USE FOR MULTI-OBJECTIVE ROUTING KONSTANTINOS THEODORESKOS, KONSTANTINOS GKIOTSALITIS
11:00-11:15	A COMPARATIVE INVESTIGATION OF THE EFFECTS OF GEOMETRIC DIFFERENCES IN WEAVING AREAS IN THE UNITED KINGDOM AND TÜRKIYE METİN MUTLU AYDIN, EREN DAĞLI
11:15-11:30	DEVELOPING PUBLIC TRANSPORTATION INFORMATION SYSTEMS AT CITY ENTRY POINTS: PUBLIC TRANSPORTATION INTEGRATION SCORE ABDULKADİR ÖZDEN, SÜLEYMAN NURULAH ADAHI ŞAHİN
11:30-11:45	EVALUATION OF EMERGENCY ENTRY MANEUVERS FOR AMBULANCES IN TERMS OF ROAD DESIGN: THE CASE OF SDÜ FACULTY OF MEDICINE AYŞE ÜNAL, MELTEM SAPLIOĞLU
11:45-12:00	STATISTICAL PREDICTION OF BITUMEN RUTTING PARAMETER JÜLİDE ÖNER
12:00-12:15	RAIL THERMAL BUCKLING RISK MANAGEMENT: COMPARATIVE ANALYSIS OF STRESS-FREE TEMPERATURE DETERMINATION IN THE USA AND TÜRKIYE MEHMET SALTAN, FERHAT ÇEÇEN, ÖMER FARUK ACAR
12:15-12:45	**KEYNOTE SESSION** **AMAN GARG (PH.D.) (INVITED SPEAKER)** BOOTSTRAP-BASED MACHINE LEARNING ALGORITHM FOR INVESTIGATING STOCHASTICITY IN COMPRESSIVE STRENGTH OF CONCRETE
12:45-13:30	**LUNCH BREAK**

13:30-14:00	KEYNOTE SESSION SELÇUK İZ (PH.D.) (INVITED SPEAKER) THE EFFECT OF WALL FORM AND RAW MATERIAL HUMIDITY AND DUST EXPLOSION ON SILO PRESSURE IN GRAIN SILOS	
14:00-14:30	KEYNOTE SESSION BORUT MACUH (PH.D.) (INVITED SPEAKER) FEASIBILITY OF USING GEOSYNTHETICS IN GEOTECHNICAL STRUCTURES	
14:30-14:45	QUESTION AND ANSWERS	
14:45-15:00	COFFEE BREAK	
15:00-15:30	KEYNOTE SESSION HALİL CEYLAN (PH.D.) (INVITED SPEAKER) AI IN TRANSPORTATION GEOTECHNICS: UNLOCKING COMPLEX Solutions for a New Era	
15:30-15:45	QUESTION AND ANSWERS	
15:45-17:00	SESSION 2	SESSION CHAIR: PROF.DR.MESUT TİĞDEMİR
15:45-16:00	INVESTIGATION OF CONDUCTIVITY AND MECHANICAL PROPERTIES OF ELECTRICALLY CONDUCTIVE ASPHALT CONCRETE PRODUCED FROM HYBRID AGGREGATE	CAHİT GÜRER , HAKKI ARDA DÜZGÜN, HÜSEYİN AKBULUT, BURAK ENİS KORKMAZ , AYFER ELMACI KORKMAZ
16:00-16:15	THE EFFECT OF MODULUS OF ELASTICITY AND LAYER THICKNESS ON THE DESIGN LIFE OF FLEXIBLE PAVEMENTS	MERVE BOŞNAK, MURAT VERGİ TACİROĞLU
16:15-16:30	INVESTIGATION OF THE EFFECTS OF USING WASTE VEGETABLE MARGARINE IN BITUMEN MODIFICATION	GİZEM KAÇAROĞLU, ÖZNUR KARADAĞ, MEHMET SALTAN
16:30-16:45	INTERVENTION MAPPING FOR TRAFFIC CRASHES IN TÜRKİYE	AHMED PAKSOY, SONER HALDENBİLEN, HALİM CEYLAN
16:45-17:00	USING ASPHALT PAVEMENT INSTEAD OF BALLAST AND SUBBALLAST LAYERS IN RAIL TRACK	TUĞÇE AKILLI TÖRER, CAHİT GÜRER, KUBİLAY ASLANTAŞ

10:30-12:15	**SESSION 3**	**SESSION CHAIR: PROF.DR.HASAN ÖZKAYNAK**
10:30-10:45	BENDING ANALYSIS OF FUNCTIONALLY GRADED BEAMS USING HIGHER ORDER SHEAR DEFORMATION THEORY INCLUDING THICKNESS STRETCHING EFFECT DOĞAN KANIĞ, YONCA BAB, AKİF KUTLU	
10:45-11:00	3 BOYUTLU YAZICILARIN İNŞAAT SEKTÖRÜNDE KULLANIMI FERDİ GEVREK, LALE ATILGAN GEVREK	
11:00-11:15	EVALUATION OF MONOLITHIC CONSTRUCTION QUALITY ACCORDING TO THE ECONOMIC INDICATOR ELINA KRISTESIASHVILI, LEILA KRISTESIASHVILI, IA MSHVIDOBADZE, IRMA GHARIBASHVILI	
11:15-11:30	STUDY OF VIBRATIONS OF FRAME BUILDINGS AS A DISCRETE CONTINUOUS SYSTEM DURING AN EARTHQUAKE UNDER IMPULSE ACTION GELA KIPIANI, ANA TABATADZE, MALKHAZ TSIKARISHVILIE	
11:30-11:45	PRODUCTION OF ENVIRONMENTALLY FRIENDLY FOAM CONCRETE USING WASTE MATERIAL: EFFECTS OF WASTE CONCRETE SLUDGE AND FIBER ADDITIVES İHSAN TÜRKEL, MEHMET UĞUR YILMAZOĞLU, İFFET GAMZE MÜTEVELLI ÖZKAN, GÖKHAN KAPLAN	
11:45-12:00	IMPACT OF THE EUROPEAN GREEN DEAL AND CIRCULARITY ON LEED PROJECTS ŞEYDA ADIGÜZEL ISTIL	
12:00-12:15	MULTIFUNCTIONAL UTILISATION OF MARBLE WASTES IN ONE-PART AND TWO-PART GEOPOLYMER PRODUCTION METHODS: APPLICATIONS AS FILLER AND FINE AGGREGATE BURAK BODUR, M.A. MECİT IŞIK,GÖKHAN KAPLAN, OĞUZHAN YAVUZ BAYRAKTAR	
15:45-17:15	**SESSION 4**	**SESSION CHAIR: PROF.DR.MURAT KANKAL**
15:45-16:00	INVESTIGATION OF MEDITERRANEAN REGION PRECIPITATION AND TEMPERATURES WITH INNOVATIVE POLYGON TREND ANALYSIS TAHSİN BAYKAL	
16:00-16:15	AN INVESTIGATION ON THE MECHANICAL BEHAVIOURS OF CONCRETE GRAVITY DAM TUBA AYDIN	
16:15-16:30	USING MACHINE LEARNING ALGORITHMS WITH OVER SAMPLING TECHNIQUES FOR SEDIMENT TRANSPORT PREDICTION TAHSİN BAYKAL	
16:30-16:45	TEMPORAL ANALYSIS OF DROUGHT AT THE ULUDAĞ METEOROLOGICAL STATION, BURSA, TÜRKIYE MURAT ŞAN, MURAT KANKAL	
16:45-17:00	KIZILIRMAK BASIN HYDROLOGICAL DROUGHT ANALYSIS ÖZLEM TERZİ, TAHSİN BAYKAL, EMİNE DİLEK TAYLAN	
17:00-17:15	INVESTIGATION OF THE EFFECTS OF TWO DIFFERENT BIOPOLYMERS ON THE STRENGTH PARAMETERS OF SILTY SOIL HALIL OĞUZHAN KARA, MEHMET UĞUR YILMAZOĞLU	

09:30-11:00	**SESSION 5**	**SESSION CHAIR: PROF. DR. SERDAL TERZİ**
09:30-09:45	FROM KEYWORDS TO TRENDS: BIBLIOMETRIC ANALYSIS OF ARTIFICIAL INTELLIGENCE METHODS IN ASPHALT PAVEMENT RESEARCH WITH R-STUDIO PROGRAM FATİH ERGEZER, SERDAL TERZİ	
09:45-10:00	EXAMINATION OF THE PROPERTIES OF 70/100 BITUMEN MODIFIED WITH ACTIVATED CARBON ÖZNUR KARADAĞ, GİZEM KAÇAROĞLU, MEHMET SALTAN	
10:00-10:15	RUTTING RESISTANCE IN BASALT FIBER REINFORCED RECYCLED ASPHALT PAVEMENT DOLUNAY ZENGİN, HALİM CEYLAN, SONER HALDENBİLEN	
10:15-10:30	A NOVEL STRUCTURAL HEALTH ASSESSMENT APPROACH FOR THE BALLASTED CONCRETE RAILWAY SLEEPERS FERHAT ÇEÇEN, BEKİR AKTAŞ	
10:30-10:45	INVESTIGATION OF RHEOLOGICAL AND CHEMICAL PROPERTIES OF BITUMEN MODIFIED WITH WASTE ENGINE AND INDUSTRIAL OILS GÜLŞAH ÖZ KICI, MEHMET SALTAN	
10:45-11:00	INVESTIGATION OF MECHANICAL PROPERTIES OF BASALT AGGREGATES IN TERMS OF USE IN ROAD PAVEMENT ALTAN YILMAZ	
11:00-11:15	**COFFEE BREAK**	
11:15-13:00	**SESSION 6**	**SESSION CHAIR: PROF.DR.MUSTAFA KARAŞAHİN**
11:15-11:30	DEMİROKSIT PİGMENTİ KULLANILARAK ÜRETILEN RENKLI BITÜMLÜ KARIŞIMLARIN ÖZELLİKLERİNİN ARAŞTIRILMASI CAHİT GÜRER, AYFER ELMACI KORKMAZ, BURAK ENİS KORKMAZ	
11:30-11:45	IMPROVING INTERSECTION EFFICIENCY: THE ROLE OF RIGHT-TURN-ON-RED (RTOR) RULE IN ISPARTA, TURKIYE AYDIN KICI, MESUT TIĞDEMİR	
11:45-12:00	DEVELOPMENT OF A DISTRESS DETECTION INDEX FOR ALLIGATOR CRACKS ON HIGHWAY PAVEMENTS ŞULE YARCI, HÜSEYIN AKBULUT, GÜR EMRE GÜRAKSIN	
12:00-12:15	DEMİRYOLU GÜZERGAH PLANLANMASINDA AHP-TOPSIS-ARAS YÖNTEMİ; ERZURUM ÖRNEĞİ MUHAMMET AYDIN, HASAN BOZKURT	
12:15-12:30	THE IMPACT OF TECHNOLOGICAL ADVANCES IN THE TRANSPORTATION SECTOR ON SUSTAINABILITY WAHABOU ATCHADE, KEMAL ARMAĞAN	
12:30-12:45	GIS-BASED ANALYSIS FOR DETERMINING HOT SPOTS OF PEDESTRIAN-INVOLVED CRASHES ORUC ALTINTASI; AHMET HAKAN ÇAY	
12:45-13:00	ASFALT ÇATLAK ONARIMINDA 3 BOYUTLU BASKI TEKNOLOJİLERİNİN KULLANIMI LALE ATILGAN GEVREK	

09:30-11:00	SESSION 7 — SESSION CHAIR: PROF.DR.HASAN ÖZKAYNAK
09:30-09:45	AN IMPROVED RAPID SEISMIC RISK ASSESSMENT TOOL FOR EXISTING LOW TO MID-RISE REINFORCED CONCRETE BUILDINGS IN TÜRKIYE UTKU KARATAŞ, MERT CAN AYDEMIR, ZIYA MÜDERRISOĞLU, HASAN ÖZKAYNAK
09:45-10:00	FIRE RESISTANCE PROPERTIES OF GEOPOLYMER BINDERS INCORPORATING CONSTRUCTION AND DEMOLITION WASTE AND SLAG HÜSEYİN ULUGÖL, SELAHATTİN GÜZELKÜÇÜK, MEHMET KAAN ERDOĞAN, OĞUZHAN ŞAHİN
10:00-10:15	INVESTIGATION OF PROPERTIES OF BARITE-LAMINATED WOOD COMPOSITE MATERIAL ŞEMSETTİN KILINÇARSLAN, YASEMİN ŞİMŞEK TÜRKER
10:15-10:30	MUZ LİFİNİN ALÇI MALZEME ÖZELLIKLERINE ETKİSİ CENK KARAKURT, MEHMET UĞUR TOPRAK, MERDAN TÖREHAN TURAN
10:30-10:45	DESIGN OF STEEL AND COMPOSITE COLUMNS WITH LOADS AFFECTING COLUMNS OF REINFORCED CONCRETE BUİLDİNG MODELS WITH DIFFERENT HEIGHTS AND SOIL CLASSIFICATIONS KIVANÇ TAŞKIN, KORAY GÜLER
10:45-11:00	ANALYTICAL STUDY OF STRUCTURAL BEHAVIOUR OF RC COLUMNS STRENGTHENED WITH CFRP WRAPS UNDER AXIAL LOAD ALİ JUMA NOORZAD, HAKAN DİLMAÇ

11:00-11:15	COFFEE BREAK

11:15-13:00	SESSION 8 — SESSION CHAIR: DOÇ.DR.KIVANÇ TAŞKIN
11:15-11:30	EFFECT OF CONCRETE STRESS MODEL ON MOMENT BEARING CAPACITY OF STRENGTHENED REINFORCED CONCRETE ELEMENTS SILA YAMAN, HAMİDE TEKELİ KABAŞ
11:30-11:45	ÖNÜRETİMLİ BETONARME YAPILARIN KOLON KİRİŞ BİRLEŞİM BÖLGELERİ İÇİN LİTERATÜR ARAŞTIRMASI MELIH SÜRMELI, CIHAN SOYDAN, HASAN ÖZKAYNAK, ERCAN YÜKSEL
11:45-12:00	INVESTIGATION OF THE USE OF ORGANIC FIBER ADDITIVES IN FOAM CONCRETE PRODUCTION İSMAİL DEMİR, KADİR ASAL
12:00-12:15	STRUCTURAL ANALYSIS OF PLASTIC VOIDED SLABS KIVANÇ TAŞKIN, İBRAHİM MÜLAZİMOĞLU
12:15-12:30	CREATING A MODEL HOUSE USING THE DESING BUILDER APPLICATION AND DETERMINING THE ENERGY PARAMETERS M. TÖREHAN TURAN, SÜLEYMAN GÜCEK
12:30-12:45	POLİPROPİLEN LİF TAKVİYELİ GEÇİRİMLİ BETONUN MEKANİK ÖZELLİKLERİNİN İNCELENMESI AYŞE BÜYÜKÜNSAL, KURTULUŞ ARTIK
12:45-13:00	VOLKANİK TÜFÜN ÇİMENTO DAYANIMINA VE KARBON SALINIMINA ETKİSİNİN ARAŞTIRILMASI ALİ NADİ KAPLAN

09:30-11:15	SESSION 9 SESSION CHAIR: PROF. DR. MEHMET AVCAR
09:30-09:45	FREE VIBRATION ANALYSIS OF SHEAR DEFORMABLE FUNCTIONALLY GRADED POROUS BEAMS BURAK İKINCI, PHAM VAN VINH, MEHMET AVCAR
09:45-10:00	FINITE ELEMENT MODELLING OF HAIL IMPACT ON STEEL SHEETS MERYEM DILARA KOP, MEHMET EREN UZ, YUZE NIAN, MEHMET AVCAR
10:00-10:15	SOLUTION OF ELASTICITY-BASED MODELING TO DETECT THE ACCURATE DESIGN OF NANO-COMPOSITE WITH CONTROL SENSING OF DENSITY MUZAMAL HUSSAIN
10:15-10:30	BENDING ANALYSIS OF FUNCTIONALLY GRADED PLATES RESTING ON ELASTIC FOUNDATIONS KHAYRA DRAOUCHE, MOHAMED AIT AMAR MEZIANE, LAZREG HADJI
10:30-10:45	OPTIMIZATION OF POLYMER CONCRETE REINFORCEMENT WITH PALM FIBERS AND WHITE MARBLE ADEL LAKEL, ZINE EL ABIDINE RAHMOUNI, LAZREG HADJI
10:45-11:00	BENDING ANALYSIS OF FUNCTIONALLY GRADED POLYMER COMPOSITE PLATES REINFORCED WITH GRAPHENE NANOPLATELETS LAZREG HADJI, MEHMET AVCAR, NAFISSA ZOUATNIA
11:00-11:15	STATIC BENDING AND BUCKLING ANALYSIS OF FG BEAMS USING A NEW FIFTH-ORDER SHEAR AND NORMAL DEFORMATION THEORY (FOSNDT). MOHAMED NASSAH, HADJ HENNI ABDELAZIZ, LAZREG HADJI
11:15-11:30	STABILITY ANALYSIS OF CNT REINFORCED VARYING CROSS-SECTION BARS PARTIALLY IN CONTACT WITH FOUNDATION SEDAT KÖMÜRCÜ
11:30-12:45	SESSION 10 SESSION CHAIR:
11:30-11:45	KİL ZEMİNLERDE KONSOLİDASYON SÜRESİNİN ZEMİNİN KAYMA MUKAVEMETİ PARAMETRELERİNE ETKİSİ MUSTAFA YILDIZ, TUBA ÖZGE NAKIPOĞLU, İREM ERKAN İYIGÖNÜL
11:45-12:00	USABILITY OF MAGNESIUM SLAG IN IMPROVING GRANULAR SOILS İSMAIL ZORLUER, SÜLEYMAN GÜCEK
12:00-12:15	RELIABILITY-BASED DESIGN OPTIMIZATION OF AN EMBEDDED RETAINING WALL ROK VARGA, BOJAN ŽLENDER, BORUT MACUH, TAMARA BRAČKO, PRIMOŽ JELUŠIČ
12:15-12:30	EFFECTIVE OF MAGNESIUM SLAG TO SOIL STABILIZATION IN CLAY SOILS SÜLEYMAN GÜCEK, İSMAİL ZORLUER
12:30-12:45	EFFECT OF CLIMATE CHANGE ON SLOPE STABILITY ANALYZES SÜLEYMAN GÜCEK, ELİF ÇAKIR

15:45-17:05	ONLINE 1	SESSION CHAIR: CONSTRUCTION+GEOTECH
15:45-15:55	BEHAVIOUR OF DIFFERENT TUNNEL CROSS SECTIONS IN DRAINED CLAY-SILTSTONE SOILS İBRAHİM UMUT YALÇINKAYA, BERRAK TEYMÜR	
15:55-16:05	ALTERNATİF MALZEMELERLE TASARLANMIŞ BACA SİSTEMİNİN BİNANIN ENERJİ VERİMLİLİĞİNE KATKISININ OPTİMİZASYONU AHMET KARAHAN, FIGEN BALO	
16:05-16:15	DEPREMİN GÖLGESİNDE BATMAN İLI: GEÇMIŞTEN DERSLER VE GELECEK İÇİN STRATEJİLER SERHAT DEMİRHAN	
16:15-16:25	INVESTIGATION OF THE EFFECT OF REPLACEABLE PLASTIC HINGE MEMBER ON DIFFERENT TYPES OF FRAMES IN PRECAST REINFORCED CONCRETE STRUCTURES USING ABAQUS SOFTWARE ALI BERK BOZAN, REŞAT ATALAY OYGUÇ	
16:25-16:35	BİNALARDA FARKLI YALITIM MALZEMESİ KALINLIKLARIYLA TASARLANMIŞ BACALARIN ÇEVRESEL ETKİLERİNİN SİMÜLASYONLA ANALİZİ AHMET KARAHAN, FIGEN BALO	
16:35-16:45	CHANGING OF REINFORCEMENT PRESTRESS IN THE FRAME-LINK SYSTEM UNDER THE INFLUENCE OF CONCRETE CREEP DEFORMATIONS NINO NAKVETAURI, MARINA KURDADZE , FATIMA VERULASHVILI , AMIRAN BUKSIANIDZE	
16:45-16:55	COMPARISON OF MECHANICAL PERFORMANCES OF MOLD-CAST GEOPOLYMER MORTARS AND 3D-PRINTED GEOPOLYMER MORTARS UNDER DIFFERENT CURING CIRCUMSTANCES MAKSUT SELOĞLU	
16:55-17:05	INTEGRATION OF ADDITIONAL INNOVATIVE METHODS WITH SMART MATERIALS TO CREATE GREEN BUILDING TECHNOLOGIES FOR A MORE SUSTAINABLE AND CONNECTED FUTURE SANJIDA SHIRIN URMI, ARNOB SARKER, NUSRAT JAHAN ROJI MOJUMDER	

QR CODE FOR ONLINE SEMINAR

CLICK THIS LINK FOR ONLINE SEMINAR

1 NOV 2024 I FRIDAY

DAY3 - ONLINE SEMINAR

09:30-10:50	**ONLINE 2**	**SESSION CHAIR: TRANSPORTATION+HYDRO**
09:30-09:40	RHEOLOGICAL BEHAVIOUR OF BITUMEN MODIFIED WITH SUSTAINABLE ADDITIVES: SBS, ANIMAL BONES, AND WASTE COOKING OIL ALİ ALMUSAWI, SHVAN TAHIR NASRALDEEN, HUSSEIN H NORRI, SARMAD SHOMAN, MUSTAFA MOHAMMED JALEEL	
09:40-09:50	IMPROPER APPLICATIONS OF THE "PEDESTRIANS FIRST" PROJECT OF ANTALYA BANİHAN GUNAY, İSMAİL YOLCU, ERDEM EDİS	
09:50-10:00	USE AND ADVANTAGES OF CONSTRUCTION WASTE TIRES IN ROAD CONSTRUCTION HÜMEYRA BOLAKAR TOSUN	
10:00-10:10	GEOLOGICAL SPATIAL BASED MODELLING FOR ECONOMIC IMPERATIVES IN PRELIMINARY SITE INVESTIGATION BERNA ÇALIŞKAN	
10:10-10:20	IMPROVING TUNNEL SAFETY THROUGH LED LIGHTING FOR LONG TUNNELS: A DRIVING SIMULATOR STUDY OMER FARUK OZTURK, YUSUF MAZLUM, EMINE CORUH, METIN MUTLU AYDIN, HALIM FERIT BAYATA	
10:20-10:30	COMPARATIVE ANALYSIS OF SEISMIC DESIGN RESULTS FOR HIGH SPEED RAILWAY BRIDGES ACCORDING TO DIFFERENT STANDARDS ÜSAME EKİCİ	
10:30-10:40	WATER POLDERS: A TOOL TO MITIGATE CLIMATE CHANGE JAKUB KOSTECKI, MARTA GORTYCH	
10:40-10:50	İÇME SUYU DAĞITIM ŞEBEKESİNDE BASINÇ, HIZ VE YÜK KAYBI DEĞİŞKENLERININ FARKLI SAYISAL YÖNTEMLER İLE ADANA İLİ ÖRNEK UYGULAMALARI ÜZERINDEN MODELLENMESİ BUSE DUYAN ÇULHA, EVREN TURHAN	
11:00-12:10	**ONLINE 3**	**SESSION CHAIR: CONSTRUCTION+GEOTECH**
11:00-11:10	CEMENT BOUND BASE COURSE WITH WASTE RUBBER – EXPERIENCES FROM TRIAL SECTION/TEST FIELD CONSTRUCTION IVANA BARIŠIĆ, MARTINA ZAGVOZDA, IVANKA NETINGER GRUBEŠA	
11:10-11:20	DIGITAL TRANSFORMATION OF CONSTRUCTION MANAGEMENT WITH THE USE OF AUTOMATED TECHNOLOGY "BUILDING MANAGER" DMYTRO CHASHYN, KJARTAN GUDMUNDSSON, DMYTRO YAREMENKO , VIKTOR KLEPA	
11:20-11:30	COST-EFFECTIVENESS AND PERFORMANCE EVALUATION OF FOUR STRUCTURAL SYSTEMS: FRAMED, SHEAR WALL-FRAMED, TUBE-IN-TUBE, AND OUTRIGGER IN G+30 STORIED BUILDINGS USING ETABS MD FAYSHAL, SANJIDA SHIRIN URMI, ARNOB SARKER, ABDULLAH AL MAHIN	
11:30-11:40	SOIL-STRUCTURE INTERACTION EFFECTS ON RC BUILDING RETROFITTED BY SHOTCRETE PANELS PINAR TEYMÜR	
11:40-11:50	MULTI-CAMERA BASED MONITORING OF THE STRUCTURAL HEALTH OF HISTORICAL MASONRY MINARETS CEMILE DUMAN, TUNAHAN ASLAN, KEMAL HACIEFENDIOĞLU, TEKIN GÜLTOP	
11:50-12:00	THE ROLE OF BUILDING MATERIALS IN HOUSING PURCHASES: A MULTI-CRITERIA DECISION-MAKING APPROACH USING THE COCOSO METHOD UFUK AYDOĞMUŞ, MERDAN TÖREHAN TURAN, HACER YUMURTACI AYDOĞMUŞ	

International Keynote Lecture

Experiments Concerning the Use of Macroscopic Fundamental Diagram-Based Hierarchical Control of Urban Traffic

Assoc. Prof. Dr. Luigi Pariota

Transportation Engineering, University of Naples "Federico II" Italy

Abstract

Traffic congestion frequently occurs on urban networks and various control frameworks are employed to mitigate such congestion at the network level. Hierarchical traffic control frameworks have also gained great interest in the recent literature, having been shown to lead to increased mobility and efficient use of network capacity.

In this presentation, we will show the results of various experiments concerning the application of a hierarchical route guidance (RG) traffic control framework based on the Macroscopic Fundamental Diagram paradigm.

The evaluation is based on the modelling of some relevant urban scenarios in the simulation software Simulation of Urban MObility (SUMO).

It will be shown that overall the proposed network-level traffic control system could significantly enhance several characteristics of the urban traffic environment.

CivilTech
2nd International Symposium on Innovations in Civil Engineering and Technologies
October 30 – November 1, 2024, Isparta / TURKIYE

International Keynote Lecture

Bootstrap-Based Machine Learning Algorithm for Investigating Stochasticity in Compressive Strength of Concrete

Assoc. Prof. Dr. Aman Garg

State Key Laboratory of Intelligent Manufacturing Equipment and Technology, School of Mechanical Science and Engineering, Huazhong University of Science and Technology, Wuhan 430074, China
Department of Multidisciplinary Engineering, The NorthCap University, Gurugram, Haryana 122017, India

Abstract

Compressive strength is the most important property of the concrete mix. In the present work, the Gradient Boosting Machine (GBM) learning algorithm is applied in the framework of Bootstrap for predicting the influence of uncertainties in the quantities of cement, blast furnace slag, fly ash, water, superplasticizer, aggregate, and age on the compressive strength of concrete. At first, the correlation coefficients are obtained for all the variables using Pearson, Spearman Rank, Kendall Tau, and Point-Biserial Correlation coefficients are obtained. The efficiency of the present approach is demonstrated by comparing the present results with those obtained using Monte Carlo simulations. It can be seen that the present model predicts the stochasticity in compressive strength with good accuracy but requires lesser dataset and computational efforts compared to the MCS. During sensitivity analysis, age is the most important parameter affecting the stochastic compressive strength of concrete at noise levels, followed by cement content.

Keywords: Bootstrap; gradient boosting machine; uncertainty; stochastic compressive strength; sensitivity.

International Keynote Lecture

Feasibility of using Geosynthetics in Geotechnical Structures

Assoc. Prof. Dr. Borut Macuh

University of Maribor, Faculty of Civil Engineering, Transportation Engineering and Architecture, Slovenia

Abstract

A comprehensive analysis of geosynthetics' technical, economic, and sustainable benefits in geotechnical structures will be presented. Case studies include road pavements, bridge abutments, strip foundations, and piled embankments. Mathematical models are developed to compare reinforced and non-reinforced options, considering cost, technical feasibility, and sustainability. Results show that geosynthetics can significantly reduce costs, especially in challenging soil conditions. For example, reinforced road pavements can be more cost-effective than traditional methods at low CBR values, and reinforced bridge abutments can be up to five times cheaper than conventional concrete ones. Reinforced pads under strip foundations are justified for high vertical loads and low horizontal loads. In piled embankments, higher-strength geosynthetics can be more economical, though they increase costs.

Keywords: Geosynthetics, geotechnical structures, reinforced soil, cost optimization, sustainable construction, piled embankments.

International Keynote Lecture

AI in Transportation Geotechnics: Unlocking Complex Solutions for a New Era

Prof. Dr. Halil Ceylan, Dist.M.ASCE

Pitt-Des Moines, Inc. Endowed Professor in Department of Civil, Construction and Environmental Engineering (CCEE)
ISU Site Director for FAA PEGASAS Center of Excellence on General Aviation
Founding Director, Program for Sustainable Pavement Engineering and Research (PROSPER) Institute for Transportation (InTrans)
Iowa State University (ISU), United States

Abstract

Transportation geotechnics deals with the geotechnical challenges faced in the construction and maintenance of transportation infrastructure systems, encompassing roads, highways, railways, underground transit systems, airfields, and waterways. The inherent complexity of soil and rock behaviors in these contexts introduces significant uncertainties in material modeling. In the past few decades, researchers have increasingly turned to artificial intelligence (AI) methods to address these challenges in transportation geotechnics, effectively predicting complex, nonlinear relationships. This presentation provides a comprehensive overview of the effectiveness of AI methods in transportation geotechnics during the recent decade. It highlights key areas where AI methods have been extensively applied and explores case studies and success stories, demonstrating the application of AI in this field. Additionally, it emphasizes the proficiency of these methods in addressing complex challenges, especially in dealing with highly nonlinear data relationships and meeting demanding optimization requirements.

Local Keynote Lecture

The Effect of Wall Form and Raw Material Humidity and Dust Explosion on Silo Pressure in Grain Silos

Assist. Prof. Dr. Selçuk İZ

Yeditepe University, Depertmant of Civil Engineering, Istanbul, Turkiye

Abstract

In our country, steel silos, which are used for grain storage, have been damaged recently. In this study, the calculation criteria between international specifications and our country's specifications were compared, the effects of the roughness and form on the silo wall pressures and friction, and the effects of the moisture content of the raw material on the silo wall pressures were investigated. Silo walls are produced in sinusoidal form in steel prefabricated silos. Sinusoidal form should not be ignored in both friction and silo pressures. The humidity ratio must be taken into consideration in the silo wall pressures of the raw material, especially in grain silos, and these raw material effects have been summarized in studies conducted for damaged silos. In addition, an algorithm is given in this study regarding the maximum pressures that may occur on the silo walls in case of a dust explosion.

Keywords: Silos, dust explosion, wall form, material humidity, wall pressure, grain

TABLE OF CONTENTS

Construction Materials

CivilTech
2nd International Symposium on Innovations in Civil Engineering and Technologies
October 30 – November 1, 2024, Isparta / TURKIYE

Comparison of Mechanical Performances of Mold-Cast Geopolymer Mortars and 3D-Printed Geopolymer Mortars under Different Curing Circumstances

Maksut Seloğlu[1]

*mseloglu@firat.edu.tr

Abstract

In this study, the mechanical strength properties of three different produced fly ash-based geopolymer mortar (GM) mixtures were compared. For this purpose, conventionally mold-cast GM samples were cured for 3, 7, and 28 days under ambient cure (20±2 °C) conditions, and GM samples produced with a 3D printer were created. In addition, conventionally mold-cast GM samples cured for 3, 7, and 28 days under heat cure (60 °C) conditions were also created. These three GM mixtures were subjected to mechanical strength tests at the end of the curing periods. For this purpose, flexural and compressive strength tests were applied. At the end of all curing periods, conventionally mold-cast GM samples cured under ambient cure conditions exhibited the highest mechanical performance. The compressive strength test results of GM samples cured for 28 days and produced with a 3D printer were found to be 20% higher than the heat-cured conventionally mold-cast GM samples. The flexural strength test results of conventionally mold-cast GM samples cured under ambient curing conditions were found to be 13% higher than the GM samples produced with a 3D printer.

Keywords: 3D-printed geopolimer; ambient cure; geopolymer mortar; flexural strength; compressive strength; heat cure.

[1] *Firat University, Organized Industrial Zone Vocational School, Elazig, Turkiye.*

1. Introduction

Geopolymer is known as a binder building material containing high levels of alumina and silica, produced by using pozzolanic materials with alkali activators. Industrial waste materials are generally used in its production (Qaidi et al., 2022). Geopolymer binders were first described and used by Davidovits (Davidovits & France, 2018), (Davidovits & Cordi, 1979). He synthesized geopolymer without the presence of cement. Geopolymer mortar (GM) is defined as mortars produced by activating alumina and silica-containing materials without cement as binders, with fine sand and alkali activators. It is an alternative binder construction material to cement in many applications with its sustainability features like little energy use and CO_2 emissions (Peled & Bentur, 2003). It is known from the literature that GM is more resilient to chemical and physical effects, and has better greater mechanical efficiency compared to cement-based mortar (Lippiatt & Ahmad, 2004).

In the last decade, production with three-dimensional (3D) printers, also known as additive manufacturing technology (AMT), has been included in the construction sector. 3D printers stand out with their ability to prevent material waste, eliminate the use of molds, and faster manufacturing and construction features (Buswell et al., 2018). While the mortar used in AMT is built on top of each other, the lower layers carry the upper layers. In this way, the desired structure or building element is created. AMT, first invented by C. Hull (Khoshnevis, 2004), is robotic-based and allows layer-by-layer production without the need for molds. However, since production with 3D printers is still very new, experimental studies, different construction methods, and production techniques continue to be applied to discover all the potential it will bring to the construction sector (Geetha et al., 2021).

In this study, three types of fly ash (FA) based GM samples were produced. For this purpose, GMs were produced by 3D printing without using molds and cement as binders. Its were cured at ambient temperature (20±2 °C). Also, conventionally mold-cast GMs were cured at ambient temperature. The third type of conventionally mold-cast GM samples were produced and heat cured at 60 °C for 24 h. Then, these three types of samples were cured at ambient temperature for 3, 7, and 28 days. The mechanical strength parameters of GM samples were tested in terms of flexural strength (FS) and compressive strength (CS) after each curing stage.

2. Material and Method

2.1 Material

In this study, FA based GMs were produced. 55% FA and 45% metakaolin (MK) were used as binder materials. The physical properties and chemical components of the binder materials used are given in Table 1.

Table 1. Properties of binder materials

Binder	**LOI**	**MgO**	**Na_2O**	**K_2O**	**Fe_2O_3**	**CaO**	**Al_2O_3**	**SiO_2**	**Specific gravity**
FA	0.91	2.42	0.92	0.99	7.25	2.58	22.95	58.25	2.31 (g/cm^3)
MK	1.11	0.16	0.24	0.55	0.85	0. 91	40.25	56.10	2.52 (g/cm^3)

NaOH (SH) solution and Na_2SiO_3 (SM) were used as alkali activators. Solid SH was used to prepare the solution. SH was selected as 12 molar and the solution was kept in room temperature for 24 h. Then, SH solution and SM were added to the GM mixture. 0.6 mm Palu aggregate (fine river sand) was used in the GM mixture, and in the mixture calculations, the water absorption rate by weight was 2.1%, and the saturated surface specific gravity was calculated to be 2.72 g/cm^3. A viscosity-increasing additive (VIA) was used as an additive to balance the increased water requirement of the produced GM and to provide

the required workability value. VIA, with a specific gravity of 1.01 g/cm^3, was used in the mixture. GM samples produced with a 3D printer in ambient cure are expressed as 3DGM, conventionally mold casting GM samples in ambient cure are expressed as GM20, and GM samples heat cured at 60 °C are expressed as GM60, and the mixing ratios used for the GMs produced from these three different mixtures are given in Table 2.

Table 2. GM mixing ratios

Mixture	**Binder**	**FA**	**MK**	**SM**	**SH**	**SM/SH**	**Aggregate**	**AAS/B**	**VIA** (%)
3DGM	1	0.55	0.45	0.60	0.25	2.4	2.51	0.85	0.01
GM20	1	0.55	0.45	0.60	0.25	2.4	2.51	0.85	0.01
GM60	1	0.55	0.45	0.60	0.25	2.4	2.51	0.85	0.01

2.2 Preparation of GM Samples and Method

The mixing process of GM samples was first mixed for approximately one minute in the presence of FA and MK. Then, fine river sand was added to the FA-MK mixture and stirred for about one minute. After allowing the SH solution to stand at room temperature for one day, SM was added and stirred for about two minutes to obtain a uniform dispersion. Following a minute of mixing, VIA was added to this liquid combination that contained an alkali activator. Two-thirds of the liquid materials and the solid mixture consisting of binder material and fine river sand were mixed with the mixer for three minutes. The process was finished when the remaining one-third of the liquid mixture was added to the combination and stirred in the mixer for a total of four minutes. It took about twelve minutes in total to mix. These three distinct GM samples were tested for mechanical strength after curing for 3, 7, and 28 days at room temperature (20±2 °C). Figure 1. a shows the schematic visual of the 3D printer, Figure 1. b shows the 3DGM sample in the production phase on the 3D printer, and Figure 1. c shows the produced 3DGM sample.

a) **b)** **c)**

Figure 1. a) Schematic of the 3D printer (SELOĞLU, 2024) , **b)** 3DGM sample in production phase (SELOĞLU, 2024), **c)** 3DGM sample

2.3 Experimental Analyzes

To determine the mechanical properties of GM specimens, FS, and CS tests were performed. For this purpose, GM samples produced in ambient temperature curing 40x40x160 mm dimensions, GM samples produced with a 3D printer without using a mold, and GM samples heat cured at 60 °C were used. For mechanical tests, three GM samples were produced from each GM mixture type, and a total of 27 GM samples were produced separately for each curing period. The mechanical (FS and CS) testing device is given in Figure 2.

Figure 2. The mechanical testing device

At the end of the curing periods, the FS of these three different GM samples were determined by the three-point flexural method in an automatically controlled press by the ASTM C348 (ASTM, n.d.) standard. The FS value of the samples belonging to each series was obtained by taking the arithmetic average of 3 samples. These values are given in the study. CS tests were performed on the GM samples subjected to FS tests and divided into two in an automatically controlled press by the ASTM C349 (ASTM, 2008) standard. The CS value of the samples belonging to each series was obtained by taking the arithmetic average of 6 samples. Figure 3. a shows a GM sample produced with conventionally mold-cast, and Figure 3. b shows a 3DGM sample produced with a 3D printer.

a) **b)**

Figure 3. a) GM sample produced with conventionally mold-cast, **b)** 3DGM sample

3. Results and Discussion

3.1 FS Test Results

Figure 4 shows the 3, 7, and 28-day FS test results of GM specimens produced under three different types. When Figure 4 is examined, the 3, 7, and 28-day FS test results of the 3DGM series were found to be 1.86 MPa, 2.5 MPa, and 2.99 MPa, respectively. The 3, 7, and 28-day FS test results of the GM20 series were found to be 2.19 MPa, 2.74 MPa and 3.38 MPa, respectively. The 3, 7, and 28-day FS test results of the GM60 series were found to be 1.77 MPa, 1.99 MPa, and 2.49 MPa, respectively. The highest FS test results were obtained from GM20 samples at the end of 3, 7, and 28-day curing periods. The FS test results of the GM20 samples increased by approximately 18%, 10%, and 13% at the end of all of curing periods, respectively, compared to the 3DGM samples produced with the 3D printer exposed to ambient temperature curing. The FS test results of GM20 samples showed an increase of approximately 24%, 38%, and 36% at the end of all cure periods, respectively, compared to the GM60 samples produced by conventionally mold casting and subjected to heat cure at 60°C. The FS test results of 3DGM samples showed an increase of approximately 5%, 26%, and 20% at the end of all cure periods, respectively, compared to the GM60 samples produced by conventionally mold casting and subjected to heat cure at

60°C. Seloğlu et al. (SELOĞLU et al., 2023) reported the FS and CS results of conventionally mold-cast geopolymer mortar samples with UK-MK-based cured for 7 and 28 days. FS test results increased in parallel with the increase in curing times.

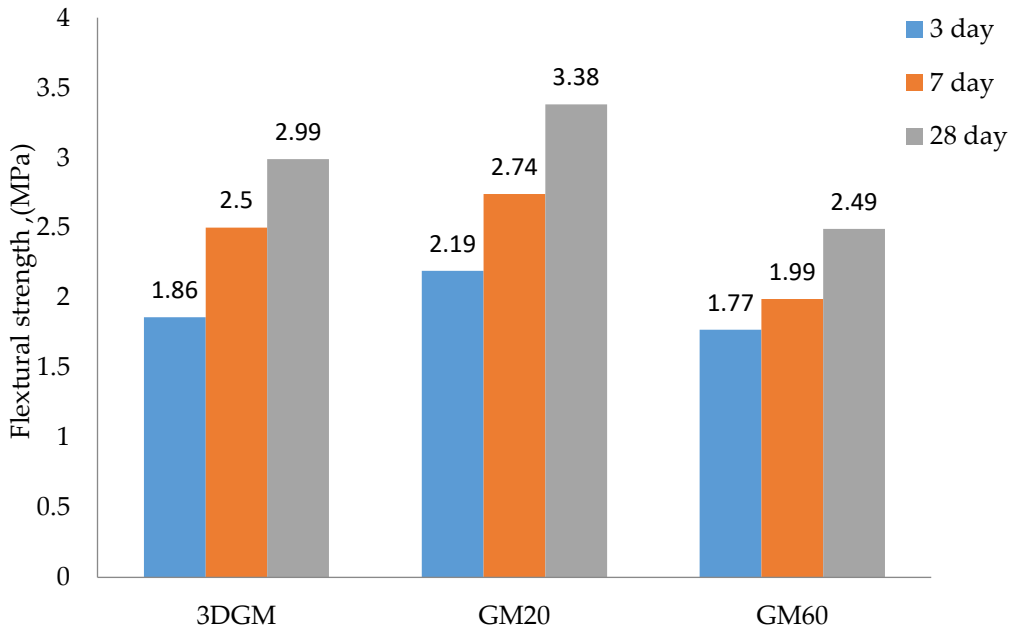

Figure 4. FS test results of GMs

3.2 CS Test Results

Figure 5 shows the 3, 7, and 28-day CS test results of GM specimens produced under three different types.

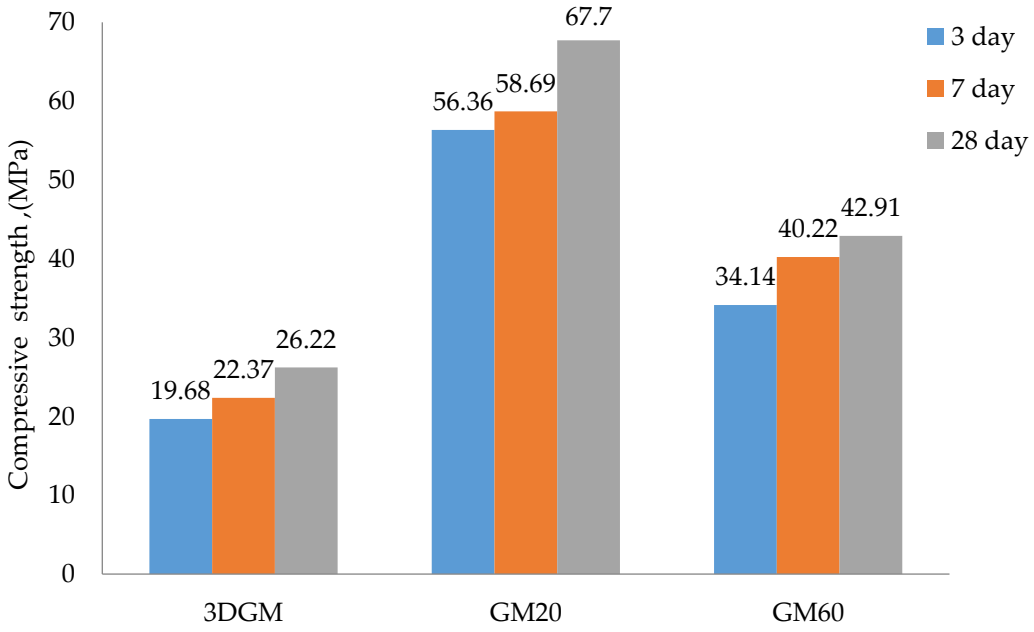

Figure 5. CS test results of GMs

When Figure 5 is examined, the 3, 7, and 28-day CS test results of GM20 samples were found to be 56.36 MPa, 58.69 MPa, and 67.70 MPa, respectively. The highest CS test results were obtained from GM20

samples at the end of all curing periods. The 3, 7, and 28-day CS test results of GM60 samples were found to be 34.14 MPa, 40.22 MPa, and 42.91 MPa, respectively. The 3, 7, and 28-day CS test results of 3DGM samples were found to be 19.68 MPa, 22.37 MPa, and 26.22 MPa, respectively. The CS test results of GM20 samples cured at ambient temperature were found to be 2.5 times higher than the CS test results of 3DGM samples at the end of all curing times and 1.5 times higher than the CS test results of GM60 samples heat cured at 60°C. It is known from the literature that curing at ambient temperature curing conditions has advantages such as easy handling and lower energy consumption in GM samples (Yunsheng et al., 2007). It is seen that the mechanical strength test results obtained in this study support this situation. In comparison to 3DGM samples cured at room temperature using a 3D printer, the CS test results of GM60 samples heat cured at 60°C were found to be, on average, approximately 1.7 times greater. This difference was observed across all curing durations. When Figure 5 is examined, it is not seen that the CS test results are parallel to the FS test results. This situation is thought to be due to the anisotropic material properties of 3DGM samples produced using layered manufacturing technology with a 3D printer. It can also be attributed to the possibility of gaps occurring in between since production is done layer by layer and the fact that the sample surface is not completely smooth like conventionally mold casting samples. Unlike conventionally mold-cast GM samples, GM samples produced with 3D printers were produced using the layer-by-layer accumulation method, resulting in defective lines, namely cold joints, between two adjacent layers. As a result, the CS of 3DGM samples produced with 3D printers were lower than conventionally mold-cast GM samples produced using the same material and mixing procedure.

4. Conclusion

In this study, the mechanical performances of three different types of GM mixtures were compared. From the findings of this mechanical experimental study, the following conclusions can be drawn:

The highest flexural strength test results were obtained from GM20 samples at 3, 7, and 28-day curing times. The highest FS was recorded as 3.38 MPa in the GM20 samples, which were cured for 28 days. The 28-day FS test results of GM20 samples increased by approximately 13% and 36%, respectively, compared to 3DGM samples produced by 3D printing and subjected to ambient temperature curing and GM60 samples produced by conventionally mold casting and subjected to heat curing at 60°C. The FS test results of 3DGM samples increased by approximately 20%, respectively, compared to GM60 samples produced by conventionally mold casting and subjected to heat curing at 60°C, at 28-day curing times.

CS test results, like FS test results, increased at the end of 3, 7, and 28-day curing periods. The highest CS test results were obtained from GM20 samples at 3, 7, and 28-day curing times. The highest CS was recorded as 67.70 MPa in GM20 samples, which were cured for 28 days. Unlike conventionally mold-cast GM samples, GM samples produced with 3D printers were produced using the layer-by-layer accumulation method, resulting in defective lines, namely cold joints, between two adjacent layers. As a result, the compressive strengths of 3DGM samples produced with 3D printers were lower than conventionally mold-cast GM samples produced using the same material and mixing procedure. Despite all these, the CS of 3DGM samples cured for 28 days was found to be 26.22 MPa. However, this CS TEST result is sufficient for many construction applications.

The feature of the production method with 3D printers, unlike the conventionally mold casting production method, is that it delivers benefits for quick manufacturing and fast skillfulness without requiring the use of molds during building, and its use is quickly increasing, especially in the building sector. However, it is recommended to use reinforcing materials, such as nano-materials and fibers, to increase their mechanical performance. Thus, it is thought that geopolymer composites will be

produced using 3D printers with faster and higher mechanical performance without the need for molds by further strengthening their flexural and compressive strength properties.

References

ASTM, A. (n.d.). C348-14 Standard Test Method for Flexural Strength of Hydraulic-Cement Mortars, ASTM Int. West Conshohocken.

ASTM, A. (2008). C349-08: Standard test method for compressive strength of hydraulic-cement mortars (using portions of prisms broken in flexure). ASTM International West Conshohocken, PA, USA.

Buswell, R. A., Leal de Silva, W. R., Jones, S. Z., & Dirrenberger, J. (2018). 3D printing using concrete extrusion: A roadmap for research. Cement and Concrete Research, 112(June), 37–49. https://doi.org/10.1016/j.cemconres.2018.05.006

Davidovits, J., & Cordi, S. A. (1979). Synthesis of new high temperature geo-polymers for reinforced plastics/composites. Spe Pactec, 79, 151–154.

Davidovits, J., & France, S. (2018). Synthesıs of New Hıgh-Temperature Geo-Polymers For Reınforced Plastıcs / Composıtes . November.

Geetha, S., Selvakumar, M., & Lakshmi, S. M. (2021). 3D concrete printing matrix reinforced with Geogrid. Materials Today: Proceedings, 49, 1443–1447. https://doi.org/10.1016/j.matpr.2021.07.212

Khoshnevis, B. (2004). Automated construction by contour crafting - Related robotics and information technologies. Automation in Construction, 13(1), 5–19. https://doi.org/10.1016/j.autcon.2003.08.012

Lippiatt, B. C., & Ahmad, S. (2004). Measuring the Life-Cycle Environmental and Economic Performance of Concrete: the Bees Approach. In International Workshop on Sustainable Development and Concrete Technology.

Peled, A., & Bentur, A. (2003). Fabric structure and its reinforcing efficiency in textile reinforced cement composites. Composites Part A: Applied Science and Manufacturing, 34(2), 107–118. https://doi.org/10.1016/S1359-835X(03)00003-4

Qaidi, S., Yahia, A., Tayeh, B. A., Unis, H., Faraj, R., & Mohammed, A. (2022). 3D printed geopolymer composites: A review. Materials Today Sustainability, 20, 100240. https://doi.org/10.1016/j.mtsust.2022.100240

SELOĞLU, M. (2024). Investıgatıon Of The Mechanıcal and Durabılıty Properties Of Geopolymer Mortars Produced Wıth A 3D Prınter Based On Metakaolın and Fly Ash Contaınıng Nanomaterıal. Dicle University.

SELOĞLU, M., TANYILDIZI, H., & ÖNCÜ, M. E. (2023). An Investigation of the Strength Properties of Fly Ash and Metakaolin-Based Geopolymer Mortars Containing Multi-Wall Carbon Nanotube, Nano Silica, and Nano Zinc. Bitlis Eren Üniversitesi Fen Bilimleri Dergisi, 12(3), 842–852. https://doi.org/10.17798/bitlisfen.1323858

Yunsheng, Z., Wei, S., Qianli, C., & Lin, C. (2007). Synthesis and heavy metal immobilization behaviors of slag based geopolymer. Journal of Hazardous Materials, 143(1–2), 206–213. https://doi.org/10.1016/j.jhazmat.2006.09.033

Structure

Güçlendirilen Betonarme Elemanların Moment Taşıma Kapasitesine Beton Gerilme Modelinin Etkisi

Sıla Yaman[1] , *Hamide Tekeli Kabaş*[1]

*silayaman@sdu.edu.tr

Abstract

Deprem performansı yetersiz olan yapıların, ekonomik ve güvenli olması koşuluyla, güçlendirilmesi meydana gelebilecek can ve mal kaybını azaltmak için önem taşımaktadır. Güçlendirme, elemanın mevcut taşıma kapasitesini, elemanın yetersiz olduğu özellikleri (kesme, eğilme vb.) doğrultusunda gidererek arttırma işlemidir. Bu kapsamda betonarme elemanın dıştan sargılama (EBR) ve/veya yüzeye yakın montaj (NSM) yöntemiyle güçlendirildikten sonraki moment taşıma kapasitesinin tasarım aşamasında hesaplanarak etkin güçlendirme detaylarının belirlenmesi gerekmektedir. Taşıma gücü hesabında yapılan kabullerden biri de kesitin taşıdığı beton basınç kuvveti hesabında betonun gerçek gerilme dağılımı yerine eşdeğer dikdörtgen basınç bloğunun kullanılmasıdır. Çalışma kapsamında literatürde bulunan deney numunelerinin moment kapasiteleri analitik olarak hesaplanmıştır. Kesitin taşıma gücü hesabında betonun gerilme-şekildeğiştirme eğrileri önce parabolik daha sonra eşdeğer dikdörtgen basınç bloğu olarak etkitilmiştir. Beton basınç bloğunun parabolik olduğu durumda beton basınç kuvveti, lifli yönteme göre belirlenmiştir. Hesaplamalarda TRM sargının beton basınç dayanımına etkisiyle birlikte CFRP levhaların kesitin moment kapasitesine etkileri dikkate alınarak numunelerin moment taşıma kapasiteleri elde edilmiş ve deney sonuçlarıyla kıyaslanmıştır. Çalışma sonucunda her iki yönteme göre hesaplanan moment taşıma kapasiteleri, deneysel sonuçlarla uyumlu elde edilmiştir. Eşdeğer dikdörtgen basınç bloğuna göre hesaplanan moment taşıma kapasiteleri, deneysel sonuçlarla daha az uyumlu ve parabolik basınç bloğuna göre belirlenen kapasitelerden %1.44 ile %3.48 oranlarında daha düşüktür. Herhangi bir güçlendirmenin uygulanmadığı, yalnızca NSM yöntemiyle ya da NSM ve EBR yöntemlerinin beraber uygulandığı yöntemle güçlendirilen betonarme elemanlarda beton gerilme dağılımı her iki şekilde kullanılarak lifli ya da eşdeğer dikdörtgen basınç bloğu yöntemlerine göre moment taşıma kapasiteleri belirlenebilmektedir.

Anahtar kelimeler: Güçlendirme, NSM, moment kapasitesi, beton gerilme dağılımı

[1] *Süleyman Demirel Üniversitesi, Mühendislik ve Doğa Bilimleri Fakültesi, İnşaat Mühendisliği Bölümü, Isparta, Türkiye*

1. Giriş

Ülkemiz aktif deprem kuşağında yer almaktadır. Son yıllarda meydana gelen büyük depremler, mevcut binaların büyük çoğunun büyük risk ve hasar potansiyeline sahip olduğunu göstermiştir. Deprem performansı yetersiz olan yapıların, ekonomik ve güvenli olması koşuluyla, güçlendirilmesi meydana gelebilecek can ve mal kaybını azaltmak için önem taşımaktadır. Betonarme yapıların güçlendirilmesinde son yıllarda fiber takviyeli polimer (Fiber Reinforced Polymer-FRP) kompozit malzemelerin kullanımı dikkat çekmektedir (Maraş, 2021). Bu malzemeler kullanılarak betonarme elemanlar dıştan sargılama (EBR) ve/veya yüzeye yakın montaj (NSM) yöntemleriyle güçlendirilmektedir. FRP kompozit malzeme, EBR yönteminde elemanın dışından yüzeyine yapıştırılırken NSM yönteminde elemanın paspayı seviyesinde açılan oluklara yerleştirilmektedir.

Güçlendirme, elemanın mevcut taşıma kapasitesini, elemanın yetersiz olduğu özellikleri (kesme, eğilme vb.) doğrultusunda gidererek arttırma işlemidir. Bu kapsamda betonarme elemanın EBR ve/veya NSM yöntemiyle güçlendirildikten sonraki moment taşıma kapasitesinin tasarım aşamasında hesaplanarak etkin güçlendirme detaylarının belirlenmesi gerekmektedir. Güçlendirilen betonarme elemanın moment taşıma kapasitesi; beton, donatı ve güçlendirme malzemelerinin taşıdığı momentlerin toplamıdır. Betonarme bir kesitin güç tükenmesi durumundaki basınç gerilme dağılımı, betonun gerilme-şekildeğiştirme eğrisine benzerdir (Celep, 2011). Taşıma gücü hesabında bazı kabuller yapılmaktadır (Celep, 2011; Doğangün, 2019). Kesitin taşıdığı beton basınç kuvveti hesabında betonun gerçek gerilme dağılımı yerine eşdeğer dikdörtgen basınç bloğunun kullanılmasıda bunlardan biridir. Beton gerilme-şekildeğiştirme eğrisinin (parabolik) doğrudan basınç bloğu olarak etkitildiği durumlarda betonun taşıdığı basınç kuvveti hesabında tabakalı (lifli/katmanlı) yöntem kullanılmaktadır (Parviz vd., 1991; Kaltakcı vd., 2001).

Ulutaş vd. (2016); beton gerilme dağılımının, betonarme kolon kesitinin karşılıklı etkileşim diyagramı, moment-eğrilik ve moment-dönme ilişkisine etkisini hazırlanan bir yazılım ile incelemişlerdir. Beton basınç bloğunun parabolik kabul edilmesi durumunda kolon kesitine ait kapasite değerleri, eşdeğer dikdörtgen basınç bloğu kabulüne göre artış göstermiştir. Köroğlu (2018) karbon fiber takviyeli (CFRP) kumaşla sargılanan betonarme kolonların moment-eğrilik ilişkisi için MATLAB tabanlı bilgisayar kodu geliştirmiştir. Bunu yaparken betonun gerilme dağılımını lifli yöntem ile belirlemiştir.

Çalışma kapsamında literatürde bulunan (Bournas ve Triantafillou, 2009) deney numunelerinin moment kapasiteleri analitik olarak hesaplanmıştır. Kesitin taşıma gücü hesabında beton gerilme dağılımı iki farklı şekilde kullanılmış ve deney sonuçlarıyla kıyaslanmıştır.

2. Materyal ve Yöntem

2.1. Materyal

Bournas ve Triantafillou (2009) yaptıkları çalışmada; 250×250 mm kare kesitli, 4Ø14 boyuna ve Ø8/200 enine donatılı 1600 mm yüksekliğinde on bir adet konsol kolon üretmişlerdir. Kolonların paspayı seviyesinde açılan oluklarına karbon fiber takviyeli polimer (CFRP) levhalar yerleştirerek NSM yöntemiyle numuneleri güçlendirmişlerdir. Bazı numuneleri ise NSM yöntemiyle güçlendirdikten sonra kolonun alt ucunu EBR yöntemiyle tekstil takviyeli polimer (TRM) kullanarak dört kat sargılamışlardır. Güçlendirilen deney numunelerine ait kesitler Şekil 1'de sunulmuştur. CFRP levhanın oluğa dik yerleştirildiği numunelerde oluklar 10×20 mm, paralel yerleştirildiği numunelerde ise 20×10 mm boyutlarında açılmıştır. Çalışma kapsamında seçilen numunelerin deney günü beton basınç dayanımı ve güçlendirme detayları Tablo 1'de verilmiştir. NSM yöntemiyle oluklara yerleştirilen CFRP levha, 2 mm kalınlığında ve 16 mm genişliğindedir. Sargılama için kullanılan TRM'nin kalınlığı ise 0.095 mm'dir. Boyuna ve enine donatı ile CFRP levha ve TRM'nin teknik özellikleri Tablo 2'de verilmiştir.

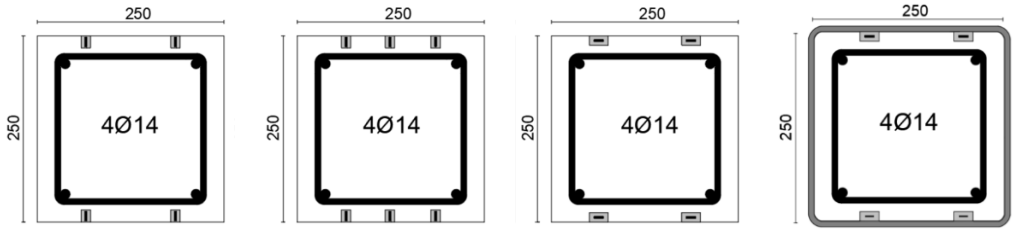

(a) C_per (b) C_per_pn2 (c) C_Par (d) C_par_J

Şekil 1. Deney numunelerine ait kesitler

Tablo 1. Deney numunelerinin detayları

Numune Adı	Beton Basınç Dayanımı	Güçlendirme Yöntemi	CFRP Levhanın Sayısı ve Oluktaki Yerleşimi
Control	25.6 MPa	-	-
C_per	27.2 MPa	NSM	4 / Dik
C_per_pn2	27.3 MPa	NSM	6 / Dik
C_Par	26.2 MPa	NSM	4 / Paralel
C_par_J	25 MPa	NSM+EBR	4 / Paralel

Tablo 2. Malzemelerin teknik özellikleri

Malzeme Türü	Akma Dayanımı	Çekme Dayanımı	Elastisite Modülü
Boyuna Donatı	372 MPa	433 MPa	200,000 MPa
Enine Donatı	351 MPa	444 MPa	200,000 MPa
CFRP Levha	-	2173 MPa	144,900 MPa
TRM	-	3800 MPa	225,000MPa

2.2. Yöntem

Betonarme kesitin moment taşıma kapasitesine betonun, donatının ve eğer mevcutsa güçlendirme malzemesinin etkisi vardır. Güçlendirme malzemelerinin etkisi, güçlendirme yöntemine göre değişiklik göstermektedir. NSM yönteminde oluklara eklenen FRP kompozit malzemeler, donatı gibi dikkate alınarak kesit merkezine olan mesafesine göre moment kapasitesine katkı sağlamaktadır. EBR yönteminde ise bu durum daha farklıdır. FRP kompozit malzemelerle sargılanan kesitin yanal sargı basıncından dolayı betonun dayanımı artmaktadır. Dolayısıyla EBR yöntemiyle güçlendirilen kesitlerde sargılı betonun davranışı dikkate alınmalıdır. C_par_J haricindeki numunelerde betonun gerilme-şekildeğişirme davranışı TBDY (2018)'de bulunan Mander yöntemine göre belirlenmiştir. Deney numunelerinde etriye sıklaştırılması bulunmadığından sargısız beton için gerilme-şekildeğiştirme eğrisi dikkate alınmıştır. C_par_J numunesinde ise ACI 549.4R-20'de verilen sargılı beton modeli kullanılmıştır. Betonun elde edilen gerilme-şekildeğiştirme eğrileri önce parabolik daha sonra eşdeğer dikdörtgen basınç bloğu olarak etkitilmiş ve hesaplamaları yapılmıştır.

TRM ile sargılanan betonun gerilme-şekildeğiştirme eğrisi aşağıdaki denklemlere göre belirlenmektedir. Yapılan hesaplamalar sonucunda C_par_J numunesinin maksimum beton basınç dayanımı 26.50 MPa olarak elde edilmiştir.

$$f_c=\begin{cases} E_c\varepsilon_c-\left[\dfrac{(E_c-E_2)^2}{4f_c^{'}}\times\varepsilon_c^2\right] & 0\le\varepsilon_c\le\varepsilon_t^{'} \\ f_c^{'}+E_2E_c & \varepsilon_t^{'}\le\varepsilon_c\le\varepsilon_{ccu} \end{cases} \quad (1)$$

$$E_c=4700\sqrt{f_c^{'}} \quad (2)$$

$$E_2=\frac{(f_{cc}^{'}-f_c^{'})}{\varepsilon_{ccu}} \quad (3)$$

$$\varepsilon_t^{'}=\frac{2f_c^{'}}{E_c-E_2} \quad (4)$$

$$f_{cc}^{'}=f_c^{'}+\psi_f\times 3.3\times\kappa_a\times f_l \quad (\psi_f=0.95) \quad (5)$$

$$f_l=\frac{2\times n\times A_f\times E_f\times\varepsilon_{fe}}{\sqrt{(b^2+h^2)}} \quad (6)$$

$$\varepsilon_{fe}=\kappa_\varepsilon\times\varepsilon_{fu}\leq 0.012 \quad (7)$$

$$D=\sqrt{b^2+h^2} \quad (8)$$

$$\varepsilon_{ccu}=\varepsilon_c^{'}\left(1.5+12\times\kappa_b\times\frac{f_l}{f_c^{'}}\times\left(\frac{\varepsilon_{fe}}{\varepsilon_c^{'}}\right)^{0.45}\right)\leq 0.01 \quad (9)$$

$$\kappa_a=\frac{A_e}{A_c}\times\left(\frac{b}{h}\right)^2 \quad (10)$$

$$\kappa_b=\frac{A_e}{A_c}\times\left(\frac{h}{b}\right)^{0.5} \quad (11)$$

$$\frac{A_e}{A_c}=\frac{1-\frac{\left[\left(\frac{b}{h}\right)\times(h-2r_c)^2+\left(\frac{h}{b}\right)\times(b-2r_c)^2\right]}{3\times A_g}-\varrho_g}{1-\varrho_g} \quad (12)$$

Burada; ε'_c, sargısız betonun maksimum basınç dayanımına (f_c') karşılık gelen şekildeğiştirme değerini; ε_{ccu}, sargılı betonun maksimum basınç dayanımına (f_{cc}') karşılık gelen şekildeğiştirme değerini; ε_c, sargılı betonun basınç dayanımına (f_c) karşılık gelen şekildeğiştirme değerini; ε_{fe}, TRM'nin koptuğu andaki etkin şekildeğiştirme değerini; ε_{fu}, TRM'nin tasarım kopma şekildeğiştirme değerini; ε'_t, parabolik kısımdan doğrusal kısıma geçiş noktasındaki şekildeğiştirme değerini; E_c, sargısız betonun elastisite modülünü; E_2, doğrusal ikinci kısmın eğimini; f_l, maksimum sargı basıncını; A_f, TRM'nin birim genişlik alanını; E_f, TRM'nin elastisite modülünü; n, TRM'nin sargı kat adedini; t_f, bir kat TRM sargının kalınlığını; κ_ε, TRM şekildeğiştirme etkinlik katsayısını; κ_a ve κ_b, kesit geometrisini dikkate alan etkinlik katsayısını; b ve h, sırayla kolonun kısa ve uzun kenar boyutunu; A_g, kesitin alanını; A_e/A_c oranı, etkili sargı alanı oranını; ϱ_g, kesitin boyuna donatı oranını; D, kolonun köşegen uzunluğunu; r_c, yuvarlatma yarıçapını; ψ_f, azaltma faktörünü belirtmektedir.

Donatının gerilme-şekildeğiştirme davranışında pekleşme dikkate alınmamıştır. Akma noktasına kadar donatıda oluşan şekildeğiştirme değerleri elasitiste modülü ile çarpılarak boyuna donatı gerilme değerleri elde edilmiştir. Akma dayanımına ulaştıktan sonra donatı gerilmeleri kopma dayanımına kadar sabit kabul edilmiştir. CFRP levhanın gerilme-şekildeğiştirme eğrisi doğrusal artarken kopma dayanımına ulaştığında güç tükenmesine ulaşmaktadır. Donatı ve CFRP levhanın gerilme-şekildeğiştirme eğrileri Şekil 2'de sunulmuştur.

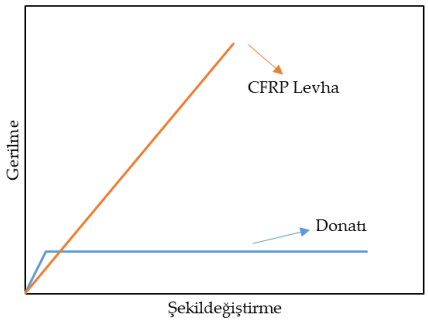

Şekil 2. Donatı ve CFRP levhanın davranışları

Deney numuneleri eksenel yük ve eğilme momenti etkisi altındadır. Dolayısıyla kesitin moment taşıma kapasitesini belirlerken betonun ezilme şekildeğiştirme değeri 0.003 kabul edilmiştir (TS 500, 2000). Betonarme kesitte betonun şekildeğiştirme değerleri tarafsız eksenden uzaklaştıkça artmaktadır. Güç tükenmesi durumundaki kesitin basınç gerilme bloğu ile betonun gerilme-şekildeğiştirme eğrisi tamamen benzerlik göstermektedir (Celep, 2011) (Şekil 3.a). Bu parabolik basınç bloğunun eşdeğer dikdörtgen basınç bloğuna çevrilmesinde önemli olan betonun taşıdığı bileşke kuvvetin değeri ve etkidiği noktadır (Ulutaş vd., 2016; Doğangün, 2019) (Şekil 3.b). Bu dönüşüm yapılırken bazı katsayılardan yararlanılmaktadır. Dikdörtgen bloğun genişliği $0.85f_{cd}$ olarak belirlenirken derinliği, beton sınıfına bağlı olan k_1 katsayısı ile tarafsız eksen derinliğinin çarpılması sonucu elde edilmektedir. TS 500 (2000)'de k_1 katsayısının, C30 beton sınıfına kadar olan dayanımlarda 0.85 alınması gerektiği belirtilmiştir. Deney numunelerinin beton basınç dayanımları 30 MPa'dan düşük olduğu için eşdeğer dikdörtgen basınç bloğuna göre yapılan hesaplamalarda betonun taşıdığı kuvvet Denklem (13)'e göre hesaplanmıştır.

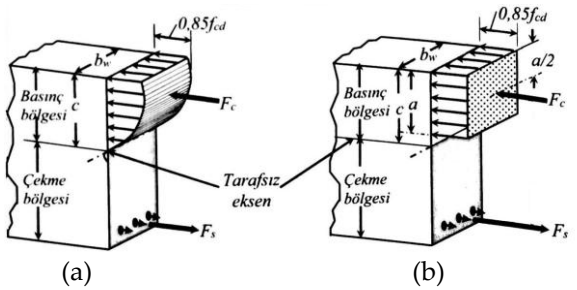

Şekil 3. Beton basınç gerilmelerinin dağılımı (Doğangün, 2019)

$$F_c=0.85\times f_c\times b\times(0.85\times c) \quad (13)$$

Burada; F_c, beton basınç kuvvetini; f_c, beton basınç dayanımını; b, kesit genişliğini; c ise tarafsız eksen derinliğini ifade etmektedir.

Beton basınç bloğunun parabolik olduğu durumda beton basınç kuvveti, lifli yönteme göre belirlenmiştir. Lifli yöntemde kesitler istenilen sayıda eşit tabakalara bölünerek o tabakaların ağırlık merkezindeki beton şekildeğiştirme değerleri, betonun ezilme şekildeğiştirme değerine bağlı olarak hesaplanmıştır. Betonun gerilme-şekildeğiştirme eğrilerinden her tabakanın şekildeğiştirme değerine karşılık gelen gerilme değerleri okunarak o tabakanın alanı çarpılmış ve tabakaların taşıdığı beton basınç kuvvetleri elde edilmiştir. Bu kuvvetlerin toplamı kesitin beton basınç kuvvetini vermektedir. Her tabakanın ağırlık merkezi için elde edilen basınç kuvvetleriyle kesit ağırlık merkezine uzaklığı çarpılarak tabakalarda betonun taşıdığı momentler elde edilmiştir. Bu momentlerin toplamı ise kesitteki betonun taşıdığı momenti vermektedir. Çekme bölgesindeki tabakalar kuvvet hesabına negatif olacak şekilde etkitilmiştir.

Deney numunelerinin moment taşıma kapasitesini belirlerken Şekil 4'te verilen kuvvet dağılımları kullanılmıştır. Burada eşdeğer dikdörtgen basınç bloğu temsilen gösterilmiştir. Eksenel yük (N) ve eğilme momenti (M) sırasıyla Denklem (14) ve Denklem (15)'e göre hesaplanmıştır.

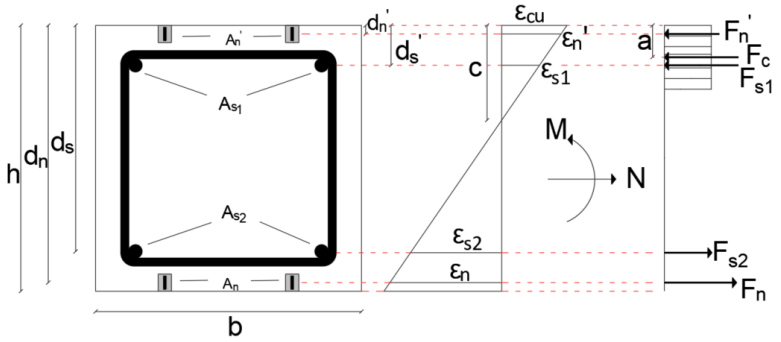

Şekil 4. Güçlendirilen kesitte kuvvet dağılımı

$$N=F_c+F_{s1}+F_n'-F_{s2}-F_n \quad (14)$$

$$M=F_c\left(\frac{h}{2}-\frac{a}{2}\right)+A_{s1}f_{s1}\left(\frac{h}{2}-d_s'\right)+A_n'f_n'\left(\frac{h}{2}-d_n'\right)+A_{s2}f_{s2}\left(d_s-\frac{h}{2}\right)+A_nf_n\left(d_n-\frac{h}{2}\right) \quad (15)$$

Burada; c, tarafsız eksen derinliğini; h kesit yüksekliğini; d_n ve d_s, CFRP levhanın ve boyuna donatının faydalı yüksekliğini; d_n' ve d_s', CFRP levhanın ve boyuna donatının paspayını; ε_{cu}, betonun ezilme şekildeğiştirme değerini; ε_{s1} ve ε_{s2}, boyuna donatıların şekildeğiştirme değerini; ε_n' ve ε_n, CFRP levhaların şekildeğiştirme değerini; F_c, beton basınç bloğunun taşıdığı kuvveti; F_{s1} ve F_{s2}, sırasıyla basınç ve çekme donatılarının taşıdığı kuvveti; F_n' ve F_n, basınç ve çekme bölgesindeki CFRP levhaların taşıdığı kuvveti; A_{s1} ve A_{s2}, sırasıyla boyuna donatıların alanını; A_n' ve A_n, CFRP levhaların toplam alanını; f_{s1} ve f_{s2}, boyuna donatıların gerilmesini; f_n' ve f_n, CFRP levhaların gerilmesini ifade etmektedir.

3. Bulgular ve Tartışma

Bournas ve Triantafillou (2009) tarafından yapılan çalışmada deney numunelerinin test edildikleri eksenel yük ile deneylerde itme ve çekme yüklemelerinde taşıdıkları yatay kuvvetler yer almaktadır. Yatay yük taşıma kuvvetleri, yatay yükün etki ettiği 1600 mm yüksekliği ile çarpılarak deneysel moment kapasiteleri elde edilmiştir. Her iki basınç bloğu yöntemine göre yapılan teorik hesaplamalarda eksenel yüke karşılık gelen moment değeri hesaplanmış ve deney sonuçları ile kıyaslanmıştır. Deney numunelerinin test edildikleri eksenel yük, deneylerde itme ve çekme yüklemeleri için taşıdıkları eğilme momentleri ile bunların aritmetik ortalamaları, teorik hesaplardan elde edilen moment taşıma kapasiteleri Tablo 3'te verilmiştir.

Tablo 3. Moment taşıma kapasitelerinin sonuçları

Numune Adı	Eksenel Yük (kN)	Deneysel Moment Kapasitesi (kNm)			Teorik Moment Kapasitesi (kNm)	
		İtme	Çekme	Ortalama	Eşdeğer Dikdörtgen Yöntemi	Lifli Yöntem
Control	320	52.93	53.90	53.42	50.77	51.50
C_per	340	66.40	68.35	67.38	64.23	66.17
C_per_pn2	341.25	74.02	70.11	72.07	69.48	71.90
C_Par	327.5	55.28	56.05	55.67	63.82	65.83
C_par_J	312.5	77.12	67.92	72.52	69.34	71.24

Teorik sonuçların ortalama deney kapasitelerine göre yüzdesel değişimleri ve eşdeğer dikdörtgen basınç bloğuna göre parabolik basınç bloğu yönteminin yüzdesel değişimleri Tablo 4'te verilmiştir. Burada DOK, ortalama deneysel moment taşıma kapasitesini; EDYK, eşdeğer dikdörtgen yöntemi için

moment taşıma kapasitesini; LYK ise lifli yöntem için moment taşıma kapasitesini temsil etmektedir. Tablodaki eksi değerler azalışı simgelerken artı değerler artışı tanımlamaktadır.

Tablo 4. Moment taşıma kapasitelerinin yüzdesel değişimleri

	Control	C_per	C_per_pn2	C_Par	C_par_J
DOK (%)	-	-	-	-	-
EDYK (%)	-5.22	-4.90	-3.73	12.77	-4.58
LYK (%)	-3.73	-1.82	-0.24	15.43	-1.79
LYK (%)	-	-	-	-	-
EDYK (%)	-1.44	-3.02	-3.48	-3.15	-2.74

Sonuçlar incelendiğinde hem eşdeğer dikdörtgen basınç bloğu hem de parabolik basınç bloğuna göre elde edilen moment taşıma kapasiteleri deneysel kapasitelerle uyumludur. Parabolik basınç bloğu için elde edilen moment taşıma kapasitelerinin deneysel sonuçlarıyla daha yakın olduğu görülebilir. Bournas ve Triantafillou (2009) tarafından yapılan çalışmada, C_Par numunesinin hasar durumu CFRP levhanın sıyrılması olarak belirtilmiştir. Teorik hesaplamalarda CFRP levhanın sıyrılması dikkate alınmadığı için hata oranları diğer numunelere göre daha yüksek (%12.77 ve %15.43) elde edilmiştir. C_Par numunesi dışındaki numunelerde hata oranları (%0.24 ile %5.22 arasında) oldukça düşüktür. Eşdeğer dikdörtgen basınç bloğuna göre elde edilen moment taşıma kapasiteleri, parabolik basınç bloğuna göre elde edilen kapasitelerden %1.44 ile %3.48 arasında daha düşük olup birbiriyle uyumludur.

4. Sonuçlar

Yapılan bu çalışmada literatürde bulunan ve NSM ya da NSM+EBR yöntemleriyle güçlendirilen betonarme konsol kolon numunelerinin deneysel moment kapasitelerini elde etmek için teorik hesaplamalar yapılmıştır. Bu hesaplamalarda TRM sargının beton basınç dayanımına etkisiyle birlikte CFRP levhaların kesitin moment kapasitesine etkileri dikkate alınmıştır. Ayrıca betonun gerilme-şekildeğiştirme davranışı önce parabolik daha sonra eşdeğer dikdörtgen basınç bloğu olarak etkitilmiş ve iki farklı yöntem için hesaplamaları yapılmıştır. Çalışma sonucunda her iki yönteme göre hesaplanan moment taşıma kapasiteleri, deneysel sonuçlarla (C_Par numunesi hariç) %0.24 - %5.22 oranında uyumlu elde edilmiştir. C_Par numunesi güç tükenme durumuna CFRP levhanın sıyrılmasıyla ulaştığı ve teorik hesaplamalarda bu durum dikkate alınmadığı için deney sonuçlarıyla %12.77 ile %15.43 oranlarında uyum elde edilmiştir. Eşdeğer dikdörtgen basınç bloğuna göre hesaplanan moment taşıma kapasiteleri, deneysel sonuçlarla daha az uyumlu olup parabolik basınç bloğuna göre belirlenen kapasitelerden %1.44 ile %3.48 oranlarında daha düşüktür. Herhangi bir güçlendirmenin uygulanmadığı, yalnızca NSM yöntemiyle ya da NSM ve EBR yöntemlerinin beraber uygulandığı yöntemle güçlendirilen betonarme elemanlarda beton gerilme dağılımı her iki şekilde kullanılarak lifli ya da eşdeğer dikdörtgen basınç bloğu yöntemlerine göre moment taşıma kapasiteleri belirlenebilmektedir.

Kaynaklar

American Concrete Institute Technical Committee 549. (2020). ACI 549.4R-20: Guide to Design and Construction of Externally Bonded Fabric-Reinforced Cementitious Matrix and Steel-Reinforced Grout Systems for Repair and Strengthening of Concrete Structures.

Ankara: Afet ve Acil Durum Yönetimi Başkanlığı. (2018). TBDY: Türkiye Bina Deprem Yönetmeliği.

Bournas, D.A., ve Triantafillou, T.C. (2009). Flexural strengthening of RC columns with NSM FRP or stainless steel. *ACI Structural Journal*, *106(4)*, 495-505. https://doi.org/10.14359/56615

Celep, Z. (2011). *Betonarme yapılar*. İhlas Matbaacılık Gazetecilik Yayıncılık Sanayi ve Ticaret A.Ş.

Doğangün, A. (2019). *Betonarme yapıların hesap ve tasarımı*. Birsen Yayınevi.

Kaltakcı, M.Y., Korkmaz, H.H., ve Korkmaz, S.Z. (2001). Basit eğilme etkisindeki betonarme elemanların moment-eğrilik ve tasarım değişkenleri üzerine analitik bir inceleme. *Pamukkale Üniversitesi Mühendislik Bilimleri Dergisi*, *7(1)*, 71-80. https://dergipark.org.tr/en/download/article-file/590955

Köroğlu, N.G. (2018). *CFRP ile güçlendirilmiş betonarme kolonların moment-eğrilik ilişkilerinin incelenmesi*. Yüksek Lisans Tezi. Sakarya Üniversitesi Fen Bilimleri Enstitüsü, Sakarya, Türkiye.

Maraş, M.M. (2021). Betonarme yapıların güçlendirilmesinde kullanılan FRP kompozitin yapısal performansa etkisi. *Avrupa Bilim ve Teknoloji Dergisi*, *23*, 108-119. https://doi.org/10.31590/ejosat.797437

Parviz, S., Jongsung, S., ve Jer-Wen, H. (1991). Axial/Flexural behaviour of reinforced concrete sections: effects of the design variable, *ACI*, *88(1)*, 17-21.

Sarafraz, M., ve Danesh, F. (2010). Experimental study on flexural strengthening of RC columns with near surface mounted FRP bars. *Journal of Seismology and Earthquake Engineering*, *12(1&2)*, 39-50. https://www.jsee.ir/article_240605.html

Türk Standartları Enstitüsü. (2000). TS 500: Betonarme Yapıların Tasarım ve Yapım Kuralları.

Ulutaş, H., Tekeli, H., Gençoğlu, M., ve Demir, F. (2016, 2-4, Mart). Beton gerilme dağılım modelinin kesit hasar sınırları üzerinde etkisi, *Uluslararası Doğal Afet ve Afet Yönetimi Sempozyumu (DAAYS'16)*, Karabük, Türkiye.

2nd International Symposium on Innovations in Civil Engineering and Technologies
October 30 – November 1, 2024, Isparta / TURKIYE

Soil-Structure Interaction Effects on RC Building Retrofitted by Shotcrete Panels

Pınar Teymür[1]

*teymurp@itu.edu.tr

Abstract

This study investigates the effects of soil-structure interaction (SSI) on the seismic retrofitting of buildings. Specifically, it evaluates the performance of a two-dimensional structure strengthened by the addition of shotcrete panels, while systematically accounting for various soil types. Utilizing a nonlinear macro-element model for shallow foundation SSI, the study uses modeling parameters that reflect the unique characteristics of each soil class. Performance assessments are conducted through static push-over analysis and nonlinear dynamic time history evaluations via the SeismoStruct software. The analysis is focused on the Tuzla region, where soil conditions vary across soil classes ZA to ZD. A specific coordinate within this area was selected to represent the building's location, and the parameters for the analysis were determined based on this coordinate. Findings from the modal analysis indicate that SSI significantly prolongs the vibration periods of reinforced concrete structures compared to fixed-base conditions, particularly when the structures are situated on softer soils. Code-based capacity assessments reveal that many columns and beams reached their bending moment capacities in fixed-base scenarios on softer soil types, like ZD and ZC. Additionally, a small number of columns and beams also reached their shear force capacities. In contrast, good performance of retrofitted structure on ZB soil suggests that the retrofitting technique is effective. This analysis highlights the importance of soil improvement measures in regions with soft soils.

Keywords: Strengthening; soil-structure interaction; pushover analysis; seismic safety, soil types

[1] *Istanbul Technical University, Civil Engineering Faculty, Department of Civil Engineering, Istanbul, Turkiye*

1. Introduction

In the design of any structural system, the civil engineer transfers all loads from the superstructure to the underlying ground. Concurrently, the design must account for and respond to the reactions from the ground. Consequently, the interaction between the superstructure and the ground must be comprehensively addressed. Therefore, the efficacy of the project depends on the accurate characterization of soil properties and the precise incorporation of soil-structure interaction into the design calculations.

In practice, seismic investigations often assume a fixed-base structure, which is only accurate if the ground is significantly more rigid than the superstructure. However, this is rarely the case, as both the superstructure and the underlying soil typically act together as a deformable system under static and dynamic loads. To more accurately estimate real behavior, it is essential to include the ground region as part of the structural system and analyze it in conjunction with the superstructure. Thus, the effects of soil on the superstructure and vice versa must be considered, acknowledging that soil-structure interaction reflects the mutual influence between the structure and the ground as a unified system.

Past earthquakes have shown how soil-structure interaction (SSI) can severely impact building safety during seismic events. For instance, in the 1970 Gediz earthquake in Turkey, a factory 135 km from the epicenter was destroyed while other nearby buildings remained intact. The destruction was due to a resonance effect, where the building's vibration period matched that of the underlying soil. Similarly, the 1999 Kocaeli earthquake in the Adapazari region demonstrated SSI's destructive potential by causing numerous foundation failures due to either uplift or soil bearing capacity issues.

Soil - structure is very important especially for tall buildings resting on soils with low bearing capacity. Therefore, this effect should be accurately reflected in the analysis. In order to accurately determine the behavior of the structure and the soil under earthquake loads, the structure and the soil should be modeled together.

Oz et al, 2020 investigated the seismic performance of 40 buildings constructed before and after the implementation of Turkey's modern seismic design code in 1998, focusing on soil-structure interaction. The researchers used non-linear time history analyses with 20 strong ground motions to assess seismic response, and they modeled soil-structure interaction using the substructure method. Four soil conditions, based on shear wave velocities, were considered: fixed-base, stiff, moderate, and soft soils. Seismic displacement demands were calculated for both roof and story levels under these soil conditions. In addition to time history analyses, static pushover analyses were performed to determine capacity curves for each building, yielding drift ratios at yield and ultimate levels. The study compared displacement demands and building capacities, evaluating the impact of soil-structure interaction on building performance across different soil types and summarized the findings.

Karaşin & Işık (2017) investigated how different soil conditions and building importance factors affect the seismic performance of reinforced concrete (RC) buildings. They analyzed the seismic responses of a 3-story school building in Çeltiksuyu, Turkey, which collapsed during the 2003 Bingöl earthquake. Their study involved eight numerical analyses, considering various soil types (Z1, Z2, Z3, and Z4) and building importance factors (R4 and R8) as specified by the Turkish Earthquake Code: Principles on buildings to be built in earthquake zones (TEC 2007). Using the SeismoStruct software for pushover analysis, they examined the seismic responses in terms of base shear force and roof displacement. The findings highlighted that soil conditions significantly impact seismic performance: as soil properties shift from hard to softer soil, seismic displacements increase while base shear force decreases due to reduced stiffness.

Shehata et al. (2015) analyzed the effects of soil-structure interaction (SSI) on typical multi-story buildings with raft foundations using three methods: equivalent static load, response spectrum methods, and nonlinear time history analysis with nine different time history records. They compared numerical results from SSI models under various soil conditions with those from fixed-base support models. Their findings suggest that conventional design procedures, which do not account for SSI, may be insufficient to ensure the structural safety of regular mid-rise moment-resisting frames on soft soil deposits.

This study aims to investigate the impact of changing local soil conditions on building performance. To achieve this, a case study is conducted on a six-story reinforced concrete (RC) building enhanced with shotcrete panels and RC jacketing. The analysis is focused on the Tuzla region, where soil conditions vary across soil classes ZA to ZD. A specific coordinate within this area was selected to represent the building's location, and the parameters for the analysis were determined based on this coordinate. The analysis employs both a single-mode pushover analysis method and a nonlinear time history analysis, in accordance with the latest version of the Turkish Earthquake Code: Building earthquake code of Turkey (TEC2018). The reference structure is evaluated under the design earthquake level (DD-2). Seismic performance assessments are conducted through parametric investigations considering variations in soil properties and base conditions. Two distinct support scenarios are examined: (1) fixed foundation and (2) flexible foundation conditions. The numerical results obtained are analyzed comparatively with respect to roof displacement-base shear force relationships, vibration periods, inter-story drifts, and damage levels in the ground story columns.

2. Analytical Model of Building Structure

The analytical study examines a two-dimensional (2D) frame of a six-story building, which represents typical reinforced concrete (RC) frame structures in Turkey, designed according to the Turkish Earthquake Code: Specifications for structures to be built in disaster areas (TEC1975). The building, depicted in Figure 1, has uniform story heights of 3.5 meters and span lengths of 5 meters, with 15 cm thick slabs. For retrofitting purposes, the two outer spans of the frame (AB and DE) are reinforced with 15 cm thick shotcrete panels, as illustrated in Figure 1b. The efficacy of this retrofitting method has been previously evaluated by Teymur (2009) and Teymur et al. (2017, 2012).

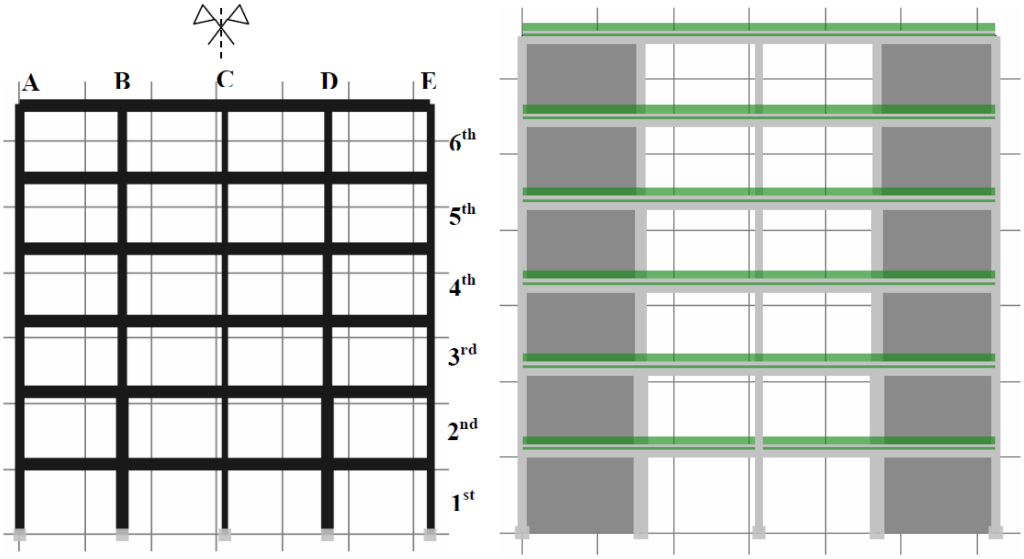

Figure 1 The representative frame for a) bare frame, b) retrofitted frame, Teymur (2009)

The steel used is of grade S420a, while the concrete quality for the frame and shotcrete panels is C16 and C20, respectively. Detailed dimensions and longitudinal reinforcement of the columns and beams

are provided by Teymur (2009) and Teymur et al. (2012). Specifically, all beams have a width of 300 mm and a depth of 600 mm, with a concrete cover of 40 mm for both beams and columns. The lateral reinforcement for the columns and beams comprises Φ10 bars spaced at 200 mm intervals.

The existing reinforced concrete (RC) bare building, designed according to outdated codes, exhibits insufficient stiffness and strength, rendering it particularly susceptible to seismic excitation. This vulnerability is evidenced by potential moment and shear failures occurring in the columns and beams as can be seen in Figure 2. To address these issues, Teymur (2009) conducted both experimental and analytical investigations into the feasibility of employing thin shotcrete panels to mitigate shear failure in the surrounding non-ductile RC columns. This approach aims to enhance the lateral structural performance by improving the lateral strength, stiffness, and ductility of the frames. The relationship between base shear and top displacement, as established through the analysis, is illustrated in Figure 3.

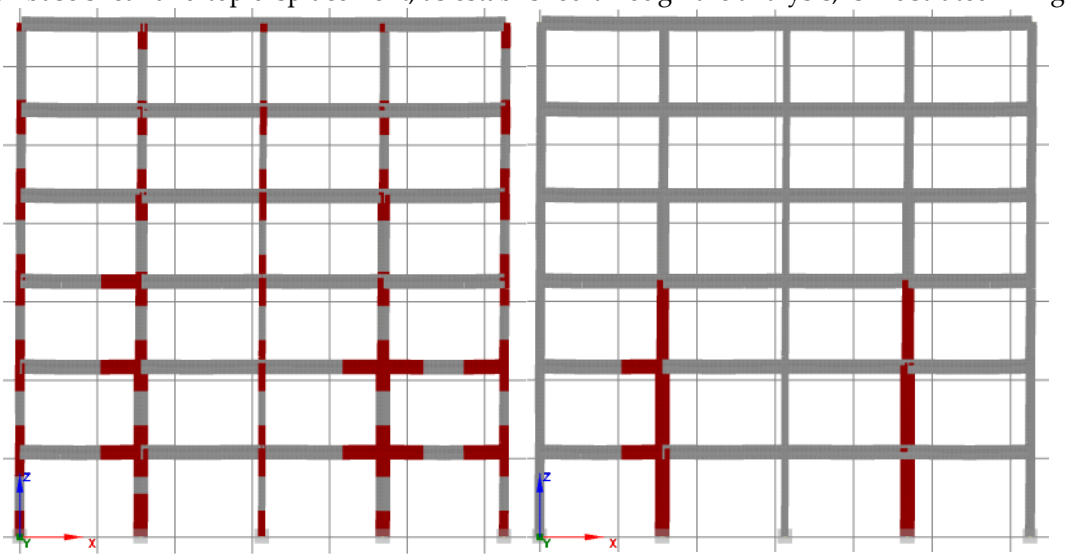

Figure 2. Damage mode of the bare frame

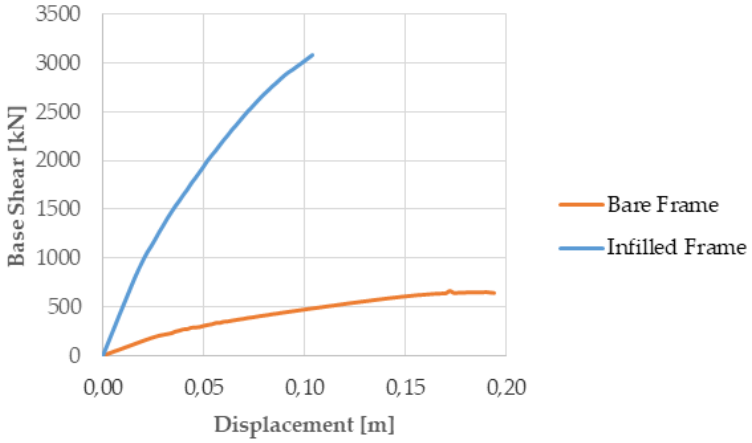

Figure 3. Base shear-top displacement diagram

SeismoStruct, a nonlinear finite element analysis software, was utilized to develop the theoretical models for the selected structure and to simulate the soil-structure interaction. A two-dimensional reinforced concrete moment-resisting frame is analyzed under two distinct support conditions. The first scenario assumes that the buildings are fixed at their bases, providing a rigid support condition. The second scenario incorporates soil-structure interaction by modeling the foundation stiffness and underlying soil stiffness as springs (i.e., foundation impedance) at each degree of freedom. The structural elements are represented as frame elements, with beams modeled using T-shaped cross-

sections and columns using rectangular cross-sections. To simplify the analytical model, slabs and infill walls are excluded; their effects are integrated into the system by translating their loads to the surrounding beams as uniform distributed loads.

Bilinear steel model is utilized to model the reinforcement and a uniaxial nonlinear constant confinement concrete model is used for concrete. Inelastic infill panel element is used to model the shotcrete panels. The details of these models can be found in SeismoStruct software manual.

Since Teymur (2009) analyzed the results using the previous version of the earthquake code (TEC2007), it has been determined that retrofitting the building in accordance with TEC 2018, as illustrated in Figure 4, has to involve the implementation of reinforced concrete (RC) jacketing on the columns surrounding the shotcrete panel. The thickness of the RC jacket is 15 cm.

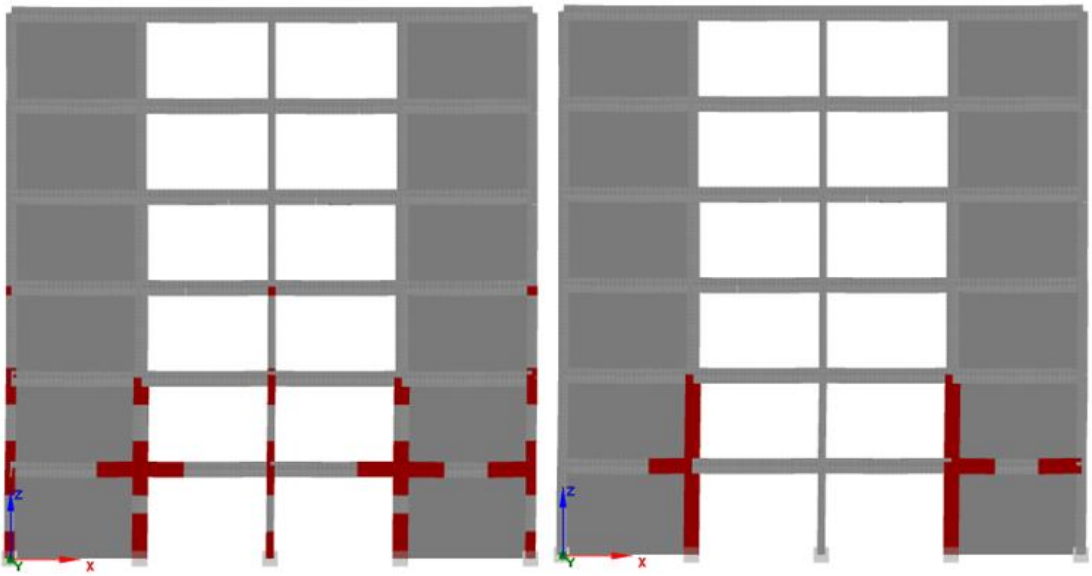

Moment Shear

Figure 4. Analysis results of the retrofitted frame according to TEC (2018)

2.3. Modeling of soil-structure interaction

The element described for modeling the soil-structure interaction is a nonlinear macro-element model used for analyzing soil-structure interactions in shallow foundations, based on Correia and Paolucci's 2019 research. This model simplifies the problem by treating both the footing and the soil as one macro-element with six degrees of freedom (DOFs) in a 3D scenario. The macro-element is defined as a zero-length link element, capturing the interaction through resultant forces and displacements. For ease of explanation, the model focuses on a rectangular rigid footing subjected to a rocking moment and vertical and horizontal forces (M_y, N, and H_x), as shown in figure 5.

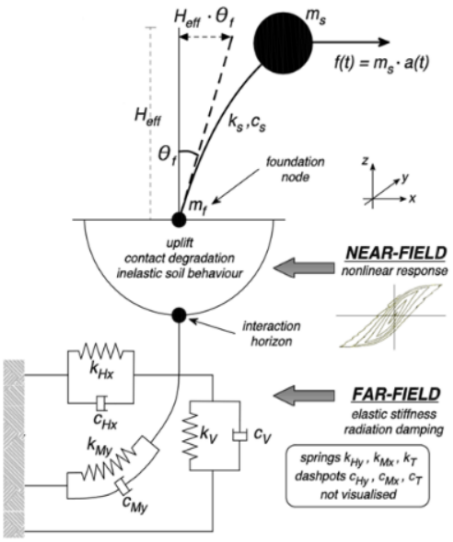

Figure 5. Hysteretic model of ssilink1 *curve*, SeismoStruct 2023

The uplift model described uses a nonlinear elastic-uplift approach that accounts for both elastic behavior and degradation at the soil/footing interface due to permanent geometric changes. Additionally, a bounding surface plasticity model is employed to accurately capture both the elastic-uplift and plastic nonlinear responses occurring simultaneously.

The bounding surface in this macro-element model varies based on soil type and drainage conditions during a seismic event. For undrained loading conditions, the ultimate bounding surface takes the shape of a "scallop," as illustrated in the figure 6, showing its intersection in the H-N and M-N loading planes.

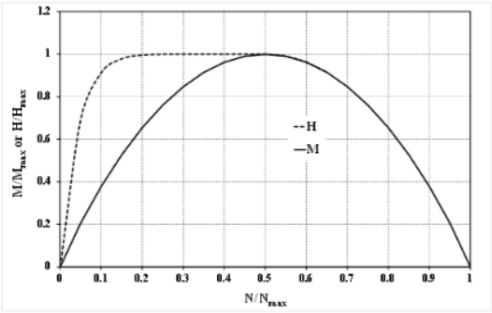

Figure 6. Ultimate surface: "scallop" shape, SeismoStruct 2023

In examining the geologic conditions of the site, this study evaluates three distinct ground conditions to assess their impact on the damage levels sustained by reinforced concrete (RC) buildings subjected to strong ground shaking. The soil profiles considered align with the ZB, ZC, and ZD classifications outlined in the TEC-2018 provisions. This approach allows for a comprehensive analysis of how varying site conditions influence the structural response and damage potential during seismic events. The dynamic interaction between the foundation and the underlying soils is typically modeled using three fundamental soil characteristics: soil shear velocity (V_S), Poisson's ratio (ν), soil shear modulus (G_0), and shear strength (c_u). The mechanical properties of the chosen local soil profiles are detailed in Table 1.

Table 1. The mechanical properties of the selected local soil profiles

Local soil types	$(V_S)_{30}$ [m/s]	G_0 [kN/m²]	ν	$(c_u)_{30}$ [kPa]
ZB	800	1280000	0,25	500
ZC	400	320000	0,35	255
ZD	200	68450	0,45	70

The design elastic response acceleration spectrum, representing the design earthquake ground motion level-2 (DD-2), is derived from the Turkish earthquake hazard map in a standardized format, assuming a 5% damping ratio.

The elastic response spectra for the design earthquake (DD-2), considering the soil properties for soil types ZD, ZC and ZB are illustrated in Figure 7.

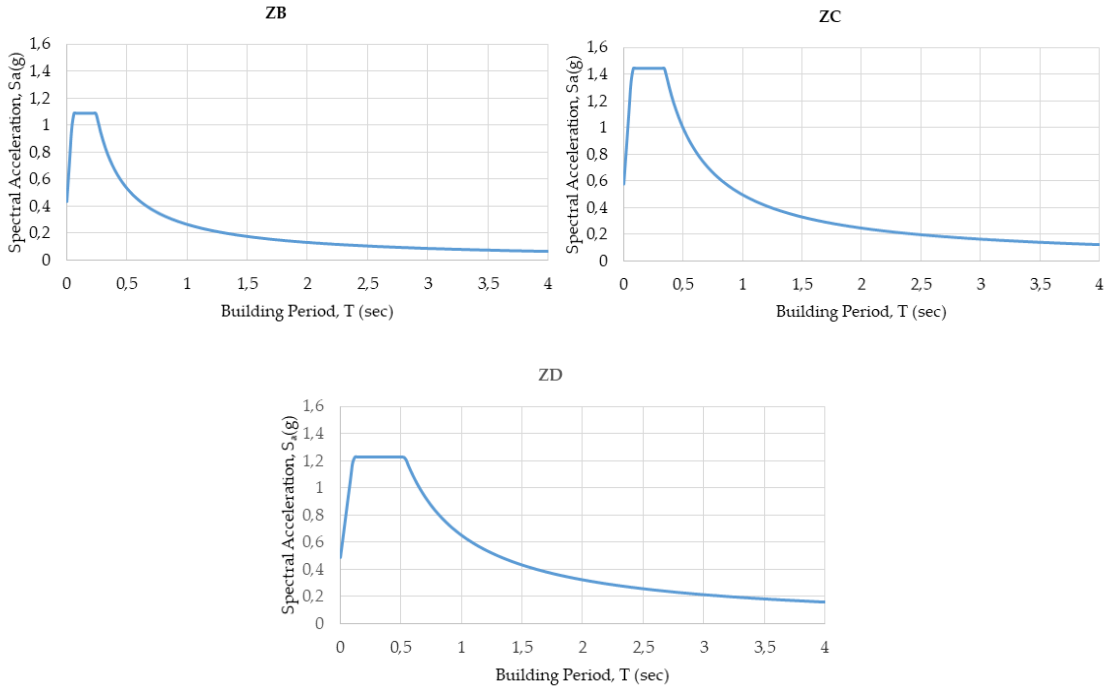

Figure 7. Elestic Response Spectrum for Soil Types a) ZB, b) ZC, c) ZD

Nonlinear dynamic time history analysis (NDTHA) is performed with Izmit Earthquake. Original and matched earthquake records according to soil types used in the analysis are given in Figure 8.

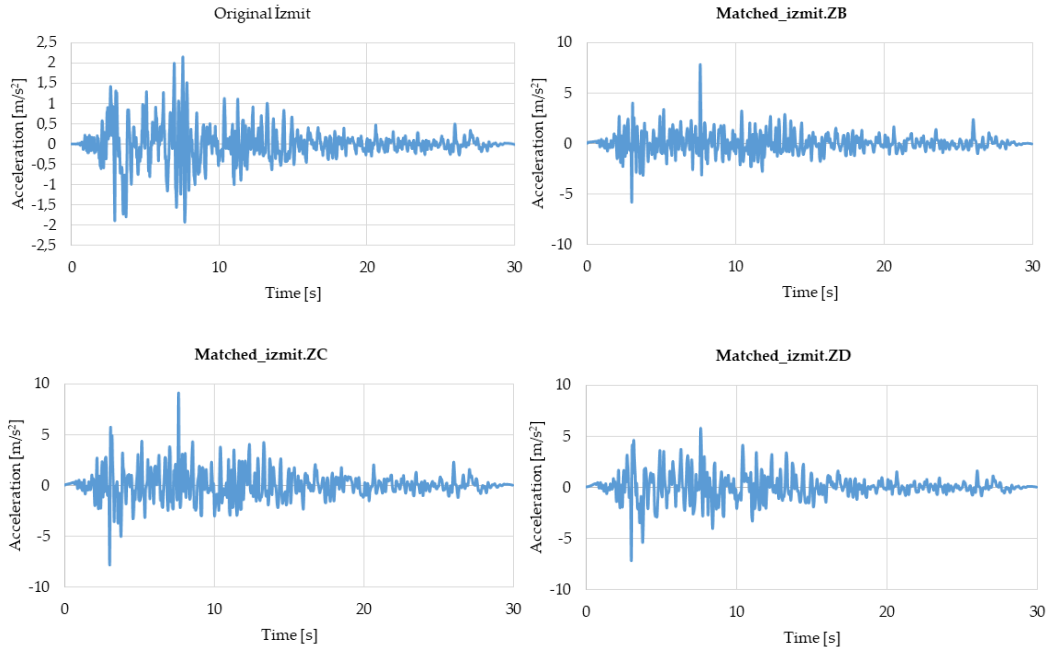

Figure 8. Earthquake records used in the analysis; a) Original, b) ZB, c) ZC, d) ZD

According to TSBC2018, DD-2 should meet the performance target of Controlled Damage (KH) under the influence of earthquake ground motion. KH defines the inelastic behavior in which the cross-sectional strength can be safely achieved. Target Displacement used for KH in the push over analysis for each soil types is given in Table 2.

Table 2. Target Displacements

Local soil types	Target Displacement [m]	
	Fixed Based	SSI
ZB	0,039	0,039
ZC	0,072	0,073
ZD	0,077	0,085

Target displacements for soil classes ZB and ZC are notably similar in both scenarios. Conversely, the target displacement for the ZD soil type, which is softer relative to the other classes, is higher in the SSI analysis. Softer soils possess lower stiffness, resulting in greater deformations under applied loads. This increased flexibility facilitates enhanced movement of the structure during its interaction with the soil.

3. Seismic response of the structures

In this section, the seismic performance of the building is evaluated for different soil conditions using single-mode pushover analysis and the nonlinear dynamic analysis. Both analyses employed a distributed plasticity model to accurately capture the structural response. The analysis results are interpreted comparatively, focusing on the relationships between base shear and roof displacement, building vibration periods, inter-story drifts, and the damage states of the ground floor columns. This comparative approach facilitates a comprehensive understanding of the structural performance under different geological ground conditions.
The values of vibration periods of the buildings, T_1 as well as the vibration due to SSI effects are presented in Table 3.

Table 3. Variation in vibration period due to the SSI effects

Foundation	T_1 (s)		
Type	ZB	ZC	ZD
Fixed Base	0.434	0.434	0.434
SSI	0.436	0.440	0.456
Variation (%)	0.46	1.38	5.07

The results obtained from the modal analysis of the studied buildings indicate that soil-structure interaction (SSI) increases the vibration periods of the reinforced concrete (RC) structures when compared to fixed-base conditions, particularly in scenarios where the structures are founded on soft soil classified as soil type ZD. This phenomenon occurs due to a reduction in the lateral stiffness of the buildings, which is attributable to the deformable behavior of the underlying soil.

3.1. The SSI effects on the structural capacity

A single-mode pushover analysis is employed to assess the influence of soil-structure interaction (SSI) on the overall behavior of the selected buildings under the design earthquake (DD-2). The buildings are subjected to incremental loading until a specified target displacement is reached. To facilitate a clearer comparison of the results, the capacity curves for both the compliant base (SSI) and fixed base (FB) conditions are plotted on the same graph.

Figure 9 illustrates the variations in pushover curves of buildings attributable to soil-structure interaction (SSI) effects under different ground conditions.

When a structure rests on a compliant base (soil), the added flexibility and energy dissipation from the soil result in larger displacements for the same applied force compared to a fixed base. This leads to a softer pushover curve and a shift toward lower stiffness. In all soil conditions, the distinction between fixed and flexible base scenarios is notably pronounced, demonstrating significant variations in the structural behavior observed in single-mode pushover analyses. It can be concluded that the use of single-mode pushover analysis has lead to an underestimation of the base shear response when soil-structure interaction (SSI) is considered.

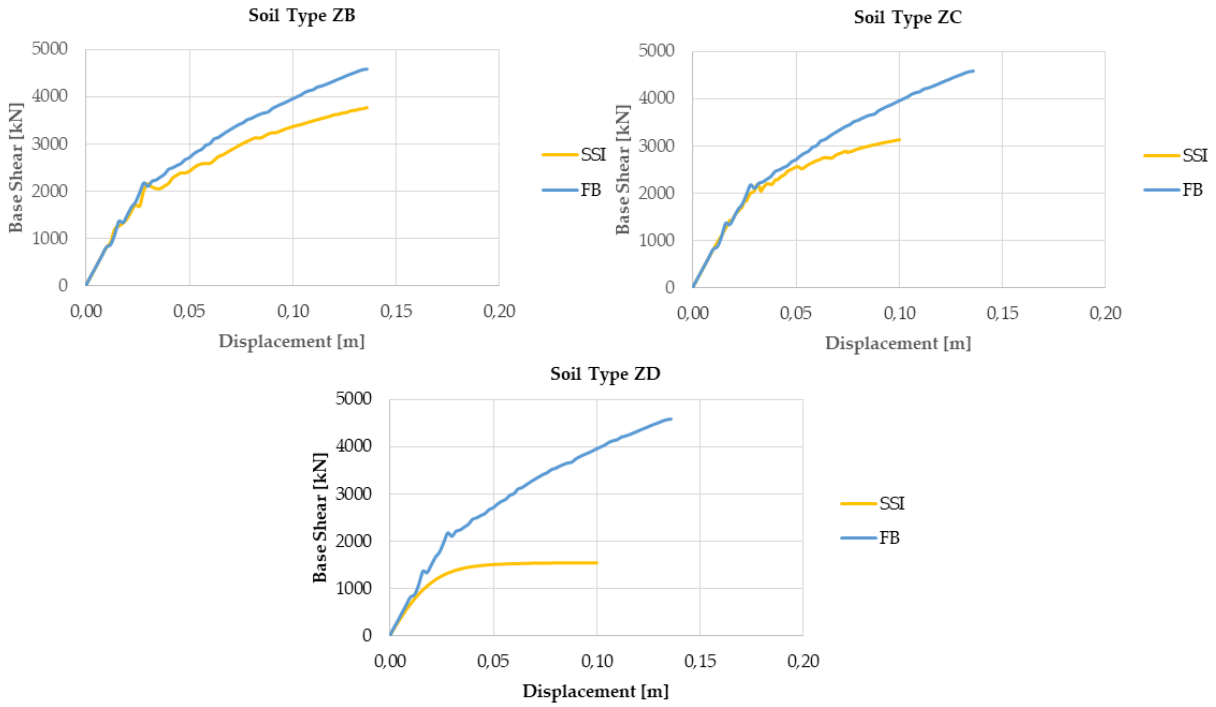

Figure 9. Pushover curves; comparison between FB and SSI conditions for a) ZB, b) ZC, c) ZD soil classes

3.2. The SSI effects on the inter-story drift ratios (IDR)

Figure 10 illustrates the variation in the inter-story drift ratio (IDR) due to soil-structure interaction (SSI) effects produced by NDTHA. The figures clearly show that the impact of SSI becomes more pronounced as soil properties transition from type ZB to type ZD. For soil type ZB, the analysis indicates no significant difference between the fixed-base assumption and the inclusion of SSI effects.

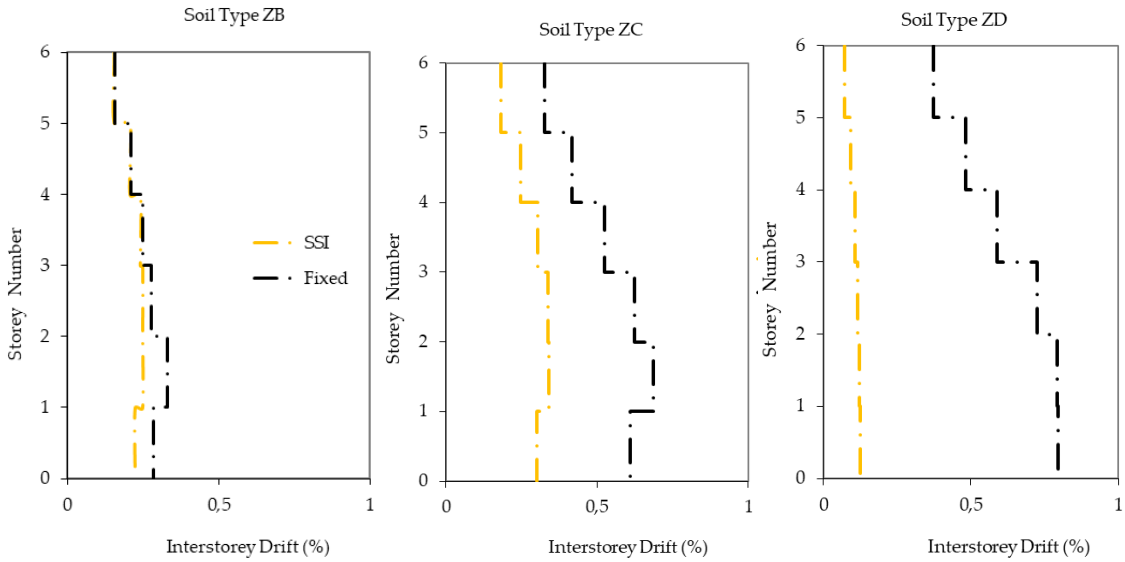

Figure 10. Inter-story drift ratios; comparison between FB and SSI conditions for a) ZB, b) ZC, c) ZD soil classes

The inter-story drifts of the buildings decrease when soil-structure interaction (SSI) is considered in the analyses, compared to their fixed base conditions. However, the observed effects are minimal and nearly negligible for stiffer soil profiles (with shear wave velocities greater than 400 m/s). In contrast, as the geotechnical conditions beneath the foundation transition to softer soil types (ZD), the effects of SSI become significantly more pronounced.

3.3. The SSI effects on the top displacement

The top displacement versus time graphs for both the fixed base and soil-structure interaction (SSI) scenarios subjected to the İzmit earthquake are presented in Figure 11. The displacement demands for the infilled frame situated on ZD, ZC, and ZB soil conditions are 0.123m, 0.107m, and 0.046m, respectively. However, when SSI is accounted for, the displacement demands decrease to 0.108m and 0.069m for the ZD and ZC conditions, respectively. Notably, the displacement demand remains unchanged for the stiff soil condition, ZB.

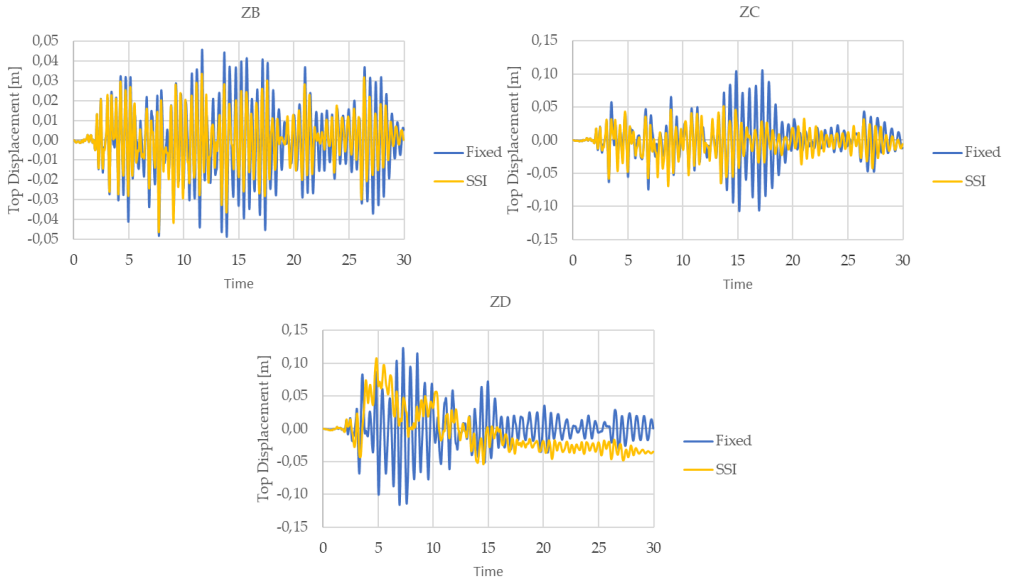

Figure 11. Time history of the top-story displacement comparison between FB and SSI conditions for a) ZB, b) ZC, d) ZD soil classes

In fixed foundation scenarios, the structure is treated as a rigid unit, directly transmitting seismic forces, which typically results in elevated displacements. In contrast, soil-structure interaction (SSI) facilitates foundation movement, allowing the surrounding soil to absorb a portion of the seismic energy, thereby reducing displacements. This reduction is particularly pronounced in stiffer soil conditions. However, in the context of this study, the interaction between the foundation and the stiff soil (ZB) appears minimal due to the soil's inherent resistance to deformation. Consequently, the structural response resembles that of a fixed base condition, leading to comparable displacement demands.

3.4. The SSI effects on the base shear forces

The base shear versus time graphs for the frame subjected to the Izmit earthquakes are presented in Figure 12. The shear force demands for the frame with a fixed foundation are recorded as 4569kN, 4072kN, and 2922kN for the ZD, ZC, and ZB seismic zones, respectively. In contrast, when soil-structure interaction (SSI) is taken into account, the base shear demands decrease to 1718kN, 3133kN, and 2640kN for ZD, ZC, and ZB, respectively.

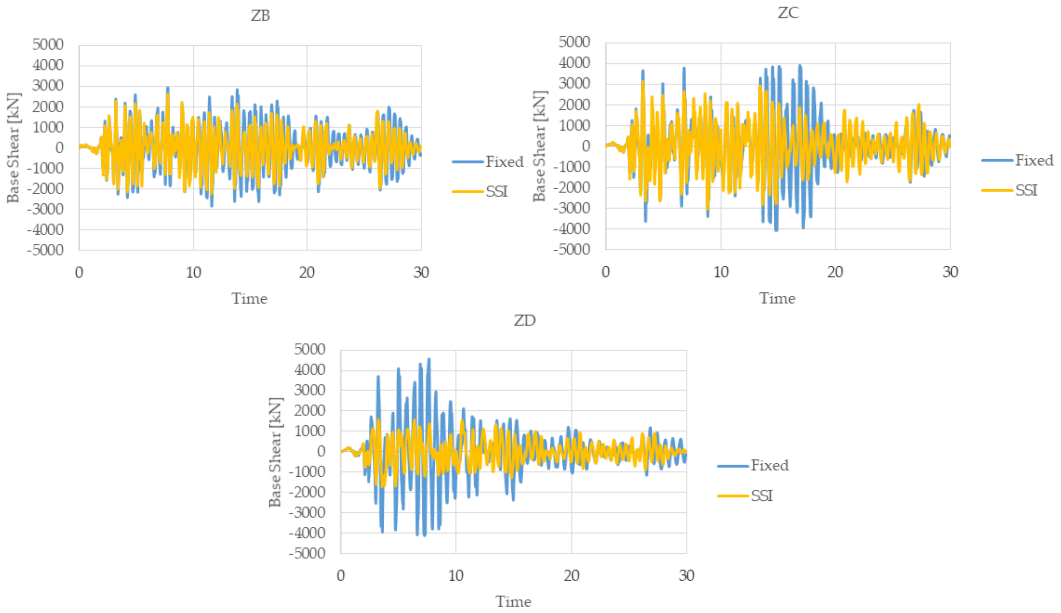

Figure 12. Base shear-time; comparison between FB and SSI conditions for a) ZB, b) ZC, c) ZD soil classes

In a fixed foundation scenario, higher shear forces occur due to direct seismic load transmission. With soil-structure interaction (SSI), the foundation absorbs and redistributes forces through the soil, leading to energy dissipation and a more distributed force pattern. This dynamic interaction reduces peak forces, resulting in a lower base shear compared to the fixed base case.

3.5. Effects of SSI on the damage mode of the system

The damage modes resulting from nonlinear time history analysis (NTHA) are illustrated in Figures 13 and 14, in accordance with code-based capacity assessments.

Code-based capacity assessments indicate that several columns and numerous beams reached their bending moment capacities in fixed-base scenarios when situated on soft soil types such as ZD and ZC. Furthermore, a limited number of columns and beams were observed to have attained their shear force capacities. In contrast, the performance under ZB soil type suggests that the retrofitting technique is effective. This analysis emphasizes the necessity for soil improvement measures in areas with soft soil.

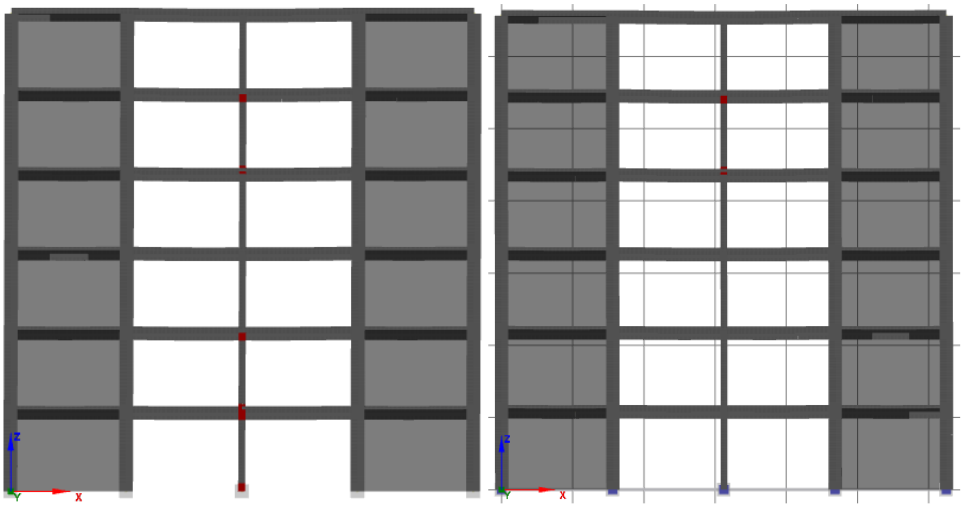

Fixed SSI

a) ZB

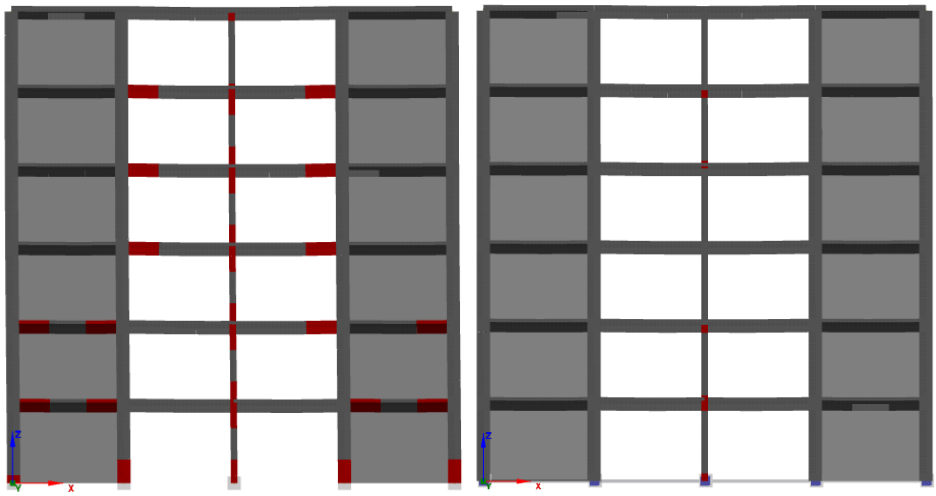

Fixed SSI

b) ZC

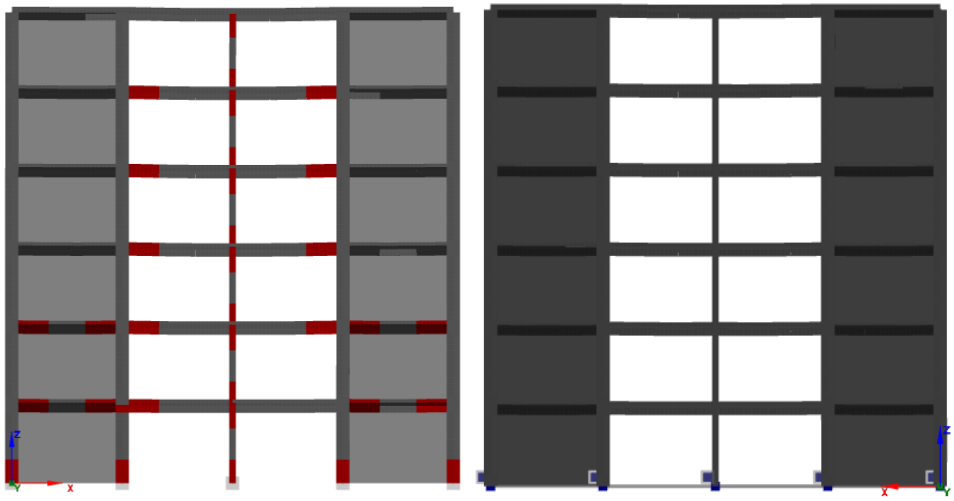

Fixed SSI

c) ZD

Figure 13. Damage levels for the structure with and without SSI according to NTHA analysis: Moment GO for a) ZB, b) ZC, c) ZD soil classes

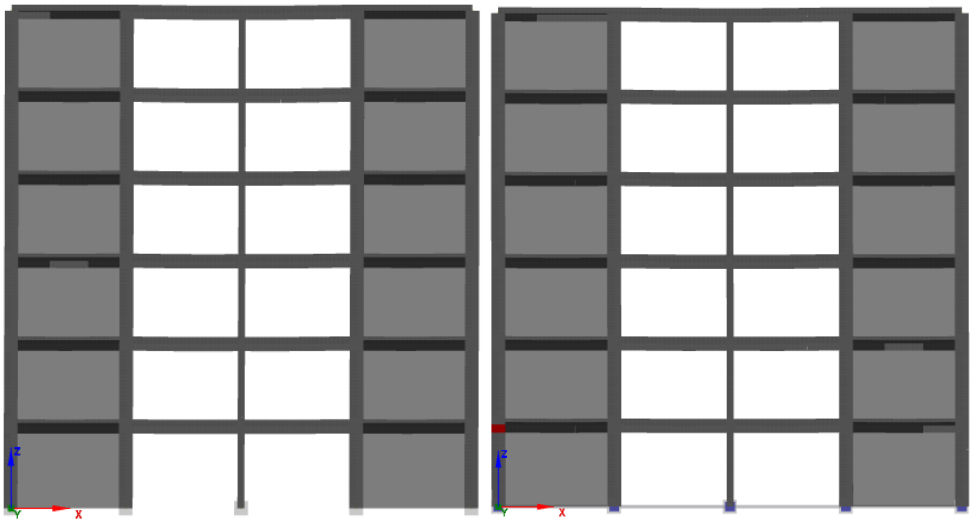

Fixed SSI

a) ZB

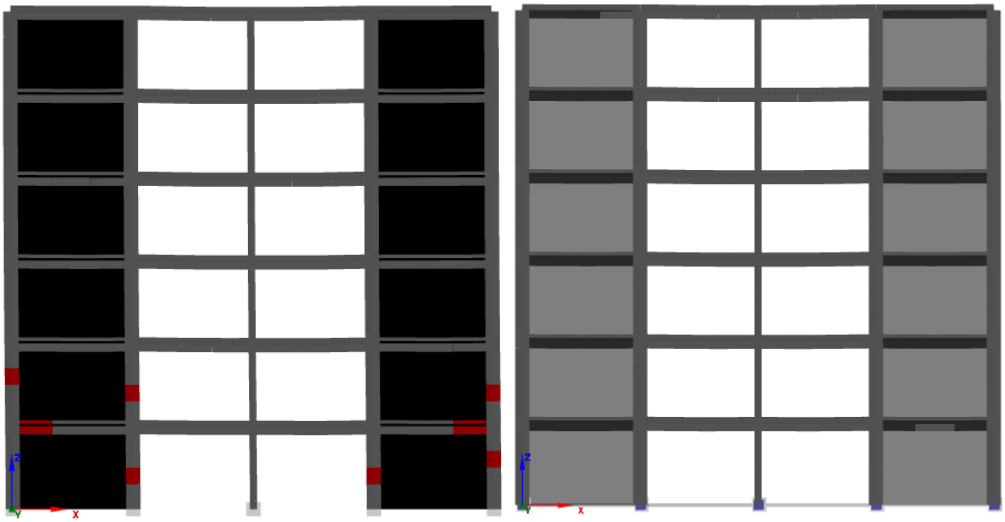

Fixed SSI

b) ZC

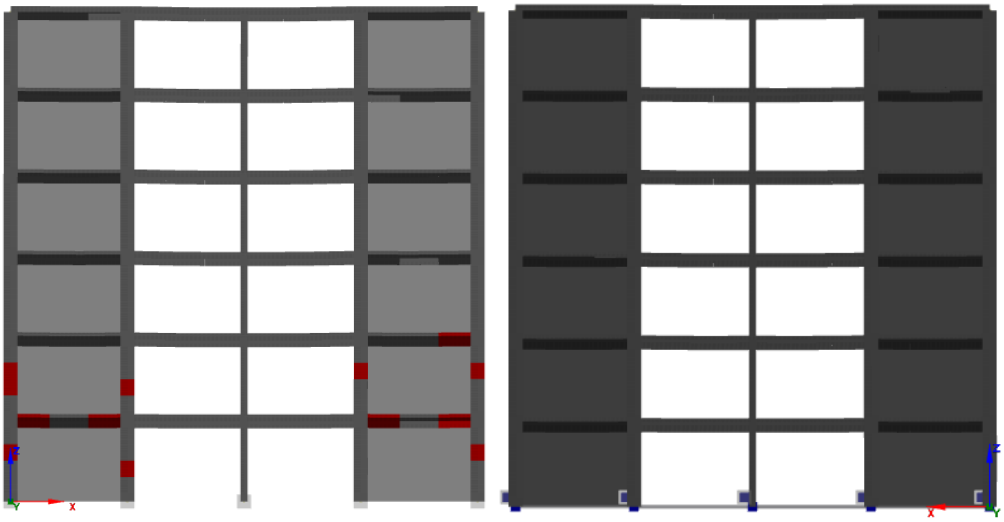

Fixed SSI

c) ZD

Figure 15. Damage levels for the structure with and without SSI according to NTHA analysis: shear GO for a) ZB, b) ZC, d) ZD soil classes

4. Conclusion

In this study, retrofitted reinforced concrete moment-resisting frame models were developed using the SeismoStruct program to conduct nonlinear static and time history analyses of the soil-foundation-structure system. Single-mode pushover analyses, in accordance with the TEC-2018 standard, were performed by subjecting the buildings to the design earthquake level (DD-2), accounting for both material and geometric nonlinearities. Various soil properties specific to the Tuzla region were considered for the soil layer beneath the foundation, and the effects of soil-foundation interaction were modeled using equivalent springs. The analyses were conducted for both flexible base (SSI system) and fixed base conditions.

The capacity curves from static pushover analyses of both fixed-based and SSI indicate that in all soil conditions, the distinction between fixed and flexible base scenarios is notably pronounced, demonstrating significant variations in the structural behavior observed in single-mode pushover analyses. It can be concluded that the use of single-mode pushover analysis has lead to an underestimation of the base shear response when soil-structure interaction (SSI) is considered.

The influence of soil-structure interaction (SSI) on the vibration periods of all reinforced concrete (RC) frame models varies according to geotechnical conditions, resulting in elongation of these periods compared to fixed base conditions across different soil profiles. Consequently, the seismic displacement demands also increase, potentially leading to a redistribution of internal forces, particularly pronounced in soft soil profiles.

The investigation into changes in seismic demands involved comparing story drift ratios. The inter-story drifts of the buildings decrease when soil-structure interaction (SSI) is considered in the analyses, compared to their fixed base conditions. However, the observed effects are minimal and nearly negligible for stiffer soil profiles (with shear wave velocities greater than 400 m/s). In contrast, as the geotechnical conditions beneath the foundation transition to softer soil types (ZD), the effects of SSI become significantly more pronounced.

Code-based capacity assessments reveal that many columns and beams reached their bending moment capacities in fixed-base scenarios on softer soil types, like ZD and ZC. Additionally, a small number of columns and beams also reached their shear force capacities. In contrast, good performance of retrofitted structure on ZB soil suggests that the retrofitting technique is effective. This analysis highlights the importance of soil improvement measures in regions with soft soils.

References

Girgin K., 1996. A method of load increments for determining the second-order limit load and collapse safety of RC framed structures, Ph.D. Thesis, ITU, (in Turkish).

Karaşın, İ. B. & Işik, E., 2017, "Farklı yapı davranış katsayıları için zemin koşullarının yapı performansına etkisi," DÜMF Mühendislik Dergisi, vol. 8, no. 4, pp. 661–673.

Oz, I., Senel, S.M., Mehmet Palanci, M., & Kalkan, A., 2020, "Effect of Soil-Structure Interaction on the Seismic Response of Existing Low and Mid-Rise RC Buildings", Applied Sciences, (10), 8357; doi:10.3390/app10238357

Shehata, E., Ahmed, M.M. & Alazrak, T.M.A., 2015, "Evaluation of soil structure-interaction effects of seismic response demands of multi-story MRF buildings on raft foundations." Int. J. Adv. Struct. Eng. 7, 11–30.

TEC 2007, Turkish Earthquake Code: Principles on buildings to be built in earthquake zones

TEC 2018, Turkish Earthquake Code: Building earthquake code of Turkey

TEC1975, Turkish Earthquake Code: Specifications for structures to be built in disaster areas

Teymur, P. & Pala, S., 2017, "Application of Wet-Mixed Shotcrete Panels for Retrofitting Purposes", Ömer Halisdemir Üniversitesi Mühendislik Bilimleri Dergisi, Cilt 6, (2), 492-510, ISSN: 2564-6605

Teymur, P., 2009. Retrofitting of Vulnerable Reinforced Concrete Frames with Shotcrete Walls, Ph.D. Thesis, ITU.

Teymur, P., Pala, S. & Yuksel, E., 2012, "Retrofitting of Vulnerable Reinforced Concrete Frames with Wet-Mixed Shotcrete Panels", Advances in Structural Engineering. V.15 (1), DOI: 10.1260/1369-4332.15.1.

Yıldız, D.H., 2008. Comparison of the evaluation methods to determine of seismic performance of buildings, M.Sc. Thesis, ITU, (in Turkish).

Construction Management

CivilTech
2nd International Symposium on Innovations in Civil Engineering and Technologies
October 30 – November 1, 2024, Isparta / TURKIYE

Digital Transformation of Construction Management with the Use of Automated Technology "Building Manager"

Dmytro Chashyn[1], *Kjartan Gudmundsson*[1], *Dmytro Yaremenko*[2], *Viktor Klepa*[3]

* *dmytrochashyn@gmail.com*

Abstract

Automated technology of construction management "Building Manager" represents a groundbreaking advancement in construction project management, leveraging state-of-the-art automated technology to optimize efficiency, streamline processes, and enhance collaboration across all design and construction operations facets. Rooted in a comprehensive network of interconnected software solutions, automated technology "Building Manager" transcends traditional project management frameworks, offering unparalleled automation, information integration, and resource optimization capabilities. Automated technology of construction management "Building Manager" traces its origins to the innovative concept of "Automated Technology" (AT), a paradigm shift in project management facilitated by the symbiotic evolution of software systems. Originally conceived within the "Building Manager" software complex framework, this automated technology embodies a transformative approach to project management, characterized by its dynamic adaptability, robust information linkage, and relentless pursuit of construction management automation. Central to AT's "Building Manager" ethos is its ecosystem of interconnected software products, meticulously curated by diverse developers to synergistically operate within a unified framework. Integrating these disparate systems transcends conventional boundaries, facilitating seamless information exchange, standardized protocols, and enhanced interoperability. This collaborative endeavor culminates in realizing a cohesive, multifunctional platform capable of orchestrating complex construction projects with unparalleled precision.

Keywords: Scheduling, resource management, construction management, project collaboration, on-site management, document management, mobile access and interoperability with a focus on BIM, automated technology of construction management, artificial intelligence, organizational and technological modelling of construction; BIM, Industry 4.0, Digital Transformation of Construction Management.

[1] *Division of Sustainable Buildings, Department of Civil and Architectural Engineering, School of Architecture and the Built Environment, KTH Royal Institute of Technology, Stockholm, Sweden*
[2] *ADA Ltd, author of AT "Building Manager", Ukraine*
[3] *Digital construction working group, Eurasian Federation of Construction Engineers, Astana, Kazakhstan*

1. Introduction

1.1. Root causes of the main problem

Results of the Digital Transformation of Construction Management with automated technology of construction management "Building Manager" must provide a realization of the encompassing myriad of cutting-edge functionalities designed to revolutionize project management practices within the construction industry. These include:

- BIM Integration and Structural Description: Leveraging Building Information Modeling (BIM), AT "Building Manager" facilitates the precise formulation of work lists and scopes, augmented by comprehensive structural descriptions of construction objects.
- Construction Network Modeling: Employing advanced approaches akin to expert systems, AT "Building Manager" automates the formation of construction network models, optimizing resource allocation and scheduling.
- Resource and Cost Estimation: Drawing upon a diverse normative base, AT "Building Manager" generates accurate resource and cost characteristics, informed by production standards and regulatory methodologies.
- Organizational and Technological Profiling: By delineating key parameters such as performers, equipment, and composition, AT "Building Manager" enables meticulous organizational and technological profiling of construction projects.
- Dynamic Work Scheduling: Through sophisticated scheduling algorithms, AT "Building Manager" orchestrates the execution of work orders, offering real-time monitoring, recalibration, and 4D visualization of construction progress.
- Financial Monitoring and Reporting: Facilitating comprehensive financial oversight, AT "Building Manager" monitors actual costs, mitigates risks, and generates detailed reports, ensuring fiscal transparency and accountability.

1.2. Main objective of the digital transformation of construction management and expected outcomes of the use of AT "Building Manager"

Digital transformation of construction management seems to be a particularly important component of Industry 4.0 technologies and should find its rightful place among these technologies (Abbasnejad 2024). AT "Building Manager" is not one software product, but a system of interconnected software products of different developers, designed to achieve the main goal of the Digital Transformation of Construction Management:

- Maximum automation and information linkage of all divisions of the design and construction organization into a single system with complex and dynamic resources – time – costs estimation.
- The creation of this automated technology required considerable efforts from developers of all software complexes included in AT, from the development and coordination of information exchange protocols to the development of special software.
- Joint operation of software complexes of different purposes within the framework of a single system not only systematized all information flows against the background of significant reduction of labor intensity of separate processes (for example: calculation of estimates or formation of network organizational and technological model of construction for calculations of calendar plans) with the significant increase of information reliability level, but also has opened such opportunities, which were unavailable when using these software complexes separately.
- Such capabilities include 4D-visualisation of the construction process (three-dimensional display of the construction object on any day of the calendar plan with or without the fact of work execution).
- Inclusion or not of different software complexes in AT "Building Manager" is not regulated by any contract between developers, but is determined by functional capabilities of software products to provide import and export of information with the use of information exchange protocols accepted in AT "Building Manager".

2. Method

The use of automated technology "Building Manager" in the processes of digital transformation of construction management is undoubtedly subordinate to the general principles of automation of construction management (Smith, 2020), (Lee, Han 2019). Automated technology "Building Manager" belongs to the class of expert systems capable of automatically planning all work and resource flows for the entire period of project implementation based on a digital information model with the use of artificial intelligence.

Creating this automated technology required considerable efforts from developers of all software complexes included in AT "Building Manager", from developing and coordinating information exchange protocols to developing special software.

Joint operation of software complexes of different purposes within the framework of a single system not only systematized all information flows against the background of significant reduction of labor intensity of separate processes (for example: calculation of estimates or formation of network organizational and technological model of construction for calculations of calendar plans) with the significant increase of information reliability level but also has opened such opportunities, which were unavailable when using these software complexes separately.

Such capabilities include 4D-visualisation of the construction process (three-dimensional display of the construction object on any day of the calendar plan with or without the fact of work execution).

Inclusion or not of different software complexes in AT "Building Manager" is not regulated by any contract between developers, but is determined by functional capabilities of software products to provide import and export of information with the use of information exchange protocols accepted in AT "Building Manager".

3. Results and Discussion

3.1. Resolving the Digital Transformation of Construction Management tasks with the use of AT "Building Manager"

Automated technology of construction and reconstruction management AT "Building Manager" was developed for the needs of enterprises of the construction complex. The solutions implemented in our automated technology can be safely used in enterprises, where there is a task of realizing complex projects with the participation of various executors and using a large nomenclature of material and technical resources.

AT "Building Manager" automates practically all functions of design and construction organization departments related to project development and construction management.

Our software complexes for project management provide:

1) Formation of the list and scope of work for individual objects from the BIM model along with the implementation of the structural description of the object (implemented in the Solaris program – as part of AT "Building Manager");

2) Automation of the formation of construction network models using approaches typical for expert systems (systems with elements of artificial intelligence);

3) Formation of resource and cost characteristics of works (based on the normative base of user's production standards or calculated according to the normative methods of EU countries);

4) Formation of organizational and technological characteristics of works (performers, composition, machines, equipment, etc.);

5) Calculation of work execution schedules by single or consolidated (unlimited number of objects in the plan) models taking into account the fact of fulfillment in comparison with the benchmark plan and forming on their basis:

- 4D display of construction objects on any day of the calendar plan with the marking of works that are behind the plan;
- delivery orders for specified and non-specified materials and equipment with daily monitoring of their fulfillment;
- work orders with daily monitoring of the fact of their fulfillment and corresponding recalculations of calendar plans;

- financing schedules with monitoring of actual costs of the objects and financial results of construction taking into account actual and planned costs as well as planned risks (inflation, credits, etc.);
- generation of certificates of completed works (periodic accounting) with the export of the fact of fulfillment to software complexes for calculation of estimates;
- generation of a report on writing off materials in comparison with production norms in connection with accounting software complexes with the entry of actually expended materials into the certificate of completed works.

"Time Stream" program complex is developed in two versions:

"TS Light" - is used to form a structured, technologically correct list of works in conjunction with the Solaris program and without it. It acts as a block of calendar planning with the possibility of 4D display of the construction or reconstruction of the object. Monitors the execution of work volumes with recalculation of the calendar plan for the object taking into account resource constraints. Exports to the volumes of completed or planned works in the period for automatic formation of certificates of completed works or sets of works of the plan for the period.

"TS Professional" - is under development. It is supposed to realize all the functions of AT "Building Manager". The new development will be deprived of such disadvantages of its predecessor as restrictions on the number of list items, the impossibility of simultaneous opening of several bases and objects, the inconvenience of the interface associated with transitions between modes, etc. The "Time Stream" is not an upgrade of "TS Professional". "Time Stream" is not a modernization of "Building Manager", but a completely new development based on the experience of 10 years of operation of "Building Manager" and modern approaches to programming.

3.2. Comparative analysis of competing software complexes to AT 'Building Manager'

"Primavera P6":

- Features: "Primavera P6" offers comprehensive project management capabilities, including scheduling, resource management, and cost control.
- Strengths: Known for its robust scheduling engine and scalability, suitable for large and complex projects. It also offers advanced reporting and analytics features.
- Weaknesses: Steep learning curve, high cost of ownership, and significant customization required for integration with other software systems.
- Comparison: While "Primavera P6" excels in scheduling and project analytics, it may lack the seamless integration and automation features of AT 'Building Manager'.

"Procore":

- Features: "Procore" is a cloud-based construction management platform offering tools for project management, collaboration, and field productivity.
- Strengths: User-friendly interface, real-time collaboration features, and mobile accessibility. It also offers integrations with various third-party applications.
- Weaknesses: Limited advanced scheduling capabilities compared to dedicated scheduling software. May lack in-depth financial management features.
- Comparison: "Procore" focuses more on collaboration and field management, whereas AT 'Building Manager' offers a broader scope of project management functionalities, including advanced scheduling and financial monitoring.

Autodesk (Technological chain: Revit – Navis Works – MS Project):

- Features: Autodesk BIM 360 is a cloud-based platform for building information modeling (BIM), project collaboration, and field management.
- Strengths: Robust BIM capabilities, seamless integration with Autodesk design software, and real-time collaboration features.
- Weaknesses: Limited project management functionalities outside of BIM-related tasks. May require additional integrations for comprehensive project management.
- Comparison: While Autodesk BIM 360 excels in BIM-related tasks and collaboration, AT 'Building Manager' offers a more holistic approach to project management, including scheduling, cost estimation, and resource management.

"Aconex":

- Features: "Aconex" is a cloud-based construction management platform offering document management, communication, and project collaboration tools.
- Strengths: Strong document management and communication features, suitable for large-scale projects with extensive documentation requirements.
- Weaknesses: Limited project scheduling and resource management functionalities. May lack advanced analytics and reporting capabilities.
- Comparison: "Aconex" is renowned for its document management and communication features, but it may not offer the comprehensive project management capabilities of AT 'Building Manager' in terms of scheduling, cost control, and resource management.

Other competing software complexes: "Alice", "Spider Project".

The results of the comparative analysis of competing software complexes to AT 'Building Manager' are shown in Table 1.

Table 1. The results of the comparative analysis of competing software complexes to AT 'Building **Manager'**

Feature	Primavera P6	Procore	MS Project	Aconex	VICO Office
Scheduling	Gantt charts, critical path analysis, and resource leveling	Gantt charts and calendar views	Gantt charts, task dependencies, and critical path analysis	Some basic features	Strong in 4D BIM scheduling (time) with features like flowline scheduling
Zone of work related to tasks and volume of work	-	-	-	-	Minimally/ partially
Resource Management	Resource allocation, leveling, and analysis	Basic resource management	Resource assignment, leveling, and utilization tracking	Limited functionality	Detailed resource allocation and optimization
Cost control	Budget tracking, cost forecasting, earned value management	Budgeting, forecasting, and change management	Cost tracking and budget management	-	Cost estimation cost analysis and forecasting
Project Collaboration	Some features	Real-time communication, file sharing, and RFI management	Basic features, often integrated with other MS tools	Strong platform designed for sharing documents, drawings, and communication across teams	Good around BIM models. IPD workflows
On site management	Limited features	Strong - including daily logs, site inspections, and punch list management.	Limited features	Mobile access for on-site management, including document control and issue tracking	Limited -integrates with other tools
Document management	Basic - integration with other Oracle solutions for enhanced functionality	Robust document management system, version control, automated workflows, and unlimited storage.	Basic features, enhanced through integration with SharePoint.	Excellent - strong version control, transmittals, and secure document sharing.	Integrates well with document management systems
Mobile access	Limited - mostly desktop-focused.	Strong - comprehensive apps for both iOS and Android	Basic - through mobile apps, can be integrated with Microsoft 365	Good - with dedicated apps	Limited native mobile access, relies on integration
BIM Interoperability	Integration with Oracle's Aconex BIM solution	Strong - model coordination, clash detection, and visualization	Limited direct BIM interoperability	Strong - Aconex Model Coordination allows integration with BIM models and tools	Exceptional 3D, 4D, and 5D BIM. detailed model coordination, clash detection, and cost estimation linked to the BIM model.
Import formats	XER, XML, MPX, CSV, MPP	CSV, XLSX, PDF, DWG, DXF, IFC	MPP, XML, MPX, CSV, XLSX	CSV, PDF, DWG, DXF, IFC	IFC, DWG, DXF, CSV, XML
Export formats	XER, XML, CSV, HTML, PDF, MPP	CSV, XLSX, PDF, DWG, DXF, IFC	MPP, XML, MPX, CSV, XLSX, PDF	CSV, PDF, DWG, DXF, IFC, XML	IFC, DWG, DXF, CSV, XML

3.3. Case study (brief results)

One such project, in which the expert system Building Manager was used for work planning, was the "Hanhikivi-1" nuclear power plant project. With the help of the Building Manager, several options for the construction of the NPP were modeled. Thanks to variable modeling, finding the most rational way of constructing the NPP was possible, which allowed to reduce the planned construction period by 12 months.

The expected savings from reducing the construction time for objects costing more than 1 billion euros is 7-10% of the construction cost.

Modeling using the expert system Building Manager made it possible to find a variant of construction of NPP "Hanhikivi-1" (Finland) 12 months earlier than the planned work schedule and to justify the technological feasibility of this variant. This was achieved in the following way:

1. The nodal method of construction (AWP- Advanced Work Package) was applied with the help of which structurally and technologically separate parts were allocated in the information model of the nuclear power plant, allowing the adjustment of separate technological units taking into account the order of their commissioning (Ryan 2017).
2. A variant of the main building construction using Open-Top technology was adopted - when the installation of heavy and large-size equipment was carried out together with general construction works.
3. To perform construction and installation works in parallel, a decision was made to create a zone with completed finishing works and climate control in the premises of the main building, which was half built.
4. The performed preparatory works determined the order of erection of buildings and structures. For the formation of the calendar-network construction model, the automated technology Building Manager was used, with the help of which the flows of works and resources (machines and mechanisms, labor resources by specialties) were modeled and synchronized.
5. Work and resource flows were analyzed, ways of their optimization were determined for the entire complex of buildings and structures, taking into account all project constraints (technological, spatial, climatic, resource, organizational) - and appropriate changes were made to the technology of construction of buildings and structures. Taking these changes into account, work, and resource flows were remodeled and synchronized with each other by using the automated technology Building Manager.
6. Ways of local optimization of works that are on the critical path of the calendar-network model of construction were found. Optimization of workflows with the help of automated technology Building Manager was performed. The resulting construction variant was shorter by 12 months of the planned work schedule and used the project resources more rationally.

Discussion

Each of the competing software complexes brings unique strengths to the table, catering to specific aspects of construction project management. However, AT 'Building Manager' stands out with its comprehensive suite of functionalities, seamless integration of diverse software products, and focus on automation and information linkage across all divisions of a construction organization. Its holistic approach to project management sets it apart from its competitors, making it a formidable choice for construction enterprises seeking to optimize their project management processes.

It should be noted that for the successful application of automated technology "Building Manager" requires a certain level of standardization of a limited list of parameters of BIM models used to determine the type of work and the calculation of their volumes. Inconsistency in item parameter lists may require additional labor costs to prepare the BIM model for use. In case of non-compliance with the list of parameters to the standard one, the total labor intensity of preparation of initial data for calculations increases, but it is still much less than the labor intensity when using traditional

technologies. Standardization of the list of parameters of elements of BIM models can be local (within the group of project participants) or within the firm or industry standard especially within the framework of the Industry 4.0 concept. To a large extent, bringing the names of an arbitrary list of parameters of BIM model elements to the standard (accepted in the system) is automated by a special software module of the system.

4. Conclusion

The adoption of AT "Building Manager" yields tangible economic benefits, including a notable reduction in labor intensity and construction costs. Empirical evidence from successful implementations underscores its efficacy in delivering substantial cost savings and operational efficiencies across a spectrum of construction and reconstruction projects.

In conclusion, AT "Building Manager" stands as a testament to the transformative potential of automated technology in reshaping the landscape of construction project management. By fostering collaboration, innovation, and efficiency, it empowers organizations to navigate the complexities of modern construction projects with confidence and precision.

Using AT "Building Manager" in the Digital Transformation of Construction Management processes and processes of Industry 4.0 allows stakeholders to approach the significant economic effect: a reduction in the labor intensity of design and management processes by 25-30% and, a reduction in construction or reconstruction costs by 20%. This economic effect has been confirmed by the successful implementation of many construction and reconstruction projects.

Acknowledgments

The authors of this paper express special gratitude to the project team of the construction site "Hanhikiwi-1" (Finland) for providing data on the results of the practical application of the studied automated construction management technology "Building Manager".

References

Abbasnejad B., et al. (2024). "A systematic literature review on the integration of Industry 4.0 technologies in sustainability improvement of transportation construction projects: state-of-the-art and future directions". Smart and Sustainable Built Environment, https://www.emerald.com/insight/2046-6099.htm

Smith, A., et al. (2020). "Automated Technology in Construction Management: A Review." Journal of Construction Engineering and Management, 146(2), 123-135.

Lee, J., Han, S. (2019). "Utilization of Project Management Systems in the Construction Industry: A Comparative Analysis" Construction Research Congress Proceedings, 598-607.

Ryan, G. (2017). Even More Schedule for Sale: Advanced Work Packaging, for Construction Projects. Bloomington: AuthorHouse, 2017. 132 p.

Impact of the European Green Deal and Circularity on LEED Projects

Şeyda Adıgüzel Istıl[1]

*seydaadiguzelistil@ohu.edu.tr

Abstract

Sustainability standards are changing in many industries, including the building industry, because of the European Union's comprehensive policy program known as the European Green Deal, which aims to achieve carbon neutrality by 2050. This study investigates the interactions between the policies of the European Green Deal and the requirements of the worldwide known LEED rating program for green buildings. In addition, the research examines how LEED standards are affected in order to meet Europe's ambitious environmental goals by examining important Green Deal components, including energy efficiency, the circular economy, and carbon neutrality. The study aims to investigate the impact of the European Green Deal and Circular Economy standards in terms of the building sector on the recently developed LEED version 5 (v5) criteria.

Keywords: European green deal; circular economy; LEED; green building certificate

[1] *Niğde Ömer Halisdemir Üniversitesi, Teknik Bilimler MYO, İnşaat Bölümü, Niğde, Türkiye*

1. Introduction

The European Green Deal has been launched by the European Union (EU) in December 2019 to make Europe the first climate neutral continent by 2050. It aims to protect, conserve and enhance the EU's natural capital, and protect the health and well-being of citizens from environment related risks and impacts (Soares, 2024). One of the main goal of the European Green Deal is to reduce greenhouse gas emissions (GHGs) by at least 55% by 2030, compared to 1990 levels to accomplish the key indicator of the Paris Agreement and European Climate Law (Brinkman, 2024).

In the analysis of the industries that are responsible for the emission of greenhouse gases, it is discovered that the building industry is ranked fourth (IEA, 2023). To achieve net zero emission goals by 2050, GHGs in the construction sector also need to be reduced. At this point, Article 2.1.4 of the European Green Deal, "Building and renovating in an energy and resource efficient way", emerges to achieve this aim. According to the Article 2.1.4. the construction, use and renovation of buildings require significant amounts of energy and mineral sources (European Commission, 2021). For this reason, it has been stated that renovation of buildings rather than new construction will reduce resource use and energy consumption and thus reduce GHG emissions. Buildings constructed by applying circular economy requirements in new and renovated buildings should be included in the system as buildings that have different functions for many years, are resilient to different climatic conditions, have low energy and water consumption and even can produce on-site.

The objective of new and renovated buildings to commit to sustainable practices and minimize energy and waste usage has led to the establishment of a system known as "green building certification systems" in the industry (Greer et al., 2019). Various green building certification systems exist globally. These are LEED (Leadership in Energy and Environmental Design), BREEAM (Building Research Establishment Environmental Assessment Method), WELL Building Standard, DGNB (Deutsche Gesellschaft für Nachhaltiges Bauen), CASBEE (Comprehensive Assessment System for Built Environment Efficiency), Green Star, etc. A common objective of all green building certification systems is to decrease energy and resource consumption in accordance with the goals outlined in the European Green Deal (European Commision, 2021) and Circular Economy (Arruda et al., 2021) to give priority to user comfort, and to guarantee sustainability objectives by delivering buildings with long-term functionality.

This study aims to demonstrate the influence of the European Green Deal and Circular Economy requirements on the LEED green building certification systems. The circular economy (CE) concept promises an alternative to the current linear economy of 'take-make-use-dispose' (Eberhardt et al., 2022) and it offers requirements such as waste management, reuse, recycle, life cycle assessment (LCA), etc. to achieve sustainability goals and green building standards. In this study, the LEED certification system has been selected due to its being the world's most widely used certification program with 197000 projects worldwide (USGBC). It is known that both of the LEED and the European Green Deal pay attention to the subjects such as material selection (Gurgun et al., 2015), energy efficiency (Rebelatto et al., 2024), water efficiency (Luo et al., 2021), waste generation, GHG emissions to evaluate the buildings' sustainability level within the scope of circularity. Thus, the study aims to investigate the impact of the European Green Deal and Circular Economy standards in terms of the building sector on the recently developed LEED version 5 (v5) criteria.

2. Material and Method

2.1. Data Collection

This study based on qualitative research on exploring correlation between LEED certificates' credits with the European Green Deal and Circular Economy requirements for building sector. To reach the research aims, data were obtained from USGBC's (United States Green Building Council) web site, articles of the European Green Deal and observing the requirements of the "Circular Economy" by searching on academic databases. The latest version of the LEED certification system, LEED v5, were examined by considering the category of Building Design and Construction: New Construction (BD+C). First, the requirements of this category were tabulated, and then the relationship between the obtained data and the European Green Deal and Circular Economy were revealed via interaction matrix (Hill, 1971).

LEED v5 is the newest certification system which requires different credits than the previous ones. The new credits have been presented to public between April 3-May 24, 2024, to get the stakeholder's feedback before releasing the certificate. LEED v5 pay more attention to climate change, decarbonization and ecological conservation and renovation (USGBC). The revised and developed credits of LEED v5 BD+C: New Construction were listed in Table 1. The prerequisite credits are shown in bold. The prerequisite credit means that; in case of applying for a category, if the category has requirements, these requirements must be achieved first. In other words, it is not possible to get points for the certification before achieving the prerequisites.

Table 1. LEED v5. BD+C:New Construction Credits (USGBC)

Integrative Process, Planning and Assessments	**Location& Transportation**	**Sustainable Sites**	**Water Efficiency**	**Energy& Atmosphere**	**Materials& Resources**	**Indoor Environmental Quality**	**Project Priorities& Innovation**
Integrative Process, Planning and Assessments	**Location& Transportation**	**Sustainable Sites**	**Water Efficiency**	**Energy& Atmosphere**	**Materials& Resources**	**Indoor Environmental Quality**	**Project Priorities& Innovation**
Carbon Assessment (R)*	Active Travel Facilities	**Minimized Site Disturbance(R)**	**Minimum Water Efficiency (R)**	**Energy Metering &Reporting (R)**	**Assess Embodied Carbon (R)**	**Building Accessibility (R)**	LEED Accredited Professional
Climate Resilience Assessment (R)	Compact and Connected Development	**Resilient Site Desing (R)**	**Water Metering and Report (R)**	**Fundamental Commissioning (R)**	**Planning for Zero Waste Operations (R)**	**Fundamental Air Quality (R)**	Project Priorities
Social Equity Assessment (R)	Electric Vehicles	Accessible Open Space	Enhanced Water Efficiency	**Fundamental Refrigerant Management (R)**	Building& Materials Reuse	**No Smoking or Vehicle Idling (R)**	
Integrative Design Process	Equitable Development	Enhanced Resilient Site Design	Water Metering and Leak Detection	**Minimum Energy Efficiency (R)**	Construction and Demolition Waste Diversion	Air Quality Testing and Monitoring	
	Sensitive Land Protection	Heat Island Reduction	Water Reuse	**Operational Carbon Projection and Decarbonization Plan (R)**	Low-Emitting Materials	Connecting with Nature	
	Transportation Demand	Light Pollution and Bird Collision Reduction		Electrification	Optimized Building Products	Enhanced Air Quality	
		Protect and Restore Biodiverse Habitat		Enhance Energy Efficiency	Reduce Embodied Carbon	Enhanced Building Accessibility	

		Rainwater Management		Enhanced Refrigerant Management		Occupant Experience	
				Enhanced& Ongoing Commissioning		Resilient Spaces	

Table 1 (continue). LEED v5. BD+C:New Construction Credits (USGBC)

				Grid Interactive			
				Reduce Peak Thermal Loads			
				Renewable Energy			

***R means "Required Credit"**

On the other hand, the European Green Deal's requirements for building sector have been listed and presented in Table 2. The subjects are detailed under 8 main headings and presented in the table. Each main heading has been clarified upon, with the requirements clearly stated.

Table 2. European Green Deal Requirements for Building Sector (European Commission, 2021)

1. **Energy Efficiency**:	• Improve energy performance of building
	• Double the renovation rate of buildings by 2030
	• Improve energy efficiency in buildings
2. Decarbonization of Heating and Cooling	• Using renewable energy resources for heating and cooling
3. Energy Performance of Buildings	• By 2030, newly built structures should be nearly zero-energy buildings (NZEBs), highly efficient, and powered primarily by renewable energy sources.
	• Existing buildings are encouraged to adopt NZEB standards via renovation.
	• Minimum energy performance standards are mandated for new buildings, and member states are required to develop long-term renovation strategies.
4. Sustainable Building Materials	• The utilization of sustainable, recyclable, and environmentally friendly building materials aims to minimize the carbon footprint associated with construction and renovation activities.
	• Life-cycle assessments (LCA) of buildings evaluate their environmental impact throughout their entire lifespan, incorporating circular economy principles.

Table 2 (Continue). European Green Deal Requirements for Building Sector (European Commission, 2021)

5. Smart Buildings and Digitalization	• Encouraging the incorporation of intelligent technologies in buildings to enhance energy utilization, increase efficiency, and facilitate demand-response in energy systems.
	• Utilization of smart meters, building management systems, and various digital tools for the monitoring and reduction of energy consumption.
6. Sustainable Transportation	• Minimizing transportation emissions and achieving sustainable transport solutions
	• Promoting the adoption of low-emission vehicles and expanding the infrastructure for vehicle charging stations.
7. Ecosystem	• Preservation of biological diversity
	• Sustainable re- and afforestation, along with the restoration of degraded forests, enhances CO_2 absorption, bolsters forest resilience, and supports the circular bioeconomy.
	• To protect the citizens and ecosystems of Europe, the EU must enhance its monitoring, reporting, prevention, and remediation of pollution affecting air, water, soil, and consumer products.
	• The natural functions of ground and surface water must be restored
8. Clean Air	• Monitoring, modeling, and developing air quality plans to assist local authorities in accomplishing improved air quality.

Within the scope of the study, Table 3 outlines the 11 principal topics identified for the achievement of a circular economy within the construction sector. Each main category is subdivided into specific requirements for achieving circular economy in the construction sector.

Table 3. Circular Economy Requirements for Building Sector

1.Design for Disassembly and Reuse	**Modular Design:** Buildings should be constructed in a way that enables components to be readily disassembled and repurposed in new constructions or renovations.
	Material Passports: A material passport is a document that records the categories, quantities, and qualities of materials used in a building, thereby enabling their future reuse or recycling.
2. Use of Recyclable and Recycled Materials	**Sustainable Material Selection**: Materials that are easily separated for recycling, have little effect on the environment, and are recyclable should be prioritized.
	Recycled Content Integration: The demand for natural resources can be reduced by incorporating materials that have been recycled from previous projects into buildings.
3. Resource Efficiency in Construction	**Minimizing Waste:** To minimize material waste, such as off-cuts and packaging, construction processes should be optimized.
	Resource Efficiency: The design and construction process should prioritize the reduction of the building's overall environmental impact by utilizing fewer materials and energy.

Table 3 (continue). Circular Economy Requirements for Building Sector

4. Longevity and Adaptability	**Durability:** To ensure that buildings stay relevant and useful for long periods of time, materials and construction methods should be selected based on their longevity.
	Adaptability: To minimize the need for demolition and new construction, buildings should be made to be able to adapt to various uses over time.
5. Circular Business Models	**Product-as-a-Service**: Supporting business models that lease rather than sold building materials or components, encouraging their recycling or reuse.
	Take-back Strategies: To guarantee that materials and components are recycled back into the production cycle, manufacturers and suppliers are urged to design take-back plans for them when their useful lifespans come to an end.
6. Deconstruction over Demolition	**Selective Deconstruction**: As an alternative to conventional demolition, structures ought to be dismantled with great care to preserve as many components as possible for recycling or future use.
	Reducing Landfill Use: The goal is to decrease the amount of waste directed to landfills by maximizing the recovery and repurposing of materials.
7. Circular Economy Principles in Building Codes and Standards	**Regulatory Support:** Building standards and regulations must incorporate circular economy principles, guaranteeing that sustainability is addressed throughout the building lifecycle.
	Performance Standards: Developing requirements that account for the whole life-cycle effects of buildings, encompassing their deconstruction and potential for material reutilization.
8. Life Cycle Assessment (LCA)	**Environmental Impact Assessment:** To assess a building's environmental impact from construction to demolition and material recovery, a life cycle assessment is recommended.
	Reduced Carbon Footprint: Including embodied carbon in materials, the LCA should be focused on reducing the building's carbon footprint over its whole life.
9. Encouraging Circular Procurement	**Sustainable Procurement Policies:** Public and private organizations should implement guidelines for procurement that give priority to circular products and solutions.
	Lifecycle Costing: Decision-making must account for the comprehensive cost of ownership, encompassing future reuse, recycling, and disposal expenses.
10. Collaboration Across the Value Chain	**Collaboration Among Stakeholders:** Encouraging cooperation between waste management firms, architects, designers, contractors, and material suppliers to develop closed-loop systems.
	Knowledge Sharing: Encouraging the sharing of innovative ideas, research, and best practices in circular architecture and construction.
11. Digital Tools and Innovation	**Building Information Modeling (BIM):** Planning, designing, and managing buildings in a way that encourages the circular economy principles using BIM and other digital tools.
	Material Innovation: Encouraging the development and application of novel materials with extended life spans or ease of recycling.

3. Results and Discussion

Within the context of the research, the interactions between;

- The LEED v5. BD+C:New Construction Credit Categories and The European Green Deal Requirements
- The LEED v5. BD+C:New Construction Credit Categories and The Circular Economy Requirements

have been listed in Table 4 and 5 orderly.
First the interaction matrix has been presented in Table 4 to show the correlation between The European Green Deal Requirements and LEED v5. BD+C: New Construction Credit Categories. Each LEED v5. BD+C: New Construction Credit's subcategories have been interacted with the European Green Deal Requirements (Table 2). In case of even having an interaction for a subcategory, it is indicated by the symbol "✓".

Table 4. The Interaction Matrix of The European Green Deal Requirements and LEED v5. BD+C: New Construction Credit Categories

LEED v5 BD+C: New Construction Credit Categories / **European Green Deal Requirements**	Integrative Process, Planning and Assessments	Location& Transportation	Sustainable Sites	Water Efficiency	Energy& Atmosphere	Materials& Resources	Indoor Environmental Quality	Project Priorities & Innovation
1. Energy Efficiency:	✓	✓			✓	✓	✓	
2. Decarbonization of Heating and Cooling	✓		✓		✓	✓	✓	
3. Energy Performance of Buildings	✓				✓	✓	✓	
4. Sustainable Building Materials	✓					✓		
5. Smart Buildings and Digitalization	✓	✓		✓	✓	✓	✓	
6. Sustainable Transportation	✓	✓	✓					
7. Ecosystem	✓	✓	✓	✓	✓	✓	✓	
8. Clean Air	✓	✓			✓		✓	

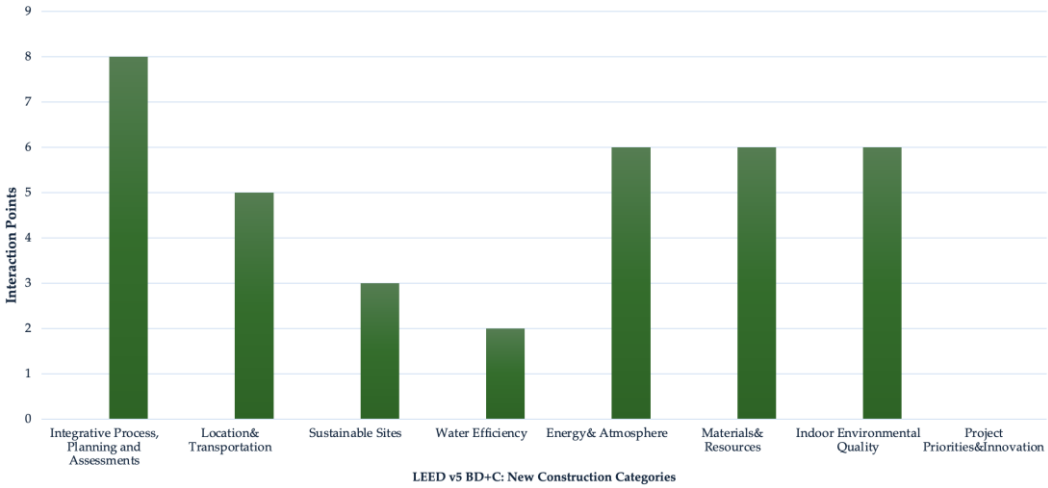

Figure 1. The Interaction Points of LEED v5. BD+C: New Construction Categories and The European Green Deal Requirements for The Building Sector

In Figure 1, the achieved interactions were shown as earned points. It has seen that the "Integrative Process, Planning and Assessments" category demonstrates the most significant influence on the implementation of the European Green Deal requirements, getting 8 points. The reason behind that is the "Integrative Process, Planning and Assessments" category has subcategories such as “Carbon Assessment, Climate Resilience Assessment, Social Equity Assessment and Integrative Design Process” which are directly related with the European Green Deal requirements. In particular, the “Integrated Design Process” category’s requirements for decarbonization, energy efficiency, sustainable material use and ecosystem protection during the pre-design phase and throughout the design phases of construction projects resulted in it receiving the highest score. Furthermore, the categories of “Energy & Atmosphere,” “Materials & Resources,” and “Indoor Environmental Quality” each obtained 6 points, indicating that 75% of the European Green Deal requirements have been met. Also, it was seen that the “Project Priorities & Innovation” category couldn’t get any point. Because the subcategories that are working with a “LEED Accredited Professional” and “Project Priorities” don’t require any decarbonization or energy efficiency implementation.

In the Table 5, the interaction between Circular Economy Requirements (Table 3) and LEED v5. BD+C: New Construction Credit Categories (Table 1) have been listed. Each LEED v5. BD+C: New Construction Credit’s subcategories have been interacted with the Circular Economy Requirements. Interactions within a subcategory are indicated by the symbol “✓” when at least one interaction is present.

Table 5. The Interaction Matrix of The Circular Economy Requirements and LEED v5. BD+C: New Construction Credit Categories

LEED v5 BD+C: New Construction Credit Categories / **Circular Economy Requirements**	Integrative Process, Planning and Assessments	Location& Transportation	Sustainable Sites	Water Efficiency	Energy& Atmosphere	Materials& Resources	Indoor Environmental Quality	Project Priorities& Innovation
Design for Disassembly and Reuse	✓					✓		
Use of Recyclable and Recycled Materials	✓				✓	✓		
Resource Efficiency in Construction	✓		✓	✓	✓	✓		
Longevity and Adaptability	✓	✓	✓			✓		
Circular Business Models	✓					✓		
Deconstruction over Demolition	✓					✓		
Circular Economy Principles in Building Codes and Standards	✓					✓		
Life Cycle Assessment (LCA)	✓	✓	✓	✓	✓	✓	✓	
Encouraging Circular Procurement	✓	✓	✓	✓	✓	✓	✓	
Collaboration Across the Value Chain	✓							✓
Digital Tools and Innovation	✓							✓

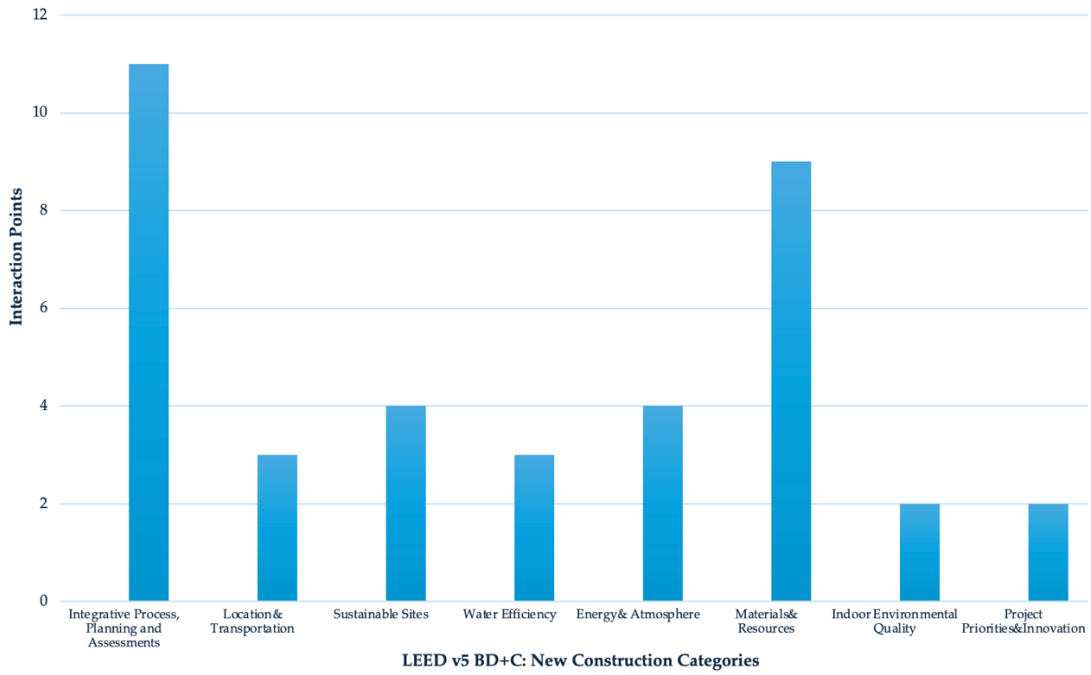

Figure 2. The Interaction Points of LEED v5. BD+C: New Construction Categories and Circular Economy Requirements for The Building Sector

Figure 2 illustrates that the "Integrative Process, Planning and Assessments" category displays the most major impact on the implementation of Circular Economy requirements within the building sector. The "Integrative Process, Planning and Assessments" category has requirements at the beginning of the project by design phase and it allows to join the stakeholders to the project at beginning of the project. During the design phase, it enables designers develop deconstruction and demolition plans, utilize recycled and renewable resources, conduct life cycle assessments (LCA) of the project, evaluate the durability of selected building materials, and create a waste management plan to mitigate environmental impacts from the very beginning of the project. Thus, this category meets all the needs of the circular economy requirements for building sector by deciding at the design phase. The interaction achievement has been followed by the "Materials and Resources" category with 9 points. The subcategories of the "Materials and Resources" category are mostly related with; planning for zero waste operations, reuse of building materials, construction and demolition waste management, reducing embodied carbon in buildings, using low-emitted building materials. Each of these subcategories have relation with the Circular Economy requirements which are listed in Table 3.

4. Conclusion

The impact of the European Green Deal and Circular Economy on LEED v5 BD+C: New Construction certification draft has been investigated for the building sector within the scope of this study. Within the aim of the study, the LEED v5 BD+C: New Construction requirements have been interacted with the requirements of the European Green Deal and Circular Economy for the building sector separately. The study reveals that the "Integrative Process, Planning and Assessment" category of the LEED v5 BD+C: New Construction has high interaction with both the European Green Deal and Circular Economy requirements for construction projects. This is since the "Integrative Process, Planning and Assessment" category requires integrative design processes, which allow the analysis and determination of the projects' needs at the beginning.

On the other hand, the "Materials&Resources" category ranked second for both European Green Deal and Circular Economy interactions. Each sub-credit within the "Materials & Resources" category imposes requirements such as the utilization of recycled materials, the reuse of materials from previous

structures, the use of low-emission materials, the reduction of embodied carbon, the pursuit of zero waste operations during construction, and the assessment and mitigation of embodied carbon. Most of the requirements of the European Green Deal and Circular Economy are required by this category. Other LEED BD+C:New Construction categories are mostly related with increasing the quality of life by applying smart building meters such as monitoring the water consumption and air quality of buildings. Additionally, the Location & Transportation category focuses on reducing fossil fuel consumption by encouraging the use of electric vehicles and public transport, aligning positively with the European Green Deal. Accordingly, this study reveals that the LEED project categories contain the European Green Deal and Circular Economy requirements for building sector. Applying a LEED project allows the automatic implementation of the European Green Deal objectives, including the reduction of carbon emissions, enhancement of energy efficiency, utilization of smart building materials, promotion of sustainable transportation, ecosystem protection, and the adoption of renewable energy sources for heating and cooling needs in buildings. Also, the circularity requirements, including design for disassembly and reuse, utilization of recycled materials, development of waste management and demolition plans, and collaboration with stakeholders, would be inherently achieved through the implementation of a LEED project.

References

Arruda, E. H., Melatto, R. A. P. B., Levy, W., & Conti, D. de M. (2021). Circular economy: A brief literature review (2015–2020). *Sustainable Operations and Computers*, *2*(March), 79–86. https://doi.org/10.1016/j.susoc.2021.05.001

Brinkman, D. (2024). EU climate law. *Sustainable Finance and Climate Change: Law and Regulation*, *2021*(June), 116–136. https://doi.org/10.4337/9781800377288.00016

Eberhardt, L. C. M., Birkved, M., & Birgisdottir, H. (2022). Building design and construction strategies for a circular economy. *Architectural Engineering and Design Management*, *18*(2), 93–113. https://doi.org/10.1080/17452007.2020.1781588

European Commission: Directorate-General for Research and Innovation. (2021). *European Green Deal : research & innovation call*. Publications Office of the European Union. **https://data.europa.eu/doi/10.2777/33415**.

Greer, F., Chittick, J., Jackson, E., Mack, J., Shortlidge, M., & Grubert, E. (2019). Energy and water efficiency in LEED: How well are LEED points linked to climate outcomes? *Energy and Buildings*, *195*(October 2017), 161–167. https://doi.org/10.1016/j.enbuild.2019.05.010

Gurgun, A. P., Komurlu, R., & Arditi, D. (2015). Review of the LEED Category in Materials and Resources for Developing Countries. *Procedia Engineering*, *118*, 1145–1152. https://doi.org/10.1016/j.proeng.2015.08.456

Hill, W. F. (1971). The Hill Interaction Matrix. *Personnel & Guidance Journal*, *49*(8), 619–623. https://doi.org/10.1002/j.2164-4918.1971.tb03693.x

IEA. (2023). CO2 Emissions in 2022. In *Encyclopedia of Sustainable Management*. https://doi.org/10.1007/978-3-031-25984-5_300288

Luo, K., Scofield, J. H., & Qiu, Y. (Lucy). (2021). Water savings of LEED-certified buildings. *Resources, Conservation and Recycling*, *175*(May), 105856. https://doi.org/10.1016/j.resconrec.2021.105856

Rebelatto, B. G., Salvia, A. L., Brandli, L. L., & Leal Filho, W. (2024). Examining Energy Efficiency Practices in Office Buildings through the Lens of LEED, BREEAM, and DGNB Certifications. *Sustainability (Switzerland)* , *16*(11). https://doi.org/10.3390/su16114345

Soares, A. G. (2024). The European Green Deal. *Revista Juridica Portucalense*, *35*, 44–67. https://doi.org/10.34625/issn.2183-2705(35)2024.ic-03

USGBC. (2024, September). *LEED rating system.* U.S. Green Building Council. https://www.usgbc.org/leed

Hydraulics

CivilTech
2nd International Symposium on Innovations in Civil Engineering and Technologies
October 30 – November 1, 2024, Isparta / TURKIYE

Kızılırmak Basin Hydrological Drought Analysis

Özlem Terzi[1] , *Tahsin Baykal*[2], *Emine Dilek Taylan*[3]

* tahsinbaykal@kku.edu.tr

Abstract

In this study, hydrological drought analysis was carried out with the Streamflow Drought Index (SDI) using data of two flow observation stations in the Kızılırmak Basin, which is the longest river that originates within Turkey's borders and flows into the sea within its own borders. Using monthly flow data between 1985 and 2015, 3-, 6-, 9- and 12- months SDI values were calculated and then drought severity and duration analysis was performed with Run Theory for these stations. As a result of the analyses, it was observed that station E15A038 had a longer and more severe drought than station E15A035.

Keywords: Streamflow drought index, run theory, Kızılırmak Basin.

[1] *Faculty of Technology, Isparta Applied Sciences University, Isparta, Turkiye*
[2] *Faculty of Engineering and Natural Sciences, Kırıkkale University, Kırıkkale, Turkiye*
[3] *Faculty of Engineering and Natural Sciences, Suleyman Demirel University, Isparta, Turkiye*

1. Introduction

Drought can generally be defined as a natural disaster that causes environmental, economic and social problems because of precipitation falling below the long-term mean value in a region. When meteorological, hydrological, agricultural and socioeconomic droughts are examined in order of occurrence, meteorological drought is observed as a deficiency in precipitation from the mean, while hydrological drought is seen as a deficiency in surface and ground water. Agricultural drought occurs as a loss of productivity when plant water needs cannot be met because of lack of soil moisture. As a result of loss of productivity, socioeconomic drought occurs when supply cannot meet demand.

Many studies have been conducted on the analysis of hydrological drought in Türkiye and in the world (Tareke and Awoke, 2022; Malik et. al, 2021; Şimşek, 2021; Jahangir and Yarahmadi, 2020). Tabari et al. (2012) conducted hydrological drought analysis with ECM for 3-, 6-, 9- and 12-month periods using the data of 14 flow observation stations in the northwest of Iran in the period between 1975 and 2009. They found that extremely dry periods in a 12-month period occurred in 1997-1998 and 2008-2009 and all stations were affected by extreme droughts. Gümüş et al. (2017) performed hydrological drought analysis using SDI for flow data between 1954 and 2005 from four streamflow gauging stations in the Asi Basin. They determined the severity, magnitude, and distribution of SDI values for 3-, 6-, and 12-month periods. They found that the number of dry years between 1980 and 2005 was much higher than the number of dry years between 1954 and 1979. They also stated that the extremely dry years were 2000 and 2001. Özfidaner et al. (2018) made drought analysis using SDI for the monthly mean flow values of two stations for the Seyhan Basin between 1967 and 2007. In their analysis for 3-, 6-, 9- and 12-month periods, they obtained similar results for 9- and 12-month periods. Myronidis et al. (2018) carried out hydrological drought analysis with SDI for rivers in Cyprus. For the analysis, streamflow data of eleven streamflow gauging stations covering the years 1979 - 2013 were used. Additionally, they found that drought increased over time with the Mann Kendall trend test.

In this study, it was aimed to perform hydrological drought analysis in the Kızılırmak Basin in 3-, 6-, 9- and 12- month periods using the streamflow drought index for E15A035 and E15A038 streamflow observation stations between 1985-2015. Also, run theory was used to determine drought duration and severity in dry and wet periods. Thus, it will be tried to describe the similarities and differences in terms of duration and severity of dry periods in these stations representing different topographic, meteorologic and hydrologic characteristics of the basin.

2. Material and Method

2.1. Study Region and Data

The basin of the Kızılırmak River, which originates from the foothills of Kızıldağ in the İmranlı district of Sivas in Turkey and contains important water resources flowing into the Black Sea in the Bafra district of Samsun, was chosen as the study area (Figure 1). The basin of the Kızılırmak River, which originates from the foothills of Kızıldağ in the İmranlı district of Sivas in Turkey and contains important water resources flowing into the Black Sea in the Bafra district of Samsun, was chosen as the study area. Kızılırmak basin, which is the second largest basin in Turkey, has an area of 82.205 km^2. The basin, located between 41°- 44' and 38°- 25' northern latitudes and 32°- 48' and 38°- 25' eastern longitudes, is surrounded by the Western Black Sea and Sakarya Basins in the west, the Konya Closed Basin in the southwest, the Seyhan Basin in the south, the Euphrates and Tigris Basins in the southeast, and the Yeşilırmak Basin in the east (TOB, 2023). Statistical information for E15A035 and E15A038 stations selected in the study are given in Table 1.

Table 1. Descriptive statistics of the stations

Stations	Mean (m^3/s)	Min (m^3/s)	Max (m^3/s)
E15A035	1065.14	42.24	10327
E15A038	207.35	8.714	1649.3

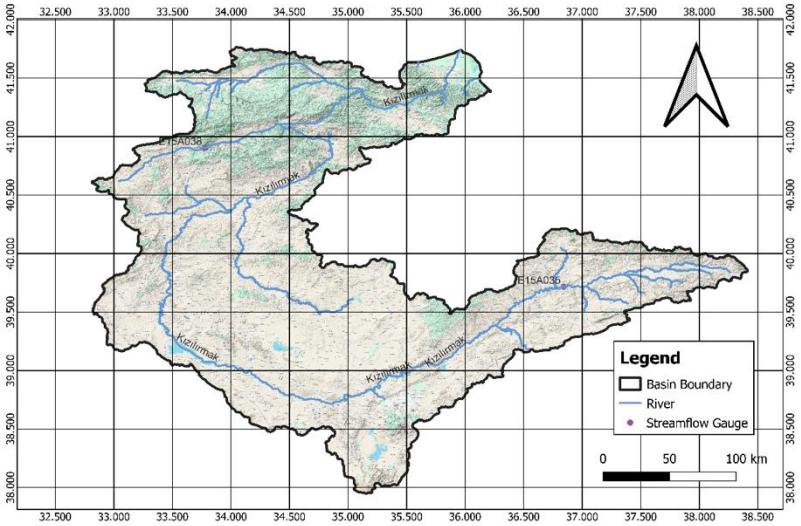

Figure 1. Study region

2.2. Run Theory

Run theory, introduced by Yevjevich in 1967, is employed to identify the severity and duration of drought when a random variable X falls below a specific threshold value X_0. According to run theory, if $X(t)$ remains continuously above X_0 over a chosen time interval Δt, this period is referred to as a positive run (wet period). Conversely, if $X(t)$ remains below X_0, it is defined as a negative run (dry period). Figure 2 illustrates the concept of run theory, where S_1 and S_2 represent drought severity, while D_1 and D_2 indicate drought duration.

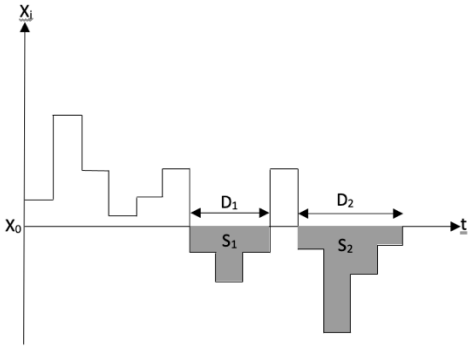

Figure 2. The concept of run theory

2.3. Streamflow Drought Index

Streamflow Drought Index (SDI), developed by Nalbantis (2008), is used to determine hydrological drought with monthly mean streamflow values. The SDI value is calculated with Equation 1, where $V_{i,k}$ (m^3/s) is the cumulative stream flow in different periods from $k=1$ to 4, V_k is the mean of cumulative streamflow for the reference period, S_k is its standard deviation and N is number of year.

$$SDI_{i,k} = \frac{V_{i,k} - \overline{V_k}}{S_k} \qquad i = 1,2,3,\dots,N \tag{1}$$

3. Results and Discussion

In this study, the severity and duration of hydrological droughts at stations E15A035 and E15A038 located in the Kızılırmak Basin were analyzed using Run Theory. For this purpose, firstly, the Streamflow Drought Index (SDI) values were calculated for the 3-, 6-, 9- and 12-months periods using the monthly total flow data for the 1987-2015 water years. Then, Run Theory was applied to the SDI values to obtain the drought severity and duration values. The threshold value was selected as "0" in Run Theory. The time series of the SDI values for the 3-, 6-, 9- and 12-months periods for station E15A035 are presented in Figure 2.

Upon examining Figure 2, it can be observed that the longest drought durations were as follows: 23 months between April 2003-February 2005 in the 3- month period; 40 months between November 2001-February 2005 in the 6- month period; 37 months between February 2002-February 2005 in the 9- month period and 35 months between April 2002-February 2005 in the 12- month period. The time series of SDI values in all periods for station E15A038 are given in Figure 3.

When Figure 3 is examined, it is seen that the longest drought periods at station E15A038 are 38 months between December 2006-January 2010 for 3- month period; 41 months between December 2006-April 2010 for 6- month period; 43 months between January 2007-July 2010 for 9- month period and 57 months between February 2006-October 2010 for 12- month period. Additionally, Figure 4 shows the drought severity for stations E15A035 and E15A038.

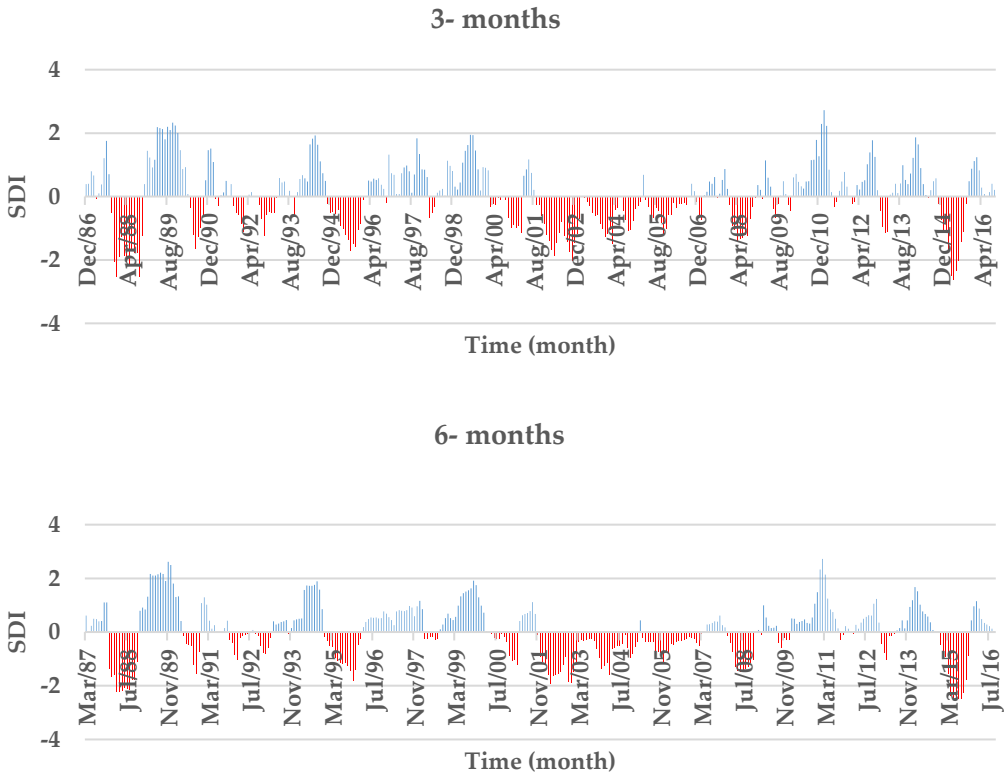

Figure 2. Time series of SDI for E15A035 station

Figure 2 (continue). Time series of SDI for E15A035 station

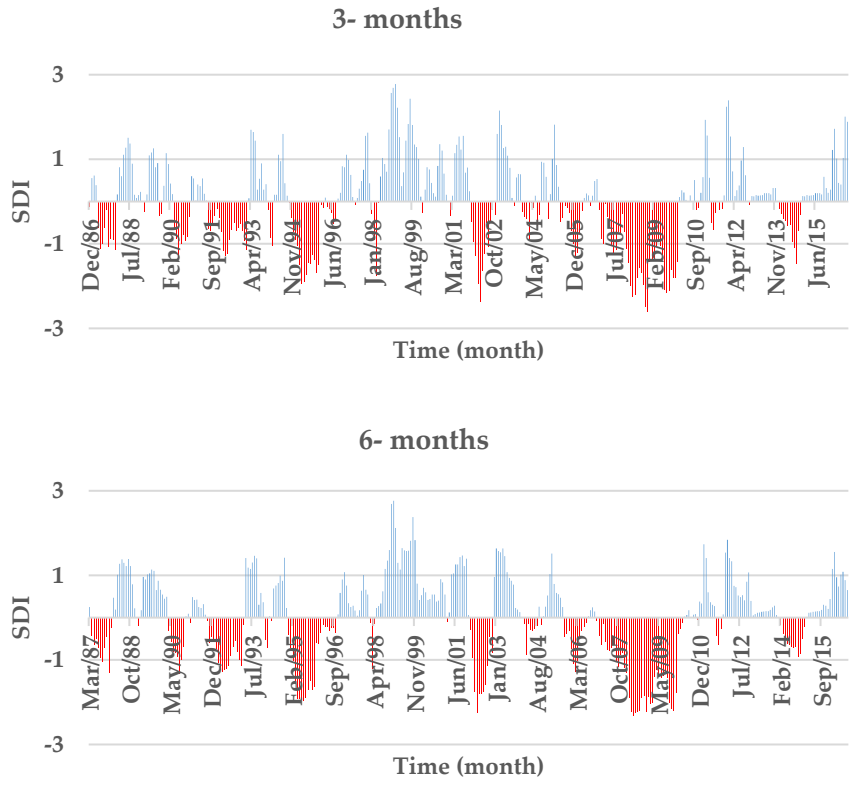

Figure 3. Time series of SDI for E15A038 station

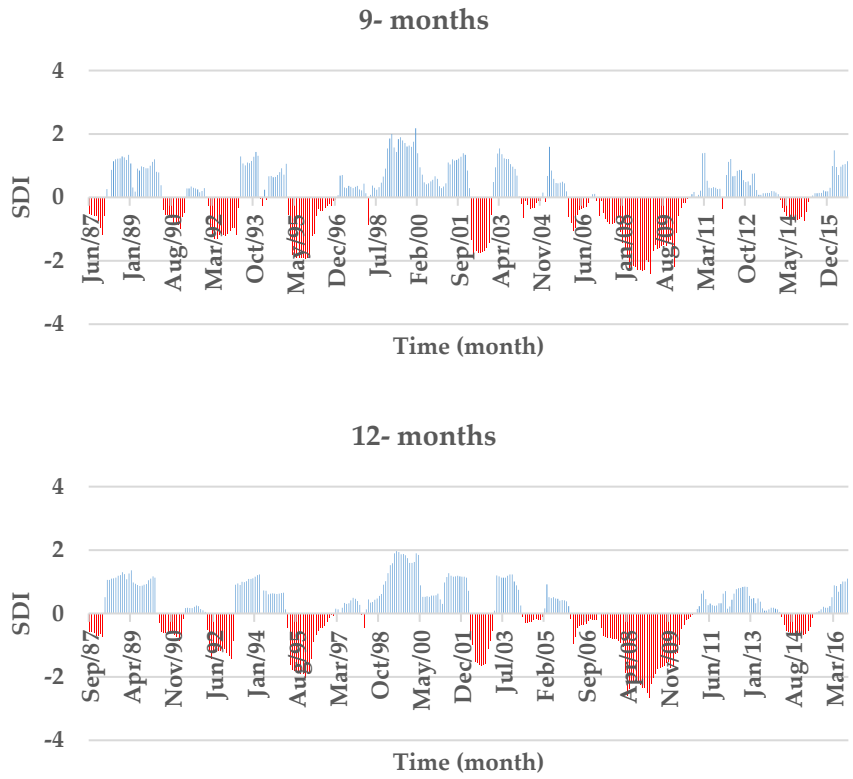

Figure 3 (continue). Time series of SDI for E15A038 station

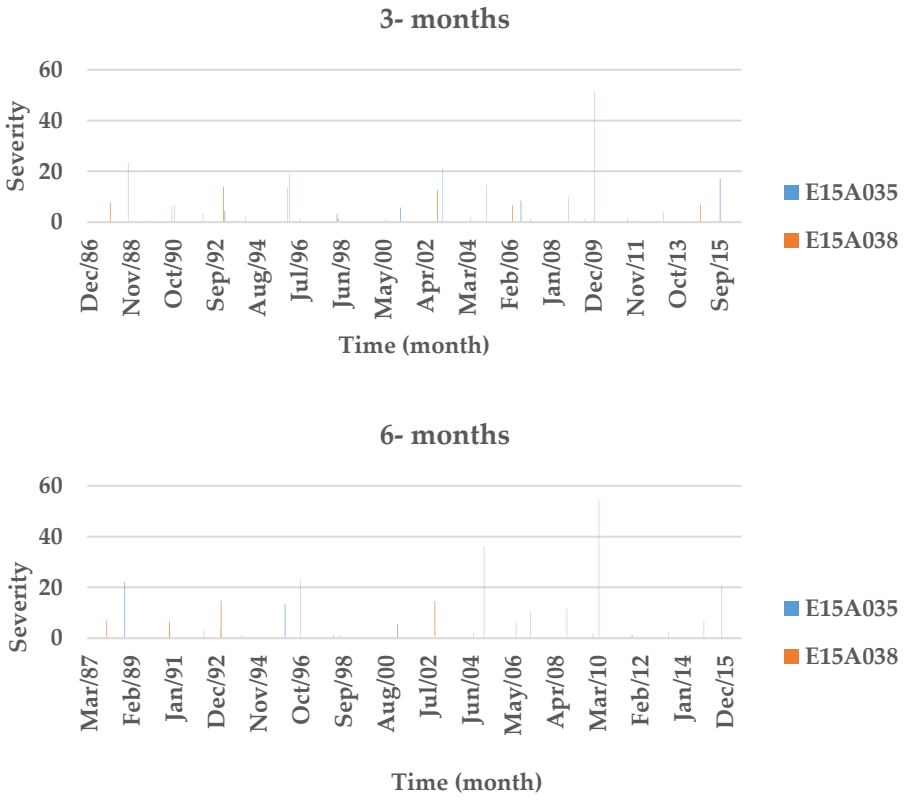

Figure 4 . Drought severity of E15A035 and E15A038 stations

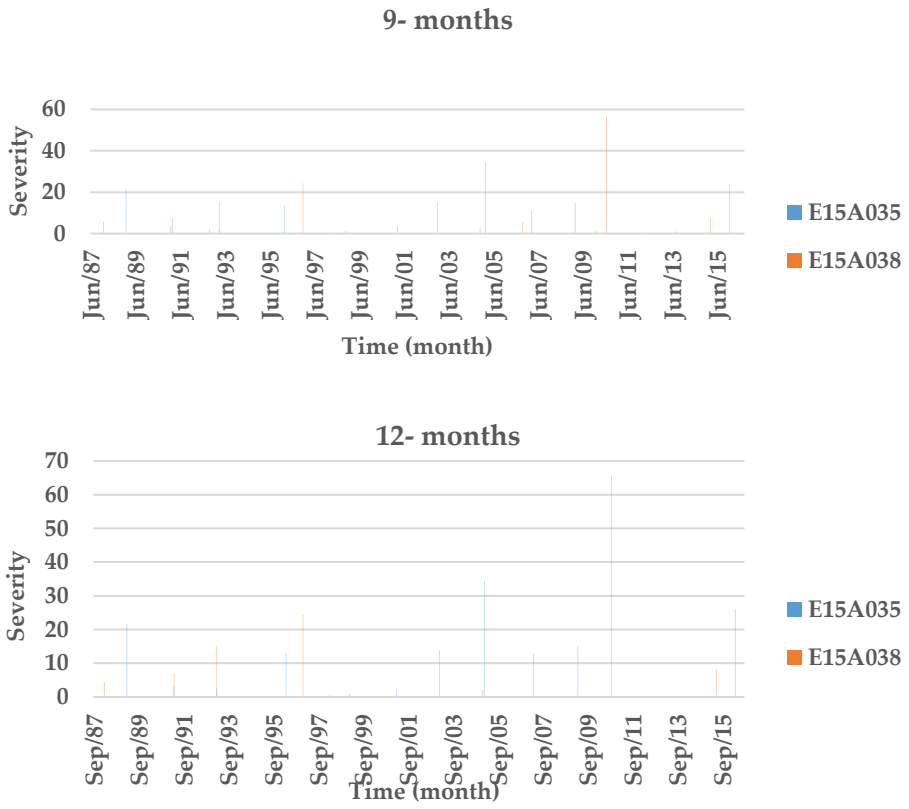

Figure 4 (continue). Drought severity of E15A035 and E15A038 stations

When examining Figure 4 to better understand the relationship between the drought severities of the two stations, it is observed that, in the 3-month period after the year 2000, the drought at the E15A035 station was more severe than at the E15A038 station. In the time interval before the year 2000, the drought severities at both stations were generally similar and occurred simultaneously. In the 6-month period, E15A038 station generally experienced more severe droughts than E15A035 station with a delay of 4 to 8 months. E015A38 station experienced more severe droughts with a delay in the 9-month period. The longest and most severe droughts were observed for E15A038 station in October 2010 and for E15A035 station in February 2005 in all periods. Since E15A038 station is downstream of E15A035 station and on a side branch, the droughts experienced in E15A038 station were delayed and more severe. Also, the drought durations of E15A035 and E15A038 stations were given in Figure 5.

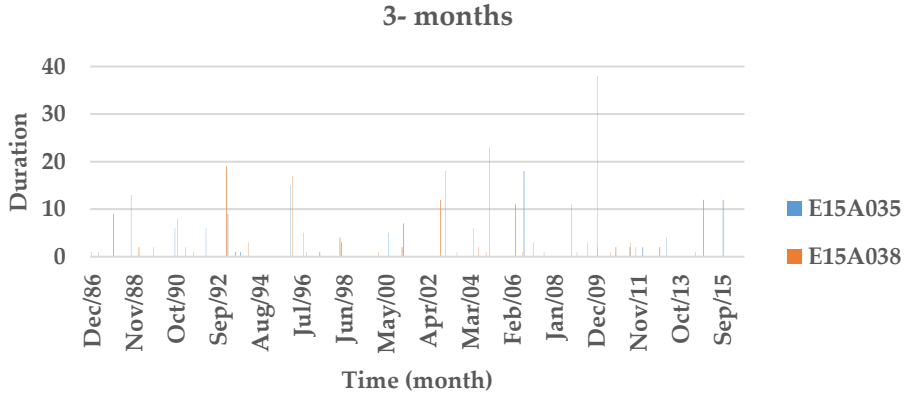

Figure 5. Drought duration of E15A035 and E15A038 stations

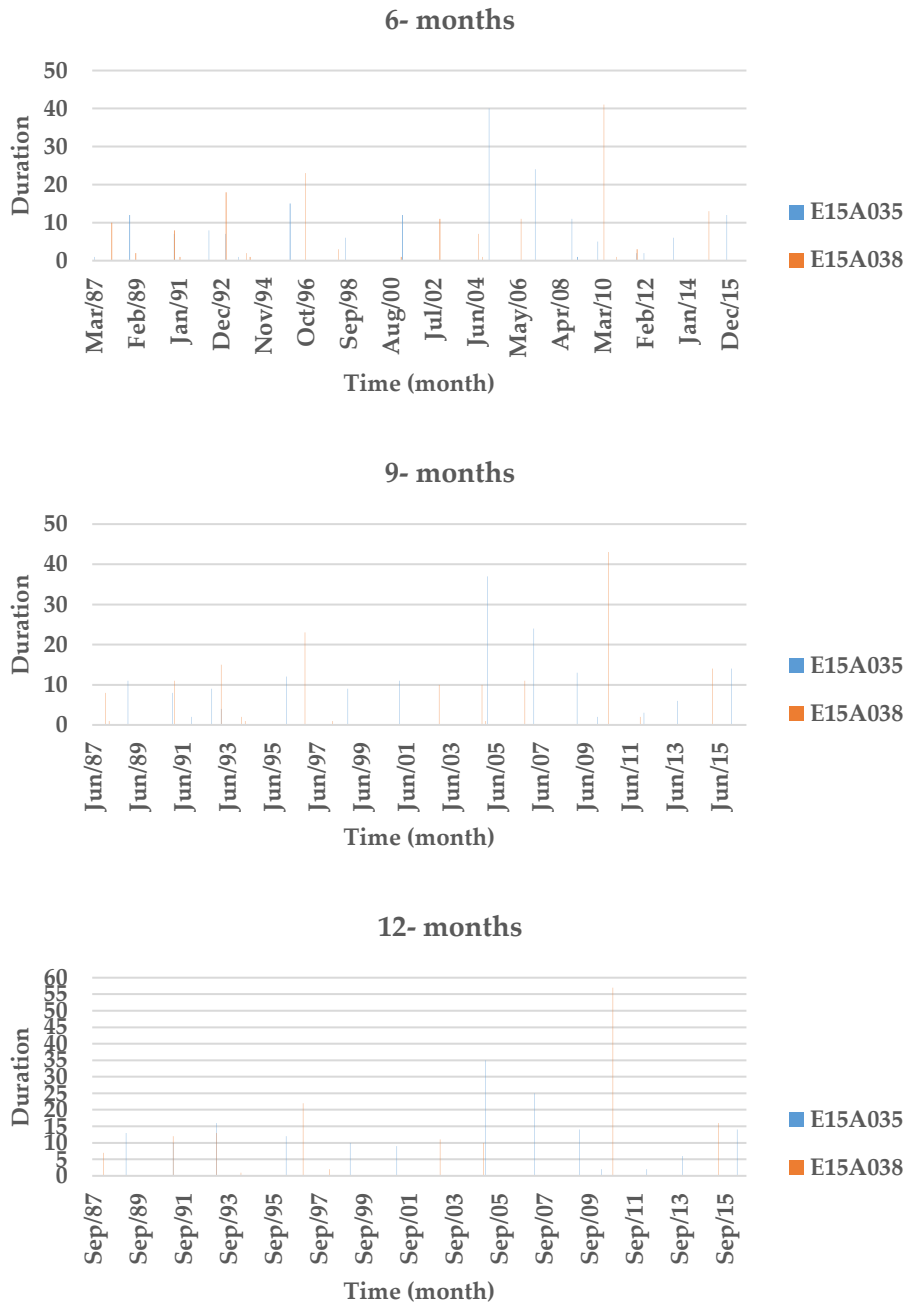

Figure 5 (continue). Drought duration of E15A035 and E15A038 stations (continue)

When the drought durations of both stations given in Figure 5 are examined, similar characteristics are observed in terms of drought severity. While longer droughts were experienced at station E15A038, a longer drought was observed at station E15A035 in February 2005.

4. Conclusion

This study aims to examine the severity and duration of droughts in the Kızılırmak Basin using the run theory. For this purpose, monthly streamflow data from the observation stations E15A035 and E15A038, covering the period 1987-2015, were used. The Streamflow Drought Index (SDI) was calculated for 3-, 6-, 9-, and 12- month periods, and drought severity and duration were analyzed using run theory. As a result of these analyses, the differences between the droughts observed at the two stations were revealed.

Station E15A035:

- **3- month period:** The longest drought occurred between April 2003 and February 2005, lasting 23 months in total. The most severe drought during this period was calculated as 23.40.
- **6- month period:** A drought lasted for 40 months between November 2001 and February 2005, with the most severe drought value recorded as 36.25.
- **9- month period:** A drought period lasting 37 months was observed between February 2002 and February 2005, and the drought severity was calculated as 34.50.
- **12- month period:** The longest drought occurred between April 2002 and February 2005, lasting 35 months, with the most severe drought value determined to be 34.45.

Station E15A038:

- **3- month period:** A drought period lasting 38 months was experienced between December 2006 and January 2010, with the most severe drought value during this time calculated as 51.70.
- **6- month period:** A drought lasting a total of 41 months was observed between December 2006 and April 2010, with the most severe drought value recorded as 54.60.
- **9- month period:** A severe drought was experienced during the 43-month drought period between January 2007 and July 2010, and the drought severity of this period was determined as 56.95.
- **12- month period:** The most severe drought value was measured as 65.61 during the 57-month drought period between February 2006 and October 2010.

The results obtained indicate that the droughts at the E15A038 station were both longer in duration and more severe compared to the E15A035 station. In particular, it is observed that drought conditions at the E15A038 station were much more pronounced in longer periods (9 and 12 months). These differences suggest that the regional topographic, meteorological, and hydrological conditions in the Kızılırmak Basin show local variability and that these conditions should be considered in water management strategies. These results are important for drought management and water resource planning and may provide guidance for future hydrological analyses and water management policies. Particularly in regions where drought durations are long and severity is high, strategies should be developed to use water resources more efficiently and reduce drought risk.

Acknowledgements

This study was carried out within the scope of the project numbered 123C431 “Development of Multivariate Drought Index Based on Copula and Entropy Weight Method for Assessment of Future Droughts” supported by TUBITAK.

References

Gümüş, V. (2017). Hydrological Drought Analysis of Asi River Basin with Streamflow Drought Index. Gazi University Journal of Science Part C: Design and Technology, 5(1), 65-73.

Jahangir, M. H., & Yarahmadi, Y. (2020). Hydrological drought analyzing and monitoring by using Streamflow Drought Index (SDI)(case study: Lorestan, Iran). Arabian Journal of Geosciences, 13, 1-12. https://doi.org/10.1007/s12517-020-5059-8

Malik, A., Kumar, A., Salih, S. Q., & Yaseen, Z. M. (2021). Hydrological drought investigation using streamflow drought index. intelligent data analytics for decision-support systems in Hazard mitigation: theory and practice of hazard mitigation, 63-88. https://doi.org/10.1007/978-981-15-5772-9_4

Myronidis, D., Ioannou, K., Fotakis, D., & Dörflinger, G. (2018). Streamflow and hydrological drought trend analysis and forecasting in Cyprus. Water resources management, 32, 1759-1776. https://doi.org/10.1007/s11269-018-1902-z

Nalbantis, I. (2008). Evaluation of a hydrological drought index. European Water, *23*(24), 67-77.

Özfidaner, M., Şapolyo, D., & Topaloğlu, F. (2018). Hydrological Drought Analysis of Streamflow Data in Seyhan Basin. Soil Water Journal, 7(1), 57-64. https://doi.org/10.21657/topraksu.410140

Simsek, O. (2021). Hydrological drought analysis of Mediterranean basins, Turkey. Arabian Journal of Geosciences, 14(20), 2136. https://doi.org/10.1007/s12517-021-08501-5

Tabari, H., Nikbakht, J., & Hosseinzadeh Talaee, P. (2013). Hydrological drought assessment in Northwestern Iran based on streamflow drought index (SDI). Water resources management, 27, 137-151. https://doi.org/10.1007/s11269-012-0173-3

Tareke, K. A., & Awoke, A. G. (2022). Hydrological drought analysis using streamflow drought index (SDI) in Ethiopia. Advances in Meteorology, 2022(1), 7067951. https://doi.org/10.1155/2022/7067951

TOB (2023). 6 Havzada Nehir Havzası Yönetim Planlarının Hazırlanması İçin Teknik Yardım. (2023, July 13). Retrieved June 26, 2024, from https://www.tarimorman.gov.tr/SYGM/Belgeler/ÖSYK%20Rapor%20Marmara-Doğu%20Akdeniz-%20Antalya%20Havzaları/Kızılırmak%20Havzası.pdf (In Turkish)

Yevjevich, V. M. (1967). An objective approach to definitions and investigations of continental hydrologic droughts (Vol. 23, p. 25). Fort Collins, CO, USA: Colorado State University.

Transportation

CivilTech
2nd International Symposium on Innovations in Civil Engineering and Technologies
October 30 – November 1, 2024, Isparta / TURKIYE

From Keywords to Trends: Bibliometric Analysis of Artificial Intelligence Methods in Asphalt Pavement Research With R-Studio Program

Fatih Ergezer[1], *Serdal Terzi*[1]

* *fatihergezer@sdu.edu.tr*

Abstract

Asphalt pavements are the most widely used pavement type in the world. There has been an increase in the use of artificial intelligence algorithms in the design and modeling processes of asphalt pavements. This study conducts a bibliometric analysis of the "asphalt pavement" keyword and its use in artificial intelligence models. Accordingly, 2544 articles in the English language in the Science Citation Index Expanded (SCI-E), Emerging Sources Citation Index (E-SCI), and Social Sciences Citation Index (SSCI) indexes were retrieved by searching the Web of Science (WOS) database, covering the period between 2000 and 2024. For the bibliometric analysis of the articles obtained, the R-Studio program was used to analyze the number of articles produced on an annual basis, the average number of citations per year, the most relevant journal analysis, the most cited journal analysis, the most relevant author analysis, the article production analysis of authors, the most relevant affiliations analysis, the country distribution analysis of corresponding authors, author-country-keyword triple match analysis, the most used word analysis, trend topic analysis, and co-occurrence analysis. The research findings were then evaluated.

Keywords: Bibliometric analysis, asphalt pavement, artificial intelligence, r-studio, web of science

[1] *Department of Civil Engineering, Suleyman Demirel University, Isparta, Turkiye*

1. Introduction

Asphalt pavements are the world's most widely used type of pavement, designed using aggregates, bitumen as a binder, and other additives if necessary (Chang et al., 2020). Asphalt pavements are temperature-sensitive and are affected by climatic factors such as precipitation, moisture, and vehicle traffic in the region they serve. These factors cause or accelerate the formation of cracks in asphalt pavements (Sun et al., 2018), rutting (Zhang et al., 2021), aging (Saleh et al., 2020), and fatigue damage (Qui et al., 2020).

Today, with the development of technology, artificial intelligence applications are widely used in the field of transportation as in every field. Especially in road engineering, studies on the use of artificial intelligence algorithms and methods such as deep learning, machine learning, artificial neural networks, time series analysis, explainable artificial intelligence, decision support systems, decision trees, long short-term memory (LSTM), classification, and artificial neural networks have gained momentum.

When examining studies on the use of artificial intelligence in asphalt pavements, several notable applications emerge: the use of ensemble machine learning to predict the International Roughness Index (IRI) in asphalt pavements (Baykal et al., 2023), the use of deep learning algorithms to evaluate the severity of crack formation in pavements (Baduge et al., 2023), the use of deep learning to classify the severity of cracks (Liu et al., 2022), the use of machine learning for pavement performance modeling in warm climate regions (Zeiada et al, 2020), the use of machine learning algorithms in recycled asphalt pavements (Botella et al., 2022), the use of deep learning algorithms to predict the surface condition of asphalt pavements based on meteorological factors (Baykal et al., 2022), the use of extreme gradient boosting algorithms to predict the modulus of elasticity of flexible pavements (Benemaran et al., 2023), and the classification of aggregate angularity (Pei et al., 2020). Additionally, the use of wireless sensors and machine learning algorithms for compaction prediction of asphalt pavements (Yu and Shen, 2023), the estimation of Jc parameters of asphalt pavements subjected to long-term aging by SCB test and mid-temperature samples using the random forest algorithm (Ma et al., 2024), prediction of rut depths of asphalt pavements using deep learning (Deng and Shi, 2024), use of an automatic decision-making preventive maintenance system for highway pavements based on deep learning (Li et al., 2022), the use of ANN modeling to predict indirect tensile test parameters for performance evaluation of asphalt pavements (Kim et al., 2021), and the use of Fuzzy C-means algorithms to determine the climate zones of asphalt pavements (Fang et al., 2023) are also notable.

Since the mechanical and physical properties of asphalt pavements vary depending on many factors, different artificial intelligence applications can be applied for each factor. The main objective of this study is to perform a bibliometric analysis of Web of Science (WOS) data to highlight the importance of using artificial intelligence methods and algorithms in asphalt pavements. Bibliometric analysis is a type of analysis that allows for a systematic literature search (Segundo et al., 2023). Recently, bibliometric analysis studies have been carried out in the field of transportation (Chang et al., 2020; Jiang et al., 2024; Rahman et al., 2023; Acebo et al., 2018; Ramirez et al., 2023). Within the scope of the study, articles are researched with keywords using WOS data between 2000 and 2024, and bibliometric analysis is carried out using the R Studio program.

2. Method

After giving brief information about bibliometric analysis in the Method section, information about the data sets to be used in the bibliometric analysis study is given.

2.1. Bibliometric analysis

Bibliometric analysis is a very important concept in searching academic studies prepared at the national or international level by searching different databases with keywords and researching trend studies in the relevant field (Alsharif et al., 2020). Bibliometric analysis has gained great importance recently. Its popularity has been supported by the developments in scientific journal databases, especially in recent years. Using large databases such as WOS and Scopus, studies can be analyzed using applications such as R-studio and Vosviewer (Donthu et al., 2021). With bibliometric analysis, data can be made sense of, and mapping can be done by listing at the desired level.

2.2. Creating the dataset

In the study, the R-Studio program is used for bibliometric analysis. WOS database is used to create the dataset. To perform the analyses in the study, keywords are selected in all fields ("*asphalt pavement*" or "highway pavement" or "flexible pavement") and ("modeling" or "algorithm" or "deep learning" or "machine learning" or "artificial neural network" or "time series" or "Shap" or "Explainable Artificial Intelligence" or 'decision tree' or 'fuzzy' or 'Ensemble' or 'random forest' or 'gradient boosting' or 'extra tree' or 'XGBoosting' or 'Adaboosting' or 'LSTM' or 'prediction' or 'Estimation' or 'KNeighborsRegressor' or 'CatBoost' or 'classification' or 'artificial intelligence'). The first keyword is searched with the connector, while the second keyword was searched with the connector and, linking it to the types of artificial intelligence in the second part. Between 2000 and 2024, 2544 articles were found by searching WOS data in the English language in Science Citation Index Expanded (SCI-E), Emerging Sources Citation Index (E-SCI), and Social Sciences Citation Index (SSCI) indexes, only in article type. The dataset characteristics of the study are given in Table 1.

Table 1. Dataset

Time interval	2000-2024
Number of articles	2544
Number of authors	5110
International co-authorship rate	26.61%
Author keyword count	6319
Number of references	55050
Average number of citations per article	15.08

3. Results and Discussion

For the bibliometric analysis of WOS data under the research findings, analyses are carried out separately according to the categorical distribution of the studies. In the study, the number of articles produced on an annual basis, the average number of citations per year, the most relevant journal analysis, the most cited journal analysis, the most relevant author analysis, the article production analysis of authors, the most relevant affiliations analysis, the country distribution analysis of corresponding authors, author-country-keyword triple match analysis, the most used word analysis, trend topic analysis, and co-occurrence analysis of the keywords are performed.
Figure 1 shows the number of articles produced on an annual basis covering the period between 2000 and 2024 when the bibliometric study was conducted. According to this, it is seen that the lowest number of articles was in 2001, while the highest number of articles was in 2023.

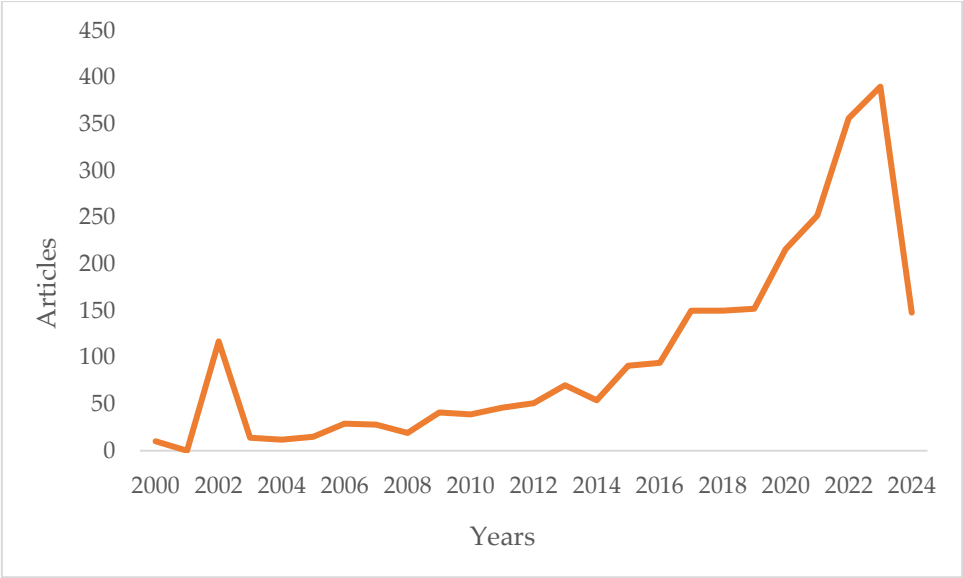

Figure 1. Number of scientific articles produced on an annual basis between 2000 and 2024.

Figure 2 shows the average number of citations per year between 2000 and 2024. Accordingly, it is seen that the lowest annual average number of citations was in 2000, while the highest annual average number of citations was in 2020.

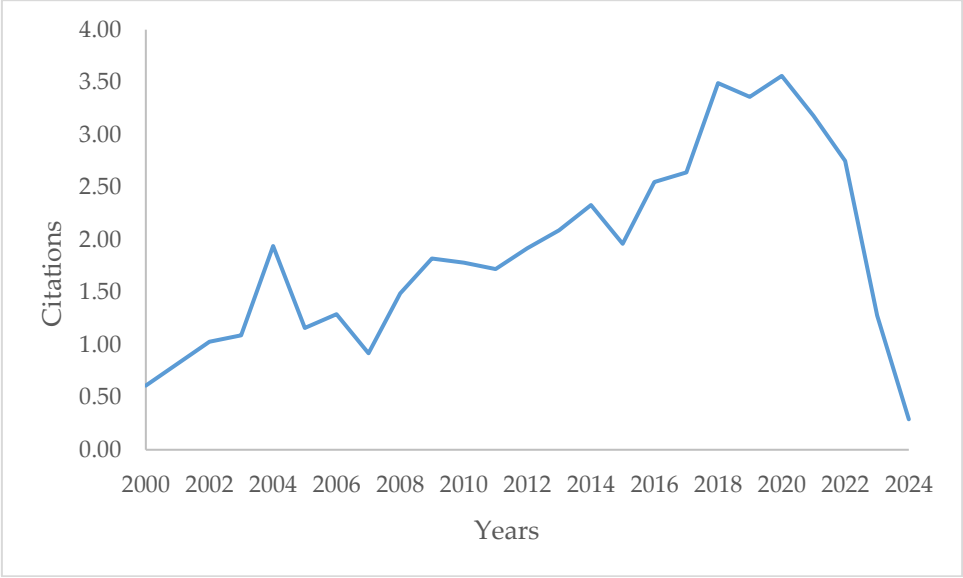

Figure 2. Average number of citations per year between 2000 and 2024

Figure 3 shows the list of the top 25 most relevant journals for the articles scanned in the WOS database for bibliometric analysis. According to this, it is seen that the highest number of publications in keyword matching is given in the journal "Construction and Building Materials" with 436 publications, followed by "International Journal of Pavement Engineering". It is seen that the least relevant journal among the top 25 is the KSCE Journal of Civil Engineering.

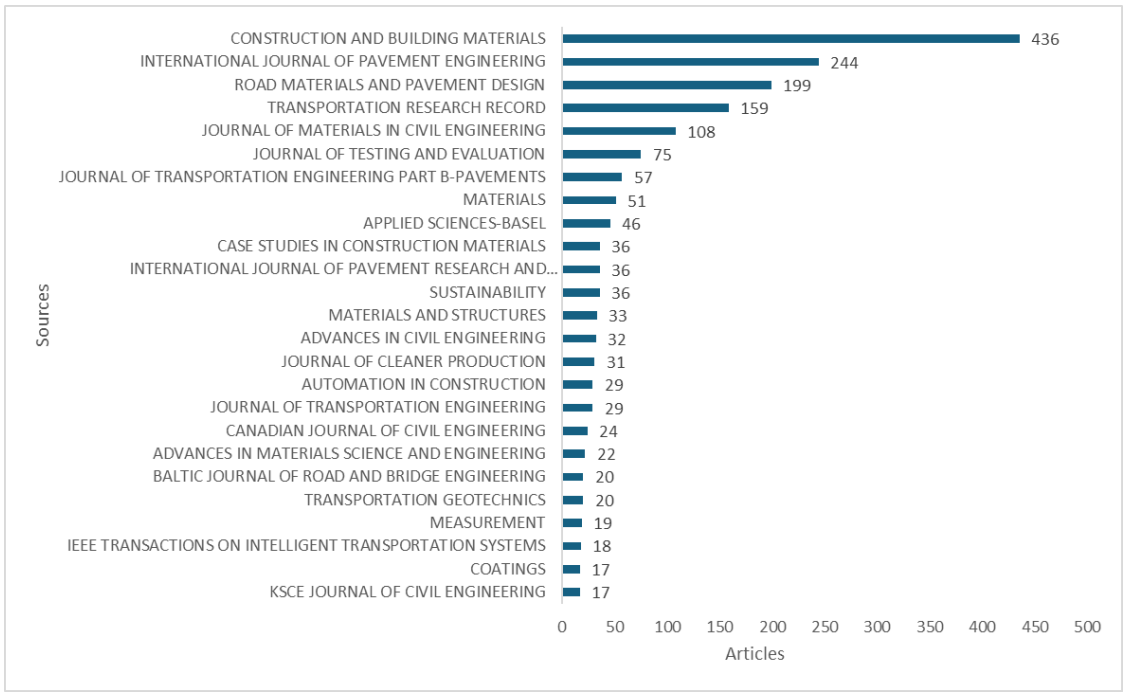

Figure 3. The most relevant journal list

In Figure 4, the journal citation analysis in the bibliometric analysis study between 2000 and 2024 is shown over the top 25 most cited journals. According to this, it is seen that the journal "Construction and Building Materials", which also ranks first in the most relevant journal list, ranks first with 8414 citations. "Transportation research record" is followed with 4916 citations. It is determined that the journal "Fuel" has the least number of citations in the top 25.

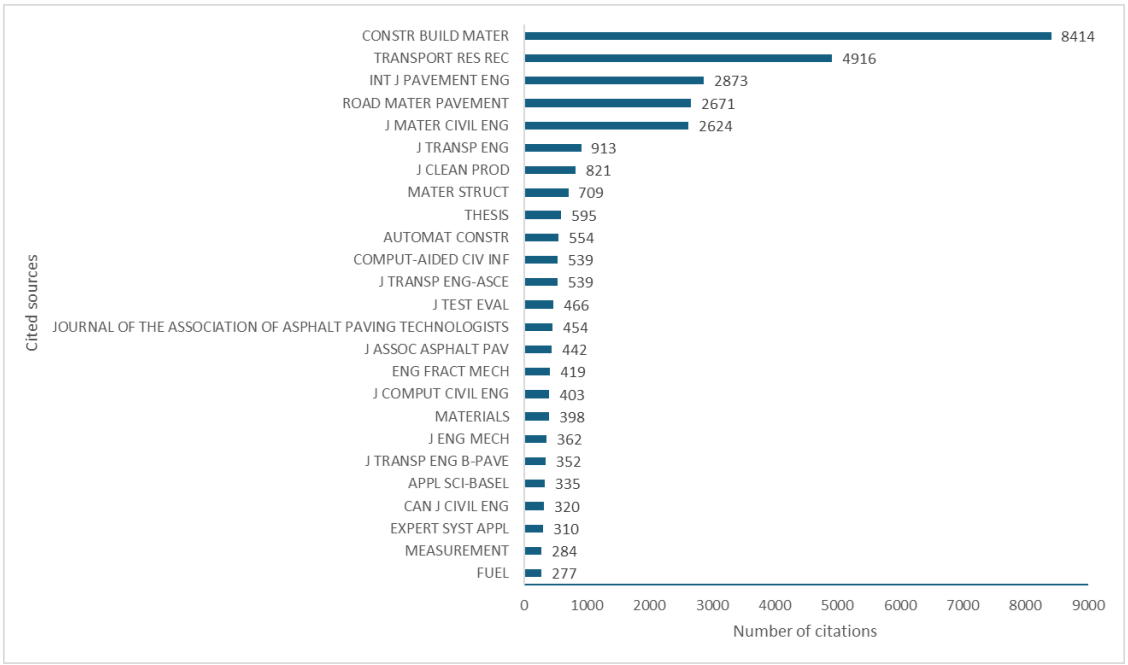

Figure 4. Journal citation analysis.

In Figure 5, within the scope of the bibliometric analysis study, according to the bibliometric analysis, Zhang Y comes in the second place with 55 WOS articles, followed by Zhang J with 49 WOS articles, considering the top 25 authors according to the most relevant author analysis based on the number of

articles according to the relevant keyword distribution between 2000-2024. Dong Q ranks 25th in the top 25 authors with 23 WOS articles.

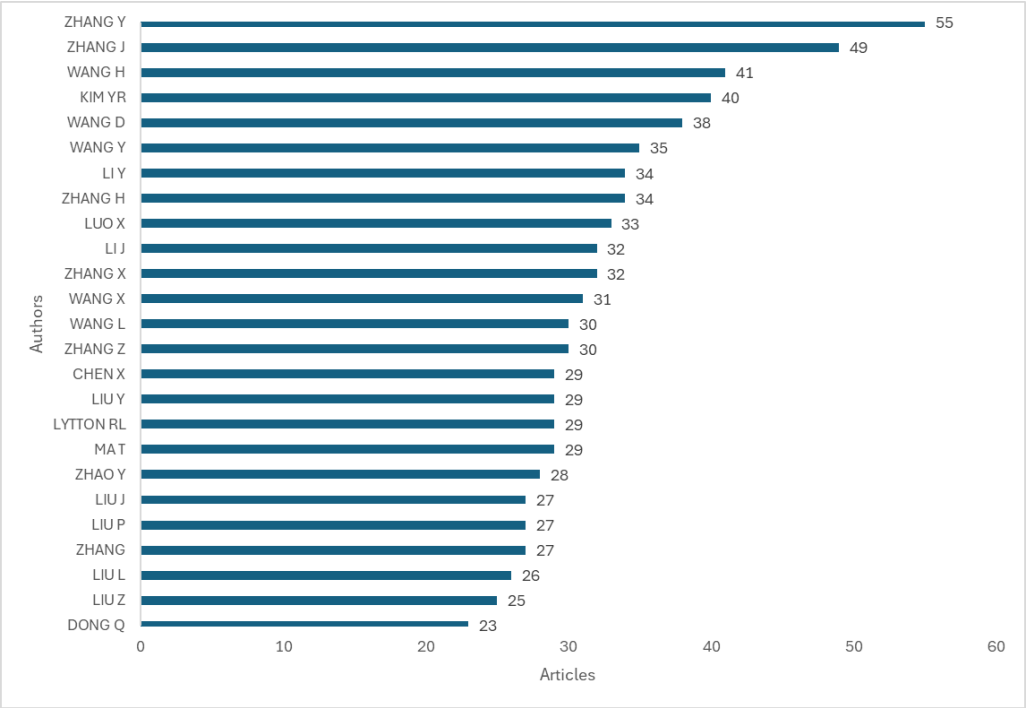

Figure 5. Most relevant author analysis

Figure 6 shows the article production performance analysis of the authors between 2000 and 2024. The first 10 authors with the highest production were included in the ranking. When Figure 6 is analyzed, it is determined that while the author Zhang Y had 1 article in 2013, he produced 6 articles in WOS in 2018 in the relevant keyword matching and reached the maximum number of articles in 2023 with 12 articles. Likewise, the author named Kim YR published his first article on relevant keyword matching in WOS in 2000 and then reached the highest number of articles in 2017 with 8 articles.

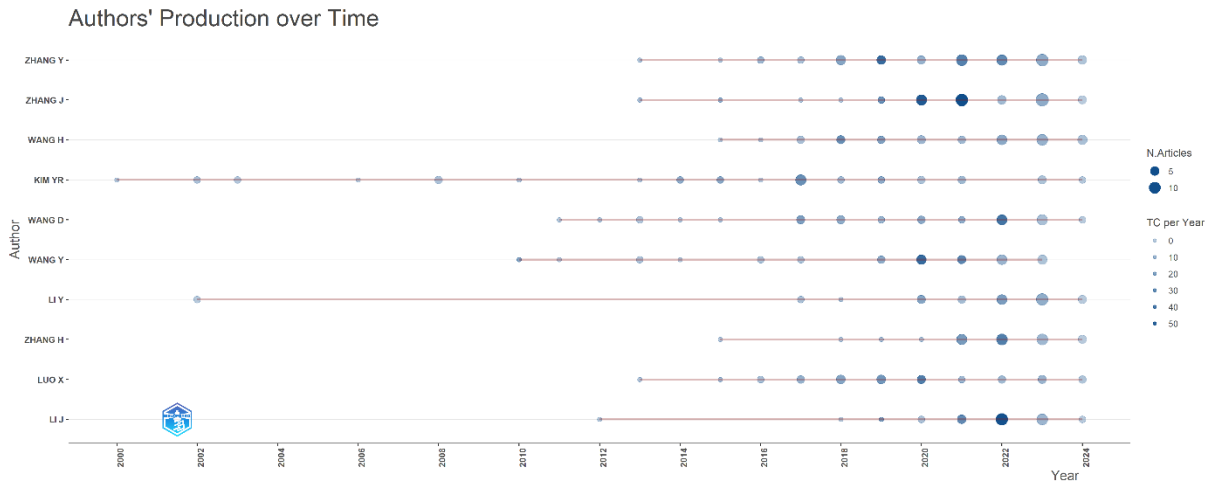

Figure 6. Authors' article production analysis

Figure 7 shows the ranking of the most relevant universities. In the analysis of the most relevant universities according to the relevant keyword matching in the WOS database between 2000 and 2024, Southeast University ranked first with 315 articles, while Changan University ranked second with 274

articles. According to the analysis of the top 25 universities, the University of Tennessee ranked 25th with 43 WOS database articles.

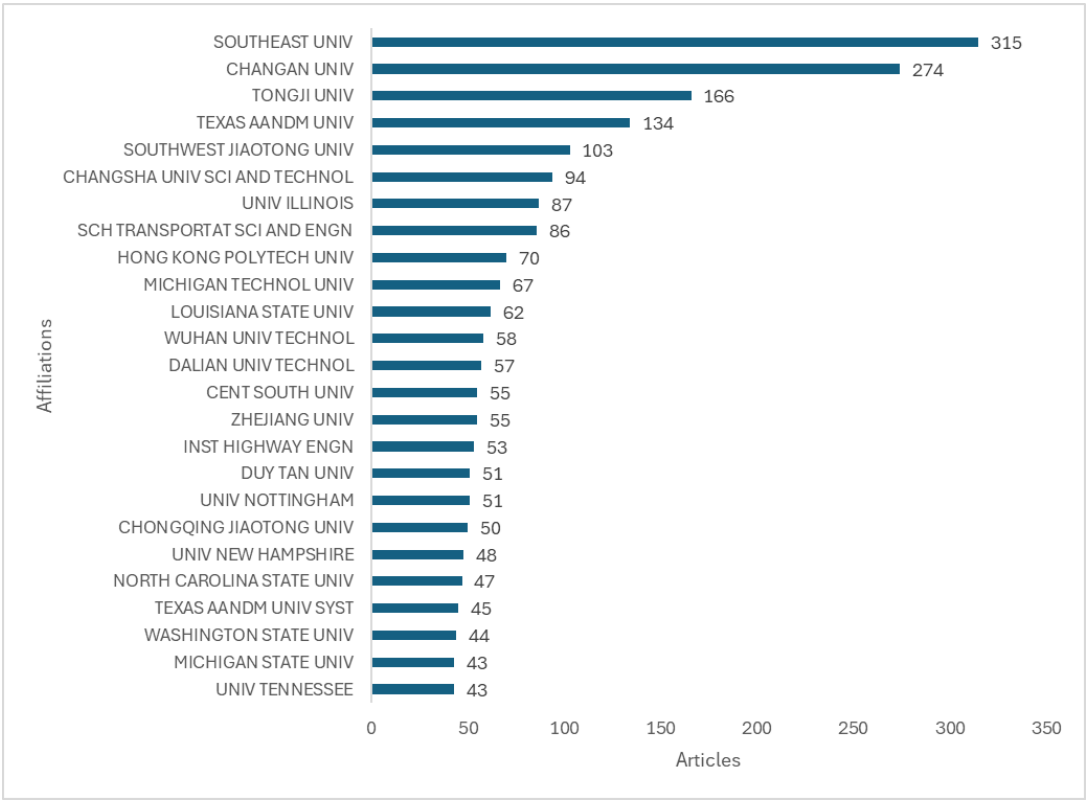

Figure 7. Most relevant affiliations

Figure 8 shows the distribution of the corresponding author's countries. According to the distinction between single-country publications and multi-country publications, China ranked first. The USA ranked second. Turkey, on the other hand, ranked 13th in the ranking, predominantly in the category of authors from other countries.

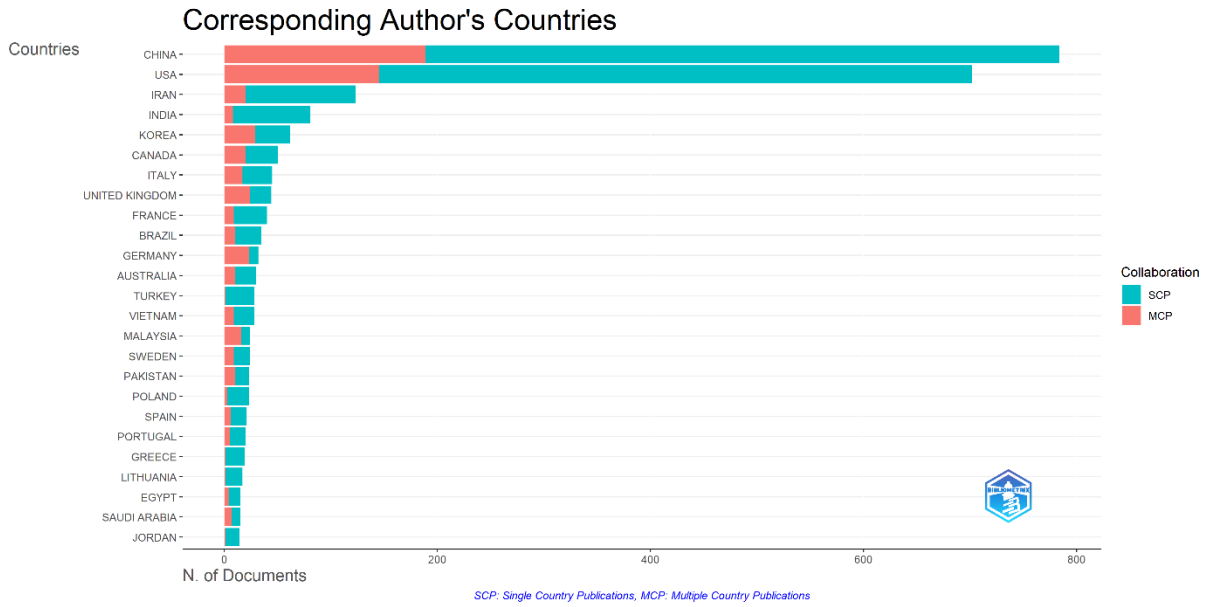

Figure 8. Corresponding author's countries analysis

Figure 9 shows a triple graph of author, country, and keyword matching. Accordingly, the keyword "asphalt pavements" appears to have a wide spectrum distribution, while China appears to have a wide distribution as a country. Among artificial intelligence methods, the keywords "machine learning", "deep learning", "prediction models", "prediction model", "prediction", "prediction", "artificial neural network", and "modeling" were included respectively. In the author matches, the distribution in the graph is given according to the country and keyword matches.

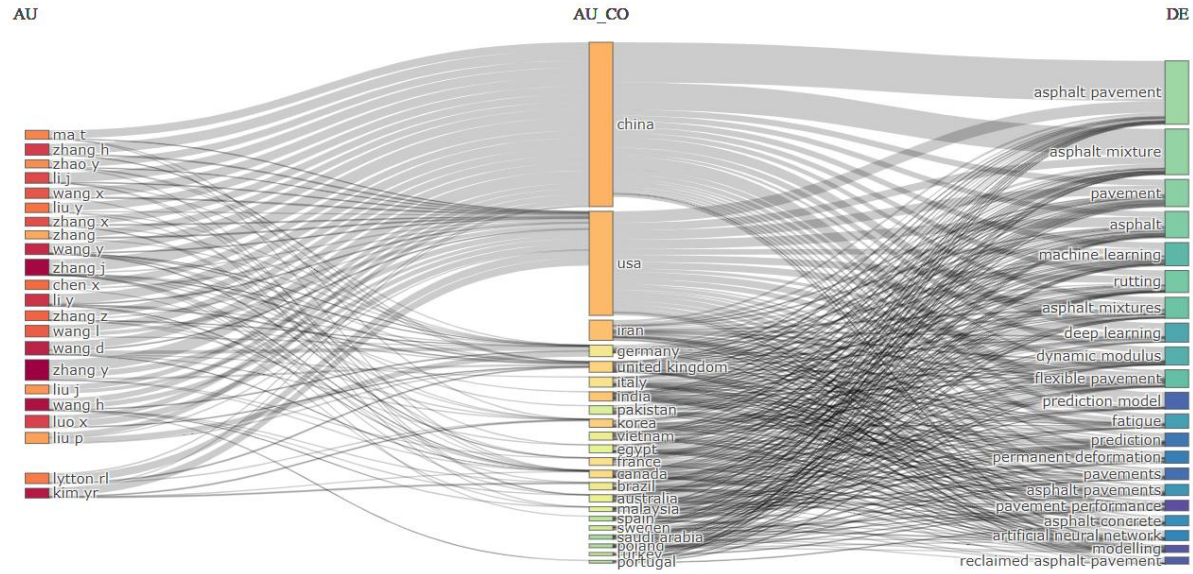

Figure 9. Relationship analysis between author, country, and keyword

Figure 10 shows a word cloud generated from the WOS data covering the period 2000-2024 analyzed in the bibliometric analysis study. According to this, the keyword "Asphalt pavement" is the most used word. Asphalt mixture is also among the words that occur predominantly. the distribution of other words is shown with a magnitude according to their weight. The distribution of terms such as machine learning, deep learning, finite element method, and neural network from artificial intelligence methods are also seen.

Figure 10. Work cloud

Figure 11 shows the trend topic analysis. According to the keyword results, the asphalt pavement keyword is seen as the most trending keyword with 229 frequencies in 2021 between 2000-2024. It is seen that the relationship between machine learning and asphalt pavements is among the trending studies with 72 frequencies in 2023.

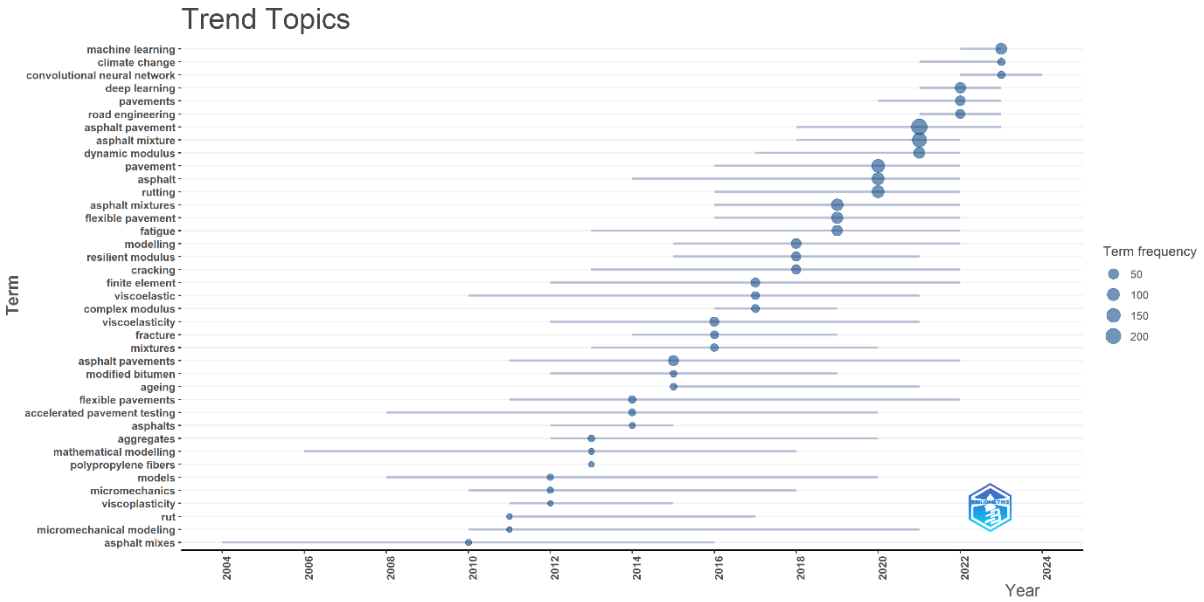

Figure 11. Trend topic analysis

Figure 12 shows the association analysis of keyword distributions. While the largest match is realized with the keyword asphalt pavement, the matches of other keywords according to their association sizes can be seen in Figure 13.

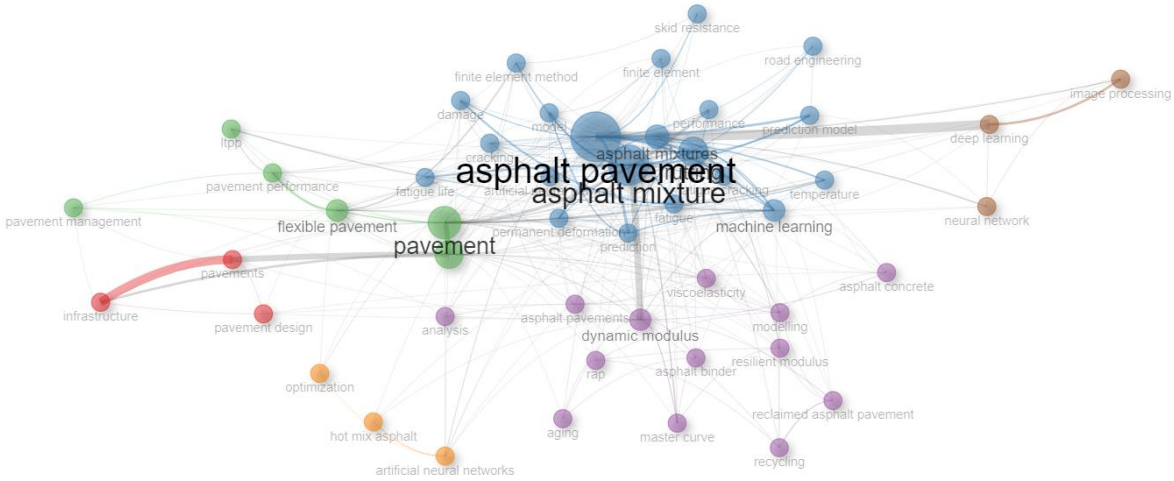

Figure 12. Co-occurrence analysis

4. Conclusions

In this study, a bibliometric analysis study was carried out for the use of artificial intelligence in asphalt pavements. For the bibliometric analysis study, 2544 articles covering the period between 2000-2024 were analyzed with the R-Studio program using the WOS database. The research findings are given below.

1. Based on the number of scientific articles produced, the highest number of publications was realized in 2023 with 390 articles. Compared to 2022, this value increased by 9.5%. In addition, the number of publications increased with the development of artificial intelligence algorithms compared to 2000, the first year of analysis, and a 38-fold increase in publications was observed in 2023 compared to 2000. Since 2024 has not yet been completed, it is thought that there will be an increase during the year.

2. When the average number of citations per year is analyzed, it is determined that the highest rate belongs to 2020. The lowest citation rate per year was determined as belonging to 2024 since 2024 has not yet been completed. Afterwards, the lowest citation rate belongs to the year 2000.

3. In the analysis of the most relevant journals according to the keyword search covering the years 2000-2024 among the journals published in the WOS database, it was determined that the journal "Construction and Building Materials" ranked first with 436 publications, while the "International Journal of Pavement Engineering" ranked second with 244 publications. According to the analysis study in which 25 journals were included in the ranking, it is seen that "KSCE Journal of Civil Engineering" ranks 25th with 17 publications.

4. In the study where the citation analysis of the journals was determined, the journal "Construction and Building Materials" was ranked first with 8414 citations, and the journal "Transportation Research Record" was ranked second with 4916 citations. According to the analysis study in which 25 journals were included in the ranking, the 25th ranked journal was "Fuel" with 277 citations.

5. After the journal analysis study, according to the keyword matching according to the author analysis, according to the most relevant author analysis, the author named "Zhang Y" ranked first with 55 publications and the author named "Zhang J" ranked second with 49 publications.
6. The article production performances of the authors from 2000 to 2024 were analyzed in the top 10 author bands. Accordingly, it was determined that while the author named Zhang Y had 1 article in 2013, he produced 6 articles in the relevant keyword match in WOS in 2018 and reached the maximum number of articles in 2023 with 12 articles. The production performances of all authors can be accessed in this way.

7. In the most relevant university analysis, "Southeast University" ranked first with 315 publications, while "Changan University" ranked second with 274 publications.

8. According to the country distribution analysis of related authors, China ranked first with 784 publications in the analysis of single-country and multi-country publications. The USA ranked second with 702 publications. Turkey ranked 13th with 28 publications and Jordan ranked 25th with 14 publications.

9. In the triple diagram with keyword, author, and country matching, the largest keyword range was determined as asphalt pavement, while China was the country.

10. According to the word cloud analysis, while the most used words were seen in large fonts, the keyword asphalt pavement was the most used word. It was determined that keywords such as asphalt mixture, pavement, deep learning, machine learning, modeling, and prediction are also frequently used in the cloud network.

11. According to the trend topic analysis study, the keyword asphalt pavement ranked first with a frequency value of 229. It was determined that other artificial intelligence keywords have also been among the trending topics recently.

12. As a final analysis, an association network for keyword matching was given. according to this, the highest number of associations was in the words asphalt pavement, asphalt mixture, pavement, and provided connections to other artificial intelligence algorithms.

According to the study, the results of the analysis were evaluated according to the matching of asphalt pavements with trending artificial intelligence models. In future studies, it is possible to add depth to the analysis by expanding the types of asphalt pavements and making the artificial intelligence models more specific.

References

Alsharif, A. H., Salleh, N. O. R. Z. M. D., & Baharun, R. (2020). Bibliometric analysis. Journal of Theoretical and Applied Information Technology, 98(15), 2948-2962.

Baduge, S. K., Thilakarathna, S., Perera, J. S., Ruwanpathirana, G. P., Doyle, L., Duckett, M., ... & Mendis, P. (2023). Assessment of crack severity of asphalt pavements using deep learning algorithms and geospatial system. Construction and Building Materials, 401, 132684.

Baykal, T., Ergezer, F., & Terzi, S. (2022). Prediction of highway pavement surface condition based on meteorological parameters using Deep Learning Method. Journal of Intelligent Transportation Systems and Applications, 5(2), 81-88.

Baykal, T., Ergezer, F., Eriskin, E., & Terzi, S. (2023). Using Ensemble Machine Learning to Estimate International Roughness Index of Asphalt Pavements. Iranian Journal of Science and Technology, Transactions of Civil Engineering, 1-12.

Botella, R., Lo Presti, D., Vasconcelos, K., Bernatowicz, K., Martínez, A. H., Miró, R., ... & Tebaldi, G. (2022). Machine learning techniques to estimate the degree of binder activity of reclaimed asphalt pavement. Materials and Structures, 55(4), 112.

Chang, X., Zhang, R., Xiao, Y., Chen, X., Zhang, X., & Liu, G. (2020). Mapping of publications on asphalt pavement and bitumen materials: A bibliometric review. Construction and Building Materials, 234, 117370.

Chang, X., Zhang, R., Xiao, Y., Chen, X., Zhang, X., & Liu, G. (2020). Mapping of publications on asphalt pavement and bitumen materials: A bibliometric review. Construction and Building Materials, 234, 117370.

da Rocha Segundo, I. G., Margalho, É. M., Lima Jr, O. D. S., Pinheiro, C. G. D. S., de Freitas, E. F., & Carneiro, J. A. S. O. (2023). Smart asphalt mixtures: A bibliometric analysis of the research trends. Coatings, 13(8), 1396.

Deng, Y., & Shi, X. (2024). Short-Term Predictions of Asphalt Pavement Rutting Using Deep-Learning Models. Journal of Transportation Engineering, Part B: Pavements, 150(2), 04024004.

Donthu, N., Kumar, S., Mukherjee, D., Pandey, N., & Lim, W. M. (2021). How to conduct a bibliometric analysis: An overview and guidelines. Journal of business research, 133, 285-296.

Fang, N., Chang, H., Hu, S., Li, H., & Meng, Q. (2023). Climate zoning of asphalt pavement based on spatial interpolation and Fuzzy C-Means algorithm. International Journal of Pavement Engineering, 24(2), 2072498.

Jiang, Q., Liu, W., & Wu, S. (2024). Technological advances and challenges of reclaimed asphalt pavement (RAP) application in road engineering—a bibliometric analysis from 2000 to 2022. Environmental Science and Pollution Research, 1-34.

Kim, D. H., Lee, S. J., Moon, K. H., & Jeong, J. H. (2021). Prediction of indirect tensile strength of intermediate layer of asphalt pavements using artificial neural network model. Arabian Journal for Science and Engineering, 46, 4911-4922.

Li, J., Yin, G., Wang, X., & Yan, W. (2022). Automated decision making in highway pavement preventive maintenance based on deep learning. Automation in Construction, 135, 104111.

Liu, F., Liu, J., & Wang, L. (2022). Deep learning and infrared thermography for asphalt pavement crack severity classification. Automation in Construction, 140, 104383.

Lozano-Ramírez, N. E., Sánchez, O., Carrasco-Beltrán, D., Vidal-Méndez, S., & Castañeda, K. (2023). Digitalization and Sustainability in Linear Projects Trends: A Bibliometric Analysis. Sustainability, 15(22), 15962.

Ma, Y., Liu, J., Mohammad, L. N., Cooper III, S. B., Cooper Jr, S. B., & Duvvuru, M. K. R. (2024). Use of Random Forest to Predict Intermediate Temperature SCB Jc Parameter of Long-Term Aged Asphalt Mixtures. Transportation Research Record, 2678(3), 177-189.

Pei, L., Sun, Z., Yu, T., Li, W., Hao, X., Hu, Y., & Yang, C. (2020). Pavement aggregate shape classification based on extreme gradient boosting. Construction and Building Materials, 256, 119356.

Pérez-Acebo, H., Linares-Unamunzaga, A., Abejón, R., & Rojí, E. (2018). Research trends in pavement management during the first years of the 21st century: A bibliometric analysis during the 2000–2013 period. Applied Sciences, 8(7), 1041.

Qiu, X., Xu, J., Xu, W., Xiao, S., Wang, F., & Yuan, J. (2020). Characterization of fatigue damage mechanism of asphalt mixtures with acoustic emission. Construction and Building Materials, 240, 117961.

Rahman, T., Irawan, M. Z., Tajudin, A. N., Amrozi, M. R. F., & Widyatmoko, I. (2023). Knowledge mapping of cool pavement technologies for urban heat island Mitigation: A Systematic bibliometric analysis. Energy and Buildings, 113133.

Saleh, N. F., Keshavarzi, B., Rad, F. Y., Mocelin, D., Elwardany, M., Castorena, C., ... & Kim, Y. R. (2020). Effects of aging on asphalt mixture and pavement performance. Construction and Building Materials, 258, 120309.

Sarkhani Benemaran, R., Esmaeili-Falak, M., & Javadi, A. (2023). Predicting resilient modulus of flexible pavement foundation using extreme gradient boosting based optimised models. International Journal of Pavement Engineering, 24(2), 2095385.

Sun, L., Wang, G., Zhang, H., & Liu, L. (2018). Initiation and propagation of top-down cracking in asphalt pavement. Applied Sciences, 8(5), 774.

Yu, S., & Shen, S. (2022). Compaction prediction for asphalt mixtures using wireless sensor and machine learning algorithms. IEEE Transactions on Intelligent Transportation Systems, 24(1), 778-786.

Zeiada, W., Dabous, S. A., Hamad, K., Al-Ruzouq, R., & Khalil, M. A. (2020). Machine learning for pavement performance modelling in warm climate regions. Arabian journal for science and engineering, 45(5), 4091-4109.

Zhang, W., Chen, X., Shen, S., Mohammad, L. N., Cui, B., Wu, S., & Raza Khan, A. (2021). Investigation of field rut depth of asphalt pavements using hamburg wheel tracking test. Journal of Transportation Engineering, Part B: Pavements, 147(1), 04020091.

2nd International Symposium on Innovations in Civil Engineering and Technologies
October 30 – November 1, 2024, Isparta / TURKIYE

Investigation of the Effects of Using Waste Vegetable Margarine in Bitumen Modification

Gizem Kaçaroğlu[1], *Öznur Karadağ*[1], *Mehmet Saltan*[1]

*gizemkacaroglu@sdu.edu.tr

Abstract

The use of various oils and their wastes in bitumen modification is quite common. In most of the studies in literature on bitumen modification, waste oils are used as rejuvenators and to soften hard neat bitumen or polymer modified bitumen. In this study, bitumen which has 50/70 penetration grade was modified with waste vegetable margarine at the ratios of 1, 2 and 3%. Physical properties of modified samples were investigated with the help of penetration, softening point, ductility and rotational viscometer tests. Penetration index values were calculated using the penetration and softening point test results to determine the temperature sensitivities of the samples. Moreover, stripping resistances and adhesion performances of them were investigated. Test results showed that the use of waste vegetable margarine results in an increase in the penetration and a decrease in the softening point. The temperature dependent susceptibility of the samples decreased as the additive ratio was increased. The rotational viscometer tests showed that both the mixing/compaction temperatures and ranges decreased as the additive ratio increased. In addition, it is possible to say that there will be a slight decrease in the stripping resistances of mixtures containing waste vegetable margarine modified bitumen. However, rising of waste vegetable margarine ratio in bitumen increased slightly adhesion performance. According to the results obtained, it was found that the modification with waste vegetable margarine can increase the resistance of bitumen to the conditions of cold climates by affecting the consistency.

Keywords: Waste vegetable margarine; bitumen modification; bitumen tests; stripping and adhesion.

[1] *Süleyman Demirel University, Department of Civil Engineering, Isparta, Turkey*

1. Introduction

Sustainable waste management, a concept that aims to protect natural resources, increase energy and resource efficiency, reduce waste and encourage recycling, by minimizing the environmental impacts of waste materials, has an increasing importance in many areas (Cucchiella et al., 2017; Rahman et al., 2020). One of these areas is the construction sector, and it is possible to say that many researches have been carried out prioritizing the protection of natural resources, especially in the construction of highway flexible pavements (Rahman et al., 2020; Milad et al., 2022). To serve this purpose, various waste materials can be added directly to asphalt mixtures as additives or used in the modification of bitumen, one of the two main materials of asphalt mixtures (Topaloğlu, 2019; Rahman et al., 2020; Duarte & Faxina, 2021; Alakara & Ağaoğlu, 2022). Thus, it is aimed to both utilize waste materials and minimize or delay deterioration that may occur in flexible pavements (Rahman et al., 2020; Ma et al., 2021).

To improve the performance of asphalt mixtures, and bitumen in particular, many different materials have been incorporated into asphalt pavements through the modification of bitumen (Porto et al., 2019; Kumandaş & Pancar, 2023). However, since some materials used for this purpose (e.g. polymers) offer very costly solutions (Fernandes et al., 2017) and, as mentioned above, ensuring sustainability has become important, the use of waste forms of most materials has begun to be preferred (Rahman et al., 2020). One of the materials that has recently become widespread in bitumen modification with an accent on sustainability is waste oils (Kumandaş & Pancar, 2023). Because waste oils are a type of waste that harms living creatures around it by polluting the environment, and has ecotoxic properties. Owing to disposal of them through bitumen modification, it is possible to get rid of these environmental damages and at the same time improve the performance of asphalt mixtures.

Due to their easy accessibility, the use of waste cooking or frying oils and waste engine oils is extremely common in studies (Kumandaş and Pancar, 2023). In most of the studies in literature on bitumen modification, these waste oils are used as rejuvenators (Zargar et al., 2012; Ji et al., 2017; Xinxin et al., 2018; El-Shorbagy et al., 2019; Joni et al., 2019; Li et al., 2019; Uz & Gökalp, 2020; Li et al., 2023; Ali et al., 2024) and to soften hard neat bitumen or polymer modified bitumen (Maharaj et al., 2015; Azahar et al., 2016; Al-Omari et al., 2018; Rasman et al., 2018; Çavdar et al., 2019; Adesina & Dahunsi 2020; Liu et al., 2020; Rodrigues et al., 2020; Eltwati et al., 2022). By softening the bitumen, these types of oils can reduce the mixing and compaction temperatures of asphalt pavements and increase the resistance of bitumen to aging and low temperature cracking. In fact, some studies have stated that by adding certain amounts of waste oils, aged bitumen can be returned to its original penetration grades and performances close to that of neat bitumen can be achieved (Xinxin et al., 2018; Joni et al., 2019; Nordiana et al., 2019; El-Shorbagy et al., 2019). Considering all these advantages, it is inevitable that waste oils will become a widely used additive. To obtain positive results regarding performance, it is recommended that the ratio of waste cooking oils in bitumen modification should not exceed 5% by bitumen weight (Hunter et al., 2015; Rahman et al., 2020). When it comes to waste engine oil, it is stated that the same ratio should be 5.5 - 6% (El-Shorbagy et al., 2019; Kumar & Aggarwal, 2023).

Within the scope of this study, bitumen which has 50/70 penetration grade was modified with waste vegetable margarine (WVM) at the ratios of 1, 2 and 3%. Physical properties of modified samples were investigated with the help of penetration, softening point, ductility and rotational viscometer tests. Penetration index (PI) values were evaluated using the penetration and softening point test results to determine the temperature sensitivities of the samples. Moreover, Nicholson stripping, California stripping and Vialit tests were carried out to investigate the stripping resistances and adhesion performances of them.

2. Material and Method

In this section, physical properties of reference bitumen and information about additive material (WVM) were given. Additionally, the test methods to be used in the study are also mentioned.

2.1. 50/70 Reference Bitumen

50/70 penetration graded bitumen was used in this study. Table 1 shows the average results of tests were applied for determining physical properties of reference bituminous binder.

Table 1. Physical properties of reference bitumen

Properties	50/70 Bitumen	
Penetration (0,1 mm)	51	
Softening Point (˚C)	49.3	
Ductility (cm)	>100	
Specific Gravity (g/cm^3)	1.017	
Viscosity (cP)	135˚C / 100 rpm	165˚C / 100 rpm
	497.8	132.5

2.2. Waste Vegetable Margarine (WVM)

Margarine is produced by adding skimmed milk, water, vitamins and milk proteins to vegetable oils such as sunflower oil, soybean oil, cottonseed oil, canola and palm. This food product, which is generally 60-70% vegetable, is the leading and perhaps the most used type of oils. Therefore, a large amount of waste of this food product is generated. Proper disposal of these waste oils is of great importance due to the environmental damage they cause. In this study, the waste of vegetable margarine (Figure 1), which was used only for frying specific products, was collected from a restaurant and included in the study after being filtered.

Figure 1. Waste vegetable margarine

2.3. Bitumen Modification

In this study, bitumen was modified to examine the effects of WVM on the 50/70 bitumen. WVM was added to bitumen at the ratios of 1%, 2% and 3% by weight. Modifications were carried out by the help of a temperature controlled high shear mixer at 160 °C and 2000 rpm for an hour.

2.4. Bitumen Tests and Penetration Index

Penetration (TS EN 1426), softening point (TS EN 1427), ductility (TS EN 13589) and rotational viscometer (ASTM D 4402) tests were carried out to determine the properties of reference bitumen and

modified samples. In addition, the PI values were calculated according to Equation (1) to determine the effect of WVM on the temperature susceptibility of the modified bitumen samples.

$$PI = \frac{1952 - 500\log(Pen_{25}) - 20SP}{50\log(Pen_{25}) - SP - 120} \quad (1)$$

2.5. Nicholson Stripping, California Stripping and Vialit Tests

When it comes to stripping performance, while the Nicholson stripping test evaluates the resistance of loose aggregate – bitumen mixtures against moisture resulting from the simultaneous presence of water and heat, the California stripping test presents the resistance of loose mixtures against water and traffic effects. Vialit is a test performed to determine how the adhesion between aggregates and bitumen is affected by the presence of water.

In this study, the Nicholson and California stripping tests were performed to examine the effect of modification of bitumen with WVM in terms of moisture – induced damage which can be observed with the help of loose mixes. In addition, the Vialit test was carried out to evaluate the adhesion between the reference and WVM modified bitumen samples and the aggregates.

3. Results and Discussion

The results of penetration, softening point and rotational viscometer tests carried out to investigate the physical properties of WVM modified samples as well as the reference bitumen are discussed in this section. PI values calculated by using softening point and penetration values were also interpreted. The results of the tests applied on the reference bitumen and WVM modified bitumen samples to investigate the adhesion and stripping performances are also included in this title.

3.1. Results of Bitumen Tests and PI Values

The effects of WVM modification on the penetration and softening point of bitumen can be seen in Figure 2. As can be seen in the graph, it is observed that the penetration values increase as the WVM ratio in bitumen increases; in parallel with this and as expected, softening point temperatures decrease. In similar studies in the literature, modification with waste oils showed similar effects on the bitumen (Azahar et al., 2016; Al-Omari et al., 2018; Rasman et al., 2018; Kumandaş & Pancar, 2023). These results show that modification with WVM softens the bitumen. This leads to the expectation that the rutting resistance that can be seen on the pavement in hot weathers will increase. However, it is also possible to say that the consistency change in this direction will increase the resistance to low temperature cracking, fatigue and ageing (Kumandaş & Pancar, 2023). In the ductility test carried out for the reference bitumen and samples with 1, 2, 3% of WVM additives, all bitumen samples showed elongation without breaking exceeding the specification limit value of 100 cm at 25 °C.

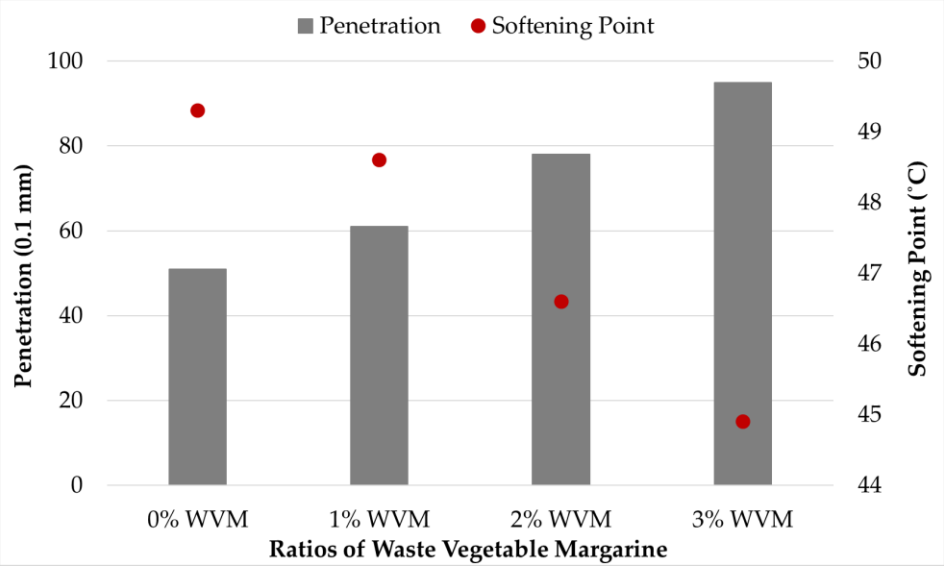

Figure 2. Penetration and softening point test results of WVM modified binders

The most commonly used measure of the temperature sensitivity of bitumen is the PI value (Geçkil et al., 2020). PI values calculated from penetration and softening point test results are shown in Figure 3. Accordingly, it is seen that the PI values increase with the increase in the proportion of WVM added to the bitumen. In this case, it can be interpreted that the temperature dependent susceptibility of the samples decreases as the additive ratio increases.

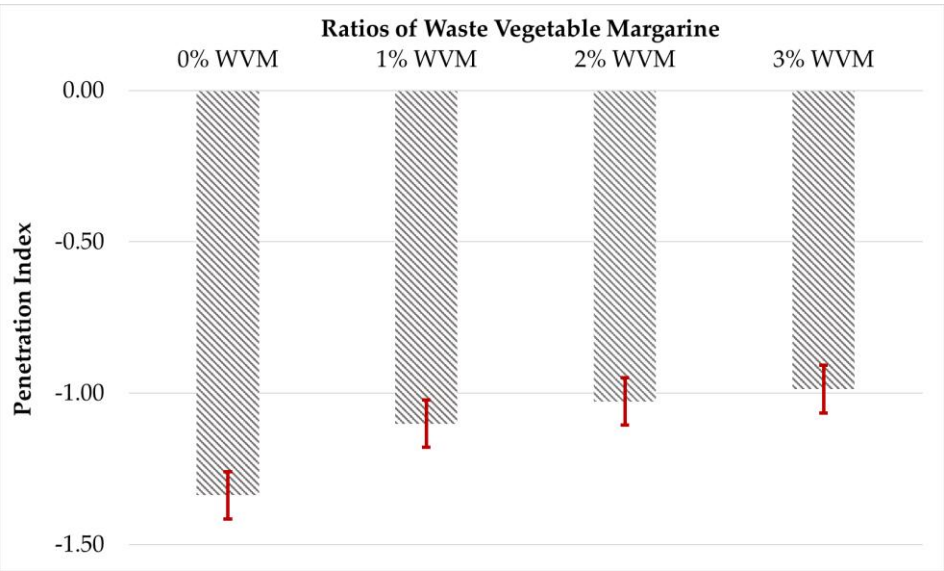

Figure 3. PI values of WVM modified binders

The results obtained from the rotational viscometer test and the specification limit values (0.17±0.02 Pa.s for mixing and 0.28±0.03 Pa.s for compaction) are given in Figure 4. Accordingly, the mixing/compaction temperatures of the samples were determined by finding the temperature vales corresponding to the points where the viscosity – temperature graph intersects. It was observed that the viscosity and mixing/compaction temperatures decreased with the increase in the additive ratio. In similar studies in the literature, modification with waste oils showed similar effects on the bitumen (Azahar et al., 2016; Al-Omari et al., 2018; Rasman et al., 2018). Also, the most significant decrease in mixing/compaction temperatures was observed at 1% WVM ratio.

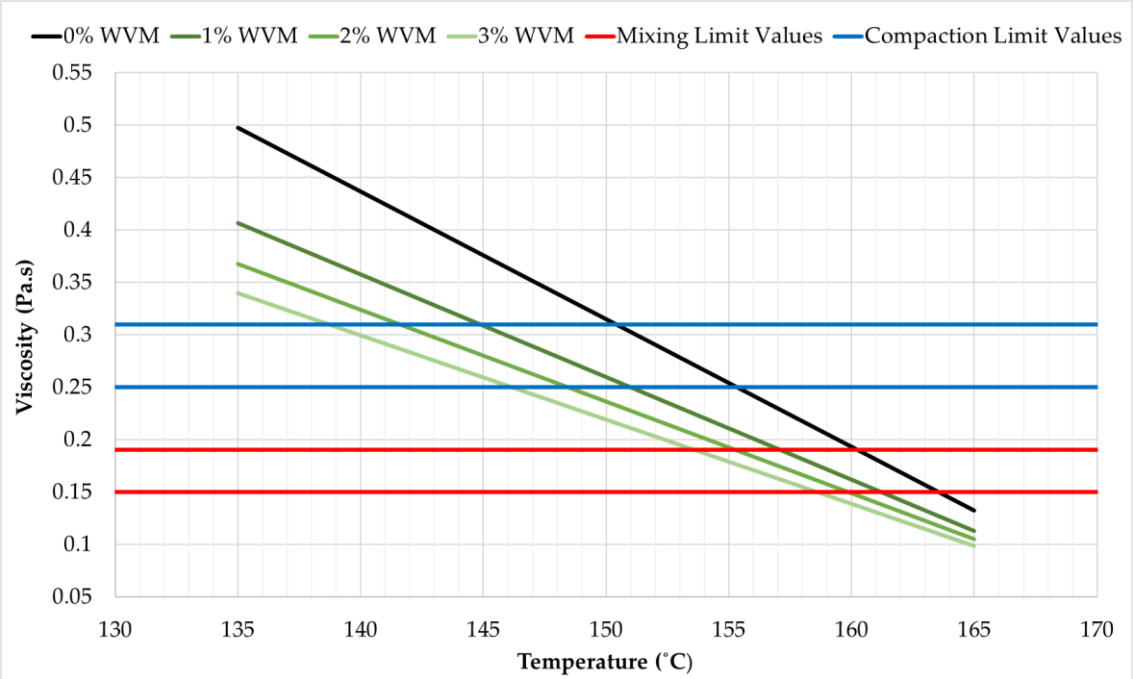

Figure 4. Rotational viscometer test results of WVM modified binders

The mixing/compaction temperatures were shown in Figure 5. The maximum decrease in mixing/compaction temperature occurred at 3% additive ratio. These decreases indicate that the workability of WVM modified bitumen is higher than the reference bitumen.

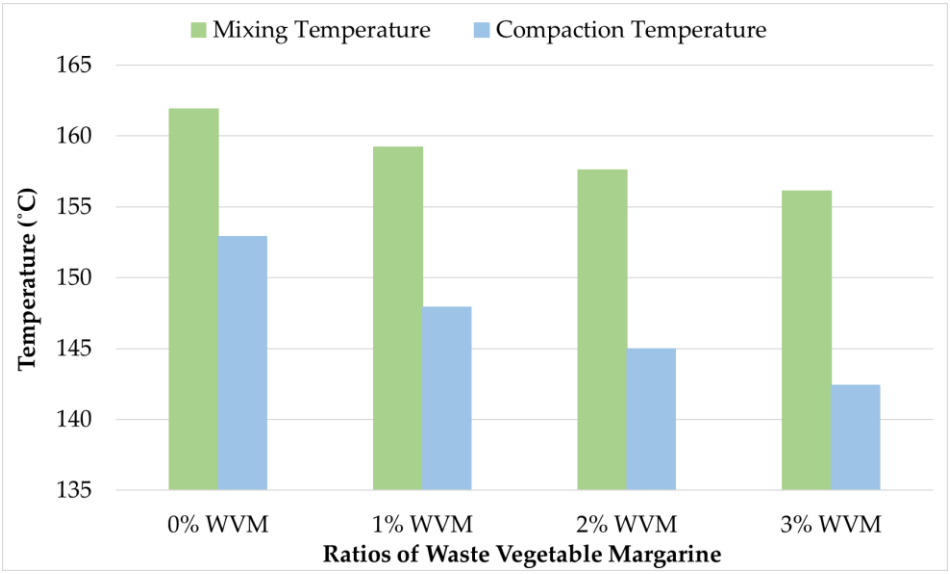

Figure 5. Mixing/compaction temperatures of WVM modified binders

3.2. Results of Nicholson Stripping, California Stripping and Vialit Tests

After bitumen modification by the addition of WVM additive to the bitumen at 1, 2 and 3% ratios, the result of the Nicholson stripping, California stripping and Vialit tests to which the samples had been subjected were compared with the reference bitumen by the help of Figure 6 and Figure 7.

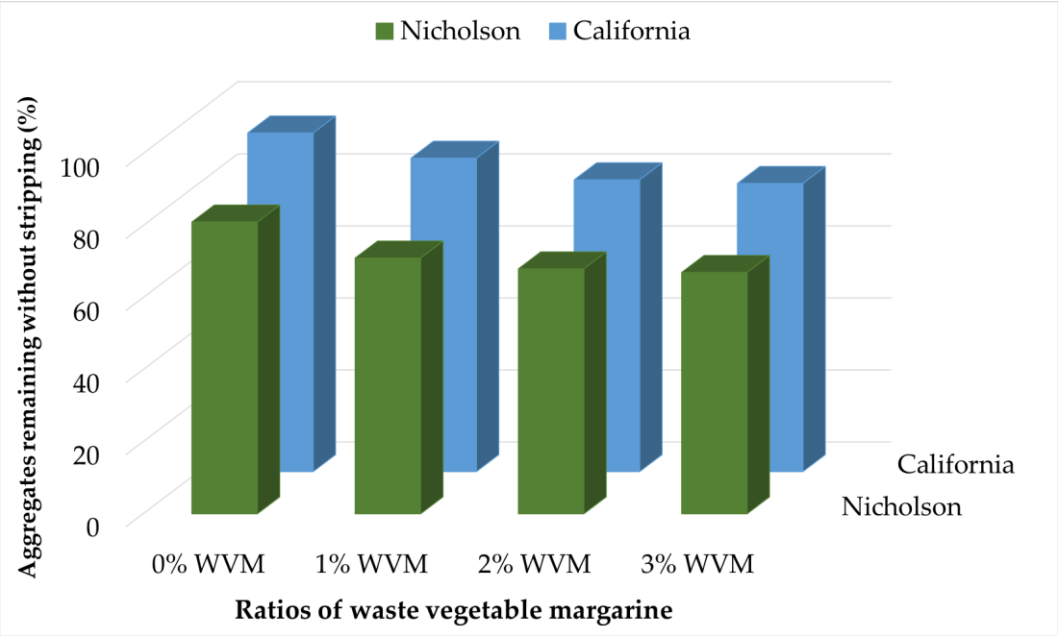

Figure 6. Results of Nicholson and California stripping tests

Figure 6 shows a comparison of the results obtained from two different stripping tests. Accordingly, it is seen that the percentage of aggregates remaining without stripping decreases with the increase in the amount of WVM additive in both cases, but the specification limit of 60% is provided at all ratios. When Figure 7 is analyzed, it can be seen that 1 and 2% WVM additives increase the adhesion performance of 50/70 penetration graded bitumen at the same rate. In addition, when 3% WVM was used, the number of falling aggregates was 0% and therefore the best adhesion performance was achieved. Based on these results, it can be interpreted that bitumen modification with WVM additive at the ratios specified in the study is suitable in terms of adhesion and stripping performance.

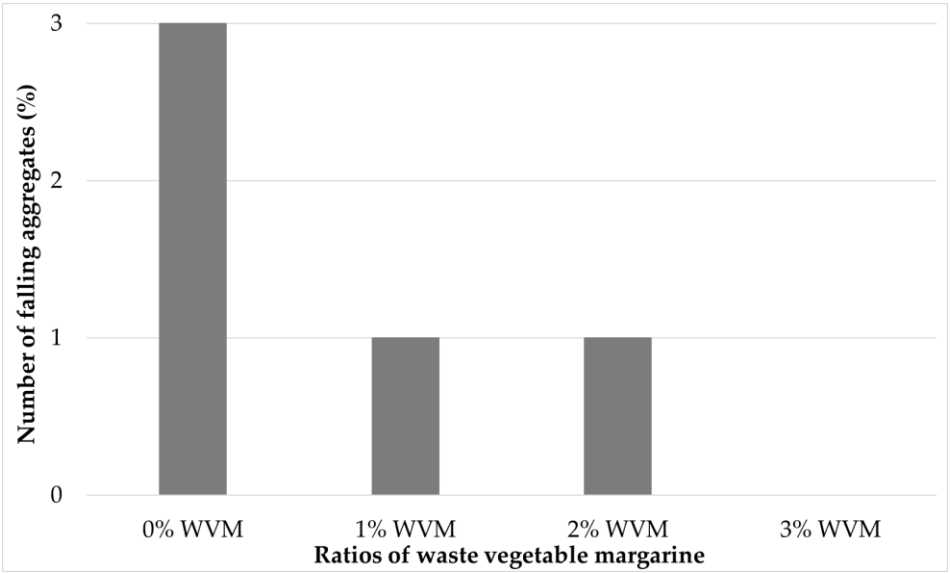

Figure 7. Results of Vialit tests

4. Conclusion

This study investigated and compared the physical properties, stripping resistances and adhesion properties of 50/70 penetration graded reference bitumen and WVM modified bitumen samples. Test results showed that the use of WVM results in an increase in the penetration and a decrease in the

softening point. The temperature dependent susceptibility of the samples decreased as the additive ratio was increased. The rotational viscometer tests showed that both the mixing/compaction temperatures and ranges decreased as the additive ratio increased. In addition, it is possible to say that there will be a slight decrease in the stripping resistances of mixtures containing WVM modified bitumen. However, rising of WVM ratio in bitumen increased slightly adhesion performance. According to the results obtained, it was found that the modification with WVM can increase the resistance of bitumen to the conditions of cold climates by affecting the consistency.

References

Adesina, P. A., & Dahunsi, B. I. (2021). Blended waste utilization in road construction: Physical characteristics of bitumen modified with waste cooking oil and high-density polyethylene. International Journal of Pavement Research and Technology, 14, 98-104. https://doi.org/10.1007/s42947-020-0040-1

Alakara, E. H., & Ağaoğlu, M. N. (2022). Estimating the Optimum Bitumen Amount of Hot Bituminous Mixtures Produced Using Concrete and Marble Wastes by Fuzzy Logic Method. International Journal of Engineering Research and Development, 14(1), 31-44. https://doi.org/10.29137/umagd.926303

Ali, B., Li, P., Khan, D., Hasan, M. R. M., & Khan, W. A. (2024). Investigation into the effect of waste engine oil and vegetable oil recycling agents on the performance of laboratory-aged bitumen. Budownictwo i Architektura, 23(1), 033-054. https://doi.org/10.35784/bud-arch.5500

Al-Omari, A. A., Khedaywi, T. S., & Khasawneh, M. A. (2018). Laboratory characterization of asphalt binders modified with waste vegetable oil using SuperPave specifications. International Journal of Pavement Research and Technology, 11(1), 68-76. https://doi.org/10.1016/j.ijprt.2017.09.004

Çavdar, E., Kumandaş, A., & Oruç, Ş. (2019, September). Effect of waste cooking oil use in the modification of sbs modified asphalt binder. In 3rd International Conference on Advanced Engineering Technologies (pp. 1653-1659).

Cucchiella, F., D'Adamo, I., & Gastaldi, M. (2017). Sustainable waste management: Waste to energy plant as an alternative to landfill. Energy Conversion and Management, 131, 18-31. https://doi.org/10.1016/j.enconman.2016.11.012

Duarte, G. M., & Faxina, A. L. (2021). Asphalt concrete mixtures modified with polymeric waste by the wet and dry processes: A literature review. Construction and Building Materials, 312, 125408. https://doi.org/10.1016/j.conbuildmat.2021.125408

El-Shorbagy, A. M., El-Badawy, S. M., & Gabr, A. R. (2019). Investigation of waste oils as rejuvenators of aged bitumen for sustainable pavement. Construction and Building Materials, 220, 228-237. https://doi.org/10.1016/j.conbuildmat.2019.05.180

Eltwati, A., Mohamed, A., Hainin, M. R., Jusli, E., & Enieb, M. (2022). Rejuvenation of aged asphalt binders by waste engine oil and SBS blend: Physical, chemical, and rheological properties of binders and mechanical evaluations of mixtures. Construction and Building Materials, 346, 128441. https://doi.org/10.1016/j.conbuildmat.2022.128441

Fernandes, S., Costa, L., Silva, H., & Oliveira, J. (2017). Effect of incorporating different waste materials in bitumen. Ciência & Tecnologia dos Materiais, 29(1), e204-e209. https://doi.org/10.1016/j.ctmat.2016.07.003

Geçkil, T., Önal, Y., & İnce, C. B. (2020). Physical, Morphological and Thermal Properties of Pure Bitumen Modified with Waste Polyethylene Terephthalate (PET). Fırat University Journal of Engineering Science, 32(1), 157-166. https://doi.org/10.35234/fumbd.618218

Hunter R N, Self A, Read J, Hobson E. The Shell Bitumen Handbook. London: ICE Publishing, 2015, 744–747

Ji, J., Yao, H., Suo, Z., You, Z., Li, H., Xu, S., & Sun, L. (2017). Effectiveness of vegetable oils as rejuvenators for aged asphalt binders. Journal of Materials in Civil Engineering, 29(3), D4016003. https://doi.org/10.1061/(ASCE)MT.1943-5533.0001769

Joni, H. H., Al-Rubaee, R. H., & Al-zerkani, M. A. (2019). Rejuvenation of aged asphalt binder extracted from reclaimed asphalt pavement using waste vegetable and engine oils. Case Studies in Construction Materials, 11, e00279. https://doi.org/10.1016/j.cscm.2019.e00279

Kumandaş, A., & Pancar, E. B. (2023). Up To Date Additives Used in Bitumen Modification: A Literature Review. OMU Journal of Engineering Sciences and Technology, 3(2), 109-140.

Kumar, V., & Aggarwal, P. (2023). Application of Natural and Waste Oils as Rejuvenator in Reclaimed Asphalt Pavement: A Review. International Journal of Pavement Research and Technology, 1-24. https://doi.org/10.1007/s42947-023-00388-7

Li, B., Liu, W., Nan, X., Yang, J., Tu, C., & Zhou, L. (2023). Development of rejuvenator using waste vegetable oil and its influence on pavement performance of asphalt binder under ultraviolet aging. Case Studies in Construction Materials, 18, e01964. https://doi.org/10.1016/j.cscm.2023.e01964

Li, H., Dong, B., Wang, W., Zhao, G., Guo, P., & Ma, Q. (2019). Effect of waste engine oil and waste cooking oil on performance improvement of aged asphalt. Applied Sciences, 9(9), 1767. https://doi.org/10.3390/app9091767

Liu, S., Zhou, S., Peng, A., & Li, W. (2020). Investigation of physiochemical and rheological properties of waste cooking oil/SBS/EVA composite modified petroleum asphalt. Journal of Applied Polymer Science, 137(26), 48828. https://doi.org/10.1002/app.48828

Ma, Y., Zhou, H., Jiang, X., Polaczyk, P., Xiao, R., Zhang, M., & Huang, B. (2021). The utilization of waste plastics in asphalt pavements: A review. Cleaner Materials, 2, 100031. https://doi.org/10.1016/j.clema.2021.100031

Maharaj, R., Ramjattan-Harry, V., & Mohamed, N. (2015). Rutting and fatigue cracking resistance of waste cooking oil modified trinidad asphaltic materials. The Scientific World Journal, 2015(1), 385013. https://doi.org/10.1155/2015/385013

Milad, A., Babalghaith, A. M., Al-Sabaeei, A. M., Dulaimi, A., Ali, A., Reddy, S. S., ... & Yusoff, N. I. M. (2022). A comparative review of hot and warm mix asphalt technologies from environmental and economic perspectives: towards a sustainable asphalt pavement. International Journal of Environmental Research and Public Health, 19(22), 14863. https://doi.org/10.3390/ijerph192214863

Porto, M., Caputo, P., Loise, V., Eskandarsefat, S., Teltayev, B., & Oliviero Rossi, C. (2019). Bitumen and bitumen modification: A review on latest advances. Applied sciences, 9(4), 742. https://doi.org/10.3390/app9040742

Rahman, M. T., Mohajerani, A., & Giustozzi, F. (2020). Recycling of waste materials for asphalt concrete and bitumen: A review. Materials, 13(7), 1495. https://doi.org/10.3390/ma13071495

Rasman, M., Hassan, N. A., Hainin, M. R., Jaya, R. P., Haryati, Y., Shukry, N. A. M., ... & Kamaruddin, N. H. M. (2018). Engineering properties of bitumen modified with bio-oil. In MATEC Web of Conferences (Vol. 250, p. 02003). EDP Sciences. https://doi.org/10.1051/matecconf/201825002003

Rodrigues, C., Capitão, S., Picado-Santos, L., & Almeida, A. (2020). Full recycling of asphalt concrete with waste cooking oil as rejuvenator and LDPE from urban waste as binder modifier. Sustainability, 12(19), 8222. https://doi.org/10.3390/su12198222

Topaloğlu, S. (2019). Ferrokrom cüruf agregasının geçirimli bitümlü karışımların performansına etkilerinin araştırılması. Master's thesis, Bartın University, Graduate School of Natural and Applied Sciences.

Uz, V. E., & Gökalp, İ. (2020). Sustainable recovery of waste vegetable cooking oil and aged bitumen: Optimized modification for short and long term aging cases. Waste Management, 110, 1-9. https://doi.org/10.1016/j.wasman.2020.05.012

Wan Azahar, W. N. A., Bujang, M., Jaya, R. P., Hainin, M. R., Ngadi, N., & Al Bakri, A. M. (2016). Performance of waste cooking oil in asphalt binder modification. Key Engineering Materials, 700, 216-226. https://doi.org/10.4028/www.scientific.net/KEM.700.216

Xinxin, C., Xuejuan, C., Boming, T., Yuanyuan, W., & Xiaolong, L. (2018). Investigation on possibility of waste vegetable oil rejuvenating aged asphalt. Applied Sciences, 8(5), 765. https://doi.org/10.3390/app8050765

Zargar, M., Ahmadinia, E., Asli, H., & Karim, M. R. (2012). Investigation of the possibility of using waste cooking oil as a rejuvenating agent for aged bitumen. Journal of hazardous materials, 233, 254-258. https://doi.org/10.1016/j.jhazmat.2012.06.021

CivilTech
2nd International Symposium on Innovations in Civil Engineering and Technologies
October 30 – November 1, 2024, Isparta / TURKIYE

A Novel Structural Health Assessment Approach for the Ballasted Concrete Railway Sleepers

Ferhat Çeçen[1], *Bekir Aktaş*[2]

*cecenferhat@sdu.edu.tr

Abstract

Concrete railway sleepers, one of the most common superstructure elements of modern ballasted railways, require effective Structural Health Monitoring (SHM) benchmarks that can be used during in-situ testing or remote monitoring. However, current or proposed techniques for detecting damaged sleepers are often complex, time consuming or unsuitable for field testing. This study investigates a novel approach that may overcome these challenges. This method uses the fundamental longitudinal resonance frequency as a benchmark of SHM. To date, researchers have generally focused on vertical, lateral or torsional mode shapes, which are highly sensitive to changes in ballast conditions and crack location/orientation. One of the main advantages of the novel approach presented is that the longitudinal resonance mode shapes are minimally affected by these changes, thereby increasing the reliability of the results. Damaged sleepers tested were found to have consistently lower longitudinal resonance frequencies, allowing cracked sleepers to be detected without the need to remove the ballast layer and carry out mandatory inspections/analyses. High repeatability was also observed on healthy sleepers, with deviations from the mean frequency not exceeding 0.5%. It was argued that this novel approach would provide a practical, rapid, and reliable means of in situ testing of concrete sleepers. Consequently, it is recommended that this approach be subjected to further validation through the implementation of more extensive in situ testing practices.

Keywords: Railway sleepers; Railroad ties; Structural Health Monitoring; Rail transportation safety; Experimental modal analysis; Naked eye crack inspection

[1] *Suleyman Demirel University, Göller Bölgesi Teknokent Coordinatorship, Isparta, Turkiye*
[2] *Erciyes University, Civil Engineering Department, Kayseri, Turkiye*

1. Introduction

Concrete sleepers are safety-critical components of ballasted railways (Kaewunruen et. al., 2016), and the monitoring of their structural health is essential for the assessment of railway safety, risk management and the reduction of maintenance costs. In most countries, this important task is carried out by visual inspection by foot patrols (Matsuoka et. al., 2015; Sengsri et. al., 2020). However, the vast majority of railway sleeper surfaces are obscured by ballast. It is therefore very difficult, if not impossible, to detect sleeper cracks with the naked eye, especially when they are covered by ballast. Even in cases where the ballast surrounding the sleepers is removed, it is not always possible to detect cracks in the sleepers by visual (naked eye) inspection due to the crack re-closing capacity of the prestressing force (applies to prestressed types) or the clogging of cracks with soil dust. Furthermore, removal of the ballast layer is not a viable solution given the significant number of sleepers to be inspected (Barke and Chiu, 2005). On the other hand, track inspection vehicles capable of measuring rail top deflections are now in use in a number of countries. However, this fast and sophisticated track inspection method is generally unable to detect damaged sleepers, especially at an early stage. This is due to the fact that a single damaged sleeper does not typically result in a notable abnormality in the rolling of the wheels. Consequently, these vehicles are unable to detect damage of this severity (Wakui and Okuda, 1997). However, these vehicles are able to detect concrete sleeper damage that is both multiple and sequential, and which could also affect railway safety (Matsuoka et. al., 2015). Therefore, it can be postulated that the use of existing methods for the detection of sleeper damage is inadequate for the purpose of early detection of sleeper damage in order to reduce track maintenance costs and increase railway safety (Sengsri et. al., 2020).

In the context of Structural Health Monitoring (SHM), Experimental Modal Analysis (EMA) is an increasingly used method today. It allows the desired modal parameters of various structures, systems and components to be determined in a non-destructive manner, both in the laboratory and in situ (Çeçen et. al., 2023; Çeçen et. al., 2022; Aktaş et. al., 2022). As expected, the EMA of railway sleepers has been the focus of numerous studies from the past to the present. In other words, attempts have been made to use the modal characteristics of railway sleepers as benchmarks for SHM. The earliest studies on this subject date back to the 1980s. While Grassie & Cox (1985) suggested that the ballast layer significantly increased the damping ratio of sleepers compared to the free-free mode, Ahlbeck and Hadden (1985) claimed that the effects of the support condition were insignificant at high frequencies. However, these results are closely related to the test equipment and analysis methods. In fact, Sadeghi (1997) pointed out that the determination of modal parameters varies significantly depending on the test and analysis method. Nevertheless, researchers from around the world, including Kaewunruen and Remennikov (2009) and Kaewunruen et al. (2018), Kumar & Shekhar (2016), Matsuoka and Watanabe (2019) and Matsuoka et al. (2018), Aikawa (2013), Sadeghi (2016), Liu et al. (2020), Va-sil'ev & Dvornikov (2000), have used EMA for SHM analysis of concrete railway sleepers. In these studies, the numerical values and percentage increases or decreases vary widely depending on several factors other than the level of damage, such as the condition of the ballast and substructure elements, which are also closely related to climatic/seasonal effects, or the EMA techniques used, etc. However, it is commonly accepted that the stiffness and homogeneity of the ballast layer under the sleepers has a significant and variable influence on the modal characteristics. It is therefore of paramount importance that an effective SHM benchmark must be able to detect sleeper damage while remaining "insensitive" to the condition of other track components, such as the ballast.

Another issue that needs to be investigated is the effect of cracks in railway sleepers, for example, on their resonance frequencies. Salim et al. (2012) conducted a study on this topic and concluded that cracks resulting from service loads reduce the flexural stiffness of railway sleepers, thereby reducing the resonance frequencies. This issue was also discussed by Kaewunruen and Remennikov (2008) after some falling weight impact tests. The uniaxial modal analysis performed by these authors after impact

loading showed that crack formation resulted in a reduction of both vertical and torsional resonance frequencies to varying degrees. The researchers subsequently carried out further studies (Janeliukstis et. al., 2018; Janeliukstis et. al., 2019) in which analyses were performed before and after three-point bending tests. It was reported that there was no significant effect on resonance frequencies as a result of low-level loading. However, changes in resonance frequencies were observed at load levels that resulted in the formation of permanent cracks. In addition, the authors investigated the potential of the mode shape curvature squares (MSCS) method. They found the results to be useful in differentiating between different levels of damage. However, it is important to note that the MSCS method requires the modal data of each sleeper in the undamaged state as well as at different levels of damage and under different ballast support conditions. Moreover, to obtain the mode shape of a single sleeper under a single set of conditions, it is necessary to mark several points on the sleeper, apply three to eight excitations to these points, record the vibrational response of the sleeper using accelerometer(s) and analyze the resulting FRF (Frequency Response Function) graphs using appropriate EMA software. Acquiring such a complex database while a large number of sleepers are waiting to be inspected on the railways requires a considerable amount of time and resources, so it is clear that using the MSCS method for railway sleeper SHM is a formidable challenge. Matsuoka et al. (2019, 2018) also investigated the modal properties of damaged sleepers using vibrational and vibroacoustic uniaxial modal analysis techniques (Matsuoka and Watanabe, 2019; Matsuoka et al., 2018). These studies confirmed that cracks that remain open (after unloading) lead to a reduction in resonance frequencies. It is important to note that, in any idealized single-degree-of-freedom (SDOF) system, the stiffness, mass, and resonance frequency are related by the following Equation 1, where ω_n=resonance frequency; k=stiffness; and m=mass:

$$\omega_n^2 = \frac{k}{m} \tag{1}$$

As can be seen from Equation 1, the cracks that cause a reduction in stiffness will also cause a reduction in resonance frequencies and vice versa. Therefore, resonance frequencies can provide a non-destructive and practical SHM benchmark. Another implication of the cited studies is that modal damping ratios are not useful as damage detection benchmarks due to the lack of certainty and the large variations observed (Matsuoka and Watanabe, 2019; Matsuoka et al., 2018). It has also been found that cracks under the rail seat are highly sensitive to some mode shapes, i.e. the third vertical mode. Therefore, it can be argued that cracks occurring in different regions will reduce different local stiffness values and affect each resonance frequency at different rates due to the different mode shapes of the different vertical/lateral resonances.

In conclusion, it is of paramount importance to monitor the condition of railway sleepers in order to ensure the safe and sustainable operation of railways. In this context, some of the modal parameters of railway sleepers can be used as benchmarks of their structural health level. Therefore, a number of studies have been carried out on the modal characteristics of railway sleepers under different levels of damage and ballast conditions. However, a major shortcoming of these studies is that they have largely neglected to investigate the longitudinal mode shapes of the sleepers. In contrast, the majority of studies have focused on vertical, lateral or torsional mode shapes, which are highly sensitive to changes in ballast conditions and damage/crack locations/orientations. Consequently, the majority of previous researchers have concluded that there is no reasonable trend in resonance frequency and damping ratio shifts with increasing damage severity for any particular mode. This study presents a novel approach to detecting damaged sleepers using their fundamental longitudinal resonance frequencies, which can be used as an effective SHM benchmark during in-situ testing or remote monitoring practices.

2. Material and Method

Currently, the most widely used and accepted modal testing and analysis method in the world is EMA (Kaewunruen et al., 2018). The details of this method have been the subject of several previous studies in the literature situ (Çeçen et. al., 2023; Çeçen et. al., 2022; Aktaş et. al., 2022). In this study, 3-axis EMA was applied to various sleepers on a railway line in Sivas, Türkiye (Figure 1). This railway is a factory branch line and has been in service for 10 years. During this time, some of the sleepers have visibly cracked under service loads.

The sleepers used on the railway section in Fig. 1 are type B58 prestressed concrete sleepers with a weight of approximately 240 kg/sleeper. The rails used on this line are UIC S-49 (49.46 kg/m) type. The fastening materials used on this line are Vossloh HM SKL-14 (flexible) and the ballast is crushed basalt aggregate with a grain size of 32/63 mm. During this study, several healthy and damaged sleepers were subjected to the EMA and those with no visible cracks (healthy) were coded as (S-1), while those with transverse cracks in the middle of the sleepers (between the rails) were coded as (S-2). Sleepers with longitudinal cracks from the ends of the sleeper towards the rail support were coded as (S-3). Figure 1 shows the track section and equipment used for in-situ modal testing. The modal hammer used in the in-situ tests is a Dytran 5802A (5000 lbs. capacity) with a hard (black) head to excite a wide frequency band (as shown in Figure 1). Three IEPE shear-type accelerometers (MMF KS76C.100 model, uniaxial sensors) combined with a mounting cube (using Loctite LB 8109 grease) and then adhesively bonded (using beeswax) to the corner points of each of the sleepers, as shown in Figures 1 and 2. The grease and beeswax provide high frequency transmission situ (Çeçen et. al., 2023). The weight of each uniaxial accelerometer is only 23 g and the measurement range is ±60 g (±600 m/S-2). The positioning of the accelerometers at the corner point made it possible to obtain all the mode shapes in the analyzed frequency band. This is because this point is not the nodal point of the first three resonance mode shapes of the sleepers in all three axes.

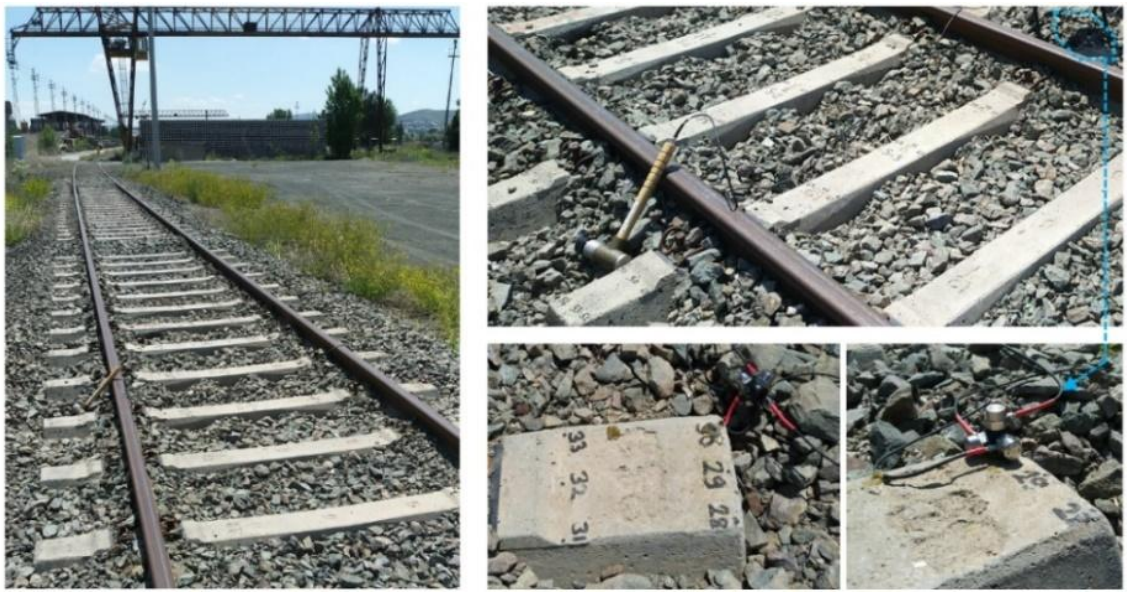

Figure 1. The track section and equipment used for in-situ modal testing

Figure 2. Accelerometer mounting details for three-axis EMA

In parallel with the field tests, a number of B58 sleepers produced in the same year (2012) and in the same factory using the same production method, but never used in the field, were taken to the laboratory and tested under free support conditions. The aim was to show the differences between these unused sleepers and their counterparts (S-1) that had been used in the field for about ten years. As shown in Figure 3, these EMA tests were carried out on two 60x60x60 cm PU blocks to obtain a free support mode. In these EMA tests, the modal hammer model was replaced by a lower capacity model (Dytran 5800 B2), as very high impact intensities are not required in laboratory studies and, on the contrary, high impacts may cause undesirable oscillations in the 3-axis analysis.

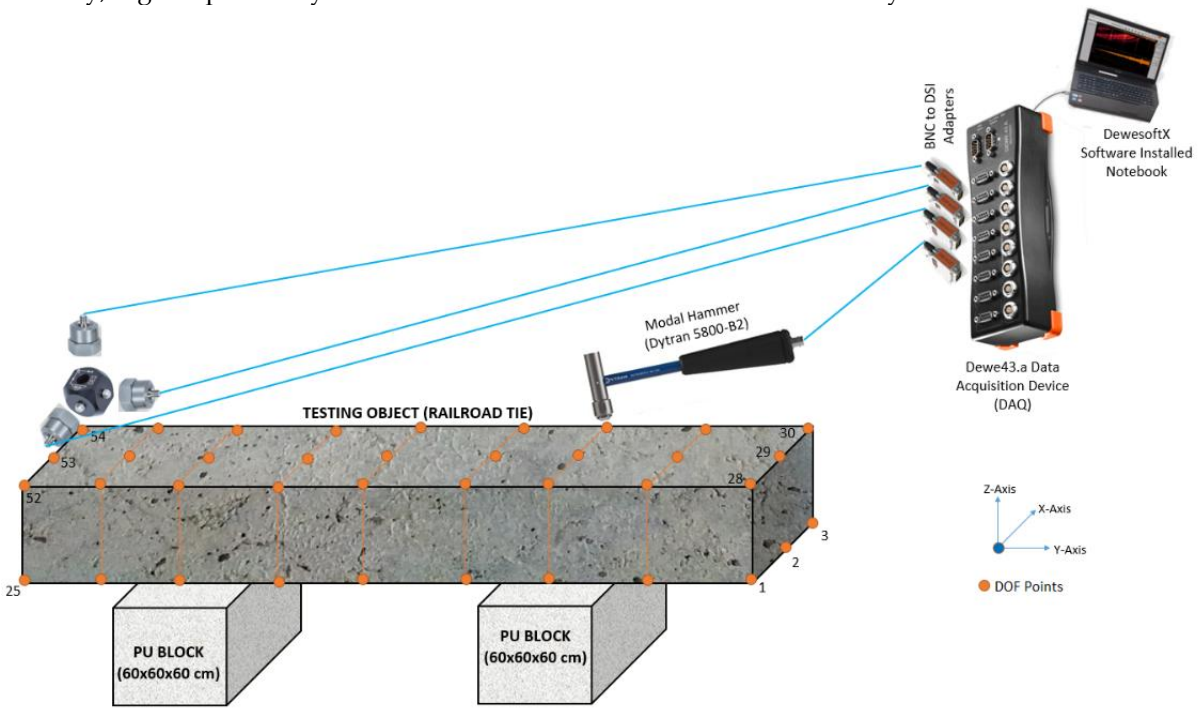

Figure 3. EMA test set-up in the laboratory and free-free support condition

The EMA laboratory tests were carried out in two stages. In the first stage, the sleepers were tested with fasteners (rail-sleeper connectors) and coded with (S-4). In the second stage, these fasteners are disassembled and these sleepers coded with (S-5). The aim of this implementation is to determine the possible changes caused by the fasteners and to provide more accurate results of the field simulation comparisons. In addition, a further set of sleepers, not used in the field, were loaded in the laboratory in a three-point bending test rig to 80 kN in the center section to produce a permanent transverse crack in the center of the sleepers. The purpose of this additional group was to simulate cracking in the field. This sleeper type was coded as (S-6) and was specifically compared to the S-2 sleeper in the field.

3. Results and Discussion

As a result of the EMA tests summarized in the previous section, the FRF graphs and mode shapes in the 3-axis (Z: vertical, X: lateral, Y: longitudinal) were obtained. An example is shown in Figure 4. In this way, the resonance frequencies for each sleeper type (S-1-S-6), for each axis (Z, X, Y) and for each excitation point were determined and presented separately in the following sections.

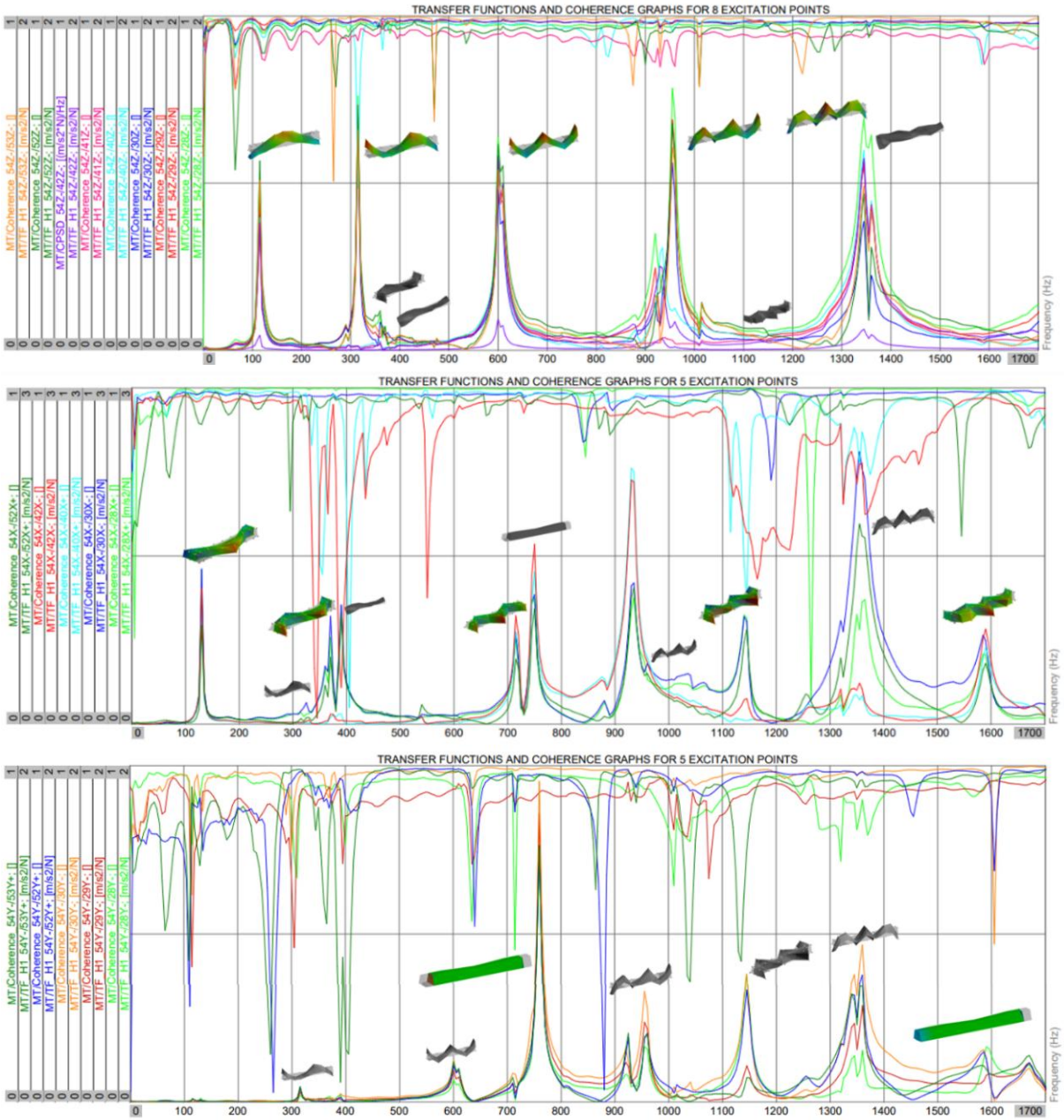

Figure 4. FRF examples for type S-4 (from top to bottom: vertical (Z), lateral (X), longitudinal (Y) axes)

3.1. Analysis results of S-1-type concrete railway sleepers

Some examples of healthy (no visible cracks observed) sleepers (S-1) found on the railway section surveyed (shown in Fig. 1) are presented in Fig. 5. The EMA results for this group of sleepers, including the measurement deviations, are summarized in Table 1. According to the results, the fundamental (first) resonance frequency values measured in each 3-axis have high reliability and repeatability, with deviations from the mean not exceeding 0.4%. However, the deviations of the second and third, vertical

and lateral resonance frequencies increased significantly, reaching 3.5% for some resonances. This is due to the fact that in some frequency bands (e.g. around 350-450 Hz) the resonances on the other axes are close to each other, as can be seen from the FRF graph examples shown in Figure 4, and this causes the closely spaced other mode shapes (CSOMS) errors explained in detail in the literature situ (Çeçen et. al., 2023).

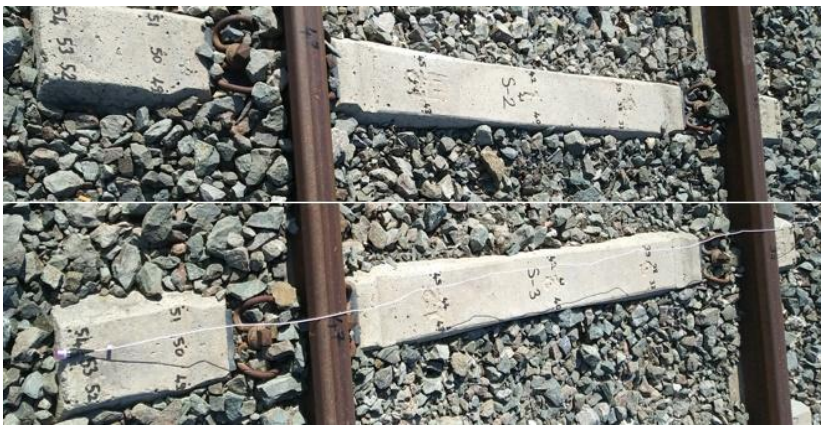

Figure 5. No visible cracks observed concrete railway sleeper samples (S-1) in the field

Table 1. Vertical, lateral and longitudinal resonance frequencies (Hz) of S-1-type railway sleepers

Parameters	1st Vertical	2nd Vertical	3nd Vertical	1st Lateral	2nd Lateral	3nd Lateral	1st Longitudinal	2nd Longitudinal
Min. (Hz)	119.31	351.30	538.05	158.23	424.38	811.85	850.58	1799.90
Max. (Hz)	120.04	376.43	551.12	158.39	446.05	814.78	855.95	1804.90
Mean (Hz)	119.68	364.02	546.18	158.31	432.39	812.96	853.71	1801.54
S.D. (Hz)*	0.52	11.00	5.14	0.11	11.89	1.59	2.28	1.94
S.D. (%)**	0.30%	3.50%	1.50%	0.10%	3.20%	0.20%	0.40%	0.20%

* Standard deviation in Hz (the square root of the average of the squares of the deviations from the mean)
** Standard deviation in % (the maximum difference from the mean)

3.2. Analysis results of S-2-type concrete railway sleepers

This section examines the sleepers that have cracks in the middle sections that are perpendicular to the longitudinal axis (transverse). Two examples of this group of sleepers (S-2) found on the railway section surveyed (in Figure 1) are shown in Figure 6. The EMA results for these sleepers, including measurement errors, are shown in Table 2.

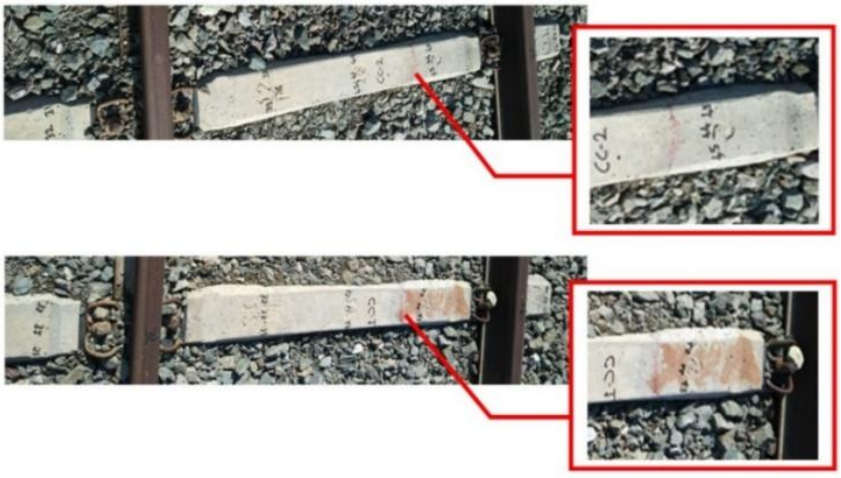

Figure 6. Central transverse cracks observed concrete railway sleeper samples (S-2) in the field

Table 2. Vertical, lateral and longitudinal resonance frequencies (Hz) of S-2-type railway sleepers

Parameters	1st Vertical	2nd Vertical	3nd Vertical	1st Lateral	2nd Lateral	3nd Lateral	1st Longitudinal	2nd Longitudinal
Min. (Hz)	118.08	339.25	545.18	146.73	411.35	792.93	837.69	1784.40
Max. (Hz)	120.43	348.27	562.70	163.21	424.11	811.58	840.92	1791.90
Mean (Hz)	118.72	343.84	551.45	153.89	416.42	803.04	839.37	1788.94
S.D. (Hz)*	0.90	4.20	6.97	7.67	6.77	9.08	1.44	3.14
S.D. (%)**	1.40%	1.30%	2.00%	6.10%	1.80%	1.30%	0.20%	0.30%

* Standard deviation in Hz (the square root of the average of the squares of the deviations from the mean)
** Standard deviation in % (the maximum difference from the mean)

As can be seen in Fig. 6, one of the sleepers was marked with red paint for replacement by the railway maintenance crews during the foot patrols. The other sleeper either cracked recently or was not identified during the visual inspections. The detection of sleeper cracks during a foot patrol is challenging, even if they are not covered with ballast, due to the size of the cracks and the necessity of inspecting a large number of sleepers. According to the results in Table 2, the deviations from the mean for the longitudinal resonance frequencies (first and second) do not exceed 0.3% and have repeatability. In contrast, deviations in vertical and lateral axes occurred significantly higher, reaching 6.1% for some resonances. It is considered that this situation is not due to test and analysis procedures, but to sleeper materials that lose their homogeneity due to damage. Because the same test and analysis method was used for S-1 type sleepers, and such a high deviation was not observed. Another possible reason is that the ballast support of the sleepers is not uniform around the sleeper. Already this heterogeneous supporting is sometimes the cause, and sometimes as a consequence, in the damage of the sleepers. A third possible cause is the combined effect of these two possibilities. But the second reason is considered to outweigh more. This is due to the fact that the longitudinal resonance frequencies (which have the mode shapes least affected by ballast heterogeneity) do not show such a deviation.

3.3. Analysis results of S-3-type concrete railway sleepers

This section examines sleepers with longitudinal cracks (parallel to the longitudinal axis, i.e. from the ends to the middle). An example of this group of sleepers (S-3) found on the railway section surveyed (in Figure 1) is shown in Figure 7. The EMA results are given in Table 3. According to the results, the longitudinal resonance frequencies again have a high repeatability and deviations from the mean do not exceed 0.5%. As before, the vertical and lateral deviations increased significantly, reaching 5.8% for some resonances. The possible reasons for these results are similar to those previously obtained for the S-2 sleepers (with central cracks). Consequently, the analysis of S-2 and S-3 sleepers shows that longitudinal resonance frequencies are a more ideal benchmark of SHM than vertical and lateral resonances, because they have mode shapes that are minimally affected by both central and longitudinal cracks in the sleepers and various heterogeneities in the ballast.

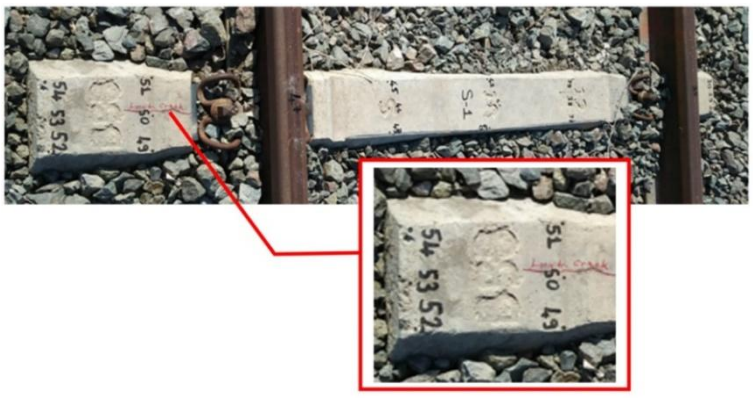

Figure 7. Longitudinal cracks observed concrete railway sleeper samples (S-3) in the field

Table 3. Vertical, lateral and longitudinal resonance frequencies (Hz) of S-3-type railway sleepers

Parameters	1st Vertical	2nd Vertical	3nd Vertical	1st Lateral	2nd Lateral	3nd Lateral	1st Longitudinal	2nd Longitudinal
Min. (Hz)	125.74	344.98	648.42	146.43	420.59	794.43	835.67	1797.60
Max. (Hz)	129.65	359.02	648.55	162.02	440.82	810.20	841.03	1808.50
Mean (Hz)	126.99	350.71	648.49	155.45	428.67	803.41	839.89	1803.42
S.D. (Hz)*	1.57	7.00	0.09	7.43	10.71	6.53	2.36	4.38
S.D. (%)**	2.10%	2.40%	0.00%	5.80%	2.80%	1.10%	0.50%	0.30%

* Standard deviation in Hz (the square root of the average of the squares of the deviations from the mean)
** Standard deviation in % (the maximum difference from the mean)

3.4. Analysis results of S-4-type concrete railway sleepers

The sleepers, produced in the same year (2012) and in the same factory using the same production method and equivalent concrete as the existing sleepers in the field, were placed on two pieces of 60x60x60 cm PU blocks (Figure 8) and subjected to EMA in the free-free supported mode and with "fasteners attached". The results show that all three resonance frequency values on all three axes have high reliability and repeatability, with deviations from the mean not exceeding 0.2%. This low level of deviation indicates that existing EMA methods are adequate and that high deviations are mostly due to undesirable ballast conditions and sleeper damage.

Figure 8. EMA test setup prepared for healthy and unused B58 type railway sleepers with fasteners

Table 4. Vertical, lateral and longitudinal resonance frequencies (Hz) of S-4-type railway sleepers

Parameters	1st Vertical	2nd Vertical	3nd Vertical	1st Lateral	2nd Lateral	3nd Lateral	1st Longitudinal	2nd Longitudinal
Min. (Hz)	112.77	314.89	603.14	131.54	388.25	717.21	759.80	1667.50
Max. (Hz)	112.90	315.20	604.88	131.86	388.57	717.56	760.27	1670.20
Mean (Hz)	112.84	315.05	603.71	131.67	388.39	717.41	760.01	1668.74
S.D. (Hz)*	0.04	0.12	0.57	0.12	0.16	0.18	0.20	0.97
S.D. (%)**	0.10%	0.10%	0.20%	0.10%	0.00%	0.00%	0.00%	0.10%

* Standard deviation in Hz (the square root of the average of the squares of the deviations from the mean)
** Standard deviation in % (the maximum difference from the mean)

3.5. Analysis results of S-5-type concrete railway sleepers

The sleeper fasteners (in Figure 8) were disassembled, as shown in Figure 9, and these sleepers were then subjected to EMA in a freely supported mode (identical to the test setup in Figure 8).

Figure 9. EMA test setup prepared for healthy and unused B58 type sleepers without fasteners

Table 5. Vertical, lateral and longitudinal resonance frequencies (Hz) of S-5-type railway sleepers

Parameters	1st Vertical	2nd Vertical	3nd Vertical	1st Lateral	2nd Lateral	3nd Lateral	1st Longitudinal	2nd Longitudinal
Min. (Hz)	112.94	318.08	611.88	131.54	388.69	739.44	767.02	1690.80
Max. (Hz)	113.14	318.79	612.31	131.76	389.11	739.97	767.25	1691.50
Mean (Hz)	113.04	318.38	612.08	131.64	388.90	739.73	767.11	1691.30
S.D. (Hz)*	0.07	0.31	0.16	0.09	0.21	0.25	0.09	0.29
S.D. (%)**	0.10%	0.10%	0.00%	0.10%	0.10%	0.00%	0.00%	0.00%

* Standard deviation in Hz (the square root of the average of the squares of the deviations from the mean)
** Standard deviation in % (the maximum difference from the mean)

As with the S-4 sleeper analysis results, the EMA results in Table 5 show that all three resonance frequency determinations in all three axes have high reliability and repeatability, with deviations from the mean not exceeding 0.1%. This low level of deviation indicates that existing EMA methods are adequate and that high deviations are mostly due to undesirable ballast conditions and sleeper damage.

3.6. Analysis results of S-6-type concrete railway sleepers

The sleepers used in the previous two sections were subjected to a static load of 80 kN in the laboratory (EN 13230-2 rail center negative moment capacity determination test set-up) to form a permanent transverse crack in the center of the sleeper, simulating cracking in the field (see Figure 6), and were coded as S-6. These sleepers were then placed on polyurethane (PU) blocks (see Figure 10) and subjected to EMA without fasteners.

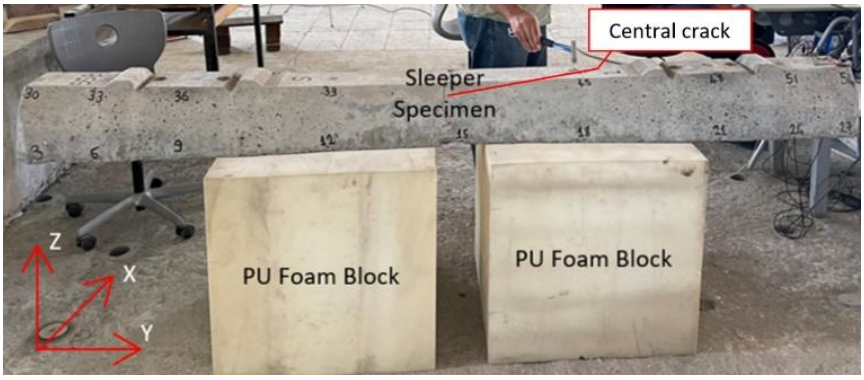

Figure 10. Test set-up prepared for centrally cracked (in the lab.) and unused (in the field) sleepers

As with the S-4 and S-5 type sleeper analysis results, the EMA results in Table 6 show that all three resonance frequency determinations in all three axes have high reliability and repeatability, with deviations from the mean not exceeding 0.2%. This low level of deviation indicates that existing EMA methods are adequate and that high deviations are mostly due to undesirable ballast conditions (i.e. air voids, pockets, contamination, compaction/stiffness heterogeneity, etc.). It also shows that for high in-situ deviations, sleeper damage has a much smaller effect than ballast irregularities.

Table 6. Vertical, lateral and longitudinal resonance frequencies (Hz) of S-6-type railway sleepers

Parameters	1st Vertical	2nd Vertical	3nd Vertical	1st Lateral	2nd Lateral	3nd Lateral	1st Longitudinal	2nd Longitudinal
Min. (Hz)	110.77	315.87	598.23	127.48	384.75	727.26	753.57	1683.00
Max. (Hz)	111.08	316.26	598.51	127.52	385.03	727.52	753.93	1683.80
Mean (Hz)	110.99	316.03	598.38	127.5	384.92	727.41	753.70	1683.54
S.D. (Hz)*	0.10	0.17	0.11	0.02	0.15	0.11	0.15	0.32
S.D. (%)**	0.20%	0.10%	0.00%	0.00%	0.00%	0.00%	0.00%	0.00%

* Standard deviation in Hz (the square root of the average of the squares of the deviations from the mean)
** Standard deviation in % (the maximum difference from the mean)

3.7. Collective evaluation of the acquired results

The collective and summarized results of the resonance frequency analysis and associated mode shapes of all these sleeper types (S-1 to S-6) analyzed in the study are presented in Table 7. As seen from this table, the frequencies of the sleeper resonances in situ or on ballast (S-1, S-2, S-3) increase by 1-2% compared to the same resonances in the free supporting condition or on PU block in the laboratory (S-4, S-5, S-6). On the other hand, the resonance frequencies of the S-4 and S-5 sleepers, which are both in the free supporting condition but differ depending on whether the fasteners are connected or not, are higher for type S-5 (in the vertical direction, where the gravitational acceleration is effective). As these materials, which weigh approximately 2-3 kg, are not connected in S-5 type sleepers, their mass decreases and the resonance frequency increases according to Eq. 1. For lateral resonances, where gravity acceleration is not directly effective, this difference is either negligible or relatively small. Conversely, longitudinal resonances were influenced by the presence or absence of fasteners, although it is also perpendicular to the acceleration of gravity. It is possible that this is largely due to the other factor in Eq. 1, stiffness, and is probably dominant rather than mass. However, this needs to be investigated further. Nevertheless, these results indicate that the presence and absence of fastenings are important considerations for accurate simulation of in-situ conditions and comparative analysis.

Table 7. Vertical, lateral and longitudinal resonance frequencies and mode shapes of all sleepers

Sleeper codes	1st Vertical	2nd Vertical	3nd Vertical	1st Lateral	2nd Lateral	3nd Lateral	1st Longitudinal	2nd Longitudinal
	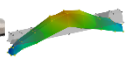	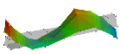	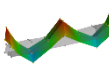	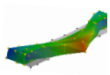	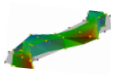	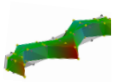		
S-1	119.68	364.02	546.18	158.31	432.39	812.96	853.71	1801.54
S-2	118.72	343.84	551.45	153.89	416.42	803.04	839.37	1788.94
S-3	126.99	350.71	648.49	155.45	428.67	803.41	839.89	1803.42
S-4	112.84	315.05	603.71	131.67	388.39	717.41	760.01	1668.74
S-5	113.04	318.38	612.08	131.64	388.90	739.73	767.11	1691.30
S-6	110.99	316.03	598.38	127.50	384.92	727.41	753.70	1683.54

A further finding was that the lowest resonance frequency values in all three axes were mostly observed for the S-6 sleeper, which was cracked in the middle in the laboratory. This is due to the fact that this type of sleeper is both in free-free mode and its stiffness decreases due to the crack effect. The fact

remains that the resonance frequency values of the sleepers tested, especially those tested in situ, varied considerably and some of the damaged sleepers had higher values than the undamaged ones. This was true for almost all resonance modes except for the longitudinal resonances. This is because the others are closely related to the ballast support conditions or because the reliability of the EMA system decreases as the frequency values increase. This shows that vertical, lateral and second longitudinal resonance frequencies can give misleading results for the SHM of railway sleepers. On the other hand, as shown in Table 1-7, the longitudinal resonance frequencies are more repeatable, less biased and provide more reliable results. Therefore, it can provide a more practical and reliable benchmark for the SHM of railway sleepers. In this context, the determination of the first (fundamental) longitudinal resonance frequency is easier because it has a frequency value almost 1 kHz lower and requires less specific EMA materials, methods and equipment. These first (fundamental) longitudinal resonance frequencies for all sleepers tested in situ are shown in Figure 14 for better understanding. As can be seen, the first longitudinal resonance frequency has the potential to discriminate well between damaged sleepers (with transverse central cracks or longitudinal cracks) and undamaged sleepers due to its high repeatability and minimal influence of ballast support conditions.

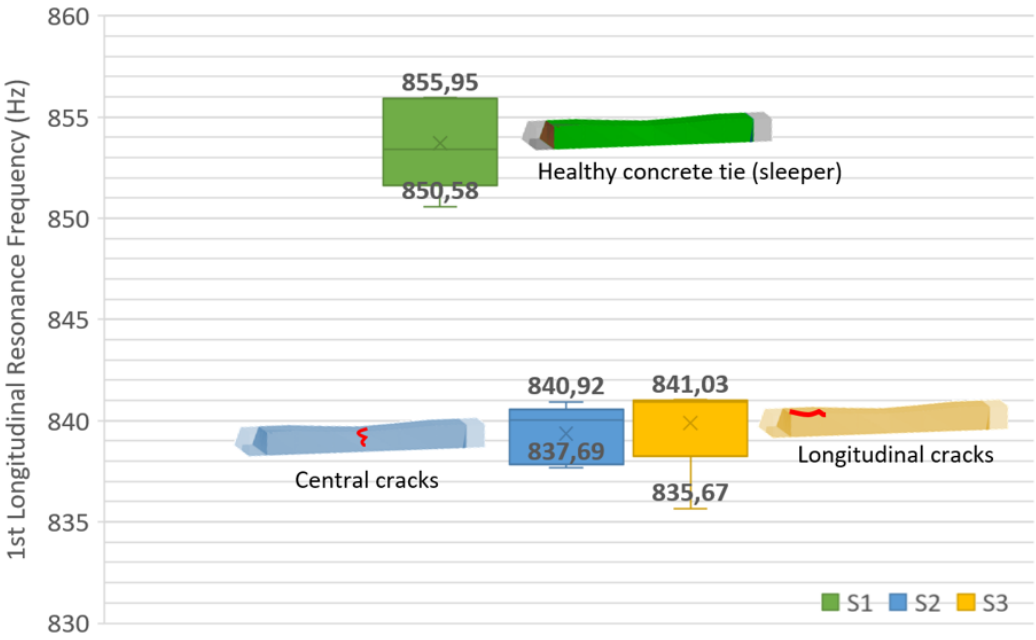

Figure 14. First (fundamental) longitudinal resonance frequencies of the S-1, S-2 and S-3-type sleepers

4. Conclusions

In this study, a comprehensive triaxial modal testing program was carried out on six groups of healthy and damaged prestressed concrete railway sleepers under in situ and laboratory conditions. Some of the main conclusions of the test and analysis results are presented below:

a. The standard deviations in the vertical and lateral axes were significantly higher than those in the longitudinal axis. While the maximum deviations reach 6.1% for the vertical and lateral resonances, only up to 0.5% deviations are observed for the longitudinal resonances. This high difference shows that the modal parameters for the vertical and lateral axes can give misleading results, whereas the longitudinal resonances are a more appropriate benchmark for the SHM of railway sleepers. It is considered that the high deviations of the vertical and lateral axes are due to some reasons such as:

i. The ballast support of the sleepers is not uniform in the field due to a number of variable reasons such as air voids/pockets, compaction/stiffness heterogeneities, contamination, climatic conditions, material losses, etc. In addition, the vertical & lateral resonances are closely related to the ballast support conditions due to their specific mode shapes (vibration directions). As a result, the standard deviations in the vertical and lateral axes increase significantly depending on the ballast conditions.
ii. The second reason for these high deviations is the damage-related heterogeneities in the sleepers, but the ballast-related comment mentioned above seems to be the most effective, since the comparative analysis presented in the study (e.g. between the S-5 & S-6-type sleepers) shows that sleeper damage has a much smaller effect than ballast irregularities.
iii. The other reason, which applies only to some specific resonances, is that in some frequency bands (e.g. around 350-450 Hz) several resonances are close to each other on different axes (e.g. second vertical, second lateral and first torsional mode) and due to this "closely spaced other mode shapes" (CSOMS) error, the resulting deviations are increased.

b. Among the several longitudinal resonances of railway sleepers, the first (fundamental) longitudinal resonance frequency is easier to determine because it has a frequency value of about 750-850 Hz, almost 1 kHz lower than the next one, and therefore requires less specific EMA materials, methods and equipment. This resonance mode is least affected by ballast heterogeneity and is sufficiently distant from resonances in other axes. Thus, according to the results obtained on six groups of healthy and damaged prestressed concrete railway sleepers under in-situ and laboratory conditions, the standard deviations from the mean for this resonance did not exceed 0.5%.
c. According to the results, the first longitudinal resonance frequency has the potential to discriminate well between damaged sleepers (with transverse central cracks or longitudinal cracks) and undamaged sleepers due to its high repeatability and minimal influence of ballast support conditions. These results indicate that the first longitudinal resonance frequency is a more ideal benchmark for SHM than other resonances because it has a mode shape that is minimally affected by crack location/orientation, various ballast heterogeneities and is easier to determine.
d. As can be seen from the triaxial EMA results presented in the study, all resonance frequency determinations are sensitive to even small changes in mass, such as fasteners (rail to sleeper connection materials) which have a total weight of approximately 2-3 kg. For example, as the total mass of the sleepers decreases (fasteners removed), the resonance frequencies tend to increase. This result demonstrates the adequacy of the EMA technique used in the study and also that the presence or absence of fasteners is an important consideration for accurate simulation of in-situ conditions and comparative analysis.

Consequently, the fundamental resonance frequency of concrete railway sleepers can provide an easy, fast, reliable, and non-destructive structural health monitoring (SHM) benchmark for railway sleeper in-situ testing or remote monitoring practices. Therefore, it is recommended that further investigation be carried out by implementing more extensive in-situ testing practices.

References

Ahlbeck, D. R., & Hadden, J. A. (1985). Measurement and Prediction of Impact Loads from Worn Railroad Wheel and Rail Surface Profiles. Journal of Engineering for Industry, 107, 197–205. https://doi.org/10.1115/1.3185985

Aikawa, A. (2013). Determination of dynamic ballast characteristics under transient impact loading, Electronic Journal of Structural Engineering, 13(1), 17-34. https://doi.org/10.56748/ejse.131581

Aktaş, B., Çeçen, F., Öztürk, H., Navdar, M. B., Öztürk, İ. Ş. (2022). Comparison of prestressed concrete railway sleepers and new LCR concrete sleepers with experimental modal analysis. Engineering Failure Analysis, 131. https://doi.org/10.1016/j.engfailanal.2021.105821

Barke, D., & Chiu W. K. (2005). Structural health monitoring in the railway industry: A review. Structural Health Monitoring, 4(1), 81-93. https://doi.org/10.1177/1475921705049764

Çeçen, F., Aktaş, B., Öztürk, H., Öztürk, İ. Ş., Navdar, M. B. (2022). Comparative modal analysis of B70 and LCR-6 type railway sleepers after repeated impact loads, Construction and Building Materials, 336, https://doi.org/10.1016/j.conbuildmat.2022.127563

Çeçen, F., Özbayrak, A., Aktaş, B. (2023) Experimental modal analysis of fly ash-based geopolymer concrete specimens via modal circles, mode indication functions, and mode shape animations. Cement and Concrete Composites, 137, http://dx.doi.org/10.1016/j.cemconcomp.2023.104951

Grassie, S. L., & Cox, S. J. (1985). The Dynamic Response of Railway Track with Unsupported Sleepers. Proceedings of the Institution of Mechanical Engineers, Part D: Journal of Automobile Engineering, 199, 123–135. https://doi.org/10.1243/PIME_PROC_1985_199_149_01

Janeliukstis, R., Clarck, A., Rucevskis, S., Kaewunruen, S. (2017). Vibration-based damage identification in railway concrete sleepers. Fourth Conference on Smart Monitoring, Assessment and Rehabilitation of Civil Structures (SMAR 2017), 9 pages. https://data.smar-conferences.org/SMAR_2017_Proceedings/papers/193.pdf

Janeliukstis, R., Ručevskis, S., Kaewunruen, S. (2019). Mode shape curvature squares method for crack detection in railway prestressed concrete sleepers, Engineering Failure Analysis, 105, 386-401. https://doi.org/10.1016/j.engfailanal.2019.07.020

Kaewunruen, S., & Remennikov, A. (2008). Dynamic Effect on Vibration Signatures of Cracks in Railway Prestressed Concrete Sleepers. Advanced Materials Research, 41-42, 233-239. https://ro.uow.edu.au/engpapers/416

Kaewunruen, S., & Remennikov, A. (2009). Application of vibration measurements and finite element model updating for structural health monitoring of ballasted railtrack sleepers with voids and pockets, Mechanical Vibrations: Measurement, Effects and Control, Chapter 12, Nova Science Publishers. https://ro.uow.edu.au/engpapers/502/

Kaewunruen, S., Janeliukstis, R., Freimanis, A., Goto, K. (2018). Normalised curvature square ratio for detection of ballast voids and pockets under rail track sleepers. The International Conference on Modern Practice in Stress and Vibration Analysis (MPSVA 2018), Cambridge, United Kingdom, https://doi.org/10.1088/1742-6596/1106/1/012002

Kaewunruen, S., Sussman, J. M., Matsumoto, A. (2016). Grand Challenges in Transportation and Transit Systems. Front. Built Environment, 2 (4). https://doi.org/10.3389/fbuil.2016.00004

Kumar, M., & Shekhar. S. (2016). Vibration Analysis of Railway Concrete Sleeper for Different Contact Condition using MATLAB. Research Journal of Engineering Sciences, 5(7), 46-55. https://www.isca.me/IJES/Archive/v5/i7/7.ISCA-RJEngS-2016-015.pdf

Liu, J., Wang, P., Liu, G., Xiao, J., Liu, H., Gao, T. (2020). Influence of a tamping operation on the vibrational characteristics and resistance-evolution law of a ballast bed. Construction and Building Materials, 239. https://doi.org/10.1016/j.conbuildmat.2019.117879

Matsuoka, K., Watanabe, T. (2019). Application of a Frequency-Based Detection Method for Evaluating Damaged Concrete Sleepers. Advances in Structural Health Monitoring, http://dx.doi.org/10.5772/intechopen.82711

Matsuoka, K., Watanabe, T., Minoura, S., Sogabe, M., Omodaka, A. (2018). Vibration modes of damaged PC sleepers and development of a simple damage detection method using sound level meter. Journal of Japan Society of Civil Engineers, Ser. E2 (Materials and Concrete Structures). 74, 158-175. http://dx.doi.org/10.2208/jscejmcs.74.158

Matsuoka, K., Watanabe, T., Sogabe, M. (2015). Damage Detection Method for Sleepers Based on Vibration Properties, 6th International Conference on Experimental Vibration Analysis for Civil Engineering Structures: EVACES'15, Vol. 24. http://dx.doi.org/10.1051/matecconf/20152405005

Sadeghi, J. (1997). Investigation of Characteristics and Modelling of Railway Track System. PhD Thesis, University of Wollongong. https://ro.uow.edu.au/theses/1249/

Sadeghi, J. (2016). Field Investigation on Dynamics of Railway Track Pre-Stressed Concrete Sleepers. Advances in Structural Engineering, 13 (1), 139–152. https://doi.org/10.1260/1369-4332.13.1.139

Salim, M. R., Abu Bakar, A., & Shariff, A. A. (2012), Investigation on Simulation of Train Loading on Prestressed Concrete Sleepers. Applied Mechanics and Materials, 157- 158, 666–670. https://doi.org/10.4028/www.scientific.net/AMM.157-158.666

Sengsri, P., Ngamkhanong, C., Melo, A. L. O., Kaewunruen, S. (2020). Experimental and Numerical Investigations into Dynamic Modal Parameters of Fiber-Reinforced Foamed Urethane Composite Beams in Railway Switches and Crossings, Vibration (MDPI), Vol. 3, pp. 174-188. https://doi.org/10.3390/vibration3030014

Vasil'ev, N. A., & Dvornikov, S. I. (2000), Experimental Study of the Vibration Characteristics of Railway sleepers. Acoustical Physics, 46 (3), 364–366. http://dx.doi.org/10.1134/1.29893

Wakui, H., & Okuda, H. (1997). A study on limit state design method for prestressed concrete sleepers. Doboku Gakkai Ronbunshu, 1997(557), 35-54. https://doi.org/10.2208/jscej.1997.557_35

Investigation of the Nylon Bag Waste Modified Bitumen Properties

Cahit Gürer[1], *Bojan Zlender*[2], *Süleyman Gücek*[1], *Primoz Jelusik*[2] , *Burak Enis Korkmaz*[1] *Şule Yarcı*[1], *Murat Vergi Taciroğlu*[3] , *Tamara Bračko*[2] *Borut Macuh*[2], *Rok Varga*[2]

*cgurer@aku.edu.tr

Abstract

Nylon bag wastes (NBW) serious environmental threats and is used in large quantities worldwide. This situation creates serious problems such as environmental pollution, damage to wildlife and micro plastic problems. Therefore, it is extremely important to reduce the use of nylon bags and to dispose of existing waste. The use of nylon bag waste in bitumen modification provides solutions to waste management problems and increases the performance of road pavement materials. In this process, nylon bags are cut into small pieces and mixed with bitumen. The resulting mixture provides more durable and long-service life road pavements. This modified bitumen is more resistant to temperature changes and reduces crack formation. In this paper, different rates of bitumen modification were performed with NBW, and the test results obtained by performing bitumen specific gravity, penetration, softening point, viscosity and Nicholson stripping tests on the samples were compared with the results of the control sample. As a result, it was assessed that the use of plastic bag waste in bitumen modification offers significant advantages both environmentally and economically, and this innovative approach is a promising method for the reusing of waste materials and the development of road construction technologies.

Keywords: Nylon bag waste; modified bitumen; bitumen test; sustainability.

[1] *Afyon Kocatepe University, Engineering Faculty, Department of Civil Engineering, Afyonkarahisar, Turkiye*
[2] *University of Maribor, Faculty of Civil Engineering, Transportation Engineering and Architecture, Slovenia*
[3] *Mersin University, Faculty of Engineering, Department of Civil Engineering, Turkiye*

1. Introduction

The widespread use of plastic bags has led to significant environmental challenges due to their non-biodegradable nature and persistence in the environment (Thompson et al., 2009). Approximately 1 trillion plastic bags are used worldwide each year. This means approximately 2 million bags using every minute (Clapp & Swanston, 2009). The majority of plastic bags are disposable and are thrown away immediately after use. This significantly increases the amount of waste (Hopewell et al., 2009). The recycling rate of plastic bags is quite low. Many countries cannot effectively recycle these bags. In the USA, only 1-3% of plastic bags are recycled (Barnes et al., 2009).

These plastic wastes, predominantly composed of polyethylene, cause to extensive pollution in terrestrial and aquatic ecosystems (Andrady, 2011). Conventional disposal methods, such as landfilling and incineration, are not sustainable solutions and pose further environmental risks (Hopewell et al., 2009). Therefore, innovative approaches to recycling and repurposing plastic bag waste are imperative. Another problem is that recycling such waste requires significant cost and also causes carbon emissions. For this reason, developed countries have begun to prefer the option of transferring the responsibility of difficult-to-process waste to lower-income countries. In such countries, this type of waste is often burned instead of recycled, which causes more carbon emissions (Web1 2024). The amount of solid waste exported from member states of the European Union to non-member countries has increased by 77% since 2004, reaching approximately 33 million tons. Among these wastes, plastic waste is seen to be at the top of the list (Web 2 2024). This situation makes the option of disposing of these wastes by reusing them in road construction for different purposes, rather than recycling, even more advantageous. The use of waste plastic as a modifier in bituminous mixtures will not only enhance the properties of mix, but will also, solve the plastic waste disposal problems that have engulfed nations thereby improving the sanitation systems and also create employment for the collectors of it.) (Kwame et al. 2015, Appaih 2017, Gökalp 2021, Victory 2022).

One promising application is the utilization of plastic bag waste in bitumen modification for road construction (Vasudevan et al., 2007). Bitumen, a byproduct of crude oil distillation, is commonly used as a binder in asphalt mixtures. However, traditional bitumen has limitations, such as susceptibility to temperature fluctuations, which can lead to cracking and pothole formation in pavements (Polacco et al., 2006). Incorporating plastic bag waste into bitumen offers a potential solution to address the plastic problem while improving the performance properties of asphalt. Punith et al. (2003) reported that it is possible to increase the performance of bituminous mixtures with waste plastics. Field tests have withstood the applied stresses and it has been concluded that plastic wastes used after being processed appropriately as additives will extend the life of the roads and also be effective in solving environmental problems. Similarly, Hınıslıoğlu and Ağar (2004) reported that waste HDPE modified bituminous binders provide better resistance to permanent deformations due to their high stability and high Marshall quotient, and contribute to the recycling of plastic wastes and the protection of the environment. In recent years, extending the life of the pavement by modifying bitumen with various polymers such as SBS has become one of the most common applications in Turkey and all over the world. However, it is known from the literature that the unit prices and carbon footprints of products such as SBS are quite high (Gürer 2015; Appiah 2017). One way to reduce the cost of pavement construction and thus make polymer-modified bitumen more usable is to use inexpensive polymers, i.e. polymers from which waste is recovered (Ahmadinia et.al, 2011).

In this study aims to contribute to sustainable road pavement construction practices by providing a viable solution for plastic waste management and enhancing the longevity and performance of asphalt pavements. The findings could pave the way for broader adoption of nylon bag waste-modified bitumen, promoting both environmental conservation and infrastructure development.

2. Material and Method

2.1. Material

Within the scope of the study, 50/70 penetration grade bitumen from TÜPRAŞ in Izmir was used. Bitumen properties are given in Table 1. Black nylon bags used as waste materials. The wastes converted to sizes suitable for the using as modifier. Figure 1 shows the images of the nylon bag waste (NBW). The NBW was cut into small 5x5 mm pieces (Figure 1).

Table 1. Material properties of 50/70 penetration grade bitumen

Properties	50/70	Standard
Specific Gravity	1.035	(ASTM D70-03 2003)
Penetration Degree (25 ºC)	52.13	(ASTM D5-06e1 2006)
Softening Point (ºC)	46.65	(ASTM D36-06 2006)
Brookfield Viscosity at 135 ºC (cP)	495.00	(ASTM D4402-06 2006)
Brookfield Viscosity at 165 ºC (cP)	131.00	

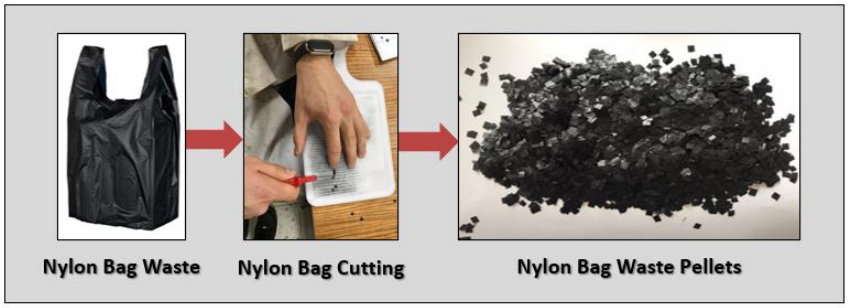

Figure 1. Steps of cutting the black nylon bag waste in 5*5 mm² dimensions

2.2. Method

The workflow diagram for preparing bitumen for modification is given in Figure 2.

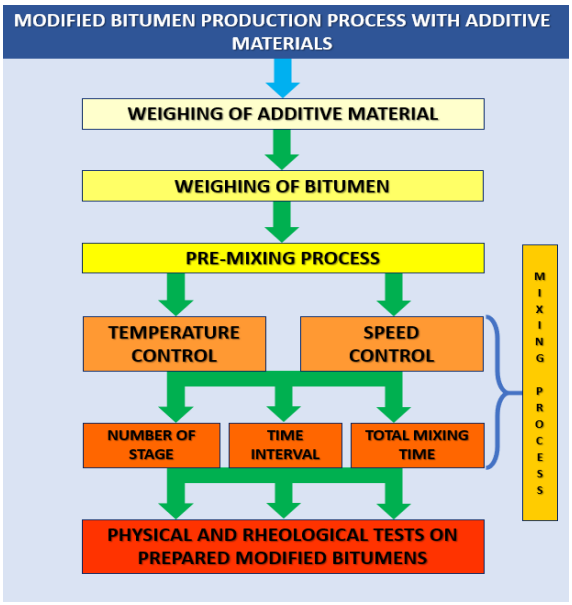

Figure 2. Bitumen Production Process

2.2.1 Penetration Test

Penetration Test, a traditional test method widely used worldwide, is applied to determine bitumen consistency under a certain load and temperature. In the mechanism, a constant load of 100-200 grams and temperature conditions of 25°C are generally used with the help of a specially shaped needle for 5 seconds. In this study, bitumen samples were subjected to this test according to the EN 1426 standard (BS EN-1426 2023).

2.2.2 Softening Point Test

Softening Point Test is determined to determine the heating temperature of bitumen and allow the bitumen to flow without interfering with its chemical structure. The mechanism consists of two rings of a certain size, a weighted steel ball, a magnetic heater to provide high temperature conditions and a gradual temperature. In this study, bitumen samples were subjected to this test according to the EN 1427 standard (CEN EN-1427 2015).

2.2.3 Nicholson Stripping Test

In the Nicholson Stripping Test (ASTM D 1664); Approximately 200 grams of the crushed aggregate sample remaining between 9.5-4.75 mm or 4.75-3.35 mm sieves are taken. After washing the test sample thoroughly and shaking it several times with pure water, it is dried in an oven at 110°C. 30±0.5 g of washed dry aggregate is taken and kept in an oven at 110 °C for 1 hour. On the other hand, 1.5±0.1 g of bituminous material (this ratio corresponds to 5% of the aggregate weight used in the experiment) is heated in a 250 cm^3 beaker in an oven at 110°C. After the bituminous material is prepared, it is immediately poured into the beaker and kept in an oven at 60°C for 24 hours, using a glass baguette, until all the crushed stones are covered with a homogeneous bitumen film. At the end of this period, the beaker is removed from the oven and transferred to a 10 cm diameter petri dish. Then, the covered gravel is smoothed with very light blows with a baguette and left at laboratory temperature for 10 minutes. Then the petri dish is filled with water. After the glass lid is closed on the Petri dish, it is placed in the oven at 60°C to wait for 24 hours. At the end of this period, the petri dish is taken outside, the water is changed, and the upper surface of the mixture is visually examined under a side light. At the end of the experiment, the ratio of the unstripped surface to the entire surface is given as resistance to stripping.

2.2.4 Rotational Viscometer Test

Rotational Viscometer Test is used to determine the fluidity properties of bitumen within the temperature ranges where it is heated during application. The experimental setup includes a rotational viscometer, measurement geometry called spindle, temperature-controlled thermal heater, special sample mold and temperature control device. When this test is performed on original binders, the viscosity value at 135°C must not exceed 3000 cP (Yüknü et al. 2021).

3. Results and Discussion

3.1 Specific Gravity Test Results

Specific gravity test results for three different sample types are shown in Figure 3. In general, in both graphs, the specific gravity results of modified bitumen tend to increase compared to pure bitumen.

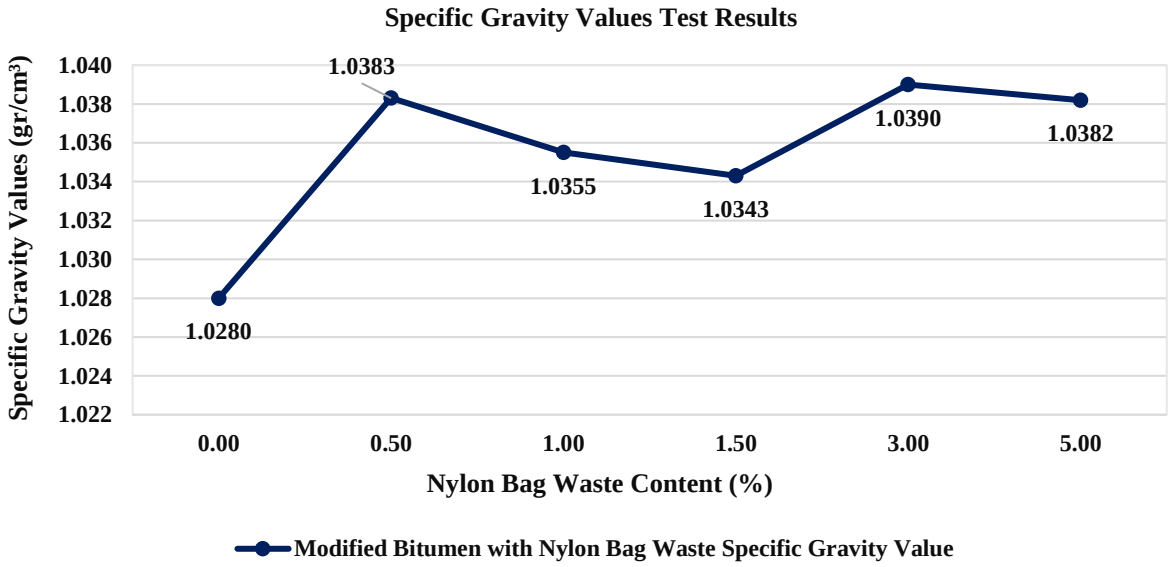

Figure 3. Specific Gravity Test Results of Bitumen Modified with 5 Different Rates of WGP

3.2 Penetration Test Results

Penetration test results for are given in Figure 4. In general, the penetration test results of modified bitumen in all series samples tend to decrease compared to pure bitumen. As a result of the penetration test, it was determined that the HM created with 1.5% NBW gave the lowest penetration value, according to the graph given in Figure 3. Penetration test results show that the temperature sensitivity of all modified bitumen samples tends to decrease.

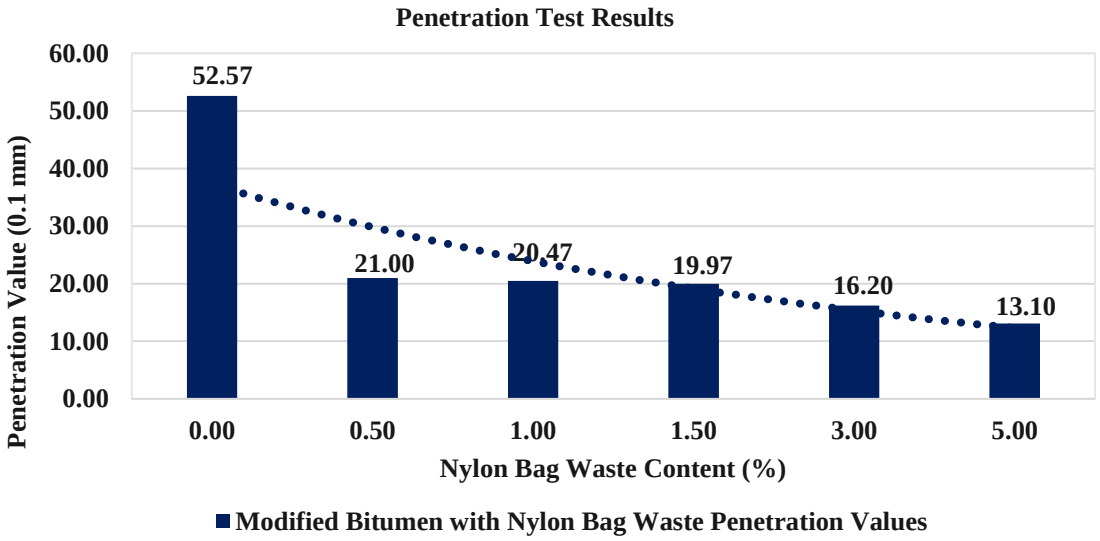

Figure 4. Penetration test results of bitumen modified with 5 different rates of NBW

3.3 Softening Point Test Results

Softening point test results are given in Figure 5. In general, the softening point values of bitumen modified with NBW tend to increase. This is an indication that the temperature sensitivity of NBW modified bitumen samples has decreased. The increasing trend in samples continues as the amount of NBW increases.

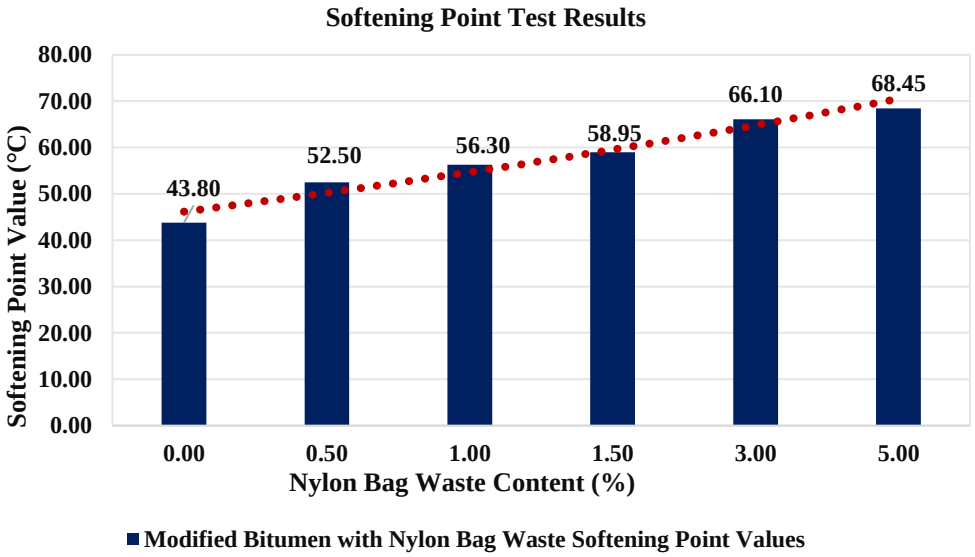

Figure 5. Softening point test results of bitumen modified with 5 different rates of NBW

3.4 Rotational Viscosity Test Results

In Figure 6, in general, a tendency to increase in viscosity is observed with the increase in the amount of NBW in the modification made with the nylon bag additive. This increasing trend is quite evident up to 3% additive amount at 135°C. While the change in viscosity is quite limited for additives higher than 3%, the increasing trend continues at 165°C.

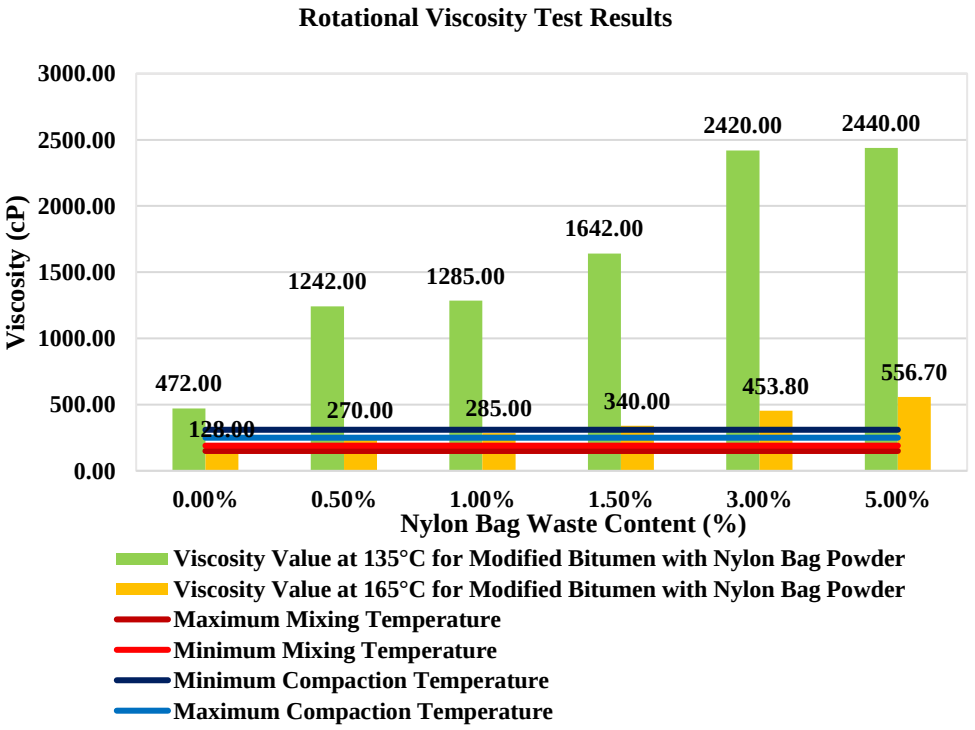

Figure 6. Rotational viscosity test results of bitumen modified with 5 different rates of NBW at 135°C and 165°C

3.5 Nicholson Stripping Test Results

To determine the stripping effect, the Nicholson stripping test was carried out and the largest aggregate surface remaining without stripping was observed in bitumen modified with 1.5% NBW additive, according to the graph given in Figure 7.

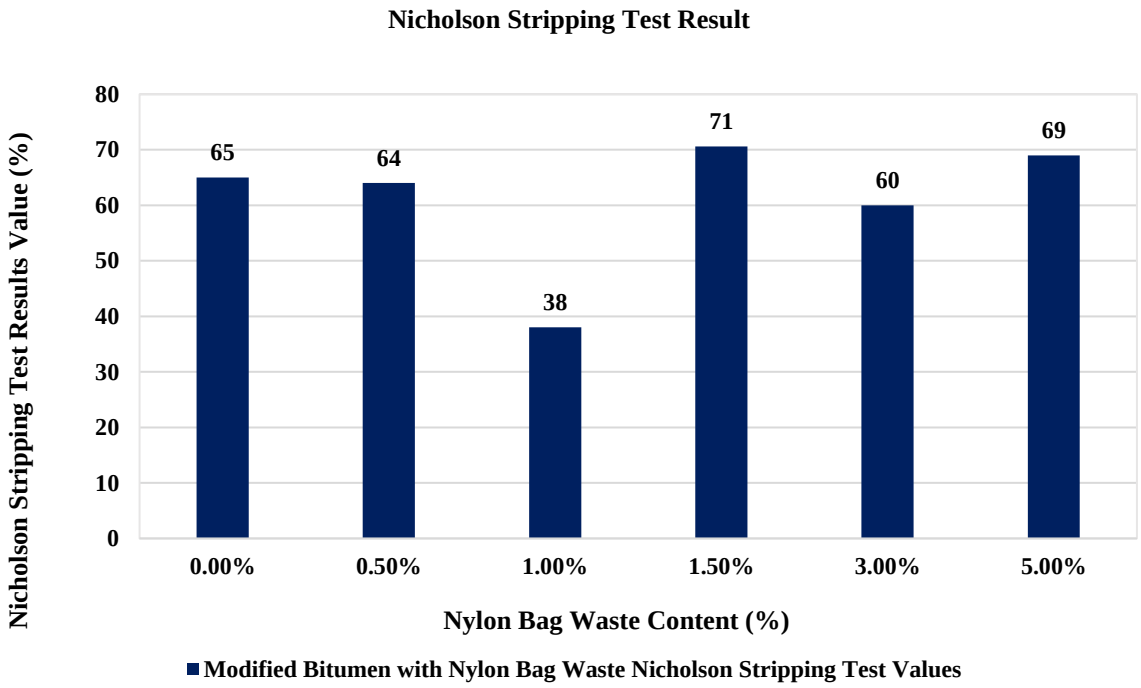

Figure 7. Nicholson test results of bitumen modified with 5 different rates of NBW

4. Conclusion

Physical and rheological bitumen tests were carried out on bitumen samples modified by using NBW 5 different amounts, and the results obtained were compared with the control bitumen results. The following results were obtained from the experimental studies.

- It was observed that both rheological and physical properties improved significantly in bitumen samples modified with NBW.
- According to the results of both penetration and softening point tests, it is understood that the temperature sensitivity of all modified samples decreases.
- According to the results of the rotational viscosity test, it was determined that all series samples had an increasing trend in viscosity values at 135 and 165 °C temperatures, and the highest increasing trends compared to the control sample were in NBW.
- In future studies, the behavior of these modified bitumen as bituminous mixtures should be examined.
- The study has shown that the use of waste nylon bag modifier will contribute to the improvement of the properties of bituminous binders, thus eliminating significant amounts of waste material and protecting the environment.

Acknowledgements

This research was funded by the Slovenian Research Agency (ARIS) and Scientific and Technological Research Council of Turkiye (TÜBİTAK) by supporting a bilateral project (grant numbers BI-TR/22-24-06 and 122N273).

References

Ahmadinia, E., Zargar, M., Karim, M. R., Abdelaziz, M., & Shafigh, P. (2011). Using waste plastic bottles as additive for stone mastic asphalt. *Materials & design*, *32*(10), 4844-4849.

Andrady, A. L. (2011). Microplastics in the marine environment. *Marine pollution bulletin*, *62*(8), 1596-1605.

Appiah, J. K., Berko-Boateng, V. N., & Tagbor, T. A. (2017). Use of waste plastic materials for road construction in Ghana. *Case studies in construction materials*, *6*, 1-7.

Barnes, D. K., Galgani, F., Thompson, R. C., & Barlaz, M. (2009). Accumulation and fragmentation of plastic debris in global environments. *Philosophical transactions of the royal society B: biological sciences*, *364*(1526), 1985-1998.

Clapp, J., & Swanston, L. (2009). Doing away with plastic shopping bags: international patterns of norm emergence and policy implementation. *Environmental politics*, *18*(3), 315-332.

Gökalp, İ. (2021). The waste transparent nylon modified bitumen properties: Experimental assessment on physical, rheological properties and storage stability. *Construction and Building Materials*, *303*, 124353.

Gürer, C., & Selman, G. Ş. (2015, June). Using tincal and colemanite wastes in bituminous hot mixtures as filler. In *International Conference on Bituminous Mixtures and Pavements, 6th, 2015, Thessaloniki, Greece*.

Hınıslıoğlu, S., & Ağar, E. (2004). Use of waste high density polyethylene as bitumen modifier in asphalt concrete mix. *Materials letters*, *58*(3-4), 267-271.

Hopewell, J., Dvorak, R., & Kosior, E. (2009). Plastics recycling: challenges and opportunities. *Philosophical Transactions of the Royal Society B: Biological Sciences*, *364*(1526), 2115-2126.

Kwame, B. A. A. W. D., & Baako, A. S. Y. (2015). Assessment of suitability of plastic waste in bituminous pavement construction. *Assessment*, *7*(11).

Polacco, G., Filippi, S., Merusi, F., & Stastna, G. (2015). A review of the fundamentals of polymer-modified asphalts: Asphalt/polymer interactions and principles of compatibility. *Advances in colloid and interface science*, *224*, 72-112.

Punith, V. S., & Veeraragavan, A. (2003). Laboratory fatigue studies on bituminous concrete mixes utilizing waste shredded plastic modifier. *Publication of: ARRB Transport Research, Limited*.

Thompson, R. C., Swan, S. H., Moore, C. J., & Vom Saal, F. S. (2009). Our plastic age. *Philosophical Transactions of the Royal Society B: Biological Sciences*, *364*(1526), 1973-1976.

Vasudevan, R., Sekar, A. R. C., Sundarakannan, B., & Velkennedy, R. (2012). A technique to dispose waste plastics in an ecofriendly way–Application in construction of flexible pavements. *Construction and Building Materials*, *28*(1), 311-320.

Victory, W. (2022). A review on the utilization of waste material in asphalt pavements. *Environmental Science and Pollution Research*, *29*(18), 27279-27282.

Web Source 1: https://medyascope.tv/2022/04/01/turkiyenin-cop-ithalati-az-gelismis-ulkeler-gelismis-ulkelerin-coplugu-olarak-goruluyor/

Web Source 2: https://tr.euronews.com/2022/05/25/ab-ulkelerinin-turkiye-ye-gonderdigi-cop-uc-kat-artarak-14-7-milyon-tona/

CivilTech
2nd International Symposium on Innovations in Civil Engineering and Technologies
October 30 – November 1, 2024, Isparta / TURKIYE

Rail Thermal Buckling Risk Management: Comparative Analysis of Stress-Free Temperature Determination in the USA and Türkiye

Mehmet Saltan[1], *Ferhat Çeçen*[2], *Ömer Faruk Acar*[3]

*cecenferhat@sdu.edu.tr

Abstract

Rail Thermal Buckling (RTB) is one of the most significant and growing risks to railway safety worldwide, driven by factors such as welded rail joints, high speed/heavy duty operations, 24-hour service, and climate change. To manage this risk, railway engineers rely on a key parameter known as Stress-Free Temperature (SFT). However, different railway organizations around the world use different approaches to determine SFT values. This study addresses this critical issue by examining the possible outcomes of practices in two different countries. The research uses data collected over the past three years at Wilmington Station, one of the rail and air temperature monitoring stations on rail lines operated by Amtrak (USA). Based on this data, SFT values were calculated according to the AREMA manual. In addition, a contrasting SFT value was calculated from the same data, based on the procedure used by TCDD (Turkish State Railways). Statistical analyses were then performed on the three years of rail and air temperature data using these two SFT values. The analysis showed that the SFT value of 41°C determined by the AREMA approach significantly reduces the RTB risk, with only 4.64% of all rail temperature data analyzed exceeding this SFT value. However, outside the summer months, this scenario is likely to result in higher tensile forces than the 24°C SFT value calculated using the second method, thereby increasing the risk of rail/weld failure.

Keywords: Railways; thermal buckling; heat related rail failure; data management; global warming

[1] *Suleyman Demirel University, Department of Civil Engineering, Isparta, Turkiye*
[2] *Suleyman Demirel University, Göller Bölgesi Teknokent Coordinatorship, Isparta, Turkiye*
[3] *Suleyman Demirel University, Department of Economics and Administrative Sciences, Isparta, Turkiye*

1. Introduction

Conventional ballasted track superstructure consists of two parallel steel rails framed by equally spaced sleepers. This framework is then positioned floating on the ballast bed. A number of different methods have been developed over the years to join these frameworks together. Old-style bolted rail joints (as shown in Figure 1.a-b), while providing flexibility against thermal effects (Esveld, 2014), are increasingly being abandoned due to their numerous disadvantages. These include discontinuities in the rolling surface (Chao, 2022), rapid deterioration of track geometry, and dangerous damage to rails, sleepers and fasteners (Esveld, 2014), which worsens with increasing operating speed (Chapman et. al., 2007). Today, especially on high-speed lines, the most common type is the Long-Welded Rail (LWR) or Continuous-Welded Rail (CWR). This modernization with welded rail joints (as shown in Figure 1.c) offers a significant reduction in total life cycle costs (Esveld, 2014), improved passenger comfort (Kjell, 2014), and higher operating speeds (Sanchis et. al., 2020). However, rails expand in heat and contract in cold weather, and welded joints do not provide flexibility against these thermal changes (Baker et. al., 2009). With the added adverse effects of climate change, this innovation is forcing railway engineers to develop additional complex solutions (Esveld, 2014).

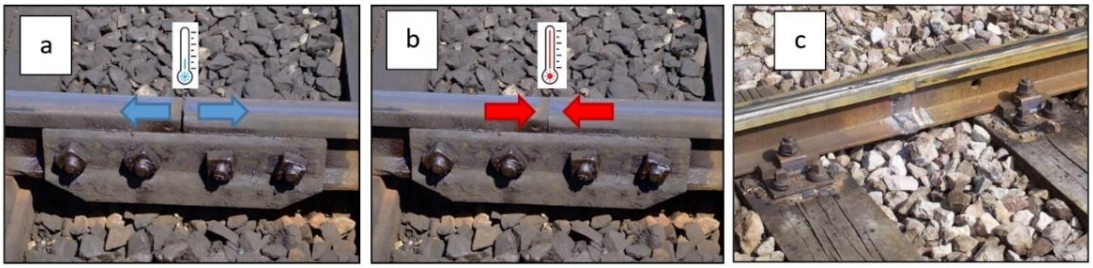

Figure 1. Rail joint examples: **a)** Conventional bolted rail joint example allowing thermal contraction, **b)** The same bolted rail joint example demonstrating its ability to allow thermal expansion, **c)** A welded rail joint example that does not allow thermal contraction or expansion.

As detailed in the literature (Chao, 2022; Çeçen and Aktaş, 2023), below a certain level known as the Stress-Free Temperature (SFT), also referred to as the Rail Neutral Temperature (RNT), railways can experience rail or weld failures at these low temperatures due to tensile stresses caused by thermal contraction of the rails. Conversely, at high temperatures, above SFT, compressive stresses due to thermal expansion progressively increase and at a certain level, known as the Critical Rail Temperature (CRT), rail thermal buckling (RTB) can occur. RTB incidents are usually due to inadequate ballast shoulder, the use of lightweight wooden sleepers or poor welds resulting in C-shaped bending or S-shaped buckling (Sanchis, 2020), as shown in Figure 2 (CNNTurk, 2010). Consequently, if the design temperature values (SFT and CRT) are underestimated, the compressive stresses in the rail will increase in hot weather conditions, leading to a higher number of RTB incidents. Conversely, if the design temperature values are overestimated, the tensile stresses in the rail will increase in cold weather conditions, leading to a higher number of rail or weld failures (Esveld, 2014; Ferranti et. al., 2016; Sanchis, 2020). Railway engineers use historical air and rail temperature data to determine the optimal SFT for the rails. During welding, maintenance, and construction, they carefully ensure that the rails are within the Desired Rail Temperature (DRT) range, which is set around the SFT value. Alternatively, they apply prestress to the rails to achieve the length that corresponds to the DRT rail length (AREMA, 2005; MEB, 2013).

Figure 2. A typical example of S-shaped RTB, Pazarcık, Kahramanmaraş, Türkiye (CNNTurk, 2010)

In this study, approximately 1050 days of rail and air temperature records obtained from the Wilmington (USA) monitoring station have been used to make a preliminary comparison of the procedures applied on the TCDD (Turkish State Railways) lines with those implemented according to the American Railway Engineering and Maintenance-of-Way Association (AREMA), e.g. Amtrak. The aim of this study is to raise awareness among railway managers and to provide a case study from which railway practitioners and engineers can benefit.

2. Method

In this study, rail and air temperature data were obtained from Amtrak, the national rail passenger service provider in the USA. As shown in Figure 3, Amtrak provides real-time rail temperature and meteorological data through an open-access website that includes data from several monitoring stations (Amtrak Engineering, 2024). The website is updated every 15 minutes, covering the past 24 hours, and also provides access to historical records dating back to 2007. This study used data from Wilmington Station, which is located on Amtrak's Northeast Corridor (AP Line). The station's GPS coordinates are 39.74914° latitude and -75.51888° longitude. According to the Google Earth images shown in Figure 4, there are no nearby structures that could cause artificial shading, and the rail lines are constructed of both concrete and wooden ties, so this site was considered suitable for the objectives of this study.

Figure 3. Screenshots taken from the AMTRAK website (Amtrak Engineering, 2024)

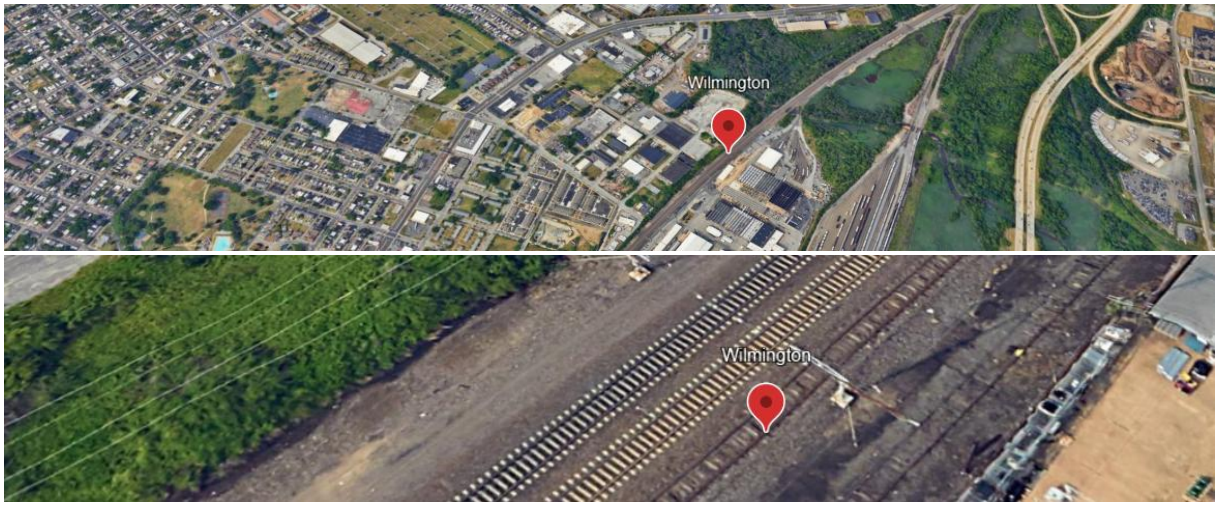

Figure 4. Satellite images (Google Earth, 2024) showing the location of sensors at Wilmington Station

This study uses data from the beginning of July 2021 to the end of July 2024, a period of 1,128 days. However, some data is missing, often in the winter months (e.g. January 2024), probably due to maintenance or equipment breakdowns. As a result, the dataset comprises 1,050 days, including 99,835 air temperature readings and 99,835 rail temperature readings. Figures 5 and 6 show monthly graphs of "air temperature" data recorded over the period mentioned. In these graphs, data for the same month from different years are juxtaposed for easy comparison. Additionally, the highest air temperature, the lowest air temperature, and the absolute difference between these two values are noted in the top right-hand corner of each graph. According to the data, the highest recorded air temperature within the analyzed period is 37.33°C, observed in July 2024. The lowest air temperature is -13.78°C, recorded in December 2022. The largest difference (delta) of 31.33°C was recorded in November 2022. This air temperature data can be considered similar to the climatic conditions of Istanbul, Türkiye (MEB, 2013). Both regions exhibit a temperate climate, characterized by the absence of extreme heat during the summer months and the lack of very low negative temperatures in the winter.

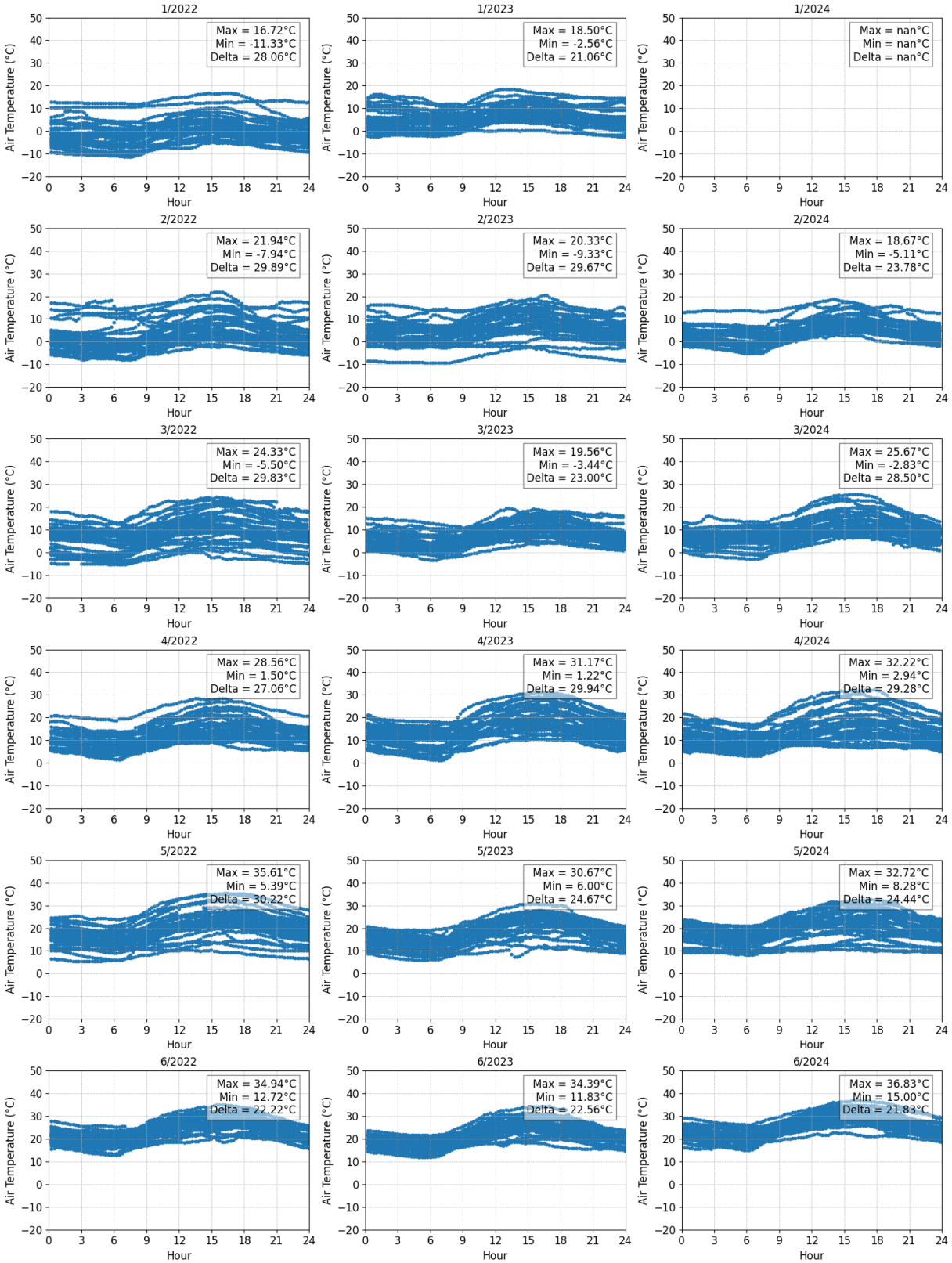

Figure 5. Hourly changes in air temperature for the first six months of the year (2021-2024)

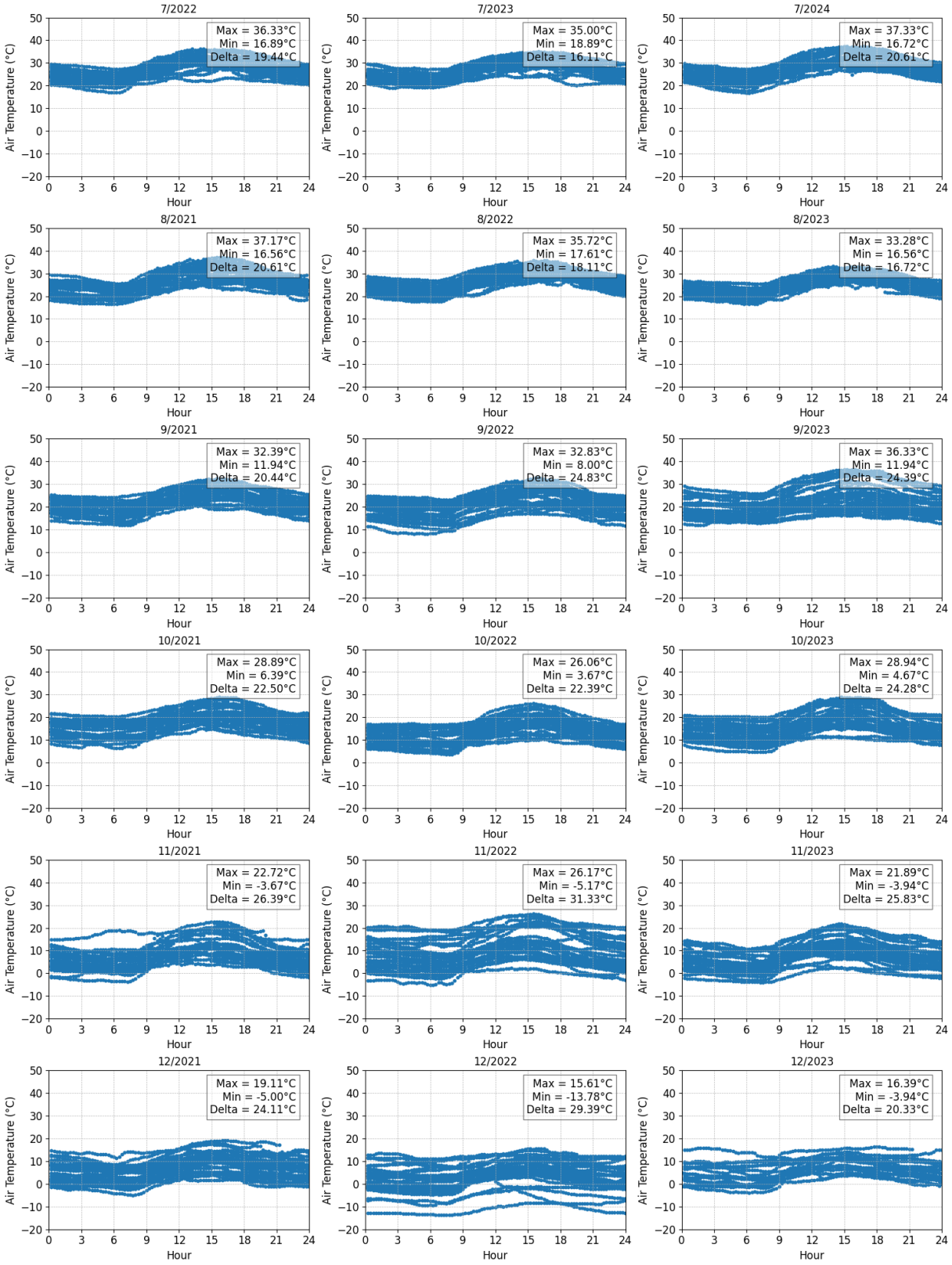

Figure 6. Hourly changes in air temperature for the second half of the year (2021-2024)

Figures 7 and 8 show monthly graphs of "rail temperature" data recorded over the same period. In these graphs, data for the same month from different years are placed side by side for easy comparison. In addition, the highest rail temperature, the lowest rail temperature and the absolute difference between these two values (delta) are noted in the top right-hand corner of each graph. According to the data, the highest rail temperature ($T_{rail_{max}} or\ H_t$) recorded within the analyzed period is 50.97°C, observed in

August 2021 and July 2023. The lowest rail temperature ($T_{rail_{min}} veya\ L_t$) is -14.58°C, recorded in December 2022. The largest difference (delta) is 44.72°C, recorded in March 2024. There are also the absolute differences between the SFT, calculated according to the AREMA, and the L_t and H_t values. These values are then categorized according to whether they represent tension (SFT_Diff_Min) or compression (SFT_Diff_Max) stresses.

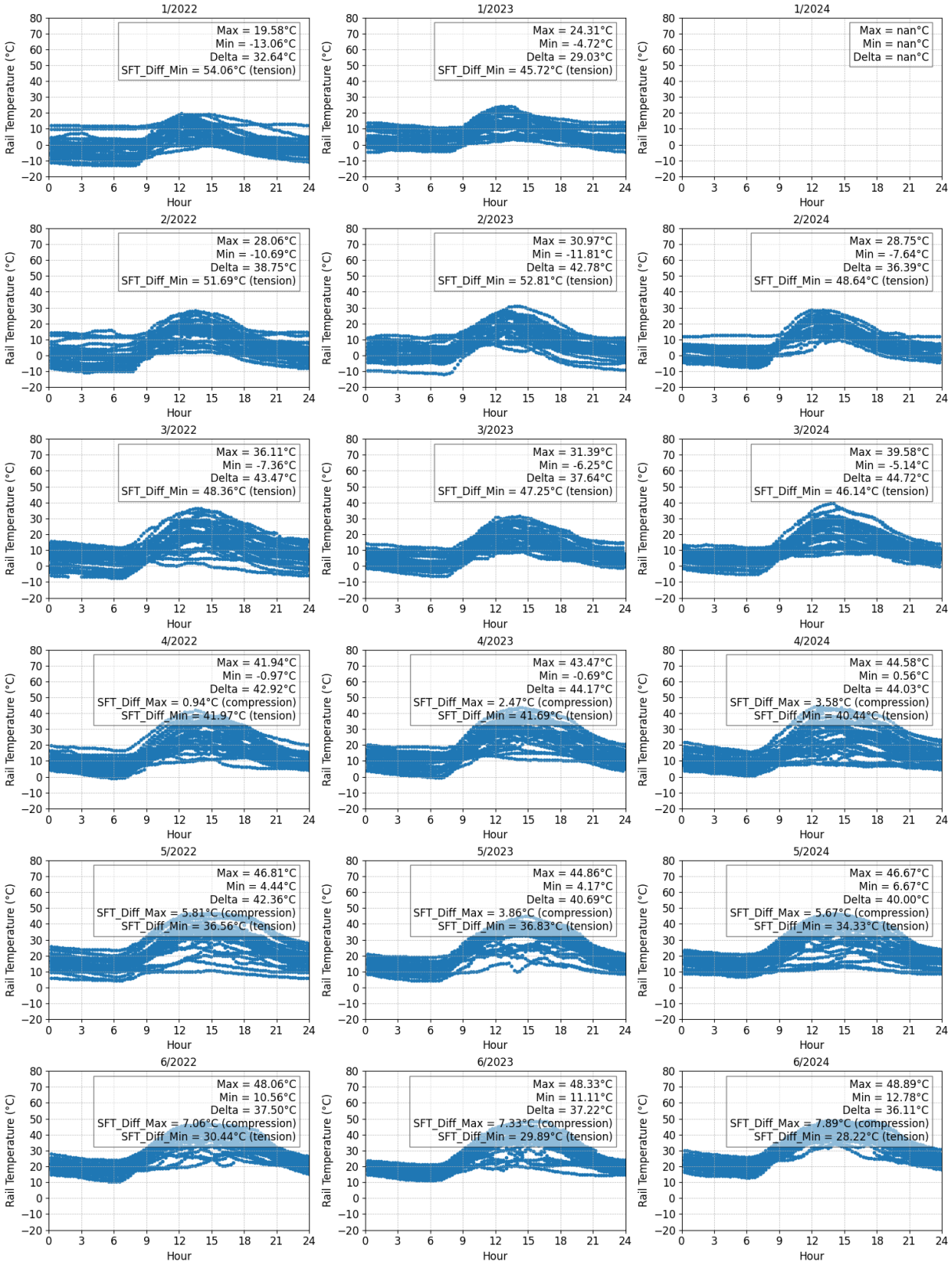

Figure 7. Hourly changes in rail temperature for the first six months of the year (2021-2024)

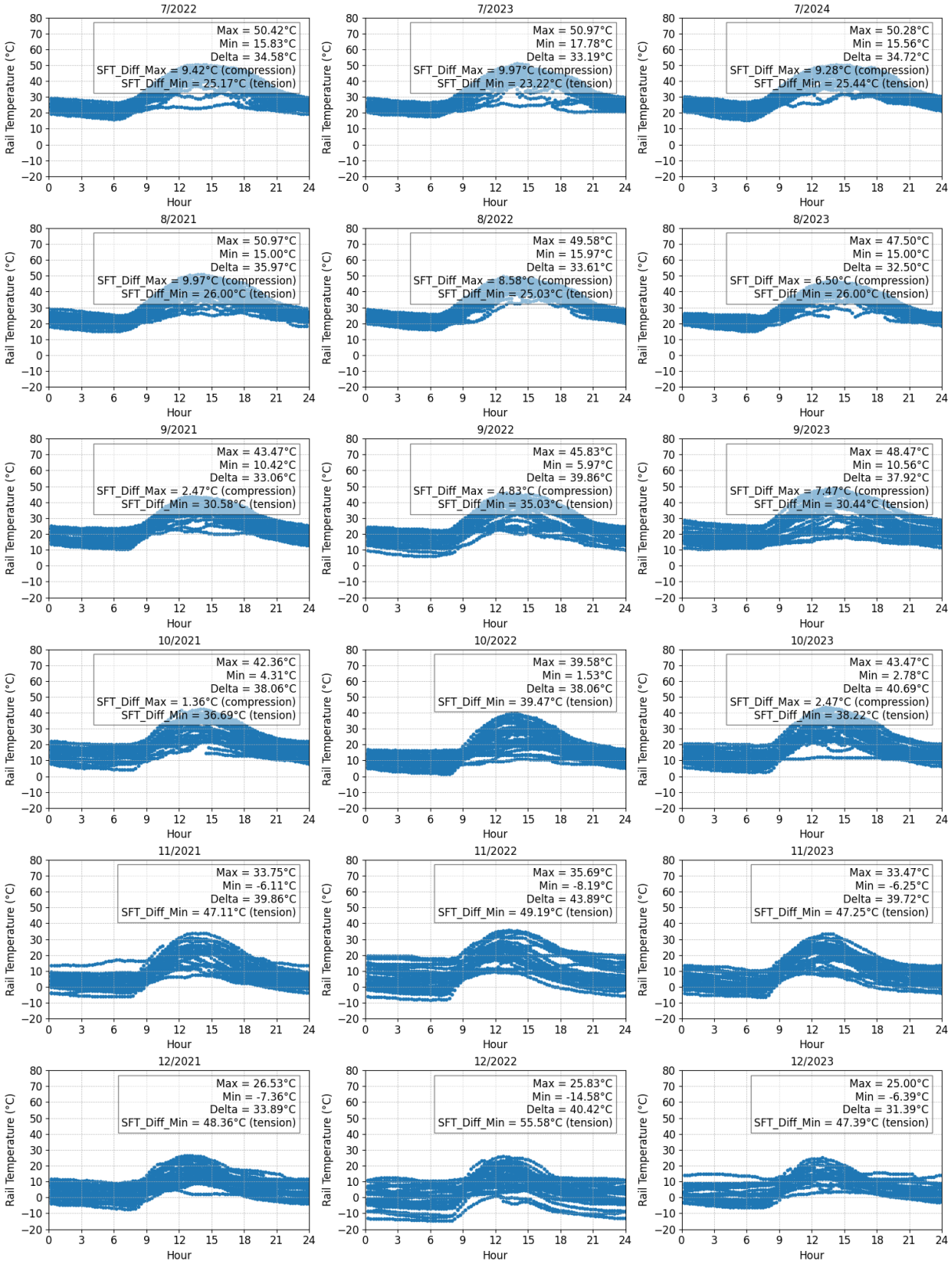

Figure 8. Hourly changes in rail temperature for the second half of the year (2021-2024)

According to AREMA manual (AREMA, 2005), rail joints should be welded within a temperature range called the Desired Rail Temperature (DRT). The maximum (Maximum DRT) and minimum (Minimum DRT) values of this range are calculated using Equations 1 and 2, based on the highest rail temperature (H_t) and the lowest rail temperature (L_t) recorded during the analyzed period. It is important to note that these equations are developed using Fahrenheit temperature units. For instance, with H_t = 123.75°F

and L_t = 5.76°F, the DRT range is calculated to be 94.42°F to 114.42°F, which converts to 34.7°C to 45.8°C in Celsius. A single SFT value of 41°C was selected from this range for comparative analysis. This SFT value was used to calculate the SFT_Diff_Max and SFT_Diff_Min values shown in Figures 7 and 8. Accordingly if the highest rail temperature for the month is above the SFT, the absolute difference is calculated as SFT_Diff_Max and a note is added in parentheses to indicate potential compressive stresses. Similarly, if the lowest rail temperature for the month is below the SFT, the absolute difference is calculated as SFT_Diff_Min and a note is added in parentheses to indicate potential tensile stresses.

$$Minimum\ DRT = \frac{2H_t + L_t}{3} + 10 \qquad (1)$$

$$Maximum\ DRT = \left[\frac{2H_t + L_t}{3} + 25\right] \pm 5 \qquad (2)$$

The SFT value calculated according to AREMA is applicable within the USA. However, due to differences in railway infrastructure, climatic conditions and, in particular, thermal buckling risk management practices, the same data set may yield significantly different SFT values for other countries. For comparison purposes, this study further analyses the SFT calculation method used by TCDD in Türkiye (Equation 3) (MEB, 2013). Based on the same three-year data set, the temperature range for rail temperature in rail welding processes was calculated to be 20.2°C to 26.2°C. A single SFT value of 24°C was selected from this range for comparative analysis.

$$DRT = \left[\frac{T_{rail_{min}} + T_{rail_{max}}}{2} + 5\right] \pm 3 \qquad (3)$$

It can be seen that, for the same set of data, a calculation result of 41°C is possible according to the AREMA manual, whereas this value corresponds to 24°C according to the TCDD practice. The difference could be even greater (45.8°C to 20.2°C) if the acceptable ranges are used. However, as an example analysis, it is considered that the values chosen provide sufficient insight and are therefore considered appropriate. In essence, the different SFT calculation methods used by different countries result in different DRT ranges despite the same rail temperature and air temperature data set. The advantages and disadvantages of these different SFT values are discussed in the following section.

3. Results and Discussion

As a result, Figure 9 shows bar graphs illustrating the number of data points (rail temperature values measured at 15-minute intervals) exceeding the SFT value of 41°C, calculated using Equations 1 and 2 according to the AREMA manual, at the top, and the number of data points exceeding the SFT_2 value of 24°C, calculated using Equation 3 according to the TCDD practice, at the bottom, at different times of the day. In the first case, data exceeding the SFT value were only recorded between 10:00 and 19:00, with a peak of about 800 data points between 13:00 and 14:00. The total number of data points exceeding the SFT value was only 4.64% of the total rail temperature data analyzed. In the second application of the SFT value, data exceeding the SFT_2 value was observed at all times of the day, accounting for a significant 29.89% of the total data analyzed, with a peak of approximately 2,500 data points between 12:00 and 13:00. Based on this initial analysis, it can be said that the RTB risk due to compressive forces in the AREMA application is significantly limited in terms of both the number of data points and the time window, whereas in the TCDD application, compressive forces are present at all times of the day, with a significantly higher number of excessive data points.

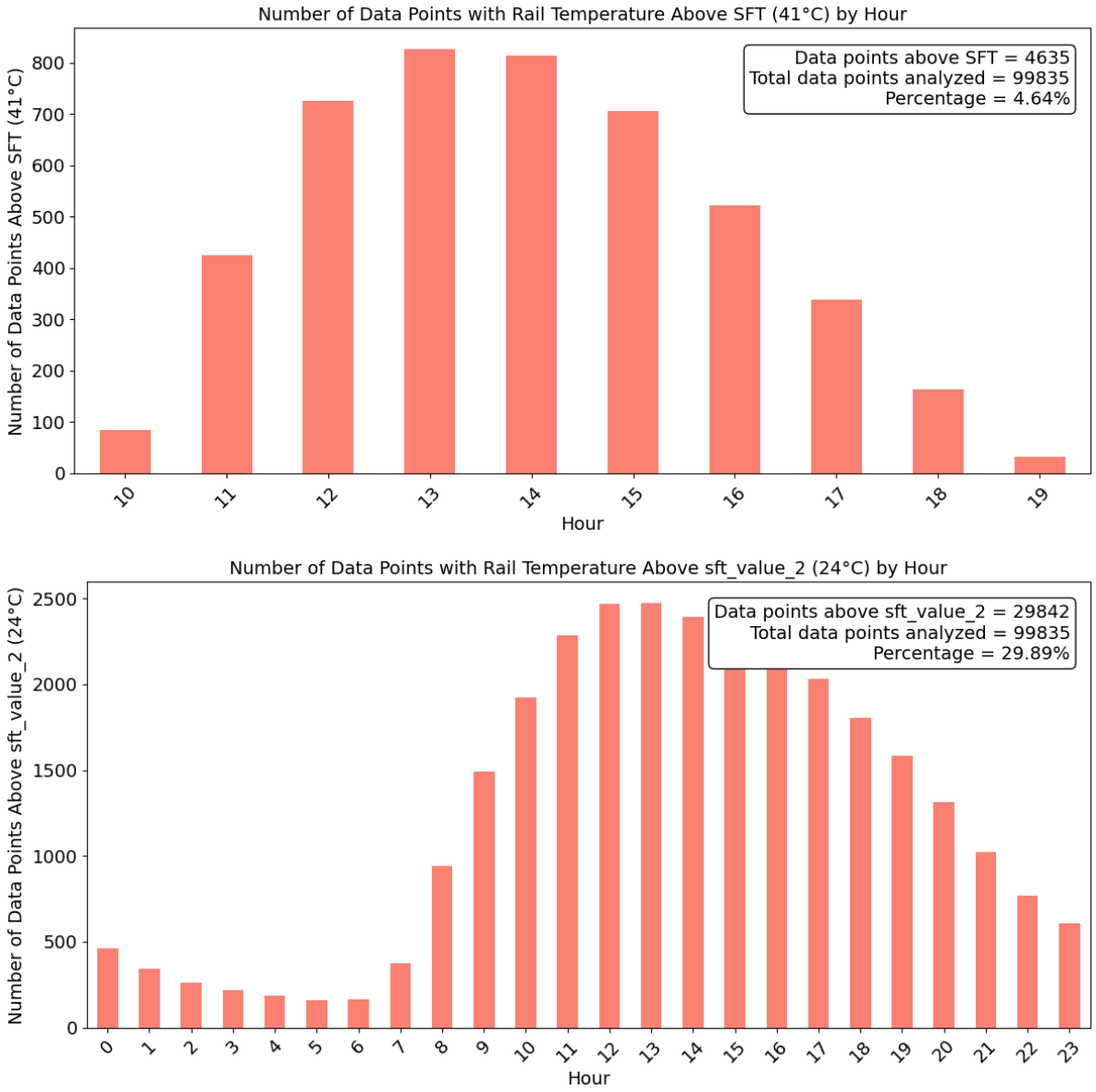

Figure 9. Distribution of data points exceeding SFT values over time (hours)

Similar analyses, this time on a monthly rather than hourly basis, were carried out as shown in Figure 10. In the first case, data exceeding the SFT (calculated according to the AREMA manual) are only recorded in April-October, with a peak of almost 80 days in July. The percentage of days exceeding the SFT within all analyzed days is limited to 24.19%. In the second SFT application (calculated according to TCDD practices), days exceeding the SFT_2 value are observed throughout the year, representing a significant 65.05% of all analyzed data, with approximately 90 days each in the summer months (June, July, August). This initial analysis shows that in the AREMA application the risk of RTB due to compressive forces is considerably limited in terms of days and months, whereas in the TCDD application compressive stresses are present throughout the year with a much higher number of excessive days. However, both methods of analysis are rather superficial and detailed analyses are needed to predict how successful the management of the RTB risk can be. In this context, the analyses in Figures 11 and 12 have been added.

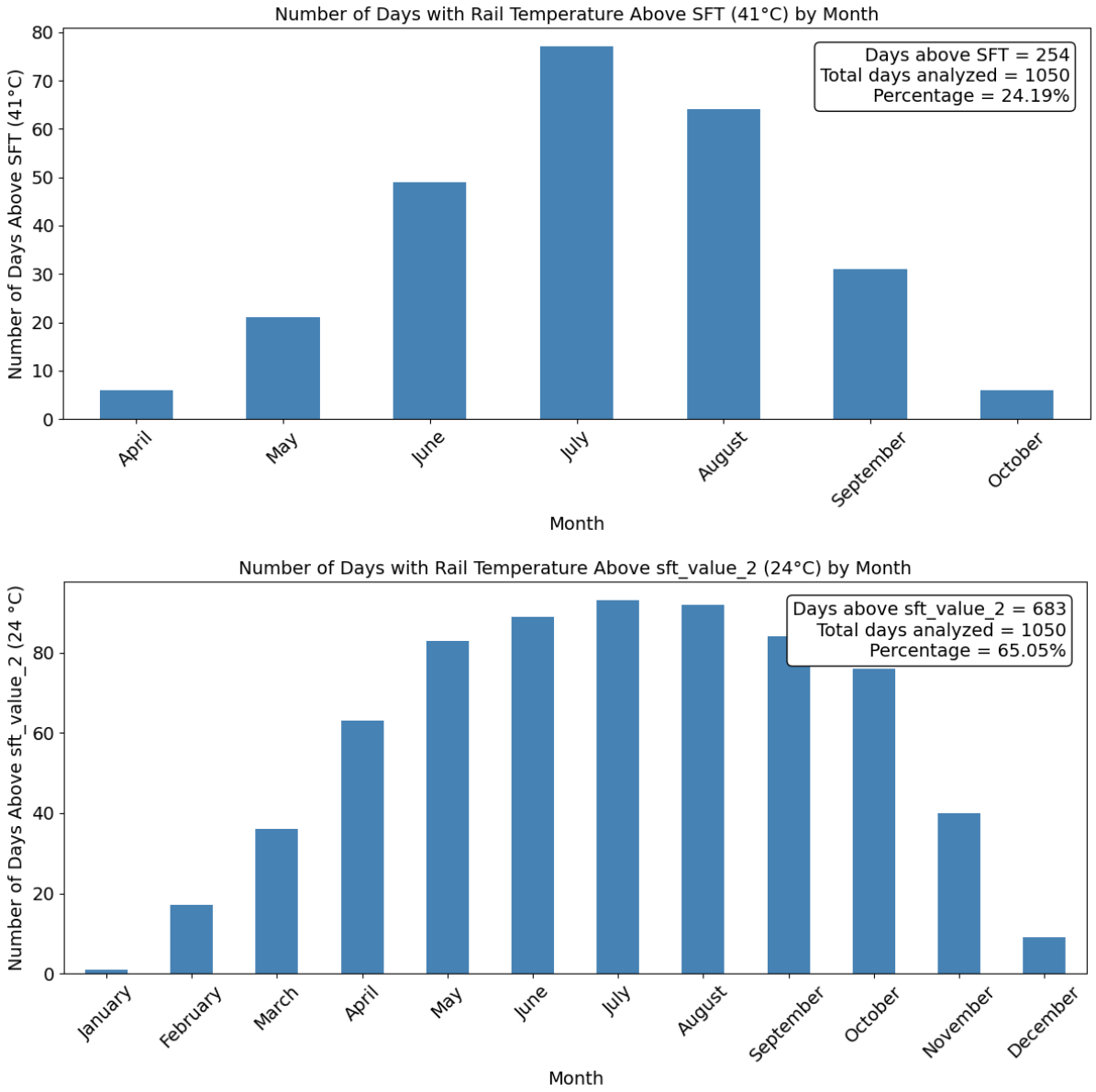

Figure 10. Distribution of days exceeding SFT values by month (total)

In Figure 11 the distribution of SFT_Diff_Max values is shown at the top, showing the levels of deviation from the SFT value of 41°C calculated using Equations 1 and 2 according to the AREMA manual. These deviations from the SFT_2 value of 24°C, calculated using Equation 3 according to TCDD practice, are shown at the bottom. These deviations are presented as bar graphs, segmented by different months and years. For the AREMA application, data exceeding the SFT value are only recorded between April and October, with particularly high exceedances of 10°C in July and August. In contrast, the TCDD application shows that days exceeding SFT_2 are present throughout the year, with exceedances reaching about 27°C in July and August. According to these last analyses, the AREMA application results in a significantly limited RTB risk due to compressive forces, both in terms of the number of days and months and the level of exceedance (in °C). However, the TCDD application shows compressive stresses throughout the year with a significantly higher number of exceedance days and much higher exceedance levels, indicating a greater RTB risk under similar infrastructure conditions. These analyses are not sufficient to give a complete picture, so additional analyses are shown in Figure 12.

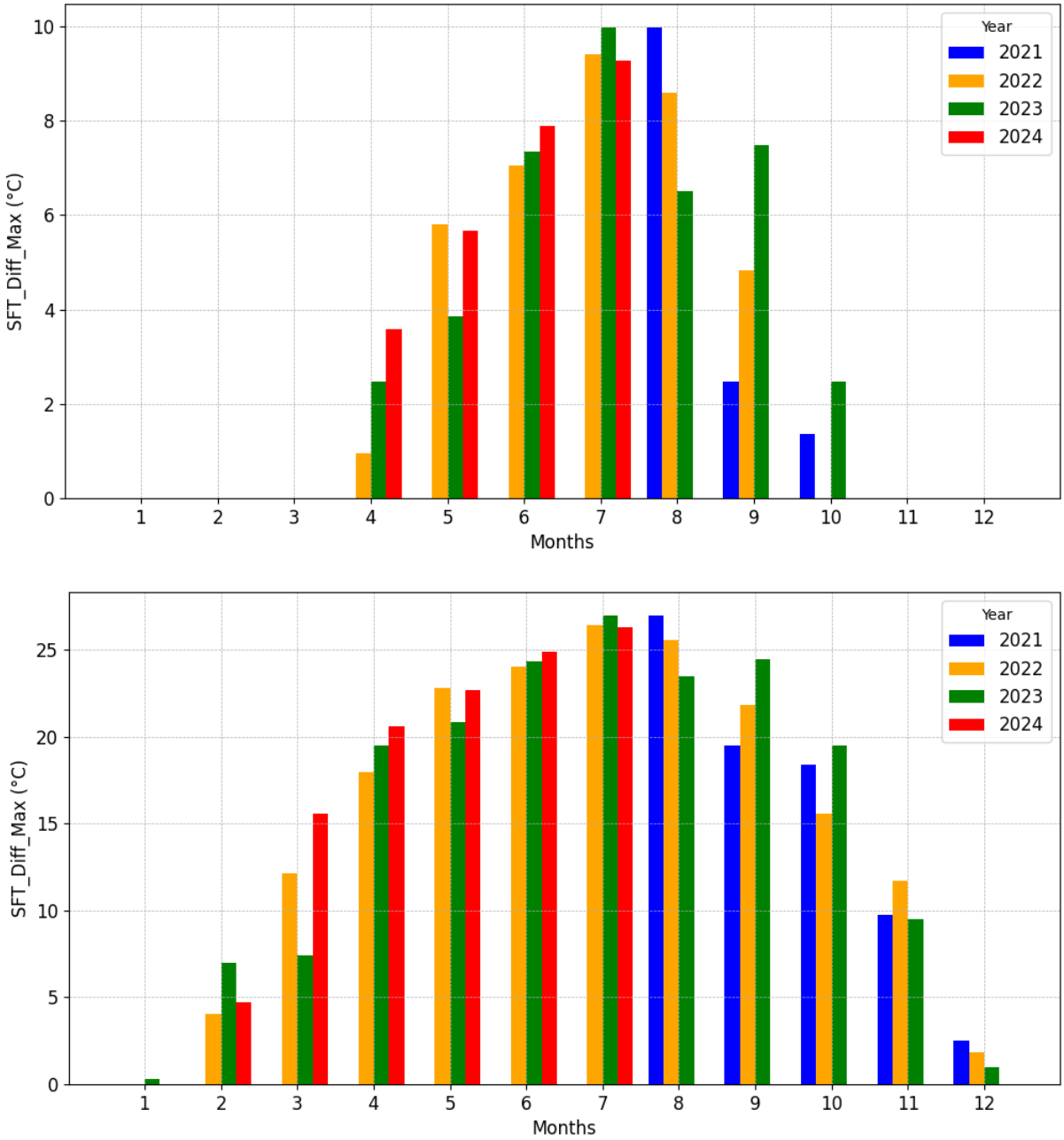

Figure 11. Monthly and annual distribution of the differences between maximum rail temperatures and SFT values

In Figure 12, similar to the previous graphs, the distribution of SFT_Diff_Min values is shown at the top, showing the levels of negative deviation from the SFT value of 41°C (the amount by which it remains below the SFT value of 41°C) calculated using Equations 1 and 2 according to the AREMA manual. These deviations from the SFT_2 value of 24°C, calculated using Equation 3 according to TCDD practice, are shown at the bottom. These are shown as bar graphs, segmented by different months and years. Both conditions show that rail temperature values below the SFT value are recorded in all months of the year, with these differences peaking in December and January. In the first case, the difference is more than 50°C, while in the second case it is closer to 35°C. This indicates that the AREMA application results in a much higher risk of rail/weld failure due to tensile forces. Specifically, the rail temperature differences (lows) with the SFT value outside the summer months (June, July, August) are equal to or greater than those observed during the harshest winter months in the second application. In other

words, rail tensile forces occurring in May or September during the first application are greater than those occurring in December or January during the second application.

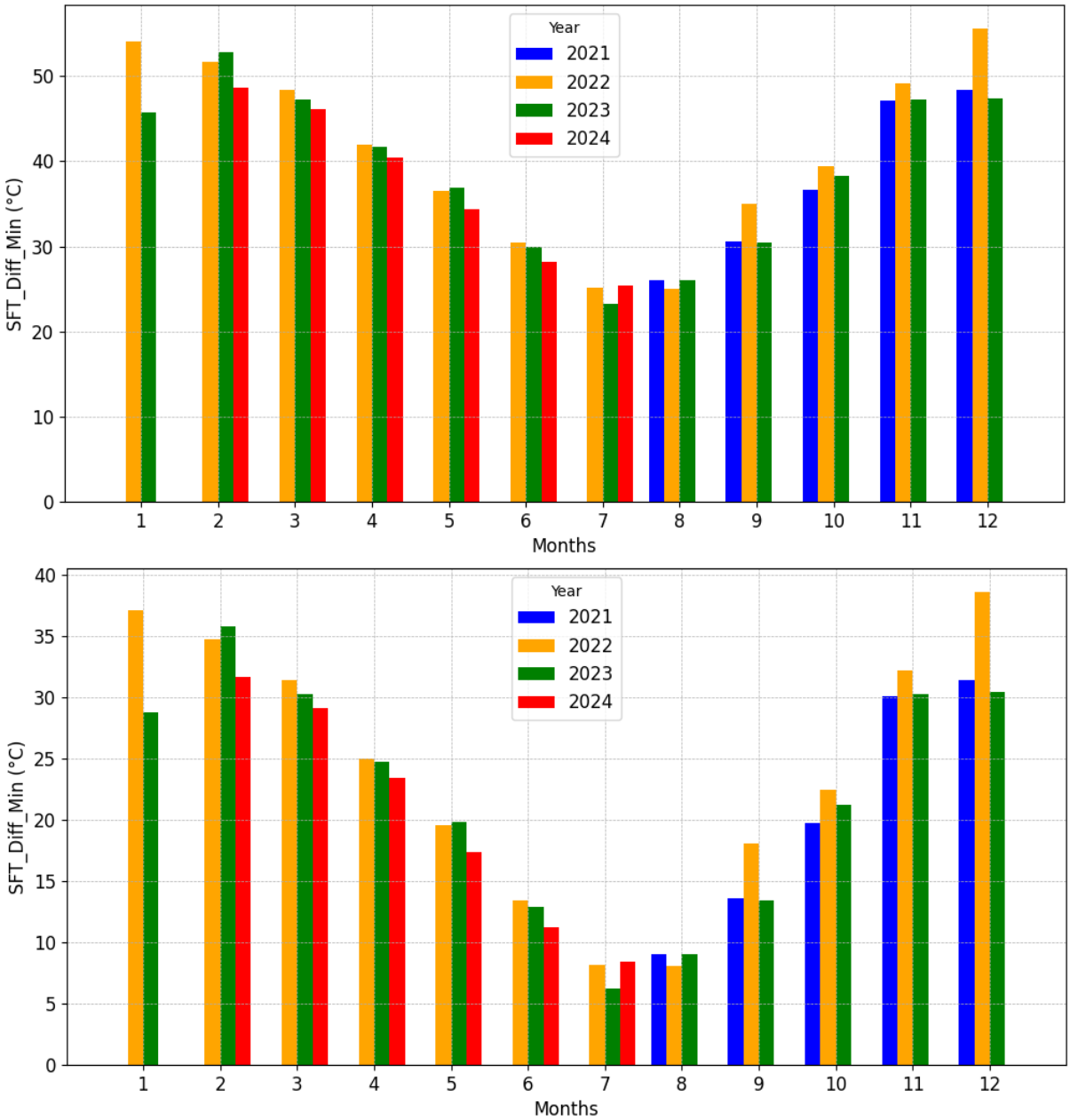

Figure 12. Monthly and annual distribution of the differences between minimum rail temperatures and SFT values

4. Conclusions

This study aims to raise awareness of the risk of Rail Thermal Buckling (RTB), which is expected to become an increasing threat to rail safety in the near future due to climate change. In this context, approximately 1,050 days of rail and air temperature records from the Wilmington (USA) monitoring station were used to compare the calculation methods of the Stress-Free Temperature (SFT) values and associated Desired Rail Temperature (DRT) ranges used by the Turkish State Railways (TCDD) and Amtrak (following the AREMA manuals). This comparison shows how different approaches to calculating SFT and DRT can lead to different levels of risk associated with RTB incidents and rail/weld failures. Some of the key conclusions of this analysis are presented below:

a. Different methods of calculating the SFT result in significantly different values. For the same rail and air temperature dataset, this case study shows an SFT calculation result of 41°C according to the AREMA manual and an SFT of 24°C according to TCDD practices.
b. Rail temperature data exceeding the 41°C SFT were only recorded between 10:00 and 19:00, accounting for 4.64% of the total. Data exceeding the 24°C SFT were recorded in each of the 24 hours, accounting for 29.89%. Compressive forces are therefore more frequent and prolonged in the TCDD application than in the AREMA application.
c. Data exceeding the 41°C SFT are only recorded from April to October, peaking in July and covering 24.19% of the days. In contrast, data exceeding the 24°C SFT occur throughout the year, representing 65.05% of the data and almost all summer days. Thus, AREMA limits the RTB risk to fewer days, whereas TCDD experiences higher compressive stresses throughout the year.
d. For the 41 °C SFT, the highest exceedances are 10 °C in July and August. In contrast, the 24 °C SFT shows exceedances up to 27 °C in the same months. AREMA limits the RTB risk with fewer exceedance days and lower levels, whereas TCDD shows higher risks with more exceedance days and higher levels.
e. The last but not least, rail temperatures below both SFT values are recorded throughout the year, peaking in December and January. The difference is over 50°C for the 41°C SFT and around 35°C for the 24°C SFT, indicating a higher risk of rail/weld failure with AREMA. It is noteworthy that, the tensile forces in May or September for the 41°C SFT exceed those in December or January for the 24°C SFT.

This study reveals notable differences between the AREMA and TCDD methods for calculating SFT values and DRT ranges. AREMA typically results in higher SFT values with fewer exceedances, potentially reducing the risk of RTB from compressive forces. Conversely, TCDD shows lower SFT values with more frequent exceedances, indicating a higher risk of compressive stresses throughout the year, however it reduces tensile stresses at colder temperatures. Although the statistical analyses in this study do not establish the superiority of any method, they do emphasize the need for accurate SFT calculations in railway design and maintenance. Correct SFT values are essential for managing both compressive and tensile stresses, as incorrect values can increase the risk of derailment in changing weather conditions.

Acknowledgments

This study used the actual rail and air temperature data published on Amtrak's open access website as part of the Rail Temperature Prediction System (RTPS), developed by ENSCO with support from the US Federal Railroad Administration (FRA) and initially deployed on Amtrak routes. The authors would like to thank these organizations and officials for their support in advancing public science.

References

AREMA (American Railway Engineering and Maintenance-of-Way Association), (2005). Manual for Railway Engineering, Chapter 5: Track, Part 5: Track Maintenance

Çeçen, F., and Aktaş, B. (2023). Use of Thermal Imaging Cameras to Identify Best Locations for Rail Temperature Monitoring Systems (RTMS): Development of Rapid Analysis Methods. Railway Engineering, 20:141-154. https://doi.org/10.47072/demiryolu.1474099

Chao, E.Y. (2022). Development of a First-Generation Prototype Laboratory System for Rail Neutral Temperature Measurements, Master's thesis, University of South Carolina, College of Engineering and Computing, Civil Engineering Faculty, 63 p.

Chapman, L., Thornes, J.E., Huang, Y., Cai, X., Sanderson, V.L., and White, S.P. (2007). Modelling of Rail Surface Temperatures: A Preliminary Study. Theoretical and Applied Climatology, 92:121–131. https://doi.org/10.1007/s00704-007-0313-5

CNNTurk. (2010). Sıcaktan tren rayları bile genleşti! August 3, 2010. Accessed July 30, 2024. https://www.cnnturk.com/turkiye/sicaktan-tren-raylari-bile-genlesti-11-12-2018

Esveld, C. (2014) Modern Railway Track. MRT-Productions, Zaltbommel.

Ferranti, E., Chapman, L., Lowe, C., McCulloch, S., Jaroszweski, D., and Quinn, A. (2016). Heat-related Failures on Southeast England's Railway Network: Insights and Implications for Heat Risk Management. Weather, Climate, and Society, 8:177–191. https://doi.org/10.1175/WCAS-D-15-0068.1

Kjell, G.B. (2014). Estimating the Total Risk for a Sun-kink by Measuring Wave Propagation in the Track, Journal of Rail and Rapid Transit, 230. https://doi.org/10.1177/0954409714562491

MEB (Milli Eğitim Bakanlığı). (2013). UKR (Uzun Kaynaklı Ray). Accessed July 30, 2024. http://www.megep.meb.gov.tr/mte_program_modul/moduller_pdf/UKR%20(Uzun%20Kaynakl%C4%B1%20Ray).pdf

Sanchis, I.V., Franco, R.I., Fernández, P.M., Zuriaga, P.S., and Torres J.B.F. (2020). Risk of Increasing Temperature Due to Climate Change on Highspeed Rail Network in Spain. Transportation Research Part D: Transport and Environment, 82. https://doi.org/10.1016/j.trd.2020.102312

CivilTech
2nd International Symposium on Innovations in Civil Engineering and Technologies
October 30 – November 1, 2024, Isparta / TURKIYE

GIS-Based Analysis for Determining Hot Spots of Pedestrian-Involved Crashes

Oruc Altintasi[1] *, Ahmet Hakan Cay*[1]

*oruc.altintasi@ikcu.edu.tr

Abstract

This study examines the spatial-temporal analysis of pedestrian-involved crashes in İzmir, Türkiye using Geographic Information System based analysis. As one of the most developed and densely populated cities, İzmir experiences a high rate of pedestrian accidents, making it a critical case for traffic safety analysis. Data from the İzmir Police Department reveal that between 2017 and 2019, a total of 6,794 pedestrian-involved crashes occurred, accounting for 15.7% of the total accidents in these years. After data cleaning and processing, the Kernel Density Estimation tool in ArcGIS Pro was employed to perform spatial density analysis and identify areas with high and low concentrations of these accidents. The study analyzed patterns of pedestrian-involved accidents by year and month to identify high-density crash areas within the core city. The results showed that while the number of pedestrians involved in accidents decreased over the years, the Kernel density estimation results indicated that the hot spot locations of the pedestrian crashes were not changed. April month was found as the highest number of accidents with 541 crashes, while January month was the lowest with 351 crashes. The lower number of accidents in winter can be attributed to people socializing less and being more cautious in bad weather conditions.

Keywords: Geographic information systems; kernel density estimation; pedestrian involved crashes; sustainable transportation

[1] *İzmir Kâtip Çelebi University, Faculty of Engineering and Architecture, Civil Engineering Department, İzmir, Turkiye*

1. Introduction

Pedestrian safety is a critical concern in urban areas, where high population density, heavy traffic, and proximity to public bus stops often increase the risk of pedestrian-involved crashes (PICs) (Craig et al., 2019). Globally, pedestrian accidents represent a significant portion of traffic-related fatalities and injuries, particularly in large cities where pedestrian and vehicular interactions are frequent (World Health Organization, 2018). LeBeau (2019) found that pedestrian crashes reached their highest level in 2018, based on an analysis of 28 years of crash data for U.S. cities. According to the Vision Zero (2019) report, the primary reason for this rise in pedestrian crashes is the lack of a comprehensive safety manual for pedestrians. As a result, pedestrian safety improvements vary between countries and even between specific locations, with one of the most widely implemented measures being the reduction of vehicular traffic speed (Ulak et al., 2021). Hence, it is important to develop common efficient strategies to reduce pedestrian crashes (Sze et al., 2007). The effectiveness of strategies developed to mitigate pedestrian-involved accidents relies on the accurate identification of hotspot locations. A thorough understanding of these hotspots is crucial to ensure that interventions are strategically targeted and effectively address the underlying causes of accidents (Özen, 2021).

In Türkiye, the rapid urbanization, increased private car ownership, private car-based transportation master plans have led to a significant raise in accident rates, especially in densely populated cities like İzmir. With a population exceeding of 4.3 million, İzmir ranks among the most developed cities in the country, making it a critical case for examining urban traffic safety challenges, particularly pedestrian-involved crashes. Understanding the spatial and temporal distribution of pedestrian accidents is vital for identifying high-risk areas and proposing effective interventions, which is the main focus of this research. Geographic Information System (GIS) software offers valuable tools for analyzing and visualizing traffic accident distributions. In this study, the Kernel Density Estimation (KDE) method was employed to identify accident hotspots using three years of traffic accident data obtained from the İzmir Police Department. By analyzing crash data across various years and months, this research seeks to uncover trends that can inform targeted traffic safety measures. The KDE analysis not only identifies accident hotspots but also reveals changes in these critical areas over time. The findings are expected to provide essential insights into the spatial patterns of pedestrian-involved crashes in İzmir, laying the groundwork for the development of urban safety interventions aimed at enhancing pedestrian safety.

2. Material and Method

The methodological framework of this research is presented in Figure 1. The analysis began with data collection, focusing on the locations and times of pedestrian-involved crashes that occurred between 2017 and 2019 within the city boundaries of İzmir, Türkiye. The traffic accident data were obtained from the İzmir Police Department. Table 1 provides an example dataset detailing the year, time, date, accident type, and the X and Y coordinates of each pedestrian accident. Using these coordinates, the spatio-temporal distribution of pedestrian crashes across the city was analyzed. The dataset was imported into the GIS environment and prepared for hotspot analyses. The study utilized GIS-based spatial data analysis methods to visualize the temporal and spatial distribution of pedestrian accidents. ArcGIS Pro software was employed to visualize and assess these distributions. To identify accident-prone areas, the Kernel Density Estimation (KDE) clustering algorithm was applied, pinpointing hot spot locations of pedestrian accidents across the various districts of İzmir. Ultimately, the hot spots of pedestrian accident locations were identified separately for each year, month, and day of the week to examine variations in critical hot spot areas over time. In total, 6,794 pedestrian-involved crashes were recorded, representing 15.7% of all traffic accidents in the city during the analysis period. Of these, 6,612 incidents resulted in injuries, while 213 led to fatalities. The spatial distribution of these accidents within the border of the İzmir is illustrated in Figure 2.

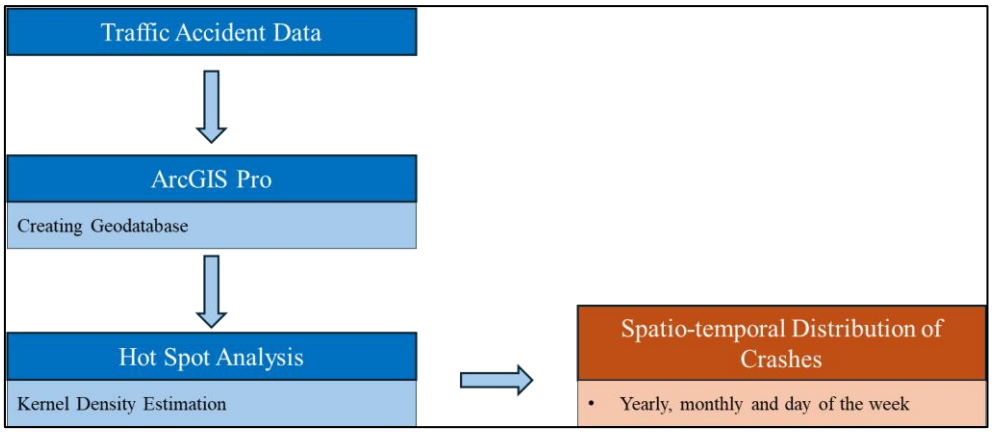

Figure 1. Methodological framework.

Table 1. Example dataset for traffic accident data

Year	Time	X	Y	Date	Accident Type	Fatal	Injury	Vehicle Type
2017	09:30	27.73052	38.08971	20170609	Pedestrian collision	0	1	Car
2017	09:30	27.73052	38.08971	20170609	Pedestrian collision	0	1	Bus
2017	09:45	27.13487	38.37309	20170823	Pedestrian collision	1	0	Truck
2017	11:20	28.20566	38.21743	20171015	Pedestrian collision	0	1	Car

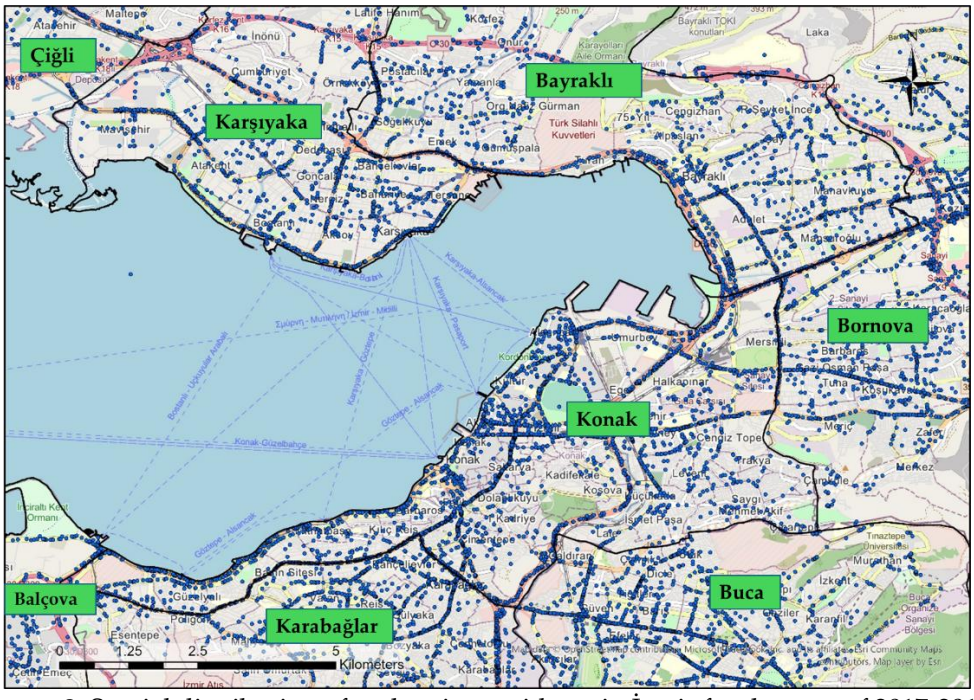

Figure 2. Spatial distribution of pedestrian accidents in İzmir for the year of 2017-2019.

3. Results and Discussion

3.1. Yearly Trends in Accident Density

Table 2 presents the descriptive evaluation results of total crashes, as well as pedestrian-involved crashes (PICs), over the analysis period. From 2017 to 2019, the population of Izmir increased by approximately 2.05%, while the number of total crashes decreased from 14,536 to 13,960, representing a nearly 4% decline. Regarding PICs, the number slightly decreased, as shown in Table 2. While the number of injuries remained almost the same in 2017 and 2019, fatalities dropped from 87 to 50,

reflecting a 42.5% reduction. The kernel density estimation enabled to analyze the spatial distribution of pedestrian involved accidents that occurred in İzmir between the years 2017, 2018, and 2019, provided in Figure 3. The color intensity on the maps represented the density of accidents in each region. While darker colors indicated a higher number of accidents, light colors indicated locations with lower accident density. When comparing the kernel density estimation results across the years, it can be concluded that accident density in certain regions has remained constant. These areas typically include central business districts with high pedestrian acitivities, such as Konak and Alsancak, as well as intersections of major roads and areas with high pedestrian activity that conflict with heavy traffic flow.

Table 2. Descriptive evaluation of the crashes for the analysis period.

Year	Population	Total Crashes	Total Injuries	Total Fatalities	PIC	#PIC Injuries	**#PIC Fatalities**
2017	4,279,677	14,536	14,328	346	2,336	2,260	**87**
2018	4,230,519	14,730	14,562	290	2,241	2,178	**76**
2019	4,367,251	13,960	13,815	242	2,217	2,174	**50**
Total	12,877,447	43,226	42,705	878	6,794	6,612	**213**

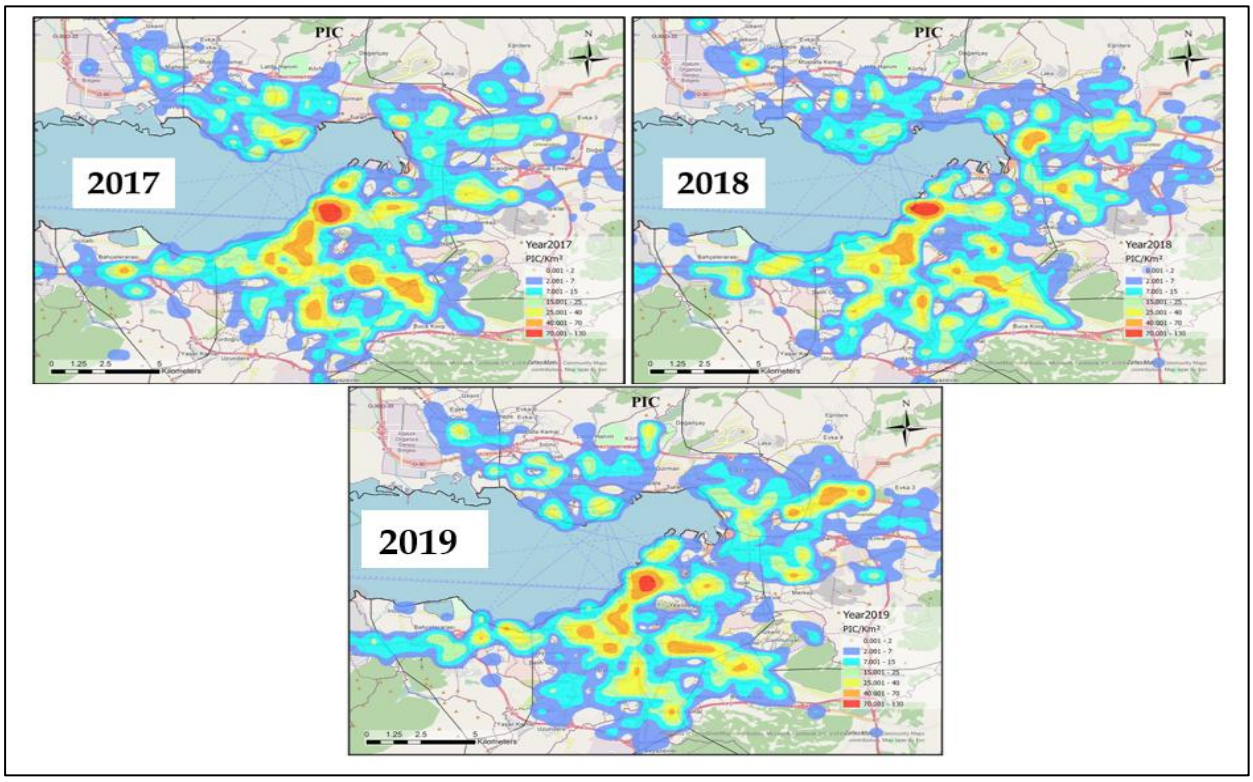

Figure 3. Kernel density estimation results for the years of 2017, 2018 and 2019.

3.2 Monthly Trends in Accident Density

Table 3 shows the monthly distribution of PICs across different districts of İzmir. The table includes the area of each district (in km²) and the number of PICs for each month. Additionally, the percentage of monthly PICs relative to the total number of PICs is also provided. It can be inferred from the Table 3 that the districts of Karabağlar and Konak consistently rank among those with the highest PIC counts throughout the year. This suggests that these areas may have higher population densities or experience more frequent occurrences of specific activities. Çiğli and Gaziemir were the regions with very few PICs occurred. Furthermore, significant fluctuations in the number of PICs are observed monthly. Certain districts exhibit increases or decreases in PIC counts during specific months, indicating that seasonal factors, special events, or other variables may influence the frequency of PICs. The months of March, April, and May were identified as the most critical periods for the occurrence of PICs, collectively accounting for 30.1% of the total. Additionally, the fall season emerged as significant, with PICs during this period constituting 25.7% of the overall total. As for the relationship between land area and PIC counts, there is no linear relationship between the land area of the districts and the number of PICs. Districts with larger land areas do not necessarily record higher PIC counts. This indicates that PIC numbers are not solely dependent on geographic size but are influenced by a range of other factors. Kernel density estimation algorithm was also employed to monthly PIC data to examine the most critical locations and hotspots of the accidents. Figure 4 shows the spatial distribution and hotspots of the PICs within İzmir for four different months. In January, it is observed that pedestrian accidents are relatively few, with limited areas exhibiting high concentrations of such incidents. In contrast, April reveals a significant clustering of pedestrian accidents, particularly in regions adjacent to Ege University in Bornova, as well as in the central business districts of Konak and Alsancak, and around the Karşıyaka Çarşı. Analysis of the July data indicates a decrease in the number of accident hotspots relative to April; however, accidents continue to be concentrated in the Konak Alsancak region. For October, accident hotspots emerge in locations that are similar to those identified in April. For both months, it can be also concluded that PICs were mostly clustered around the Izmir Gulf because of the existence of social and recreational areas which resulted in higher pedestrian activity and, consequently, a higher incidence of accidents. These findings suggest that serious precautions must be taken to enhance pedestrian safety in these areas.

Table 3. Monthly distribution of PICs across different districts of İzmir.

District	Area (km²)	Jan	Feb	Mar	Apr	May	Jun	Jul	Aug	Sep	Oct	Nov	Dec
Gaziemir	70.53	10	15	25	20	22	16	16	11	23	16	13	4
Karabağlar	89.11	63	47	64	61	87	66	70	61	63	66	57	67
Buca	178.00	55	70	92	108	96	83	56	68	86	86	72	60
Balçova	16.21	11	10	17	17	18	15	10	9	8	14	16	14
Konak	24.01	76	77	120	133	101	102	88	62	96	126	88	90
Bayraklı	29.92	35	28	39	52	26	33	48	26	38	30	38	28
Karşıyaka	52.11	37	34	43	40	23	23	23	22	29	35	36	34
Çiğli	138.20	10	11	13	17	14	10	11	9	16	17	9	10
Bornova	220.10	43	59	54	66	73	48	58	57	57	60	63	67
Total		351	368	489	541	482	411	407	346	429	465	420	388
Percent (%)		6.9	7.2	9.6	11.0	9.5	8.1	8.0	6.8	8.4	9.1	8.2	7.6

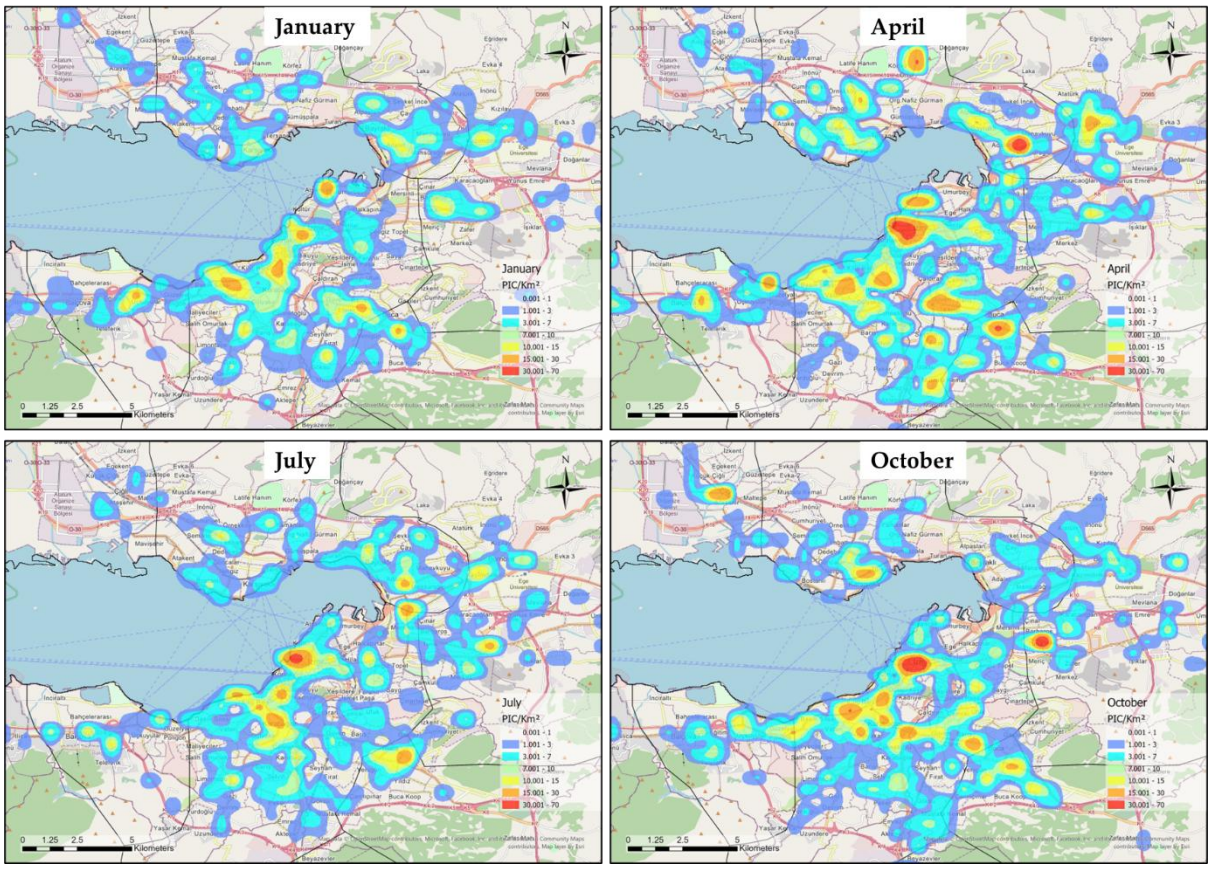

Figure 4. Kernel density estimation results showing the pedestrian accident density for selected months.

4. Conclusions

This study conducted a spatial-temporal analysis of pedestrian-involved crashes (PICs) using Geographic Information System (GIS) tools to identify accident hot spots and temporal trends between 2017 and 2019. The analysis revealed that despite a slight overall reduction in the number of pedestrian crashes and fatalities over the study period, certain regions remained consistent hot spots for accidents, particularly the central business districts of Konak and Alsancak, as well as other areas with high pedestrian and vehicle interaction, such as near Ege University and Karşıyaka Çarşı. Seasonal fluctuations in crash counts were also observed, with the months of April, March, and May accounting for the highest number of incidents, while winter months saw fewer accidents. This suggests that weather conditions, pedestrian activity levels, and possibly special events significantly affect crash frequency. Importantly, the spatial analysis revealed that accident hotspots are not uniformly distributed across the city's districts, and the size of a district is not a determinant of higher PIC counts.

Acknowledgements

This work has been supported by the National Research Project of Izmir Katip Celebi University, grant number of 2024-TYL-FEBE-0022. The authors also express their thanks to Izmir Police Department for sharing the accident data.

References

Craig, C. M., Morris, N. L., Van Houten, R., & Mayou, D. (2019). Pedestrian safety and driver yielding near public transit stops. Transportation research record, *2673*(1), 514-523.

LeBeau, P., 2019. Pedestrian deaths hit 28-year high, and big vehicles and smartphones are to blame [WWW Document]. CNBC. https://www.cnbc.com/2019/02/28/pedestrian-deaths-hit-a-28-year-high-and-big-vehicles-and-smartphones-are-to-blame.

Özen, M. (2021). Yaya kazalarının yaralanma şiddetinin incelenmesi: İkili lojistik regresyon modeli uygulaması. *Teknik Dergi*, *32*(3), 10859-10883.

Sze, N. N., Wong, S. C. (2007). Diagnostic Analysis of the Logistic Model for Pedestrian Injury Severity in Traffic Crashes. Accident Analysis & Prevention, 39(6), 1267-1278.

Ulak, M. B., Kocatepe, A., Yazici, A., Ozguven, E. E., & Kumar, A. (2021). A stop safety index to address pedestrian safety around bus stops. Safety Science, *133*, 105017.

Vision Zero, 2019. Vision Zero NYC [WWW Document]. https://www1.nyc.gov/site/visionzero/index.page

World Health Organization. (2018). Global Status Report on Road Safety 2015. World Health Organization.